
Novel chromatin interactions
by structural rearrangements
and aberrant enhancer functions
drive oncogenic programs
in unfavorable neuroblastoma

Dissertation

Dipl. Biol. Moritz Gartlgruber, M.Sc.

Biowissenschaften



Dissertation

submitted to the
Combined Faculty of Natural Sciences and Mathematics
of the Ruperto Carola University Heidelberg, Germany
for the degree of
Doctor of Natural Sciences

Presented by
Dipl. Biol. Moritz Johannes Gartlgruber, M.Sc.
born in: Darmstadt
Oral examination: 21.09.2018



Novel chromatin interactions by structural rearrangements and aberrant enhancer functions drive oncogenic programs in unfavorable neuroblastoma.

Referees: Prof. Dr. Thomas Höfer

PD Dr. Frank Westermann

Declaration

The work presented in the following dissertation was carried out from April 2013 until June 2018 in the Division of Neuroblastoma Genomics at the German Cancer Research Center (DKFZ) in Heidelberg (Germany) and was supervised by PD Dr. Frank Westermann.

I declare that I have written and submitted this dissertation myself and in this process have not used any other sources than those indicated. To the best of my knowledge this thesis, and the research to which it refers, are the product of my own work except where due to acknowledgement is made in the thesis itself.

Parts of the results of section 3.1.1 and 3.2 of this dissertation have been published in *Nature* in October 2015 (Peifer et al. 2015) and are ongoing work of a manuscript in preparation, respectively. Contributions in terms of data processing or experiments by other co-authors on the manuscripts are indicated in the materials and methods section or at the beginning of the respective results section of this dissertation.

I hereby declare that I have not applied to be examined at any other institution, nor have I used the dissertation in this or any other form at any other institution as an examination paper, nor submitted it to any other faculty as a dissertation.

Place, Date

Moritz Gartlgruber

Table of content

Zusammenfassung.....	V
Summary	VII
Figures.....	IX
Abbreviations.....	XII
1. Introduction.....	1
1.1 Neuroblastoma.....	1
1.1.1 The molecular principles of Neuroblastoma for targeted therapy	2
1.2 Epigenetics.....	9
1.2.1 DNA methylation.....	10
1.2.2 Histone modifications	12
1.2.3 Enhancer and super-enhancer	15
1.2.4 Chromatin organization – interaction and insulation	16
1.2.5 Motivation and aim of the thesis	17
2. Materials and methods.....	19
2.1 Materials	19
2.1.1 Chemicals and consumables.....	19
2.1.2 Laboratory equipment.....	21
2.1.3 Kits.....	22
2.1.4 Antibiotics.....	23
2.1.5 Cell lines.....	23
2.1.6 Enzymes.....	24
2.1.7 Antibodies.....	24
2.1.8 Secondary antibodies and ladder.....	25
2.1.9 Primer.....	25
2.1.10 Puffer and solutions.....	26
2.1.11 Software.....	30
2.2 Methods.....	31
2.2.1 General molecular biological methods	31

2.2.2	General cell culture methods	31
2.2.3	ATRA (all-trans retinoic acid) treatment.....	32
2.2.4	Quantification of proteins - SDS-PAGE/Western blot.....	32
2.2.5	CTB (CellTiter Blue) viability assay	35
2.2.6	Colony formation assay using GIEMSA staining.....	35
2.2.7	RNA interference using siRNA.....	36
2.2.8	Fluorescence <i>in situ</i> hybridisation (FISH)	36
2.2.9	Multicolour fluorescence <i>in situ</i> hybridisation (mFISH)	36
2.2.10	RNA isolation, purification and RNA sequencing (RNA-seq)	36
2.2.11	Chromatin immunoprecipitation sequencing (ChIP-seq)	37
2.2.12	Tumor ChIP-seq.....	38
2.2.13	ChIPmentation	38
2.2.14	4C sequencing (4C-seq)	38
2.2.15	HiChIP sequencing.....	39
2.2.16	ATAC sequencing (ATAC-seq).....	40
2.2.17	DNA preparation and whole genome sequencing (WGS).....	41
3.	Results.....	43
3.1	Global enhancer hijacking landscape in NB	43
3.1.1	Telomerase activation by genomic rearrangements in high-risk NB	43
3.1.2	Further rearrangements affecting oncogenes	53
3.1.3	WGS identified rearrangements affecting oncogenes.....	70
3.1.4	HAND2 SE cluster is recurrent donor-region in rearrangement events.....	81
3.2	Global super enhancer landscape analysis in NB	85
3.2.1	Epigenetic profiling defines NB SE landscape.....	86
3.2.2	SE defined NB epigenetic subtypes	89
3.2.3	Core regulatory circuitries of NB subtypes.....	95
3.2.4	Functional and clinical relevance of NB epigenetic subtypes	100
4.	Discussion.....	106
4.1	Global enhancer hijacking landscape in NB	106
4.1.1	Telomerase activation by genomic rearrangements in high-risk NB	106

4.1.2	Further rearrangements affecting oncogenes	110
4.1.3	HAND2 SE cluster is recurrent donor-region in rearrangement events.....	115
4.2	Global super enhancer landscape analysis in NB	116
4.2.1	Epigenetic profiling defines NB SE landscape.....	117
4.2.2	SE defined NB epigenetic subtypes	118
4.2.3	Core regulatory circuitries of NB subtypes.....	119
4.2.4	Functional and clinical relevance of NB epigenetic subtypes	121
4.3	Conclusion and perspective.....	123
5.	Appendix.....	126
5.1	ChIP-seq step-by-step protocol.....	126
5.2	Tumor ChIP-seq step-by-step protocol.....	129
5.3	ChIPmentation step-by-step protocol	130
5.4	4C-seq step-by-step protocol	132
5.5	Further figures and tables	137
	References	138
	Publications.....	150
	Acknowledgements.....	151

Zusammenfassung

Das Neuroblastom (NB) ist ein von migrierenden Neuralleistenzellen abgeleiteter, embryonaler Tumor, der im gesamten sich entwickelnden sympathischen Nervensystem auftreten kann. Kürzlich haben mehrere umfangreiche Sequenzierungsstudien im NB ein heterogenes Mutationsspektrum und eine geringe Mutationsfrequenz beschrieben. Es gibt viele Hinweise, dass im NB epigenetische Deregulation eine wichtige Rolle spielt. Dies verdeutlicht den dringenden Bedarf, epigenetische Profile für entitätsspezifische Regulatoren wie „enhancer“ und „super-enhancer“ (SE) zu lokalisieren, da diese regulatorischen Elemente zellspezifische Genexpression und dadurch Zellidentität bestimmen oder Onkogene in Tumoren regulieren. Durch diesen Ansatz könnten wichtige Krebsgene für eine zielgerichtete Tumorthherapie identifiziert werden. Im Rahmen dieser Studie wurden mittels Sequenzierung des gesamten Genoms (WGS) einer NB Kohorte, bestehend aus 60 Tumoren, wiederkehrende Umlagerungen in der Nähe des *TERT* Gens in 24% aller Hochrisiko-Patienten mit schlechter klinischer Prognose gefunden. Chromatin-Immunpräzipitation mit anschließender Sequenzierung (ChIP-seq) Analyse zeigte, dass Umlagerungen von starken „enhancer“ Regulatoren hin zum *TERT* Gen stattfinden und die RNA- und Protein-Expression sowie die Aktivität des Genprodukts Telomerase fördern. Zusätzlich wurden weitere wiederkehrende Umlagerungen von regulatorischen „SE“ Elementen hin zu Onkogenen wie *MYC* und *MYCN* in NB Zelllinien identifiziert, was in den spezifischen Fällen eine Erklärung für deren bisher unerklärbar hohe Expression lieferte. Mittels Integration von WGS Daten sowie auf RNS Sequenzierung basierten Expressionsdaten einer Kohorte, bestehend aus 111 NB Tumoren, konnte nach weiteren hochregulierten Genen in der Nähe von Bruchpunkten gesucht werden. Anhand dieses Vorgehens wurden weitere „enhancer-hijacking“ Kandidaten wie *IGF2BP1* und *ATOH1* in NB Tumoren und Zelllinien identifiziert. Durch anschließende ChIP-seq Analysen der betroffenen Tumoren und Zelllinien konnten hoch aktive „SE“ Bereiche, die durch Umlagerung in die Nähe der Onkogene gebracht wurden, und deren Expression sie höchstwahrscheinlich regulieren, identifiziert werden. Schließlich wurden mittels Chromatin Interaktionsanalyse mit anschließender Sequenzierung (4C-seq) physikalische Interaktionen zwischen regulatorischen „enhancer“ Elementen und durch Umlagerung in deren Einflussbereich geratenen Onkogenpromotoren in Zelllinien bestätigt. Zusätzlich wurde eine für die Entität spezifische regulatorische SE Region identifiziert, welche zwischen den Genen *HAND2* und *FBXO8* gelegen ist und die wiederkehrend in Umlagerungen mit den zuvor genannten Onkogenen involviert ist.

Des Weiteren wurden in dieser Studie mittels ChIP-seq Analysen der Azetylierung von Histon 3 Lysin 27 (H3K27ac) in einer NB Kohorte aus 60 Tumoren und 23 Zelllinien gewebespezifische

„SE“ inklusive ihrer assoziierten Zielgene identifiziert. Durch bioinformatische Analysen der „enhancer“ Daten konnten drei Gensignaturen definiert werden welche mit unterschiedlichen klinischen Subtypen assoziiert sind. Diese den Gensignaturen zugewiesenen Subtypen waren solche mit (i) amplifiziertem *MYCN*-Onkogen, sowie (ii) Niedrigrisiko- und (iii) Hochrisiko-Patienten ohne amplifiziertes *MYCN*-Onkogen. Bemerkenswerterweise konnte eine vierte Gensignatur gefunden werden, die mit mesenchymalen Attributen assoziiert war. Diese „SE“ definierte Subgruppe konnte, basierend auf einem großen Satz an RNA-seq-Daten, auf Expressionsebene, reproduziert werden und zeigt innerhalb der vier Signaturen höchste Stabilität zwischen Zelllinien und Tumoren. Die mesenchymale Signatur wies starke Assoziationen mit dem Auftreten von Rezidiv-Tumoren auf sowie mit erhöhter Expression des RAS und JUN/FOS Signalweges. Durch die erstmalige Integration von epigenetischen „SE“ und Genexpressionsdaten von Tumoren wurde ein NB-spezifisches Regulom sowie ein Subgruppenspezifischer Satz an essentiellen Haupttranskriptionsfaktoren definiert, die im Weiteren funktionell validiert wurden.

Zusammenfassend wurde in dieser Studie mit der Entdeckung von wiederkehrenden Umlagerungen von regulatorischen SE Elementen, welche in der Folge das *TERT* Gen aktivieren, ein erstmaliger Beweis für „enhancer-hijacking“ in NB Primärtumoren geliefert. Durch die Identifizierung weiterer wiederkehrender Onkogen-Umlagerungen, welche wesentliche Onkogene wie *MYC*, *MYCN*, *IGF2BP1* und *ATOH1* betreffen, wurde bewiesen, dass wiederkehrende „enhancer-hijacking“ Ereignisse *in vivo* nicht nur auf das *TERT* Gen beschränkt sind. Basierend auf ChIP-seq Analysen einer großen Tumorkohorte identifizierte diese Studie erstmalig spezifische dem NB sowie den NB Subgruppen zugrundeliegende spezifische „SE“-Landschaften, deren assoziierten Zielgene sowie die zugehörigen Sätze an essentiellen Haupttranskriptionsfaktoren. Die Studie identifizierte zudem viele für das NB essentielle deregulierte Gene, welche durch selektive Inhibition ihrer abnormalen Funktion potentiell die Möglichkeit für eine gezielte und personalisierte Therapie bieten können.

Summary

Neuroblastoma (NB) is an embryonal tumor derived from migrating neural crest cells and can occur within the whole developing sympathetic nervous system. Recently, several comprehensive sequencing studies in NB revealed a comparatively low mutation frequency and a heterogeneous mutation spectrum. Evidence accumulates that epigenetic deregulation play a prominent role in NB. Therefore, there is an urgent need to define entity-specific enhancer and super-enhancer (SE) profiles as regulatory elements control cell identity or oncogenes in a cancer context through cell type-specific gene expression. This will identify critical oncogenic driver genes essential for NB and help to devise a targeted therapy strategy. In the present study, whole genome sequencing (WGS) analysis of a 60 NB tumor cohort identified recurrent rearrangements in close proximity to the *TERT* gene in up to 24% of high-risk NB cases with poor clinical outcome. ChIP-sequencing analyses revealed that strong enhancers were juxtaposed to the *TERT* gene by these rearrangements likely driving increased *TERT* expression and TERT activity in the respective cases. In addition to *TERT*, discovery of recurrent repositioning of SE elements explained remarkably high expression levels of *MYCN*, *MYC* oncogenes in NB cell lines. Integrative analysis of WGS-based rearrangement data and RNA-seq based expression data in a cohort of 111 NB tumors allowed to identify highly upregulated genes in proximity to breakpoints. This approach located several other enhancer-hijacking candidate oncogenes including *IGF2BP1* and *ATOH1* in NB tumors and cell lines. Subsequent ChIP-seq analysis of the affected tumors and cell lines confirmed that highly active SE regions were juxtaposed to the oncogenes, which likely drives their high expression. Finally, physical interactions of juxtaposed enhancer elements with the oncogene promoters were confirmed by chromatin interaction analyses (4C-seq) in cell lines. Intriguingly, a lineage-specific SE region downstream of *HAND2* and upstream of the *FBXO8* gene locus was recurrently involved in the above mentioned rearrangements.

In a set of 60 NB tumor specimen and 23 NB cell lines, the present study identified groups of tissue-specific SEs and associated target genes based on histone mark H3K27ac ChIP-seq data. In depth bioinformatic analysis of the enhancer data retrieved three gene signatures, associated with previously established clinico-biological association, namely *MYCN*-amplified, high-risk- and low-risk *MYCN* non-amplified. Intriguingly, a fourth SE-defined NB subgroup was resolved, as defined by a gene signature highly associated with mesenchymal (Mes) gene ontology terms. This subgroup was reproducibly recovered by an analogue and extended approach based on RNA-seq expression of SEs assigned signature genes and further proved its stability by its consistent presence in NB cell lines and tumors. Importantly, the Mes signature was associated

with relapsed NB cases as well as with increased RAS and JUN/FOS signature expression. For the first time, integration of SE and expression data of primary tumors enabled the establishment of an NB entity and NB subgroup-specific regulome resulting in the definition and subsequent functional validation of subgroup-specific core-regulatory networks. Taken together, with the discovery of recurrent rearrangements of SE elements activating the *TERT* gene, the present study provides initial evidence for “enhancer hijacking” in NB tumors. The identification of further recurrent oncogene rearrangements involving known NB oncogenes *MYC* and *MYCN* in cell lines and as well as new candidates *IGF2BP1* and *ATOH1* in NB tumors demonstrates that recurrence of enhancer hijacking *in vivo* is not restricted to *TERT*. Importantly, the present study reveals the first entity and subgroup-specific SE landscape including assigned target genes and downstream core transcription factor networks based on CHIP-seq analyses in a large cohort of tumors. This study identifies several critical NB cancer genes, which may open a therapeutic window for selective inhibition of those dysregulated key genes.

Figures

Figure 1: The international staging system for NB tumors (INSS).	2
Figure 2: Epigenetic landscape involved in cell fate.	9
Figure 3: DNA methylation and CpG sites.....	10
Figure 4: Cytosine methylation and demethylation.	12
Figure 5: Posttranscriptional histone modifications.	13
Figure 6: Histone modifications define chromatin conformation.	14
Figure 7: Enhancer and SE definition.....	16
Figure 8: Chromatin conformation influences enhancer-promoter interaction.	17
Figure 9: The mechanism of enhancer hijacking.	43
Figure 10: WGS revealed recurrent genomic rearrangements in NB.	44
Figure 11: TERT rearrangement is associated with poor survival in NB.....	45
Figure 12: TERT mRNA expression in NB.	46
Figure 13: Structural aberrations involving TERT.....	47
Figure 14: Genome-wide interactions of TERT promoter.	48
Figure 15: Genome-wide interactions of TERT promoter.	48
Figure 16: Epigenetic profiling of TERT locus.	50
Figure 17: Epigenetic profiling of TERT locus.	50
Figure 18: Epigenetic profiling of rearranged regions involving TERT.....	51
Figure 19: Ranking of histone mark H3K27ac signal.....	52
Figure 20: DNA methylation of CpG islands at TERT locus in NB.....	53
Figure 21: MYCN mRNA expression in NB.	54
Figure 22: MYC mRNA expression in NB.	55
Figure 23: MYCN protein expression in NB cell lines.	55
Figure 24: MYC protein expression in NB cell lines.....	56
Figure 25: High MYCN is associated with poor survival in NB.	56
Figure 26: Structural aberrations involving MYCN.	57
Figure 27: Structural aberrations involving MYC.....	59
Figure 28: Genome-wide interactions involving MYCN promoter.....	60
Figure 29: Genome-wide interactions involving MYC promoter.....	61

Figure 30: Genome-wide interactions of MYCN promoter.....	61
Figure 31: Epigenetic profiling of rearranged regions involving MYCN.....	62
Figure 32: Epigenetic profiling of rearranged regions involving MYC.....	63
Figure 33: Epigenetic profiling of rearranged regions involving MYC.....	64
Figure 34: Epigenetic profiling of rearranged regions involving MYC.....	65
Figure 35: Epigenetic profiling of rearranged regions involving MYC.....	66
Figure 36: Ranking of histone mark H3K27ac signal.....	67
Figure 37: Ranking of histone mark H3K27ac signal.....	68
Figure 38: Impact of RNAi-mediated knockdown targeting MYC.....	69
Figure 39: IGF2BP1 mRNA expression in NB.....	71
Figure 40: IGF2BP1 protein expression in NB cell lines.....	71
Figure 41: High IGF2BP1 is associated with poor survival.....	72
Figure 42: Structural aberrations involving IGF2BP1.....	73
Figure 43: Genome-wide interactions involving IGF2BP1.....	74
Figure 44: Genome-wide interactions involving IGF2BP1.....	75
Figure 45: Epigenetic profiling of rearranged regions involving IGF2BP1 locus.....	76
Figure 46: Ranking of histone mark H3K27ac signal.....	77
Figure 47: ATOH1 mRNA expression in NB.....	78
Figure 48: High ATOH1 is associated with poor survival.....	79
Figure 49: Epigenetic profiling of rearranged regions involving ATOH1 locus.....	80
Figure 50: Ranking of histone mark H3K27ac signal.....	80
Figure 51: Epigenetic profiling and mRNA expression of genes within rearranged regions.....	83
Figure 52: HAND2 protein expression of NB cells.....	84
Figure 53: Impact of RNAi-mediated knockdown targeting HAND2.....	85
Figure 54: SE landscape of NB tumors.....	86
Figure 55: Tissue specificity of NB SE cohort.....	87
Figure 56: Validation of SE to target gene assignment using chromatin conformation data.....	88
Figure 57: Ranking of target gene assigned SEs in NB tumor cohort.....	89
Figure 58: NMF analysis of NB tumors.....	90
Figure 59: NMF analysis of the NB cell lines.....	91
Figure 60: t-SNE analysis of NB tumors and cell lines.....	92

Figure 61: Extended NMF analysis of NB tumors based on RNA-seq data.....	93
Figure 62: Scatterplots of NMF-based signatures for NB tumors.....	94
Figure 63: Recovery analysis of clinical variables of NMF-based signatures for NB tumors.....	95
Figure 64: Definition of NB-specific CRCs.	96
Figure 65: Validation of exemplar CRC TFs using chromatin conformation data.....	97
Figure 66: Functional validation via RNAi-induced knockdown of exemplar CRC TFs.....	98
Figure 67: Validation of RNAi-induced knockdown of exemplar CRC TFs.	99
Figure 68: Interactions and chromatin conformation of NB subgroup and specific CRC TFs.	100
Figure 69: ATRA-induced shifts of NB subtype exposure values of ChIP-seq data.	101
Figure 70: ATRA-induced shifts of NB subtype exposure values of RNA-seq data.	102
Figure 71: NB subtype exposure values of relapsed patients.	103
Figure 72: Pathway gene correlation of Mes signature.	104
Figure 73: Pathway gene enrichment in relapsed patients.....	104
Figure 74: CRC TF enrichment in relapsed patients.	105
Figure 75: Fragment distribution of ChIP-seq library.....	128
Figure 76: Fragment distribution of 4C-seq library.....	136
Figure 77: Summary of rearrangements in NB cell lines (hg19).....	137

Abbreviations

°C	celsius
μ	micro
4C-seq	Circularized Chromosome Conformation Capture with high-throughput sequencing
5caC	5-carboxylcytosine
5fC	5-formylcytosine
5hmC	5-hydroxymethylcytosine
5mC	5-methylcytosine
A	ampere
A, C, T, G, U, (N)	adenine, cytosine, guanine, thymine, uracile, (N: any nucleotide)
AFA	adaptive Focused Acoustics
ALT	alternative lengthening of telomeres
AML	acute myeloid leukemia
Amp	ampicillin
APS	ammonium-persulfate
ARACNE	algorithm for the reconstruction of accurate cellular networks
ATAC-seq	assay for transposase-accessible chromatin with high-throughput sequencing
ATL	T-cell leukemia/lymphoma
ATP	adenosine-5'-triphosphat
ATRA	all-trans retinoic acid
BAC	bacterial artificial chromosome
BAM	Binary Alignment Map
BET	bromodomain and extra-terminal
BFGF	basic fibroblast growth factor
BGH	bovine growth hormone polyadenylation
BMPs	bone morphogenetic proteins
bp	base pair
BSA	bovine serum albumin
CCD	charge-coupled device
CCHS	congenital central hypoventilation syndrome
cDNA	complementary DNA
CFS	common fragile sites
CGH	comparative genomic hybridization arrays
ChIP-seq	chromatin immunoprecipitation coupled with sequencing
chr.	chromosome
CLL	chronic lymphocytic leukemia
CML	chronic myeloid leukaemia
CMV	cytomegalovirus
CRC	core regulatory circuitry
cSCC	cutaneous squamous cell carcinoma
CTB	CellTiter Blue
dAMP	desoxyadenosine-monophosphate
DAPI	4,6-diamino-2-phenylindol

DCC	deleted in colon cancer
DEPC	diethylpyrocarbonate
der	derivate
DMEM	Dulbecco's modified eagle's medium
dmins	double minutes chromosomes
DMRs	differentially methylated regions
DMSO	dimethylsulfoxid
DNA	desoxyribonucleic acid
DNase	desoxyribonuclease
DNMTs	DNA methyltransferases
dNTP	2'-deoxyribonucleoside 5'-triphosphate
DOC	Na-deoxycholate
dsDNA	double-stranded DNA
DTT	dithiothreitol
<i>E. coli</i>	<i>Escherischia coli</i>
ECL	enhanced chemiluminescence
EDTA	ethylendiamintetraacetic acid, Na-salt
EFS	event-free survival
EGF	epidermal growth factor
EMT	epithelial-mesenchymal transition
ES	embryonic stem
et al.	et alii (and other)
EtOH	ethanol
FA	formaldehyde
FACS	fluorescence activated cell sorting
FANTOM5	functional annotation of the mammalian genome
FBS	fetal bovine serum
FCS	fetal calf serum
FDR	false discovery rate
FISH	fluorescent in situ hybridization
FPKM	fragments per kilobase of transcript per million mapped reads
g	gram
GC	gastric adenocarcinoma
gDNA	genomic DNA
GFP	green fluorescent protein
GSEA	gene set enrichment analysis
GTex	genotype-tissue expression
GWAS	genome-wide association study
h	hour(s)
H3/4/2A/2B	histone 3/4/2A/2B
H3K27ac	acetylathin of histone 3 at lysine residue 27
H3K27me3	trimethylation of histone 3 at lysine residue 27
H3K36me3	trimethylation of histone 3 at lysine residue 36
H3K4me1	monomethylation of histone 3 at lysine residue 4
H3K4me3	trimethylation of histone 3 at lysine residue 4

H3K9me3	trimethylation of histone 3 at lysine residue 9
HATs	histone acetyl transferases
HDACs	histone deacetylases
HDMs	histone demethylases
HEPES	4-(2-hydroxyethyl)-1-piperazineethanesulfonic acid
hg19	human genome 19
HiC	high-throughput chromosome conformation capture
HiChIP	high-throughput chromatin immunoprecipitation
HMTs	Histone methyltransferases
HR	high-risk
HRP	horse reddish peroxidase
HRPT1	hyperparathyroidism 1
HSCR	Hirschsprung disease
hsrs	homogenously staining regions
ICF syndrome	immunodeficiency, centromeric region instability, facial anomalies syndrome
igG	immunoglobulin G
IgH	immunoglobulin H
IGV	integrative genomics viewer
INSS	international neuroblastoma staging system
K	lysine
kb	kilo base
KD	knockdown
kDa	kilo dalton
l	liter
LB	Luria-Bertani
LMRs	low methylated regions
LOH	loss of heterozygosity
LR	low-risk
m	milli
M	molar
MACS	model-based analysis of ChIP-Seq
MAE	monoallelic expression
Mb	mega base
Mes	mesenchymal
min	minute(s)
MNA	<i>MYCN</i> -non amplified
mRNA	messenger RNA
MYB	myeloblastosis
n	nano
NB	neuroblastoma
NDRs	nucleosome-depleted regions
NMF	non-negative matrix factorization
NP-40	nonyl phenoxypolyethoxyethanol
P/S	Penicillin/Streptomycin
PAGE	polyacrylamide gel electrophoreses

PBS	phosphate buffered saline
PCR	polymerase chain reaction
PI	propidium iodidie
PIP	peak incident power
PIQ	protein interaction quantification
QuASAR	quantitative allele specific analysis of reads
R	arginine
RA	retinoic acid
RISC	RNA-induced silencing complex
RNA	ribonucleic acid
RNAi	RNA-interference
RNAPolII	RNA polymerase II
RNase	ribonuclease
RNS	Ribonucleinsäure
ROSE (tool)	rank ordering of super-enhancers
rpm	rotation per minute
RPMI1640	Rosvell park memorial institute, medium formulation 1640
RT	room temperature
RT-PCR	reverse transcription reaction followed by PCR
RT-qPCR	quantitative real-time RT-PCR
SDHA	succinate dehydrogenase
SDS	sodiumdodecylsulfat
SE	super-enhancer
sec	second(s)
Shh	sonic hedgehog
shRNA	short hairpin RNA
Sig	signature
siRNA	small interfering RNA
t	translocation
TAD	topologically associating domain
T-ALL	T cell acute lymphoblastic leukemia
TARGET	therapeutically applicable research to generate effective treatments
TBE	Tris/Borat/EDTA
TBS	Tris buffered saline
TCGA	the cancer genome atlas
TDG	thymine DNA glycosylase
TE	Tris/EDTA
TEMED	N, N, N', N'-tetramethylethylendiamin
Tet	tetracycline
TF	transcriptionfactor
Tris	tris-(hydroxymethyl)-aminomethan
Triton X-100	octyl-phenoxy-ethylenoxide
t-SNE	t-distributed stochastic neighbor embedding
TSS	transcriptional start site
U	unit (enzyme activity)

UDG	uracil-DNA glycosylase
UV	ultraviolet
V	volt
VIPER	virtual pathway explorer
VP	viewpoint
W	watt
WB	western blotting
WGS	whole genome sequencing
Wnt	wingless-type MMTV (mouse mammary tumor)

1. Introduction

1.1 Neuroblastoma

Neuroblastoma (NB) is an embryonal tumor deriving from migrating neural crest cells and affects the whole developing sympathetic nervous system including the adrenal medulla, sympathetic ganglia and paraganglia (Johnsen et al. 2009). NB accounts for 7 – 10 % of paediatric malignancies and approximately 15 % of all deaths of childhood tumors (Castleberry 1997; Castleberry 1997; Brodeur 2003). The clinical behaviour of this pediatric tumor is quite heterogeneous, with localized cases and excellent outcome, including spontaneous regression even without any therapy (Maris et al. 2007). Indeed, NB exhibits the highest spontaneous regression rate of all malignant neoplasms, which is 10 – 100-fold higher than for any other human entity (Pritchard and Hickman 1994; Castleberry 1997). On the other hand, in face of an intensive therapy for high-risk and metastatic diseases, which account for almost 50 % of the cases, long-term survival is still less than 40 % (Westermann and Schwab 2002; Oldridge et al. 2015). Comparison of world-wide results, in this clinical and biological extremely heterogeneous cancer, with regards to stage assignment and treatment strategy is still challenging. By establishing the international NB staging system (INSS) (Figure 1), this problem was approached and paved the way for a consistent assignment strategy (Brodeur et al. 1993). According to the INSS and irrespective of minimal residual disease or affected lymph nodes, gross resected, localized tumors of stage 1 are associated with a favourable outcome (Matthay et al. 1989; Hata et al. 1990).

Both, INSS stage 2A and 2B, represent 10-15 % of NB cases, which are described as localized tumors without metastases. The event-free survival (EFS) for patients classified stage 1 is with 92 % (n=209) significantly higher than EFS of 78 % (n=103) for patients classified stage 2A and 2B (Monclair et al. 2009). Patients with low risk tumors with the best outcome are classified INSS stage 4S, which are younger than one year, have in addition the ability of spontaneous regression and less than 1 % tumor cells in the bone marrow (Hayes et al. 1983). INSS stage 3 tumors are described as intermediate risk with EFS of 75 % (Monclair et al. 2009). Advanced stage 4 tumors are considered as high-risk NB tumors that are already metastatic (Jiang et al. 2011).

Stage 1

Localized tumor confined to the area of origin; complete gross resection, with or without microscopic residual disease; identifiable ipsilateral and contralateral lymph node negative for tumor.

Stage 2A

Unilateral with incomplete gross resection; identifiable ipsilateral and contralateral lymph node negative for tumor.

Stage 2B

Unilateral with complete or incomplete gross resection; with ipsilateral lymph node positive for tumor; identifiable contralateral lymph node negative for tumor.

Stage 3

Tumor infiltration across midline with or without regional lymph node involvement; or unilateral tumor with contralateral lymph node involvement; or midline tumor with bilateral lymph node involvement.

Stage 4

Dissemination of tumor to distant lymph nodes, bone marrow, liver, or other organs except as defined in 4s.

Stage 4s

Localized primary tumor as defined for stage 1 or 2 with dissemination limited to liver, skin or bone marrow (< 10% of nucleated marrow cells are tumor cells).

Figure 1: The international staging system for NB tumors (INSS).

(modified from Castleberry et al., 1997 – licence obtained.)

1.1.1 The molecular principles of Neuroblastoma for targeted therapy

A detailed understanding of the molecular principles of a cancer cell, regardless of its origin, is indispensable for the development of a targeted therapy approach. In the future this will pave the way from nonspecific therapy towards personalized approaches. Conventional approaches (i.e. cytotoxic chemotherapeutics) come with non-specific toxicity and troubling side effects. Therefore, identification of novel and specific targets, which represent molecular drivers of a particular malignancy, will increase the impact of treatment, whereas side effects should decrease (Sawyers 2004).

Retrospectively, applying a targeted therapeutic approach to NB, led to various challenges caused by the molecular nature and genetic complexity of this disease.

Genomic aberrations

Analysis of karyotypes of cancer cells, in the early 70s, already revealed genomic aberrations i.e. the rearrangement of chromosome 9 to chromosome 22, the notorious “Philadelphia translocation” in chronic myeloid leukaemia (CML). This results in a fusion protein BCR-ABL1, which is a highly active protein involved in tyrosine kinase signalling, driving the progression in this type of cancer (Rowley 1973). In the beginning of 1980, first cytogenetic studies in NB revealed genetic aberrations like ploidy changes, deletions, allelic losses and gains of recurrent locations as well as amplifications. All of these genomic aberrations correlate with the clinical outcome of the patient and are of prognostic relevance (Bown 2001).

1p deletion

In 1977, recurrent deletions of the short arm of chromosome 1 (1p) have been described in NB tumors and cell lines (Brodeur et al. 1977). Later on it was confirmed that this genetic aberration is the most frequent one occurring in NB. 1p deletion correlates with amplified *MYCN* (62 % of 1p loss of heterozygosity (LOH) tumors) and is associated with unfavourable clinical outcome (Fong et al. 1989). The recurrent deleted region of 1p is known to contain important genes for NB tumorigenesis but also tumor suppressors, like the calmodulin binding transcription activator 1 (CAMTA1), essential for neuronal differentiation of NB cells (Henrich et al. 2006; Henrich et al. 2011).

Ploidy

New methods to detect the cellular DNA content by flow cytometry (Look et al. 1984) or the level of ploidy changes by cytogenetic approaches (Kaneko et al. 1987; Hayashi et al. 1989) revealed findings of prognostic relevance. Tumors with hyperdiploid cellular DNA content or near triploidy are associated with a more favourable clinical course. In contrast to this, tumors with normal DNA content and diploid or tetraploid tumors are associated with a reduced survival probability.

17q gain

The genetic aberration of up to five copies of chromosome arm 17q and in addition translocation events of 17q was detected by multicolour fluorescence *in situ* hybridisation (mFISH) (Savelyeva et al. 1994; Meddeb et al. 1996). For NB tumors and cell lines, the most recurring event besides 1p loss is an unbalanced translocation with 17q. Both events are associated with

poor patient survival, while 17q gain reflects a more favourable clinical outcome (Van Roy et al. 1994; Bown et al. 1999).

Amplified MYCN

An amplified domain on the short arm of chromosome 2 was first described by Schwab and colleagues in 1983 (Schwab et al. 1983). The size of this amplified domain, with limited homology to the *MYC* oncogene, is varying in size and includes different co-amplified genes like e.g. *DDX1* (DEAD-Box Helicase 1). The *MYCN* oncogene was found to be amplified in the shape of hrsrs (homogenously staining regions) integrated at different chromosomes or in primary NB tumors mainly in form of circular extra-chromosomal dmins (double minutes chromosomes) (Cox et al. 1965; Kohl et al. 1983; Schwab et al. 1984; Emanuel et al. 1985). These crucial amplification events very frequently co-occur with either 1p loss or 17q gain (Abel et al. 1999). Lab tools for detecting the *MYCN* status for clinical evaluation as a biomarker for high-risk disease include southern blotting, genomic PCR or interphase *MYCN* FISH (Squire et al. 1996; Gallego et al. 1998).

Amplified *MYCN* occurs in half of all high-risk tumors of stage 3-4 with advanced stage disease and in 20% of all NBs (Brodeur et al. 1984). This association of amplified *MYCN* and increasing *MYCN* copy numbers with increased risk, reduced survival probability and poor clinical outcome was confirmed later (Seeger et al. 1985).

Recurrent somatic mutations in NB

Recurrent mutations of the *RAS* (*N-RAS*, *H-RAS*, and *K-RAS*) genes play a key role in many human cancer types and serve as a prognostic marker. First evidence that a single point mutation (G into T) leads to an amino acid substitution (valine instead of glycine) and thereby *HRAS* oncogene activation and cancer cell conversion into human bladder carcinoma cells was described in the early 80s (Reddy et al. 1982). Approximately 20-30% of non-small cell lung carcinomas and large fraction of colon cancers harbor a *K-RAS* mutation (Forrester et al. 1987; Aviell-Ronen et al. 2006). In NB primary tumors and cell lines, only few *RAS* mutations have been described, including NB cell line SK-N-SH, harboring a point mutation in one *N-RAS* allele (Moley et al. 1991; Iolascon et al. 1993). A whole-genome sequencing (WGS) study from 2015 identified an enrichment of *RAS*-MAPK (mitogen-activated protein kinase) pathway gene mutations, in relapsed NBs as compared to the matched primary samples. In 78% of the relapsed NBs, activating *RAS*-MAPK pathway gene mutations were detected, which is in 38% exclusive for the relapsed samples (Eleveld et al. 2015).

The most prominent and intensively studied gene being affected by inactivating mutation events, is the tumor suppressor gene *TP53*. While *TP53* mutations are, with a high mutation rate, one of the most common mutations in human cancer entities, they are rarely detected in primary NBs (Imamura et al. 1993; Vogan et al. 1993; Muller and Vousden 2014).

The first NB predisposing gene, the paired-like homeo-box 2B gene (*PHOX2B*), that harbors germ line mutations, has been identified by locus-specific sequencing (Trochet et al. 2004). In a study from 2007, 6.4% of supposedly hereditary NBs had a germ line mutation within the *PHOX2B* gene. This did not occur in sporadic neuroblastomas (Raabe et al. 2008). In addition, mutations of the *PHOX2B* gene were identified as the cause of congenital central hypoventilation syndrome (CCHS) or Hirschsprung disease (HSCR), which is another disorder of neural crest cells (Amiel et al. 2003).

Another predisposition gene, harboring germ line mutations, which is held responsible for most familial cases is the anaplastic lymphoma kinase (*ALK*) gene. A sequencing approach of 194 high-risk NB samples detected in approximately 10% of all tumors a mutation in the tyrosine kinase domain, resulting in *ALK* overexpression and a constitutively active kinase. In addition, comparative genomic hybridization arrays (CGH) of 592 NB samples identified increased copy numbers or even amplification of the *ALK* gene locus (Mosse et al. 2004; Chen et al. 2008; George et al. 2008; Janoueix-Lerosey et al. 2008).

Whole genome sequencing (WGS) NB studies

The first WGS study of 87 NB tumors without focus on any risk group confirmed the already suspected small number of recurrent amino-acid-changing mutations (Molenaar et al. 2012). Besides recurrent structural aberrations of genes involved in neuronal growth cone stabilization, point mutations in the *ATRX* (5.7%), *TIAM1* (T-cell lymphoma invasion and metastasis 1) (3.4%) and *RAC/RHO* (Rho family members of G proteins) pathway genes were identified. In addition, 18% of high-risk NBs revealed tremendous alterations called chromotripsis, which is defined as shredding of whole chromosomes (Molenaar et al. 2012).

NB-specific low median exonic mutation frequency was confirmed by a sequencing study of 240 NB samples. Here, whole-exome, genome and transcriptome sequencing were combined within the TARGET (therapeutically applicable research to generate effective treatments) initiative (Pugh et al. 2013). Several additional genes with significant recurrent somatic mutations like *ALK* (9.2%), *PTPN11* (tyrosine-protein phosphatase non-receptor type 11) (2.9%), *ATRX* (2.5%) and *NRAS* (0.83%) were identified. Further studies, like the genome-wide association study (GWAS), a combined cohort of four case series counting more than 2000 patients, identified additional putative oncogenes in NB, including the *LMO1* gene (Wang et al. 2011).

In summary, novel technologies, such as WGS and RNA-sequencing helped to identify additional putative NB-specific oncogenes and potential candidates for therapy, i.e. *ALK* (Wang et al. 2016). Despite of comprehensive and extensive sequencing studies in NB, the number of recurrent somatic coding mutations is rare and the mutation spectrum is heterogeneous, which will hinder the development of rational therapeutics. It is assumed that additional structural aberrations and epigenetic alterations contribute to the differential clinical heterogeneity of NB. This would help further defining the high-risk NB tumors, with the worst prognosis and outcome, at the molecular level.

Epigenetic alterations in paediatric cancer like NB and future perspectives

The fact that cancer is described equally as an epigenetic disease as well as genetic disease supports the fact that epigenetic changes serve as precursors of genetic transformations (Iacobuzio-Donahue 2009). One of the first epigenetic alterations described in cancer is the reduction of DNA methylation of colon cancer cells in contrast to normal tissue, like hypomethylation of the *RAS* oncogenes (Feinberg and Vogelstein 1983; Feinberg and Vogelstein 1983). The first study of DNA-methylation in NB primary tumors revealed methylation of caspase-8 as well as hypermethylation of promoter CpGs of the *RAS*-association domain family 1 isoform A (*RASSF1A*) (Teitz et al. 2000; Astuti et al. 2001). This recurrent hypermethylation of *CASP8* apoptosis gene is associated with relapse susceptibility (Grau et al. 2011), whereas hypermethylation of the putative tumor suppressor gene *RASSF1A* is correlated with survival (Decock et al. 2011). In addition, promoter hypermethylation in NB leading to inactivation of further putative tumor suppressor genes was reported for *PTEN* (Phosphatase and tensin homolog) and *CDH1* (Cadherin-1), which are both associated with reduced event-free survival (Hoebeeck et al. 2009). A genome wide methylation analysis of 105 primary NB samples, combining 450K methylation arrays, transcriptome and low copy WGS, revealed two distinct patient clusters (Henrich et al. 2016). Here, cluster 2, enriched for MNA (*MYCN*-non amplified) samples, was further subdivided in subgroup 2s, being enriched for low risk tumors with rare chromosomal aberrations. Cluster 1 consists of *MYCN*-amplified tumors, classified as high-risk cases and patients with a higher age at diagnosis.

There are several events, like chromosomal translocations, promoter methylations or deletions that cause monoallelic expression (MAE), which significantly more often affects oncogenes, including *hTERT* (Telomerase reverse transcriptase), than tumor suppressors in tumors (Walker et al. 2012).

Mutations lead to altered transcription factor binding within enhancer elements

A polymorphism within a super-enhancer region assigned to *LMO1* (LIM domain 1) alters a GATA to a TATA binding motif in NB. This causes disruption of transcription factor binding like GATA3, decreases *LMO1* expression and thereby leads to tumorigenesis (Oldridge et al. 2015). Another example is a mutation of *HOXB13* (homeobox B13) binding site within a regulatory enhancer, which causes increased *HOXB13* binding and leads to upregulation of *RFX6* (regulatory factor X6) gene expression in prostate cancer. *RFX6* gene expression is associated with prostate cancer cell proliferation, metastasis and relapse (Huang et al. 2014).

Deletions within enhancer elements

Deletions within enhancer elements of tumor suppressor genes can lead to tumor development. In prostate cancer, a deletion within enhancer regions that are bound by members of the activator protein 1 (AP-1) complex, like *c-JUN* transcription factors, has been described. HiC interaction data indicates a possible interaction of this enhancer region with several genes that act protective against prostate cancer (Demichelis et al. 2012).

De novo enhancer and transcription factor binding site creation

Oncogene regulation and activation by regulatory elements including enhancers, is a common event in many human cancers (Mansour et al. 2014). One of these oncogene drivers is *TAL1* (T-cell acute leukemia 1) in T cell acute lymphoblastic leukemia (T-ALL), which is regulated by an upstream super-enhancer (SE) established by a somatic mutation. Insertions of 2 – 18 bps create the MYB (myeloblastosis) binding motif, which leads to acetylation of H4K27 by CBP (CREB-binding protein) and formation of the transcription factor complex (Mansour et al. 2014).

Focal amplification or duplication of enhancer elements

There are many human tumors harboring focal amplifications and copy number gains, which affect enhancer elements that are driving oncogene expression. Many of these focal amplifications affect the *MYC* gene, which is independent of the tumor entity and reveals an important role for the *MYC* enhancer and *MYC* gene in tumorigenesis (Herz 2016). This is in line with *MYC* focal amplifications that affect a 500 kb region upstream of *MYC* in 5% of chronic lymphocytic leukemia (CLL), a 400 kb region downstream of *MYC* in 2% of lung adenocarcinoma and a 800 kb region downstream of *MYC* in 4% of uterine corpus endometrial carcinoma. In addition, 5% of T-ALL and 3-5% of adult acute myeloid leukemia (AML) are characterized by a duplication of an enhancer element 1,7 Mb downstream of *MYC* (Edelmann et al. 2012; Shi et al. 2013; Herranz et al. 2014; Zhang et al. 2016).

Structural rearrangements leading to enhancer hijacking events

The principle of alternative oncogene activation by enhancer rearrangements (enhancer hijacking) is defined as a process placing an enhancer into the proximity of an oncogene consequently resulting in ectopic oncogene activation. The phenomenon of enhancer hijacking, firstly described in 1982 in Burkitt's lymphoma, revealed immunoglobulin H (*IgH*) enhancer rearrangement juxtaposing the *MYC* gene and causing increased *MYC* expression (Taub et al. 1982). Subsequently, several translocation events were identified, like translocation of the *IgH* assigned enhancer into the proximity of the *BCL2* (B-cell lymphoma 2) gene, which leads to increased expression of the anti-apoptotic *BCL2* gene in follicular lymphoma (Bakhshi et al. 1987). In AML, rearrangements of the *GATA2* (GATA-binding factor 2) enhancer juxtaposing *EVII* (ecotropic virus integration site 1) activate its expression ectopically, resulting in a haplo-insufficient *GATA2* functionality. In addition, enhancer excision or BET (bromodomain and extra-terminal) inhibitor treatment reversed this process and led to tumor growth inhibition (Groschel et al. 2014). Another way of oncogene activation in paediatric cancers has been reported by Northcott and colleagues in 2014 (Northcott et al. 2014). Medulloblastoma represents a heterogeneous entity with four distinct subgroups. While *WNTs* and *SHH* (sonic hedgehog) are well known oncogenic drivers of subgroup 1 and 2, in the remaining subgroups central genes driving tumorigenesis are still unknown. However, these subgroups reveal an exclusive way of alternative *GFII* or *GFIIIB* (growth factor independent 1 family proto-oncogenes) oncogene activation. In this enhancer hijacking events, genomic rearrangements frequently juxtapose active enhancer and super enhancer elements to the *GFII* or *GFIIIB* gene locus (Northcott et al. 2014).

Deletion or inversion of a topologically associating domain (TAD)

Deletion of one of these conserved TAD regions (described more in detail in 1.2.3 and Figure 8) can alter gene expression by changing the interaction capability of regulatory elements (Valton and Dekker 2016). Two types of TAD disruptions are found in cancer cells. First, deletion of a TAD is leading to a TAD fusion, creating an enlarged interaction context of regulator elements, like increased *PDGFRA* (platelet-derived growth factor receptor A) expression in gliomas (Flavahan et al. 2016). Second, a rearrangement event that is creating new TADs and a new interaction context of regulatory elements as described for the *GATA2* enhancer juxtaposing and subsequently upregulating the *EVII* gene (Groschel et al. 2014).

In contrast to this, inhibition of super-enhancers (SE) using chromatin modifying enzymes or BET-bromodomain inhibitors, like JQ1, causes loss of BRD4 (Bromodomain Containing 4) at

regulatory elements and disrupts regulation of oncogenic drivers like *MYC* in multiple myeloma (Filippakopoulos et al. 2010; Loven et al. 2013).

Taken together, it could be hypothesized that there is a strong epigenetic involvement in NB tumorigenesis. This is supported by a sequencing study in paediatric cancers, including NB, which revealed that almost 20% of mutations are found in epigenetic regulator genes (Huether et al. 2014). A better understanding of the epigenetic landscape could pave the way for the development of specific epigenetic drugs and personalized therapies as well as epigenetic marker screens as a basic diagnostic analysis tool for paediatric cancer, including NB.

1.2 Epigenetics

Various definitions of the term “epigenetics” exist firstly described by Conrad Waddington in 1942 as the phenotypical result of the interplay of genes and their products - or basically, acts that could not be explained simply by genetic processes (Goldberg et al. 2007). Epigenetics connect the genotype and phenotype as all cells in an organism share the same genetic information and only different regulation of gene expression generates the tremendous diversity of cell types and cellular functions (Figure 2). A more recent definition describes epigenetics as a stable heritable phenotype that results from alterations in a chromosome without changing the DNA sequence (Berger et al. 2009).

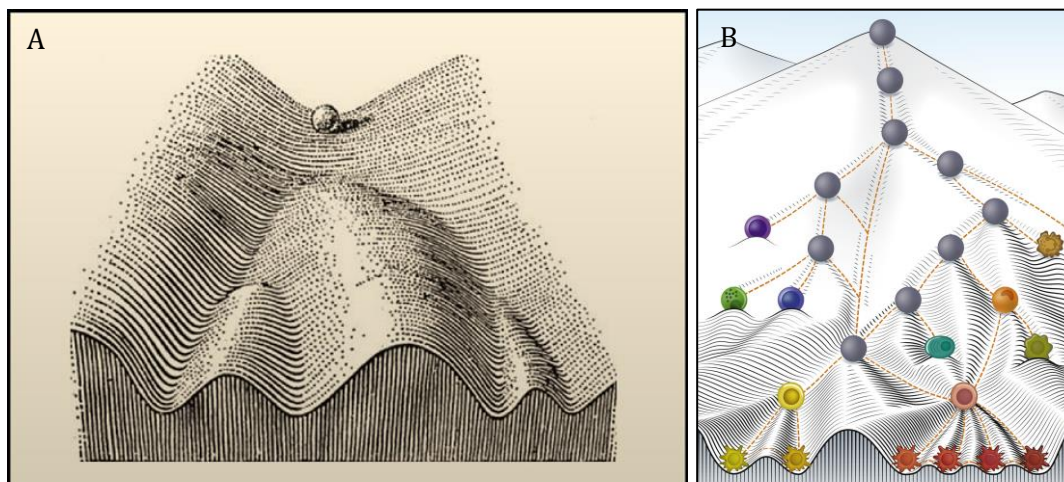


Figure 2: Epigenetic landscape involved in cell fate.

(A) Conrad Waddingtons epigenetic landscape – concept of developmental decision making of a cell results in different cell fates (adapted from Waddington, 1952 and (Goldberg et al. 2007) – licence obtained.). (B) Model of dendritic cell fate in a more recent interpretation, which is based on Conrad Waddingtons epigenetic landscape (Paul and Amit 2014) – licence obtained.

Nowadays, investigating epigenetic mechanisms are focused on modifications of DNA and histone proteins that influence the chromatin status. Disruption of this epigenetic balance is an essential cause for cancer development (Egger et al. 2004). New therapeutic strategies that restore the epigenetic balance will pave the way for more specific epigenetic drugs to fight cancer.

1.2.1 DNA methylation

DNA methylation is the first characterized epigenetic and probably best characterized chemical modification of chromatin (Holliday and Pugh 1975; Riggs 1975; Goldberg et al. 2007). Already in 1975, de novo DNA methylation by enzymatic reactions that is inherited from one cell to another and involved in gene silencing has been reported. DNA methylation was described in plants and fungi but at least in mammals shown to occur at the pyrimidine ring of cytosine residues of CpG dinucleotides (Figure 3). Regions of CpG dinucleotide accumulation are called CpG islands and their methylation at the transcriptional start site (TSS) is associated with transcriptional repression (Goll and Bestor 2005). In vertebrates, at least half of the genome contains CpG regions of approximately 1 kb length (Jones 2012).

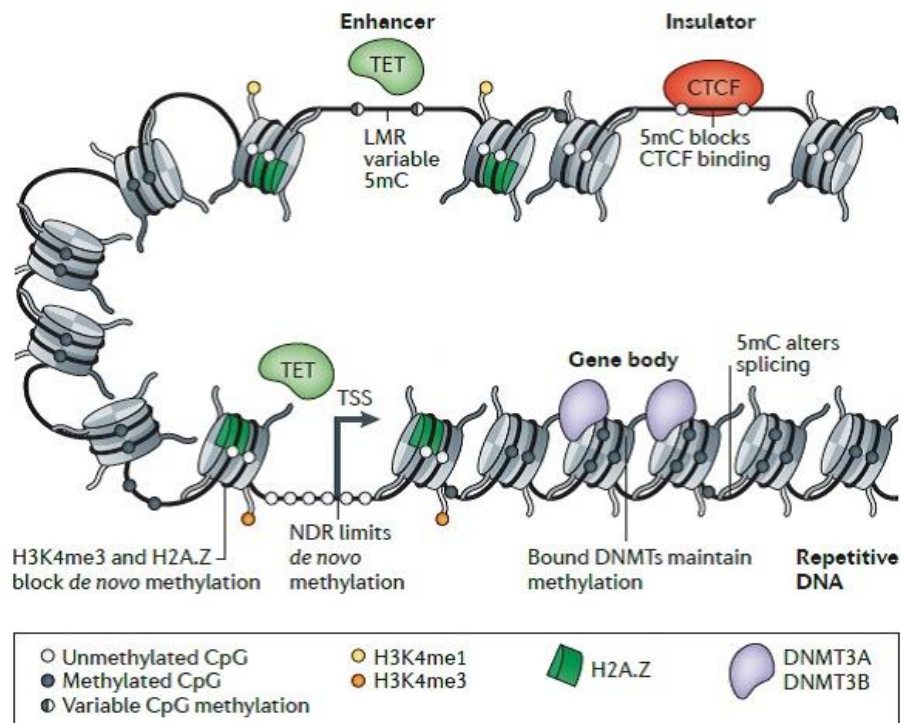


Figure 3: DNA methylation and CpG sites.

CpG sites within the genome have different functions in respect to transcriptional regulation. Low methylated regions (LMRs) at enhancers and nucleosome-depleted regions (NDRs) are

demethylated and associated with the presence of ten-eleven translocation (TET) proteins. Contrary, presence of 5-methylcytosine (5mC) is blocking CCCTC-binding factor (CTCF) binding and influences the process of splicing. DNA methylation is catalyzed and maintained by DNA methyltransferases. Adapted from (Jones 2012) – licence obtained.

The region up to 2 kb surrounding CpG islands are defined as “shores” (Irizarry et al. 2009). Initially, methylation of the gene body was shown to be associated with actively transcribed genes (Wolf et al. 1984). Nowadays, this dogma gets more and more dynamic as gene body methylation is tissue- and cell-specific and might have more diverse functions. Regulatory elements like enhancers are mostly CpG poor and have variable methylation, calling them low methylated regions (LMRs) (Stadler et al. 2011). In T cells, methylation of CpG sites within differentially methylated regions (DMRs) of enhancers leads to reduced enhancer activity (Schmidl et al. 2009). DNA binding enzymes with binding sites at enhancers like glucocorticoid receptors might foster CpG demethylation and thereby restore enhancer activity (Wiench et al. 2011). Methylation at insulators like CTCF binding-sites, which prevent promoter-enhancer interactions, might be involved in splicing (Shukla et al. 2011). Methylation of CTCF binding sites prohibit CTCF binding and thereby regulate gene expression of this locus (Bell and Felsenfeld 2000).

The enzymatic process of DNA methylation is maintained by three different DNA methyltransferases (DNMTs) (Figure 4). DNMT1 is the essential enzyme maintains DNA methylation patterns after DNA replication (Hermann et al. 2004). Therefore, it mainly binds hemi-methylated DNA target sites, which are defined by one of the strands methylated. *De novo* DNA methylation, which is necessary to establish DNA methylation patterns during early mammalian development, is catalyzed by DNMT3A and DNMT3B (Okano et al. 1999). A mutation of *DNMT3B* in humans leads to hypomethylation of pericentromeric regions, which are causing defects during human development (ICF syndrome).

Demethylation of DNA is catalyzed by three enzymes of the TET (ten-eleven translocation) protein family members, which are named after a frequently occurring translocation in cancer of chromosome 10 and 11 (Huang and Rao 2012).

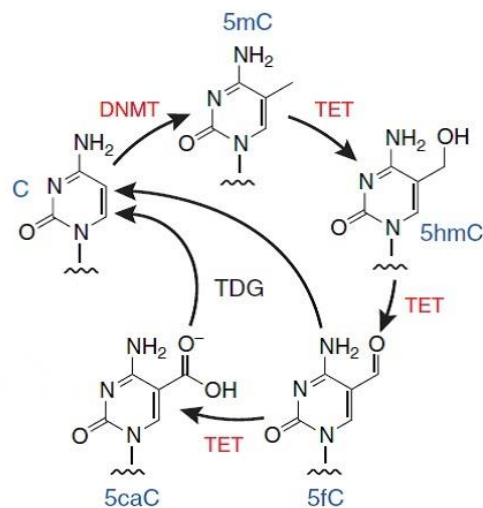


Figure 4: Cytosine methylation and demethylation.

DNA methyltransferases (DNMTs) and TET proteins act on Cytosine methylation and demethylation. Adapted from (Huang and Rao 2012) – licence obtained.

The first enzymatic step is the oxidation of 5-methylcytosine (5mC) and to 5-hydroxymethylcytosine (5hmC). The next oxidation leads to formation of 5-formylcytosine (5fC) and finally to 5-carboxylcytosine (5caC) (Tahiliani et al. 2009; Ito et al. 2011). Finally, restoration of unmodified cytosine is catalyzed by the DNA repair enzyme thymine DNA glycosylase (TDG) (He et al. 2011). In embryonic stem (ES) cells, enrichment of 5hmC at TSS, exonic sequences and enhancers were reported. At the TSS, 5hmC was strongly enriched with bivalent histone marks such as H3K4me3 and H3K27me3 (He et al. 2011).

1.2.2 Histone modifications

Posttranscriptional modified histones, like histone acetylation or methylation, have been firstly described by Vincent Allfrey in 1964. Besides DNA methylation, histone modifications represent another level of epigenetic regulation by modulating nucleosome dynamics during transcription (Allfrey et al. 1964; Allfrey and Mirsky 1964).

One feature of nucleosomes is packaging of 147 bps of DNA around a nucleosome that allows regulation of DNA accessibility for transcription, DNA repair mechanisms and replication (Figure 5) (Venkatesh and Workman 2015). A nucleosome itself consists of an octamer, subdivided into two copies of the histones H3, H4, H2A and H2B (Kornberg 1974; Kornberg and

Thomas 1974). Modification of specific amino acids of the histone amino-terminal-tail extensions are predominantly lysines (K) or arginines (R).

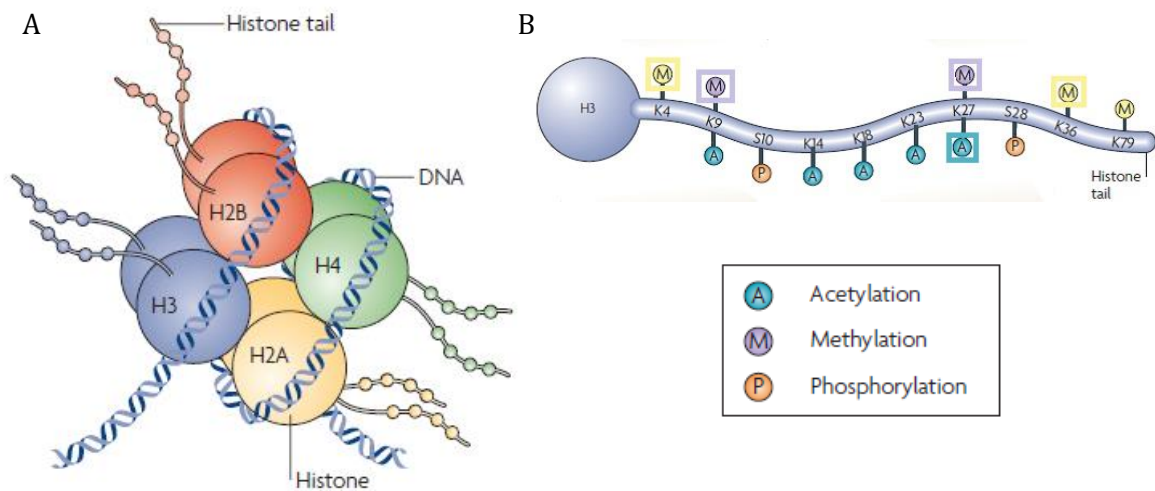


Figure 5: Posttranscriptional histone modifications.

(A) DNA-Nucleosome complex including two copies of the histones H3, H4, H2A and H2B as well as the outward facing amino-tails. (B) Histone modifications of lysine residues of H3 with a focus on methylation of K4 (K4me1 and K4me3), K9 (K9me3), K27 (K27me3) and K36 (K36me3) as well as acetylation of K27 (K27ac). Adapted from (Tsankova et al. 2007) – licence obtained.

Possible modifications that have an impact on chromatin structure and gene regulation range from methylations, acetylations and phosphorylations to ubiquitinilations or SUMOylations (Bannister and Kouzarides 2011). Acetylation reaction is conducted by histone acetyl transferases (HATs) and inverted by histone deacetylases (HDACs). Histone methyltransferases (HMTs) and histone demethylases (HDMs) catalyze methylation and demethylation, respectively (Tsankova et al. 2007). The chromatin is organized in functional inactive, compact (heterochromatin) and active, less dense chromatin packaging (euchromatin). These domains are crucial for genome organization and epigenetic regulation of gene expression (Foret et al. 2014). Further identification of histone modifications at distinct genomic locations, like promoters and enhancers, via ChIP-seq links epigenetic information to transcriptional regulatory activity (Figure 6) (Heintzman et al. 2007). One of the most studied histone modifications are those of histone H3 and especially trimethylated H3K4 (H3K4me3), which can be found at transcription start sites (TSS) and are associated with actively transcribed protein-coding promoters (Kim et al. 2005; Hon et al. 2009).

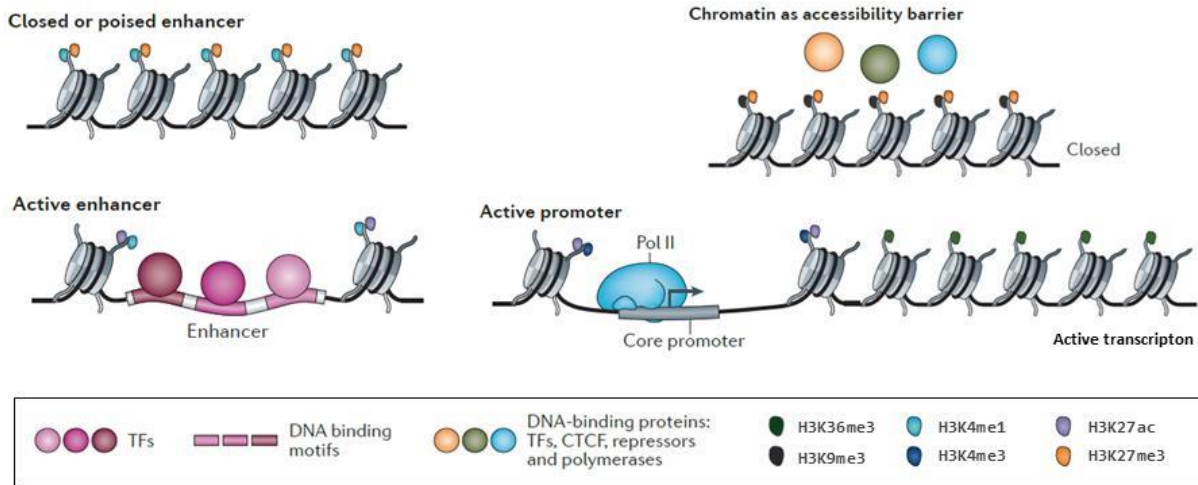


Figure 6: Histone modifications define chromatin conformation.

Chromatin accessibility changes rendered by histone modifications are essential for transcription factor binding, enhancer activity and transcription. Chromatin signature of repressive histone marks H3K9me3 together with H3K27me3 is associated with condensed chromatin, which prevents binding of transcription factors or RNA polymerase II. In contrast, enrichment of histone modifications H3K4me3, H3K4me1 or H3K27ac at the TSS leads to RNA polymerase II binding and active transcription. Chromatin signature of H3K36me3 at the gene body is likewise associated with elongation and active transcription. Enrichment of H3K4me1 in combination with H3K27me3 is associated with closed or poised enhancers. An active enhancer, accessible for transcription factor binding, is enriched for H3K4me1 and H3K27ac in the absence of H3K4me3. Adapted from (Shlyueva et al. 2014) – licence obtained.

Likewise, the chromatin signature of trimethylated H3K36 (H3K36me3) is enriched at the gene body of active genes. The accumulation of H3K36me3 is not randomly distributed throughout the gene body but significantly higher in exons than introns (Guenther et al. 2007; Kolasinska-Zwierz et al. 2009). Enhancer- and promoter-specific chromatin features are enriched for acetyltransferases, like p300 as well as monomethylated H3K4 (H3K4me1), while enhancers are lacking H3K4me3 marks (Hatzis and Talianidis 2002; Heintzman et al. 2007). Enhancers are usually defined as the sequences with binding motifs for transcription factors (approximately 1700) that release condensed chromatin structure and enable binding of the transcription machinery at the TSS (Heintzman and Ren 2009; Vaquerizas et al. 2009). The promoter and TSS itself can be located a long way off the *cis*-regulatory enhancer elements and therefore enhancers act independently of orientation or distance (Creighton et al. 2010). Definition of enhancers only by H3K4me1 mark leads to a significant ratio of inactive genomic regions. Based on this, Jeanisch and colleagues suggested acetylated H3K27 as an additional histone modification that defines active in contrast to poised enhancers, without a H3K27ac mark

(Creighton et al. 2010). H3K27ac mark is set by P300 and CREB binding protein (CBP), which have both a histone acetyltransferase (HAT) activity. In addition, an active TSS shows enriched H3K27ac mark, which can be used in the presence of H3K4me1 at enhancer sites to assess enhancer activity according to the level of enrichment (Tie et al. 2009; Wang et al. 2011).

In contrast to transcriptional activation, gene silencing and repression are another important mechanism to establish and maintain tissue- and cell-specific expression patterns (Foret et al. 2014). Post-transcriptional modifications of histones, like trimethylation of H3K27 (H3K27me), are associated with gene silencing and repressive function, which goes along with chromatin compaction. The trimethylation of H3K27 is polycomb mediated by the polycomb repressive complex 2 (PRC2), which is enzymatically catalyzed by the histone-lysine N-methyltransferase subunits EZH1 and EZH2 (Enhancer of zeste homolog 1 and 2) (Schuettengruber and Cavalli 2009; Simon and Kingston 2009; Margueron and Reinberg 2011). Genomic locations with enriched trimethylation of H3K4 and H3K27 histone mark have a bivalent promoter that is characteristic e.g. for the pluripotent status of an embryonal stem cell (Bernstein et al. 2006). Another negative regulation of transcription can be achieved by trimethylation of histone H3K9 (H3K9me3), which is crucial for heterochromatin formation and epigenetic repression. This modification is catalyzed by site-specific histone methyltransferase (HMT) SUV39H. H3K9me3 acts as specific binding site for heterochromatin protein 1 (HP1 α), a main component of heterochromatin (Peters et al. 2002; Stewart et al. 2005). The repressive marks, H3K27me and H3K9me3, both are hallmarks of constitutive and facultative heterochromatin, regularly co-localize at the same genomic region (Boros et al. 2014). Co-localization of H3K27me3 and H3K9me3 at silent gene promoters was detected at the deleted in colon cancer gene (DCC) and defines bivalent gene promoters (Derks et al. 2009).

1.2.3 Enhancer and super-enhancer

In a mammalian cell, thousands of active enhancer elements are defined as DNA regulatory units that are bound by transcription factors and control cell type-specific gene expression (Bulger and Groudine 2011; Thurman et al. 2012). The term super-enhancer (SE) was first introduced by Hnisz and colleagues to describe a large cluster of transcriptional enhancers that drive gene expression, thus defining cell identity (Hnisz et al. 2013). SEs differ from normal enhancer in size, enrichment for binding of transcription factors and their ability for transcriptional activation (Whyte et al. 2013). In a cancer context, SEs are located close to key driver oncogenes like *MYC* in multiple myeloma. This might offer an opportunity for epigenetics-based therapeutic approaches, i.e. using the BET-bromodomain inhibitor, JQ1 (Loven et al. 2013).

SEs are defined in a three step procedure (Figure 7). First, normal enhancers are defined by enrichment of H3K27ac ChIP-seq peaks. Second, H3K27ac ChIP-seq peaks within 12.5 kb of each other are combined to form one single enhancer unit. Third, all enhancers and combined enhancer units are ranked according to their H3K27ac signal within the genomic region. Enhancers with the highest H3K27ac signal above the cut-off where the slope of the curve is one are considered as super-enhancers (Hnisz et al. 2013; Pott and Lieb 2015).

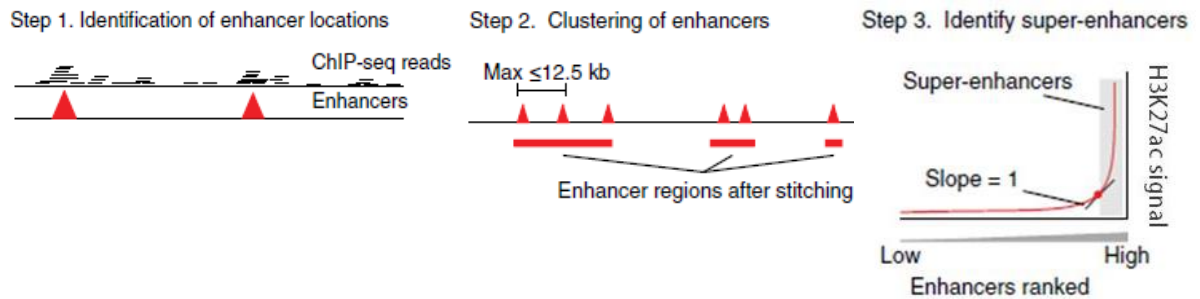


Figure 7: Enhancer and SE definition.

Step-to-step procedure of SE definition. 1. Enhancer definition by peak calling of H3K27ac ChIP-seq data. 2. Combining/concatenating enhancers within 12.5 kb of each other. 3. Super-enhancer definition. All enhancers (combined and single enhancers) are ranked according to their H3K27ac signal. Enhancers with higher H3K27ac signal from the inflection point are considered as super-enhancer. Adapted from (Pott and Lieb 2015) – licence obtained.

Instead of using H3K27ac as surrogates for SE identification, master transcription factor binding, such as OCT4 (octamer-binding transcription factor 4), SOX2 (SRY (sex determining region Y)-box 2) and Nanog (Whyte et al. 2013) as well as MED1 (Mediator of RNA polymerase II transcription subunit 1) can serve for SE prediction (Loven et al. 2013). In any case, defining a SE by surrogate enrichment (H3K27ac, MED1 or master transcription factors) is solely a prediction and does not evaluate enhancer-promoter interactions and thereby functional enhancer activity resulting in active transcription.

1.2.4 Chromatin organization – interaction and insulation

The mechanism of differential transcriptional regulation is based on (promoting and preventing) physical interactions between regulatory elements of distant enhancers and promoters. New methods, like locus-specific 4C-seq (circularized chromosome conformation capture with high-throughput sequencing) or a genome wide chromatin immunoprecipitation conformation method (HiChIP) improved the understanding of genomes architecture (van de Werken et al. 2012; Mumbach et al. 2016). This essential process of facilitating enhancer looping

of interacting elements requires on the contrary as well shielding functions of neighboring domains that are blocking enhancer activity (Figure 8) (Ali et al. 2016). Those regions, which allow interactions within domains but prevent interactions between neighboring domains, are called topologically associating domains (TAD) or bordering insulators (Ong and Corces 2014). Essential for this 3D organization are the architectural proteins CTCF (CCCTC-binding factor) and SMC1A and SMC3 (structural maintenance of chromosomes protein 1A and 3) as core subunits of the cohesion complex (Peters et al. 2008).

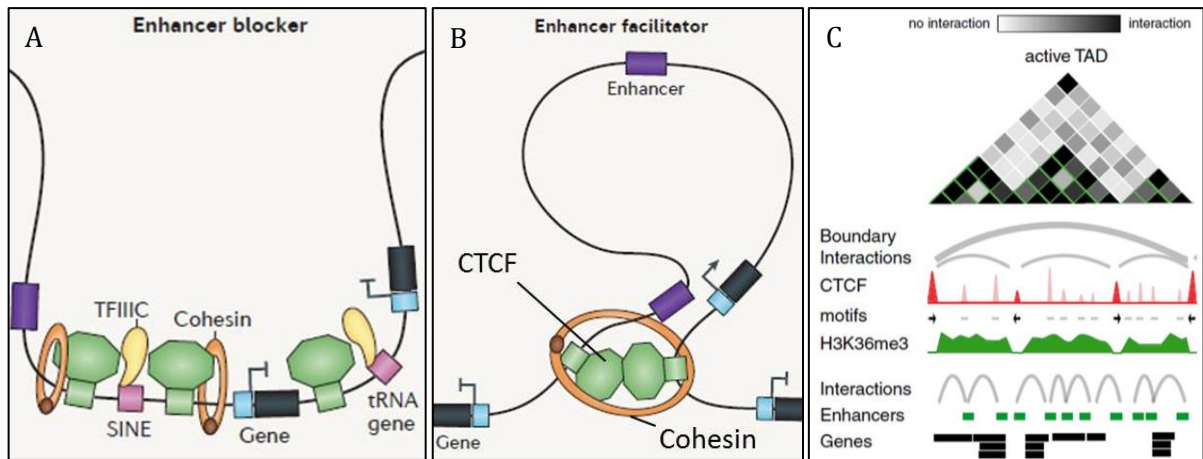


Figure 8: Chromatin conformation influences enhancer-promoter interaction.

(A) Coinciding CTCF binding sites together with transcription factor complex TFIIC and architectural cohesin proteins lead to TAD border formation. These insulator regions prevent interaction across such borders and block enhancer function. (B) CTCF binding and recruitment of cohesin within TAD regions supports physical enhancer-promoter interactions by enhancer looping. (C) Virtual HiC matrix represents interaction frequency within the TAD. CTCF peaks in red are involved in binding TAD boundaries in contrast to pale red peaks. Interactions in grey represent active enhancer-promoter looping. Adapted from (Ong and Corces 2014; Ali et al. 2016) – licence obtained.

1.2.5 Motivation and aim of the thesis

Several structural aberrations of specific chromosomes as well as the amplification of the oncogene *MYCN* in subsets of high-risk neuroblastomas (NBs) are known till today, which are associated with poor NB outcome and are likely driver events. However, exome sequencing studies have shown that NBs harbor a low overall mutation rate with only few recurrently mutated genes leaving the molecular etiology of a large proportion of NBs elusive. (Molenaar et al. 2012; Pugh et al. 2013). Recent studies in NB and other pediatric cancer entities revealed that epigenetic deregulation may be a significant driver component in these cancer types (Northcott et al. 2014; Henrich et al. 2016). The present study is based on the hypothesis that deregulated

enhancer networks may be responsible for NB development, progression and heterogeneity. A deeper understanding of underlying mechanisms will offer the perspective for targeted molecular therapies based on epigenetic drugs.

1. Do structural rearrangements contribute to NB pathogenesis by generating activating *de novo* interactions between enhancers and oncogenes?

Regulatory elements, like SEs that recruit and build up transcription factor networks and thereby regulate gene expression play an essential role in cell specificity and identity as well as aberrant function in human cancers (Demichelis et al. 2012; Huang et al. 2014; Mansour et al. 2014; Oldridge et al. 2015). The principle of alternative oncogene activation by locating enhancers in the proximity of oncogenes was described for several cancer entities and is referred to as enhancer-hijacking (Taub et al. 1982; Bakhshi et al. 1987; Groschel et al. 2014; Northcott et al. 2014). The present study aims at discovering single and especially recurrent structural rearrangement events leading to oncogene activation by enhancer hijacking. Candidate rearrangements and enhancer gene couples will be validated via expression analyses, chromatin interaction analyses and functional testing in cell line models.

2. What are NB- or NB subtype-specific SEs and their innate transcription factor network? SEs are the regulatory units of core regulatory circuitries, which consist of small, auto-regulatory sets of cell type-specific master TFs determining identity and fate of cells. Evidence accumulates that differential SE landscapes have the potential to discriminate between cancer entities and subgroups. Furthermore, elucidating the networks of entity- and subtype-specific SEs and their downstream targets promises to unravel specific vulnerability nodes in view of potential targeted therapy (Wong et al. 2017). This subproject aims to define the SE landscape of NB, resolve epigenetically defined subgroups and functionally test vulnerabilities e.g. by knockdown of specific core regulators derived from these networks.

2. Materials and methods

2.1 Materials

2.1.1 Chemicals and consumables

Product	Supplier
Acrylamid/ Bis 40%	Bio-Rad, München
Agarose NEEO Ultra quality	Roth, Mannheim
Agencourt AMPure XP	Beckman Coulter, Sinsheim
AlamarBlue	MorphoSys AbD, Düsseldorf
Ammonium persulfate (APS)	Merck, Darmstadt
BFGF	Invitrogen, Carlsbad, USA
Bioruptor Pico 1.5 ml microtubes with caps	Diagenode, Liège, Belgium
Bovine serum albumin (BSA)	Sigma Aldrich, Munich
Bradford Reagent	Biorad, München
Bromphenol blue	Serva, Heidelberg
Cell culte well plates	TPP, Trasadingen
Cell culte well plates	Nunc, Wiesbaden
Cell culture cryotubes	Nunc, Wiesbaden
Cell culture flasks	TPP, Trasadingen
Cell culture plates	TPP, Trasadingen
Chloroform	Sigma Aldrich, Munich
Citrat Monohydrat	Riedel DeHaën, Seelze
Cover slips	Menzel, Braunschweig
DEPC	Roth, Mannheim
Dimethylformamide	Serva, München
Dimethylsulfoxide	Sigma Aldrich, Munich
Disodiumhydrogenphosphate	Merck, Darmstadt
Dithiothreitol	AppliChem, Darmstadt
DMEM	PAA, Pasching
dNTPs	Amersham-Pharmacia, Freiburg
DTT	Roth, Mannheim
ECL Plus Western Blotting Detection Reagent	GE Healthcare, Freiburg
ECL Prime Western Blotting Detection Reagent	GE Healthcare, Freiburg
EDTA	Roth, Mannheim
EGF	Genaxxon, Ulm
Electroporation cuvettes (1 mm gap width)	Biorad, München
Ethanol abs.	Sigma Aldrich, Munich
FBS	Biochrom, Berlin
Filter tips, graduated (10, 100, 200, 1000 µl)	Star Lab, Hamburg
Formaldehyde	Sigma Aldrich, Munich
GelRed	Genaxxon, Ulm
GeneRuler™ 100bp DNA Ladder	MBI-Fementas, St.Leon-Rot

GeneRuler™ 1kb DNA Ladder	MBI-Fementas, St.Leon-Rot
Giemsa's Azure Eosin Methylene Blue solution	Merck, Darmstadt
Glass slides	Thermo Fisher Scientific, Waltham, USA
Glycerol	Roth, Mannheim
Glycine	Biorad, München
Glycogen	Roche Diagnostics, Mannheim
Harnstoff	Merck, Darmstadt
Heparin	Sigma Aldrich, Munich
HEPES	Sigma Aldrich, Munich
Isopropanol	Sigma Aldrich, Munich
KCl	Roth, Mannheim
KH ₂ PO ₄	Merck, Darmstadt
L-Glutamin	Lonza, Basel
Lipofectamine RNAiMAX	Thermo Fisher Scientific, Waltham, USA
Luna Cell Counter Slides	Logos Biosystems, Annandale, USA
Manganese (II) chloride solution	Sigma Aldrich, Munich
Methanol	Sigma Aldrich, Munich
MgCl ₂	Roth, Mannheim
Milk powder	Sigma Aldrich, Munich
Na- Citrat	Roth, Mannheim
Na ₂ HPO ₄	Sigma Aldrich, Munich
NaCl	Sigma Aldrich, Munich
NaHCO ₃	Merck, Darmstadt
Natriumacetat	Roth, Mannheim
NH ₄ Cl	Merck, Darmstadt
Nitrocellulose membranes, 0.2 mm	Whatman, Dassel
Nitrocellulose membranes, 0.45 µm	GE Healthcare, Munich
PCR plate 96 twin-tec, skirted, colorless	Eppendorf, Hamburg
Phenol/ chloroform/ isoamylalcohol	Roth, Mannheim
Pipette tips	Starlab, Hamburg
Plastic pipettes (5, 10, 25, 50 ml)	Corning, Tewksbury, USA
Plastic plates (black)	Greiner bio-one, Frickenhausen
Plastic reaction tubes (0.1-2ml)	Eppendorf, Hamburg
Plastic reaction tubes (15-50ml)	Greiner bio-one, Frickenhausen
Polyacrylamide	Serva Electrophoresis, Heidelberg
Ponceau-S	Sigma Aldrich, Munich
Potassium chloride	Roth, Mannheim
Powdered milk (blotting grade)	Roth, Mannheim
Proteinase inhibitor cocktail, EDTA	Roche Diagnostics, Mannheim
RPMI-1640	PAA, Pasching
Sodium dodecyl sulfate (SDS)	Gerbu, Heidelberg
Sodium hydrogen carbonate	Merck, Darmstadt
TEMED	BioRad, München
Tris Base	Sigma Aldrich, Munich
Tris HCl	AppliChem, Darmstadt

Triton X-100	Serva, Heidelberg
Trypan Blue	AppliChem, Darmstadt
Trypton	AppliChem, Darmstadt
Tween 20	Merck-Schuchardt, München
Whatman 3MM Paper	Whatman, Dassel
β -mercaptoethanol	Merck, Darmstadt

2.1.2 Laboratory equipment

Product	Supplier
<u>CCD-cameras:</u>	
CH250	Photometrics, München
SenSys 1400	Photometrics, München
<u>Centrifuges:</u>	
5417R	Eppendorf, Wesseling-Berzdorf
Allegra X-12	Beckman Instr., München
Avanti J-25 I	Beckman Instr., München
Biofuge fresco 17	Heraeus, Osterode
J 2-21 M/E	Beckman Instr., München
Minifuge RF	Heraeus, Osterode
Varifuge 3.2RS	Heraeus, Osterode
<u>Rotors:</u>	
5310	Heraeus, Osterode
JA 10	Beckman Instr., München
JA 20	Beckman Instr., München
JS 13.1	Beckman Instr., München
<u>Thermo incubators:</u>	
Cell culture incubator Hepa Class 100	Thermoelectron Corp., Waltham, USA
Setri-Cult	Thermo Fisher Scientific, Waltham, USA
Termicon T	Heraeus, Osterode
2100 BioAnalyzer	Agilent Technologies, Santa Clara, USA
Analytical Balances PM 4600	Mettler, Gießen
Axiovert 10, Imager Z1	Zeiss, Oberkochen
Beckmann Coulter Z2	Beckman Instr., München
Bioruptor Pico	Diagenode, Liège, Belgium
Cat RM5 (Membrane roller)	Neolab, Heidelberg
Cellgard Class 2	INTEGRA Biosciences, Biebertal
Covaris LE220	Covaris, Woburn, USA
Covaris S-Series	Covaris, Woburn, USA
Fluoroscan Ascent FL	Thermo Electron, Dreieich
Gel documentation system Geldoc	BioRad, München
Horizontal mini-gel systems	GIBCO/BRL, Darmstadt
Light cyclers 480 II	Roche, Mannheim
Luna automated cell count	Logos Biosystems, Annandale, USA

Magnetic Mixers	Heidolph, Schwabach
Mini trans-blot cell	BioRad, München
Mini-PROTEAN 3 electrophoresis system	BioRad, München
Mini-PROTEAN 3 multi-casting chamber	BioRad, München
MS3 Vortexer	IKA, Staufen
Nano-Drop 1000	Peq-Lab, Erlangen
pH-Meter pMX 2000	WTW, Weilheim
Photometer GeneQuant 1300	General Electric, Boston, USA
Pipetboy	Integra Bioscience, Fernwald
Platereader FLUOstar OPTIMA	BMG Labtech, Ortenberg
Polymax 2040	Heidolph, Schwabach
Power supply units, PHEROlab	Fisher Scientific, Schwerte
Qubit 2.0 Fluorometer	Invitrogen, Carlsbad, USA
Safe 2020	Thermo Fisher Scientific, Waltham, USA
Shacking platform, IKA KS250	Janke & Kunkel, Staufen
Tank-transfer unit	Biorad, München
Thermo Block Biometra Trio	Biometra, Goettingen
Thermo water bads	GFL, Mannheim
Thermocycler DNA-Engine PTC200	BioRad, München
Thermocycler Tetrad 2	BioRad, München
Thermo-shakers G25, G24	New Brunswick Scientific, Offenbach
Vacuum concentrator	Bachofer, Reutlingen

2.1.3 Kits

Product	Supplier
NEBNext Ultra DNA Library Prep Kit for Illumina	NEB, Ipswich, USA
BM Chemiluminescence Blotting Substrate kit	Roche, Basel, Switzerland
CellTiter-Blue® Cell Viability Assay	Promega, Madison, USA
NEBNext Ultra Directional RNA Library Prep Kit for Illumina	NEB, Ipswich, USA
Ribo-Zero rRNA Removal Kit	Illumina, San Diego, USA
TRIZOL Reagent	Invitrogen, Carlsbad, USA
Effectene transfection Reagent	Qiagen, Hilden
First Strand cDNA Synthesis Kit for RT-PCR	Roche, Basel, Switzerland
High pure PCR template preparation kit	Roche, Basel, Switzerland
QIAquick Gel Extraction kit	Qiagen, Hilden
QIAquick PCR purification kit	Qiagen, Hilden
RNeasy mini kit	Qiagen, Hilden
NucleoSpin Kit for RNA	Macherey-Nagel
NEBNext End Repair Module	NEB, Ipswich, USA
NEBNext Quick Ligation Module	NEB, Ipswich, USA
NEBNext dA-Tailing Module	NEB, Ipswich, USA
NEBNext High-Fidelity 2X PCR Master Mix	NEB, Ipswich, USA
NEBNext Multiplex Oligos for Illumina (Index Primers Set 1)	NEB, Ipswich, USA

NEBNext Multiplex Oligos for Illumina (Index Primers Set 2)	NEB, Ipswich, USA
Nextera DNA Library Prep Kit	Illumina, San Diego, USA
Nextera Index Kit (24 Indexes)	Illumina, San Diego, USA
KAPA library Amp Illumina with primers	KAPA Biosystems, Wilmington, USA
Expand Long Template PCR System	Roche, Basel, Switzerland
Agilent DNA 12000 Kit	Agilent, Santa Clara, USA
Agilent High Sensitivity DNA Kit	Agilent, Santa Clara, USA
Agilent DNA 1000 Kit	Agilent, Santa Clara, USA
Agilent RNA 6000 Nano Kit Guide	Agilent, Santa Clara, USA

2.1.4 Antibiotics

Product	Stock concentration	Supplier
Ampicillin	(50 mg/ml)	Serva, Heidelberg
Kanamycin	(25 mg/ml)	Serva, Heidelberg
Blasticidin	(41,25 mg/ml)	MP Biomedicals, Illkirch, France
Penicillin/Streptomycin	(10000 U/ml)	Serva, Heidelberg
G418 Sulfate	(200 mg/ml)	Sigma, München
Zeocin	(100 mg/mL)	Invitrogen, Karlsruhe
Tetracycline	(10 mg/ml)	Sigma, München

2.1.5 Cell lines

MNA = *MYCN* non-amplified

Neuroblastoma cell line	<i>MYCN</i> status	Reference/Established
CHLA15	MNA	(Keshelava et al., 1998)
CHLA20	MNA	(Keshelava et al., 1998)
CHLA90	MNA	(Keshelava et al., 1998)
CLB-GA	MNA	(Combaret et al., 1995)
GI-M-EN	MNA	(Donti et al., 1988)
LAN6	MNA	(Wada et al., 1993)
NB69	MNA	(Mena et al., 1989)
NBL-S	MNA	(Cohn et al., 1990)
SH-EP	MNA	(Ross et al., 1983)
SH-SY5Y	MNA	(Biedler et al., 1978)
SK-N-AS	MNA	(El-Badry et al., 1989)
SK-N-FI	MNA	(Suigimoto et al., 1984)
HD-N-33	<i>MYCN</i> -amplified	(Schwab, unpublished)
IMR-32	<i>MYCN</i> -amplified	(Tumilowicz et al., 1970)
IMR5/75	<i>MYCN</i> -amplified	(Tumilowicz et al., 1970)
KELLY	<i>MYCN</i> -amplified	(Schwab et al., 1983)
LAN2	<i>MYCN</i> -amplified	(Seeger et al., 1977)
LS	<i>MYCN</i> -amplified	(Rudolph et al. 1991)

NGP	<i>MYCN</i> -amplified	(Brodeur et al., 1977)
NMB	<i>MYCN</i> -amplified	(Brodeur et al., 1977)
P4	neural crest derived cell line	(Hauser et al., 2012)
P5	neural crest derived cell line	(Hauser et al., 2012)
SK-N-BE-(2)-C	<i>MYCN</i> -amplified	(Biedler and Spengler 1976)
SK-N-DZ	<i>MYCN</i> -amplified	(Suigimoto et al., 1984)
SMS-KCNR	<i>MYCN</i> -amplified	(Reynolds et al., 1986)
TR14	<i>MYCN</i> -amplified	(Cowell and Rupniak 1983)

2.1.6 Enzymes

Product	Supplier
Benzonase	Merck, Darmstadt
<i>Bgl</i> I	Fermentas, Waltham, USA
<i>Eco</i> RI	NEB, Ipswich, USA
<i>Hind</i> III	Fermentas, Waltham, USA
<i>Pfu</i> Turbo DNA polymerase	Applied Biosystems, Foster City, USA
Proteinase K	Gerbu, Heidelberg
RNAse A	Sigma, München
T4 DNA ligase	NEB, Ipswich, USA
<i>DPN</i> I	NEB, Ipswich, USA
<i>Csp6</i> I	Thermo Fisher Scientific, Waltham, USA

2.1.7 Antibodies

Antigen	Application	Supplier	Cat.nr.:
H3K4me3	ChIP-seq	abcam, Cambridge, UK	ab8580
H3K36me3	ChIP-seq	abcam, Cambridge, UK	ab9050
H3K9me3	ChIP-seq	abcam, Cambridge, UK	ab8898
H3K27me3	ChIP-seq	Active Motif, Carlsbad, USA	39155
H3K27ac	ChIP-seq/HiChIP	abcam, Cambridge, UK	ab4729
H3K4me1	ChIP-seq	abcam, Cambridge, UK	ab8895
H3K79me3	ChIP-seq	abcam, Cambridge, UK	ab2621
CTCF	ChIP-seq	Diagenode, Liège, Belgium	C15410210
SMC1A	HiChIP	Bethyl, Montgomery, USA	A300-055A9
ETS1	western blot	Santa Cruz, Dallas, USA	sc-55581
SMAD3	western blot	abcam, Cambridge, UK	ab40854
RARB	western blot	Santa Cruz, Dallas, USA	sc-56864
HAND2	western blot	Santa Cruz, Dallas, USA	sc-398167
IGF2BP1	western blot	abcam, Cambridge, UK	ab82968
MYC	western blot	abcam, Cambridge, UK	ab32072
MYCN	western blot	(Wenzel <i>et al.</i> 1991)	
a-tubulin	western blot	Santa Cruz, Dallas, USA	sc-5286

β -actin	western blot	Sigma-Aldrich, St. Louis, USA	A-5441
----------------	--------------	-------------------------------	--------

2.1.8 Secondary antibodies and ladder

Antigen/description	Host	Supplier	Cat.nr.:
Anti mouse (rabbit)-HRP	goat	Dianova, Hamburg	115-035-003
Anti rabbit-TxRed	goat	Dianova, Hamburg	111-075-003
Anti goat igG-HRP	donkey	Santa Cruz, Dallas, USA	sc-2020
GeneRuler 100bp (0.1 μ g/ μ l)		Thermo Scientific, Waltham, USA	#SM0243
Quick-Load 1 kb DNA ladder		NEB, Ipswich, USA	#N0552S
BenchMark, prestained protein ladder		Invitrogen, Carlsbad, USA	10748-010
PageRuler, prestained protein ladder		Fermentas, Waltham, USA	26616

2.1.9 Primer

Primer name	Sequence 5'-3'	Appl.
HAND2 P300_1_f	aatgatacggcgaccaccgaacactctttccctacacgacgctctccgatctagatgatgtttcaggatc	4C-seq
HAND2 P300_1_r	caagcagaagacggcatacagatagtttctgttctgaagccc	4C-seq
HAND2 P300_2_f	aatgatacggcgaccaccgaacactctttccctacacgacgctctccgatctccattgtccaatctgatc	4C-seq
HAND2 P300_2_r	caagcagaagacggcatacagatccaaatactgagccatgat	4C-seq
HAND2 P300_3_f	aatgatacggcgaccaccgaacactctttccctacacgacgctctccgatctcaagtctaactagccagatc	4C-seq
HAND2 P300_3_r	caagcagaagacggcatacagatagcttcaattactgcccc	4C-seq
HAND2 TSS_f	aatgatacggcgaccaccgaacactctttccctacacgacgctctccgatctctcccgtgtggaaggatc	4C-seq
HAND2 TSS_r	caagcagaagacggcatacagactgaaccagagaggaaag	4C-seq
IGF2BP1 TSS_f	aatgatacggcgaccaccgaacactctttccctacacgacgctctccgatctgggagaacacataaaagatc	4C-seq
IGF2BP1 TSS_r	caagcagaagacggcatacagaggggaatcaacaaaagat	4C-seq
MYC endo_f	aatgatacggcgaccaccgaacactctttccctacacgacgctctccgatctgccaacttctaaaaggatc	4C-seq
MYC endo_r	caagcagaagacggcatacagacttgatttatggaggggtg	4C-seq
MYCN endo_f	aatgatacggcgaccaccgaacactctttccctacacgacgctctccgatctgaaggcatcgtttgaggatc	4C-seq
MYCN endo_r	caagcagaagacggcatacagactggggaacatttctgtaa	4C-seq
TERT TSS_f	aatgatacggcgaccaccgaacactctttccctacacgacgctctccgatctctaaagatgggaccaggatc	4C-seq
TERT TSS_r	caagcagaagacggcatacgaaggagggtgaccttcttg	4C-seq
Primer1	aatgatacggcgaccaccgagatctacactcgtcggcagcgtcagatgtg	ATAC-seq
P2.1_TAAGGCCGA	caagcagaagacggcatacagagattcgcttagtctcgtgggctcggagatgt	ATAC-seq
P2.2_CGTACTAG	caagcagaagacggcatacagagatctagtagctcgtgggctcggagatgt	ATAC-seq

2.1.10 Puffer and solutions

10x Amresco	1x	1 l
Tris Base	25 mM	30.3 g
Glycin	192 mM	144 g
SDS	0.1%	50 ml of 20% SDS
H ₂ O		up to 1 l

Annealing buffer	1x	100ml
Potassium acetate	100 mM	1 g
HEPES-potassium hydroxide	30 mM	0.83 g
Magnesium acetate	2 mM	0.043 g

DNA lysis buffer		100 ml
NH ₄ Cl		0.83 g
KHCO ₃		0.1 g
EDTA		0.037 g
H ₂ O		up to 100 ml
autoclave		

Laemmli buffer	1x	50 ml
Tris	0.5 M	4 g
SDS	4%	10 mL of 20% SDS
Glycerol	20%	10 ml
β- Mercaptoethanol		5 ml
H ₂ O		25 ml
Bromphenolblue		small amount

Protein lysis buffer		50 ml
Tris Base	1 M	1 ml
Triton X-100		500 µl
Harnstoff		21 g
DTT	1 M	5 ml
MgCl ₂	1 M	2 ml
Protease inhibitors		2 tablets
H ₂ O		42 ml

Separating gel buffer (pH 8.8)	1x	1 l
Tris Base	1.5 M	182.1 g
SDS	0.4%	20 mL of 20% SDS
H ₂ O		up to 1 l

Stacking gel buffer (pH 6.8)	1x	1 l
Tris Base	0.5 M	60.1 g
SDS	0.4%	30 mL of 20% SDS
H ₂ O		up to 1 l
10x PBS (pH 7.4)	(1x)	1 l
NaCl	137 mM	8 g
KCl	2,68 mM	0,2 g
Na ₂ HPO ₄	10 mM	1,42 g
KH ₂ PO ₄	1,76 mM	0,24 g
H ₂ O		up to 1 l
10x TBE (pH 8.3)	1x	1 l
Tris Base	89 mM	108.9 g
Boric acid	89 mM	55 g
EDTA	2 mM	7.4 g
H ₂ O		up to 1 l
10x TBS (pH 7.6)	1x	1 l
Tris	50 mM	6 g
NaCl	150 mM	8.8 g
H ₂ O		up to 1 l
Transfer buffer	1x	1 l
Tris Base	25 mM	3 g
Glycin	192 mM	14.4 g
Methanol	20%	200 ml
H ₂ O		up to 1 l
Versene (pH 7.0)		1 l
EDTA	10 mM	0.3 g
1x PBS		up to 1 l
autoclave		
4C lysis buffer		10 ml
TRIS pH 7.5	50 mM	500 µl of 1 M
NaCl	150 mM	300 µl of 5 M
EDTA	5 mM	1300 µl of 0.5 M
NP-40	0.5%	500 µl of 10%
Triton X-100	1%	100 µl
H ₂ O		8.5 ml

4C ligation buffer	10x	10 ml
TRIS pH 7.5	660 mM	6.6 ml of 1 M
DTT	50 mM	500 µl of 1 M
MgCl ₂	50 mM	500 µl of 1 M
ATP	10 mM	500 µl of 0.2 M
H ₂ O		1.9 ml
TE	1x	0.1 l
TRIS pH 8.0	10 mM	1 ml of 1 M
EDTA pH 8.0	1 mM	1 ml of 0.1 M
H ₂ O		98 ml
Na-deoxycholate (DOC)	5%	0.1 l
Na-deoxycholate (DOC)	5% (w/v)	5 g
H ₂ O		0.1 l
Glycine	2.5 M	0.1 l
Glycine		18.76 g
H ₂ O		0.1 l
RIPA buffer	1x	0.1 l
Tris-HCl pH 8.0	10 mM	1 ml of 1 M
EDTA, pH 8.0	1 mM	1 ml of 100 mM
NaCl	140 mM	2.8 ml of 5 M
Triton x-100	1%	10 ml of 10%
SDS	0.1%	0.5 ml of 20%
DOC	0.1%	2 ml of 5%
H ₂ O		82.7 ml
Binding/ blocking buffer	1x	0.1 l
BSA	0.5%	0.5 g
Tween-20	0.5%	0.5 ml
1x PBS		99.5 ml
RIPA I buffer	1x	0.1 l
Tris-HCl pH 8.0	10 mM	1 ml of 1 M
EDTA, pH 8.0	1 mM	1 ml of 100 mM
NaCl	140 mM	2.8 ml of 5 M
SDS	0.2%	1 ml of 20%
DOC	0.1%	2 ml of 5%
H ₂ O		92.2 ml

RIPA-500 buffer	1x	0.1 l
Tris-HCl pH 8.0	10 mM	1 ml of 1 M
EDTA, pH 8.0	1 mM	1 ml of 100 mM
5 M NaCl	500 mM	10 ml
Triton x-100	1%	10 ml of 10%
SDS	0.1%	500 µl of 20%
5% DOC	0.1%	2 ml of 5%
H ₂ O		
LiCl wash-buffer (ChIP-seq)	1x	0.1 l
Tris-HCl pH 8.0	10 mM	1 ml of 1 M
EDTA, pH 8.0	1 mM	1 ml of 100 mM
5 M LiCl	250 mM	5 ml
Triton x-100	1%	10 ml of 10%
NP-40	0.5%	5 ml of 10%
5% DOC	0.5%	10 ml of 5%
H ₂ O		
Direct elution buffer	1x	0.1 l
Tris-HCl pH 8.0	10 mM	1 ml of 1 M
EDTA, pH 8.0	5 mM	5 ml of 100 mM
5 M NaCl	300 mM	5.5 ml
20% SDS	0.5%	2.5 ml of 20%
H ₂ O		
HiChIP lysis buffer	1x	10 ml
Tris-HCl pH 8.0	10 mM	100 µl of 1 M
NaCl	10 mM	20 µl of 5 M
Nuclear lysis buffer	1x	10 ml
Tris-HCl pH 7.5	50 mM	500 µl of 1 M
EDTA, pH 8.0	10 mM	200 µl of 500 mM
SDS	1%	1 ml of 20%
Protease Inhibitor (50x, 1 ml)	1x	200 µl
H ₂ O		8.3 ml
ChIP dilution buffer	1x	10 ml
Tris-HCl pH 7.5	16.7 mM	167 µl of 1 M
EDTA	1.2 mM	24 µl of 500 mM
5 M NaCl	167 mM	334 µl of 5 M
Triton x-100	1.1%	1.1 ml of 10%
SDS	0.01%	5 µl of 20%
H ₂ O		8.37 ml

Low salt wash buffer	1x	10 ml
Tris-HCl pH 7.5	20 mM	200 µl of 1 M
EDTA	2 mM	40 µl of 500 mM
NaCl	150 mM	300 µl of 5 M
Triton x-100	1%	1 ml of 10%
SDS	0.1%	50 µl of 20%
H ₂ O		8.86 ml

High salt wash buffer	1x	10 ml
Tris-HCl pH 7.5	20 mM	200 µl of 1 M
EDTA	2 mM	40 µl of 500 mM
NaCl	500 mM	1 ml of 5 M
Triton x-100	1%	1 ml of 10%
SDS	0.1%	50 µl of 20%
H ₂ O		8.16 ml

LiCl wash-buffer (HiChIP)	1x	10 ml
Tris-HCl pH 7.5	10 mM	100 ml of 1 M
EDTA	1 mM	20 µl of 500 mM
LiCl	250 mM	500 µl of 5 M
NP-40	1%	1 ml of 10%
DOC	1%	2 ml of 5%
H ₂ O		6.38 ml

STE buffer	1x	1 l
NaCl	100 mM	100 ml of 1 M
EDTA	1 mM	1 ml of 1 M
Tris-HCl pH 8	10 mM	10 ml of 1 M
H ₂ O		889 ml

2.1.11 Software

Software	Company/Source
FLUOstar Optima	BMG Labtech, Ortenberg
IGV 2.3	Broad Institute of MIT and Harvard
IGV viewer	Broad Institute, Cambridge, USA
ImageJ version 1.47	Wayne Rasband
Inkscape 0.91	
Microsoft Office package 2010	Microsoft Corp., Redmond, USA
R2	https://hgserver1.amc.nl

2.2 Methods

2.2.1 General molecular biological methods

Agarose gel electrophoresis

The gel electrophoretic separation of DNA was conducted in 1-4% agarose in 1x TBE buffer. Agarose was heated up in 1xTBE buffer until it was completely dissolved. The DNA samples were loaded onto the gel in the ratio of 5:1 with 6x loading dye containing 2% GelRed. The electrophoretic separation was performed in 1x TBE buffer at 20 - 90 V.

2.2.2 General cell culture methods

Culturing of NB cells

NB cell lines were cultured in either RPMI1640 or DMEM supplemented with 1% penicillin/streptomycin and 10% FCS. Cells were incubated at 37°C, 5% CO₂ and standard cell culturing procedures were used. Cell culture medium was replaced with pre-warmed medium every 2 - 4 days. Cells were split at ratios from 1/3 to 1/12 depended on confluency and cell line. Therefore, cells were gently detached by incubation in 1 - 5 ml versene chelating agent for 1 - 5 min. Cell morphology was observed at least every second day by light microscopy (Zeiss Axiovert microscope). Cell count was performed using the Luna automated cell count (Logos Biosystems) according to the manufacturer's protocol.

Thawing of NB cells

In liquid nitrogen or -80°C freezer preserved cells were thawed at 37°C for approximately 1 min. Subsequently, cells were resuspended with 10 ml pre-warmed cell culture media. Thereafter, cells were centrifuged at 800 rpm for 5 min and supernatant was removed. Finally, the cell pellet was resuspended and transferred into a cell culture flask (25 cm) containing pre-warmed cell culture media, which was replaced after 24 h.

Cryo-preservation of NB cells

For cryo-preservation, special freezing medium containing 70% RPMI1640 or DMEM, 10% sterile filtered DMSO and 20% FCS was prepared and stored on ice. Medium of cells in preparation for cryo-preservation was changed the previous day and cells did not exceed confluency higher than 80%. Approximately $2 \cdot 10^8$ cells were harvested, centrifuged at 800 rpm for 5 min and the supernatant was removed. The cell pellet was resuspended with

approximately 1 ml freezing medium, split into cryo tubes and cells were cooled down using a freezing container.

2.2.3 ATRA (all-trans retinoic acid) treatment

The NB cell line SK-N-BE(2)-C served as a well-established *in vitro* model for neuronal differentiation (Dreidax et al. 2014). All-trans retinoic acid (ATRA) is an established element of high-risk NB therapy (Matthay et al. 1999). ATRA induces neuronal differentiation in some but not all high-risk NBs. Cells were cultured in media containing 10 μ m ATRA (Sigma) (+ATRA) or ethanol solvent control (+EtOH). Cells were harvested at the indicated time points for subsequent ChIP-seq (24 h and 144 h after ATRA treatment) or as replicates for RNA-seq (0 h, 1 h, 3 h, 6 h, 12 h, 24 h, 48 h, 96 h and 144 h after ATRA treatment) analysis.

2.2.4 Quantification of proteins - SDS-PAGE/Western blot

Total protein extraction and purification of

For preparation and quantification of total protein cell culture samples, cells were detached by versene, washed with cold PBS and pelleted. Cell pellets are resuspended in 20 – 60 μ l (depending on the pellet size) MPER lysis buffer and can be stored at -80°C or directly used for total protein extraction and purification. For digestion of high molecular weight DNA or RNA, lysed samples were treated with 1 μ l benzonase (endonuclease) and incubated for 15 – 30 min at 37°C. To remove insoluble membranes the samples were centrifuged at 13000 for 1 min and the protein containing supernatants were used for protein quantification and further analysis.

Protein quantification (Bradford 1976)

First, 800 μ l autoclaved H₂O were mixed with 200 μ l Bradford reagent in a cuvette. Then 1 μ l of the protein sample was added to each cuvette and mixed thoroughly while a Bradford/H₂O mixture served as a blank. The absorption at 595 nm was measured with a photometer and the total protein concentration was determined due to a corresponding serial protein dilution with known concentrations. The absorption switch from 470 nm to 595 nm is caused by the stabilization of the anionic dye bound to cationic protein side chains, which built a colored protein complex.

Protein sample preparation

For protein denaturation, 50 µg of each sample was mixed up to 15 µl with 1x Laemmli buffer including β-mercaptoethanol to generate reducing conditions. The sample mix was incubated at 95°C for 2 min, shortly centrifuged and loaded onto a polyacrylamide gel.

SDS-PAGE

The SDS-polyacrylamide gel electrophoresis enables the separation of proteins under denaturing conditions in the presence of SDS according to their electrophoretic mobility. This depends on the percentage of the polyacrylamide in the separating gel matrix (12.5%) as well as shape and size of the denatured proteins.

SDS-PAGE was performed in Tris-glycine buffered system (Laemmli) using a stacking and subjacent separation gel while all ions are moving towards the anode during gel electrophoresis. Due to the pH-value of 6.8 in the stacking gel buffer, glycine exists as a dipolar ion and Cl⁻ is negatively charged. All denatured proteins are moving in between these two ions, were accelerated and concentrated due to lack of charge carrier. Additionally, the proteins are stacked while reaching the border to the separating gel, holding a higher percentage of polyacrylamide. Secondary, the pH-value shift of 6.8 to 8.8 in the separating gel buffer leads to a negatively charged glycine ion and a removal of the lack of charge carrier. Thereby, the denatured proteins are separated due to their electrophoretic mobility.

First, for the separating gel (12.5%), 4.7 ml of 40% polyacrylamide solution, 6.4 ml H₂O, 75 µl 20% SDS solution and 3.75 ml separating gel buffer were mixed.

Thereafter, 6 µl TEMED served as catalyst of the polymerization reaction and 150 µl 10% APS solution for initiation. The casted separating gels were overlaid with H₂O saturated isobutyl alcohol for approximately 2 h until the polymerization process was completed.

After polymerization of the separating gel, the isopropyl alcohol was removed, components for the stacking gel were mixed (0.375 ml 40% polyacrylamide solution, 1.2 ml stacking gel buffer, 2.75 ml H₂O, 25 µl 20% SDS solution, 6 µl TEMED and 150 µl 10% APS solution) and poured above the separating gel.

For electrophoresis, two gels were assembled into the chamber. The inner chamber between the two assembled gels and the outer tank were filled with 1x Amresco buffer.

The combs were removed and the cavities were thoroughly rinsed with a syringe. For each sample 15 µl containing 50 µg protein sample in Laemmli buffer were loaded onto the gel. As a marker for determination of the protein size, 10 µl of BenchMark prestained protein ladder or 5 µl of PageRuler prestained protein ladder were used. The separation of the proteins was carried

out at 80 V until the samples entered the stacking gel and subsequently increased up to 110 V for approximately 2 h.

Protein transfer – Western blot

After separation of proteins via SDS-PAGE, they were electro transferred onto a 0.45 µm nitrocellulose membrane using the tank blotting method. The assembly for the electro blotting was conducted and every component was soaked in transfer buffer. The final assembly was rolled with a bar to remove residual air blowing. Afterwards, the electro transfer was performed twice for 45 min at 125 V / 440 mA at 4°C.

After successful protein blotting, the nitrocellulose membrane was washed with 1x TBS and incubated in complex blocking solution or alternatively in a 1:10 dilution of ECL plus blocking solution at 4°C overnight. Blocking of binding sites with unspecific proteins is important to decrease unspecific signals during immunodetection. Afterwards, the membrane was washed three times with approximately 5 ml TBS.

Immunodetection

For immunodetection of proteins, a primary antibody was added in a concentration of 1-10 µg/ml to 5 ml of 5% nonfat-milk in H₂O (2.1.7). The common dilution of primary antibody to nonfat milk solution was between 1:300 - 1:5000 except of beta-actin with a ratio of 1:10000, which served as a loading control. Incubation was performed at 4°C overnight, anti-β-actin had an incubation time of 45 - 60 min at RT. After incubation, the membrane was washed three times with approximately 5 ml 1x TBS and incubated with the appropriate secondary antibody conjugated with HRP in 5% nonfat milk solution for 2 h at 4°C. Subsequently, the membrane was washed three times with 1x TBS and the chemiluminescence reaction was started by adding BM Chemiluminescence or ECL plus reagent with extended stability according to the manufacturer's protocol. The added solution served the secondary antibody conjugated horseradish peroxidase as substrate to catalyze the chemiluminescence reaction after 1 - 5 min of incubation. The signal was detected using Chemi-Capt 5000 (Vilber).

Protein quantification

Quantification of protein level was performed using ImageJ version 1.47. The image of the chemiluminescence reaction was inverted using ImageJ and bands were encircled fitting all bands that have to be analyzed. The mean value of the analyze/measure function was used for all bands and the background, which was subtracted. Protein samples after knockdown by RNA interference were divided by the value of the loading control (actin or tubulin). Finally, the

normalized value of the protein samples after knockdown (RNA-interference; RNAi) were divided the normalized value of the negative control to achieve the reduced protein level.

2.2.5 CTB (CellTiter Blue) viability assay

CTB viability assay (Promega, Mannheim, Germany) measures the metabolic activity and was performed to evaluate the effect of RNAi-induced gene silencing experiments or drug treatments on NB cells viability.

The NB cell lines SH-EP (1500 cell/well), GI-ME-N (2000 cells/well) and NMB (3500 cells/well) were seeded in 96well plates in 100 µl medium and RNAi experiments were performed after 24 h as described below (2.2.7). 72 h or 96 h after siRNA mediated knockdown, 10 µl of CTB reagent was added to the cells in 100 µl medium (ratio 1:10) and incubated for 5 h under cell culture conditions. Fluorescence was detected using a flouro-scan plate reader with the setting 540 nm excitation and 580 nm emission filters. Empty medium with CTB reagent served as a blank for normalization of the fluorescence of the samples. The relative cell viability was evaluated by setting the highest fluorescence value to 1, representing viable and metabolically active cells.

2.2.6 Colony formation assay using GIEMSA staining

Colony formation assay was performed to evaluate the effect of RNAi-induced gene silencing experiments or drug treatments on NB cells colony formation capacity.

The NB cell lines SH-EP (1500 cell/well), GI-ME-N (2000 cells/well) and NMB (3500 cells/well) were seeded in 96well plates in 100 µl medium and RNAi experiments were performed after 24 h as described below (2.2.7). 72 h or 96 h after siRNA mediated knockdown, cells were fixed (11% glutaraldehyde) and incubated for 30 min. After removing the fixation solution, the cells were washed twice with 100 µl PBS. Subsequently, the cells were stained using 100 µl of a 10% Giemsa Azure Eosin Methylen Blue solution in 1x PBS and incubated overnight. The stained cells were washed twice with 100 µl PBS, once with 100 µl water and dried afterwards. For evaluation of the cells colony formation capability, the wells were scanned and analyzed by the ImageJ software version 1.47 and ColonyArea plugin.

2.2.7 RNA interference using siRNA

For detection of the candidate gene impact on cell viability or gene expression, RNAi-induced gene silencing experiments were performed using siRNAs.

NB cells were seeded 24 h before the transfection in 96-well plates or in 10/25 cm dishes to achieve 50% confluency at transfection. First, Lipofectamine RNAiMAX reagent was diluted 1:100 – 1:25 (cell line depended), in Opti-MEM medium (serum- and antibiotic-free). SiRNAs (50 μ M stock solution) were diluted in Opti-MEM medium in a ratio of 1:250. Subsequently, both solutions were mixed in equal amounts and incubated for 15 min at room temperature. Depending on the cell culture vessel (96-well plates up to 10/25 cm dishes), the siRNA-lipid complex were added to the cells (10 μ l/96-well wells and 1 ml/10 cm dish) and incubated for the desired time (24 h - 72 h).

2.2.8 Fluorescence *in situ* hybridisation (FISH)

FISH experiments and analysis were performed by Olga Sepman and Larissa Savelyeva. The preparation was performed according to the published protocol (Brueckner et al. 2013) for NB cell lines CLB-GA, GI-ME-N, KELLY, NBL-S, NB69, SH-SY5Y, CHLA15/20 and SK-N-AS. Labeled BAC clones were selected by Olga Sepman with the exception of TERT and IGF2BP2 (Larissa Savelyeva).

2.2.9 Multicolour fluorescence *in situ* hybridisation (mFISH)

mFISH experiments and analysis were performed by Olga Sepman and Larissa Savelyeva. To generate mFISH karyotypes of cell lines CLB-GA, GI-ME-N, KELLY, NBL-S, NB69, SH-SY5Y, CHLA15/20 and SK-N-AS the 24xCyte multicolour FISH probe mix (MetaSystems, Altlusheim, Germany) was used according to the manufacturer's protocol (Brueckner et al. 2013).

2.2.10 RNA isolation, purification and RNA sequencing (RNA-seq)

RNA isolation

For RNA isolation, approximately $3 \cdot 10^6$ cells were used. Therefore, the culture media was discarded and cells were detached by incubation with 3 ml versene for 1 - 5 min. The cells were pelleted by centrifugation at 800 rpm and the supernatant was removed. The cell pellet was

resuspended in 1 ml Trizol reagent and thoroughly mixed. Subsequently, the isolate was directly stored at -80°C to avoid RNA degradation. Afterwards, total RNA was isolated using the miRNeasy Mini Kit (Qiagen) according to the manufacturer's protocol.

RNA isolation of primary tumors

For RNA isolation of primary tumors, the NucleoSpin Kit for RNA (Macherey-Nagel) isolation was used and tumor slices were prepared according to the manufacturers' protocol.

RNA sequencing

RNA was depleted from ribosomal RNAs using the Ribo-Zero rRNA Removal Kit (Illumina) according to the manufacturer's protocol. RNA libraries were prepared using the NEBNext Ultra Directional RNA Library Prep Kit for Illumina (New England Bio Labs) according to the manufacturer's protocol with the following changes: RNA was fragmented for 20 min at 94°C followed by first strand cDNA synthesis for 10 min at 25°C, 50 min at 42°C and 15 min at 70°C. Size selection of adapter-ligated DNA was done with a bead:DNA ratio of 2/5 (AMPure XP beads, Beckman Coulter) removing index primer and short fragments. Quality, quantity and sizing (approximately 320 bp) of the RNA library were analyzed using a DNA High Sensitivity DNA chip run on a 2100 Bioanalyzer (Agilent Technologies). Libraries were sequenced (50 bases single-end) on the Illumina sequencing platform (German Cancer Research Center Core facility).

Data analysis of RNA-seq samples was performed by Naveed Ishaque.

2.2.11 Chromatin immunoprecipitation sequencing (ChIP-seq)

The tumor ChIP-seq protocol was established by modifying the previously published protocol by Blecher-Gonen and colleagues (Blecher-Gonen et al. 2013). A detailed step-to-step description of the ChIP-seq protocol is given in the appendix (5.1).

Data analysis of ChIP-seq as follows was performed by Carl Herrmann and is described briefly. Single end reads were aligned to the hg19 genome using Bowtie2 (version 2.1.0). Only uniquely aligned reads were kept. BAM-Files of aligned reads were further processed using the deepTools suite (Ramirez et al. 2014). Input files were subtracted from the treatment files using the bamCompare tool, applying the SES method for normalization of signal to noise. Resulting signals were normalized to an average 1X coverage to produce signal (bigWig) files. Peaks were called using the MACS 1.4 tool using default parameters.

2.2.12 Tumor ChIP-seq

The tumor ChIP-seq protocol was established by modifying and combining two previously published ChIP protocols from Dahl as well as Blecher-Gonen and colleagues (Dahl and Collas 2008; Blecher-Gonen et al. 2013). A detailed step-by-step description of the tumor ChIP-seq protocol is given in the appendix (5.2).

The tumor ChIP-seq protocol is based on a distinct tissue disruption step, which is essential for high performance and reproducibility of experiments. For disruption, a standard microtome-cryostat is used to cut a number of slices (dependent on the volume of the biopsy) of defined thickness from frozen biopsies. Roughly six milligrams of these slices are sufficient for six ChIP reactions of histone marks or two ChIP reactions of transcription factors, respectively. The slices are transferred to standard reaction tubes in which they can be stored or directly processed. SDS-based lysis of the tissue is supported by dounce homogenization with a micro-pestle and brief sonification in the reaction tube. Chromatin shearing via sonification is performed under standard ChIP-seq conditions. After sonification, the tissue ChIP-seq protocol follows a slightly modified version of a previously published high-throughput ChIP-seq protocol (Blecher-Gonen et al. 2013) with all the downstream convenience and high-throughput compatibility.

Data analysis of tumor ChIP-seq was performed by Carl Herrmann according to ChIP-seq processing described in 2.2.11.

2.2.13 ChIPmentation

The ChIPmentation protocol, which describes the tagmentation of immunoprecipitated chromatin, was established by modifying and combining two previously published protocols (Schmidl et al, 2016 (Schmidl et al. 2015), Blecher-Gonen *et al.*, 2013 (Blecher-Gonen et al. 2013)). A detailed step-to-step description of the tumor ChIPmentation protocol is given in the appendix (5.3).

Data analysis of ChIPmentation data was performed by Carl Herrmann according to ChIP-seq processing described in 2.2.11.

2.2.14 4C sequencing (4C-seq)

For a better understanding of long range *cis*- and *trans* gene regulation via interaction of regulatory DNA elements with promoters, we applied a technique called “circularized

chromosome conformation capture with high-throughput sequencing” (4C-seq) (van de Werken et al. 2012). 4C allows the examination of the regulatory environment of a certain locus of choice (viewpoint) with each individual regulatory element genome wide as a high resolution interaction profile. This technique starts with the formaldehyde fixation of the genome conformation and thereby the three-dimensional proximity of regulatory elements. This is followed by two subsequent processes of restriction enzyme digestion and fragment ligation. A PCR amplification step using primers of the viewpoint of interest is followed by sequencing of the product. A detailed step-by-step description of the 4C-seq protocol is given in the appendix (5.4).

Data analysis of 4C-seq samples was performed by Carl Herrmann and Paul Saary and is described briefly. Unpaired 4C reads were demultiplexed allowing zero miss-matching between barcodes and aligned to the hg19 ref-genome with bwa-mem v. 0.7.17. Aligned reads were then matched and filtered to match expected restriction fragments using FourCseq using default parameters (Klein et al. 2015). Far *cis*- and *trans*-interactions were detected as suggested by Splinter et al. (Splinter et al. 2012). *Trans*-interactions with more than 50 supporting reads were subsequently visualized using circlize (Gu et al. 2014). 4Cker was used to detect close bait, *cis* and/or *trans*-interactions (Raviram et al. 2016). Domainograms for whole chromosomes were created according to Splinter et al. and for regions of interest were computed according to the method published by http://compgenomics.weizmann.ac.il/tanay/?page_id=367. Using adaptive windows domainograms for regions of interest in close and far *cis*-interactions were computed, by comparing the signal to a localized background.

2.2.15 HiChIP sequencing

To obtain information of genome wide chromatin conformation in NB cells, we performed HiChIP with subsequent sequencing in two NB cell lines (SK-N-AS and KELLY). The HiChIP method was performed according to the previously published protocol by Mumbach and colleagues (Mumbach et al. 2016) with slight modifications as described briefly.

1x10⁶ cells were detached, pelleted and subsequently resuspended in 1 ml of 1% FA for 10 min crosslinking. Decrosslinking, lysis and restriction using MboI restriction enzyme, was performed according to the published protocol. Incorporation of biotin-ATP was achieved using 15 µl 1 mM Biotin-14-dATP (NU-835-BIO14-S, Jena Bioscience) to the master mix instead of 37.5 µl of 0.4 mM biotin-dATP (819524016, Thermo). Proximity ligation was performed according to the protocol with the only variation of ligation incubation over night at 16°C.

Sonication of the material was accomplished using the Covaris LE220 and 1 ml tubes instead of Covaris E220 as described in the protocol. The change of sonication device altered the sonication parameters as follows:

Duty Cycle	15%
PIP	350 W
Cycles/Burst	200
Time	4 min

The subsequent IP reaction was performed using SMC1A (Bethyl A300-055A9) and H3K27ac (ab4729) antibodies. After ChIP DNA elution in 27 μ l water, the obtained post ChIP DNA amount reached from 30ng for SMC1A to more than 150ng for H3K27ac HiChIP samples. During the biotin-capture step the Streptavidin C-1 beads were incubated at RT for 30 min instead of 15 min. For the PCR reaction, Illumina Nextera i5/i7 primer (Illumina Nextera Index Kit 24 Indexes – 96 samples - Illumina 15055289) and Nextera PCR master mix (Illumina Nextera DNA Library Prep Kit 24 samples – Illumina 15028212) were used and reaction was performed for 8 cycles in total. Ampure XP beads (AMPure XP beads, Beckman Coulter) were used for a size selection to obtain fragments greater than 300 and smaller than 700 bps of the amplified libraries. For final quantification and fragment size distribution of libraries, a Bioanalyzer assay was performed. The libraries were sequenced paired-end and one per lane with 100 bps read length adding 10% PhiX to increase sequence complexity.

Data analysis of HiChIP-seq samples was performed by Carl Herrmann and Paul Saary and is described briefly. HiChIP reads were aligned using HiC-pro with the default configuration (Servant et al. 2015). Valid pairs were analyzed using step 4 and 5 of a slightly modified Mango version (Phanstiel et al. 2015). A FDR of 0.05 was applied to all samples.

2.2.16 ATAC sequencing (ATAC-seq)

For genome-wide mapping of chromatin accessibility and to perform transcription factor footprinting analysis we conducted Assay for Transposase-Accessible Chromatin with high-throughput sequencing (ATAC-seq) using the protocols published by Buenrostro and colleagues (Buenrostro et al. 2013; Buenrostro et al. 2015) with the following changes. In total 50.000 cells were used for lysis and transposase reaction. After purification Nextera PCR primer (2.1.9) were used in a 11 cycle amplification PCR. ATAC-seq library was finally cleaned up and the

concentration and fragment distribution were tested. The libraries were pooled, 15% PhiX was added to increase sequence complexity and finally sequenced using a HiSeq 2000 V4 platform with 50 bp single read.

Data analysis of ATAC-seq samples was performed by Carl Herrmann and is described briefly. Differential ATAC-seq analysis between SK-N-AS and Kelly cell lines was done based on the footprints of a collection of transcription factor binding motifs containing in particular motifs for all TFs identified in the CRC analysis. Footprinting was done using the PIQ method (Sherwood et al. 2014). For each motif, we filtered the motif occurrences for which the purity score was larger than 0.7 in at least one of the two cell lines and computed a paired t-test on this set of filtered motifs. Hence, we obtained a value of the t-statistics for each motif, indicating a tendency of these motifs to be more accessible in one or the other of the two cell lines.

2.2.17 DNA preparation and whole genome sequencing (WGS)

DNA isolation cell lines

Cells were seeded into 15 cm cell culture plates until they reached a density up to 80%. Subsequently, cells were incubated in an appropriate volume of versene for detachment and were transferred into a 15 ml tube. Afterwards the cells were centrifuged at 800 rpm for 5 min and the supernatant was removed. For the following DNA isolation, the High Pure PCR Template Preparation Kit (Roche) was used according to manufacturer's protocol.

DNA isolation primary tumors

Tumors were sliced in small fractions while cooled with dry-ice. Subsequently, tumor fractions were diluted in STE buffer and 100 - 200 µl proteinase K (20 mg/ml) and 50 µl SDS (20% solution) were added to the resuspended cell pellet and mixed. For protein digestion, the mixture was incubated at 65°C for at least 2 h. The cell suspension was mixed occasionally and proteinase K concentration was increased if necessary.

DNA purification

By the time, the suspension was no longer highly viscous, the DNA was purified using a phenol/chloroform mixture (Kirby 1956). The removal of the proteins was carried out by adding an equal volume of phenol/chloroform/isoamylalcohol (25:24:1) with a pH-value of 7.8 - 8. All further steps were performed on ice. The two phases were mixed rapidly inverting the tube followed by a centrifuge step at 3000 rpm for 10 min at 4°C. The aqueous phase containing nucleic acids was carefully transferred into a new tube. Thereby, phenol denatured proteins

were collected at the interphase, lipids in the organic and the DNA in the aqueous phase. This process was repeated and finally the aqueous phase was mixed with chloroform and centrifuged again at 3000 rpm for 10 min at 4°C to remove any residual phenol. Finally, the DNA-containing aqueous phase was transferred into a fresh tube.

DNA precipitation

DNA was precipitated by adding 3 ml of 3 M sodium acetate and 30 ml of ice cold 100% ethanol. Directly afterwards, the tube was carefully inverted until the precipitated DNA became visible. The DNA was coiled on a little rod and washed in ice cold 70% ethanol. Subsequently, the DNA was dried until all residual ethanol was evaporated and resuspended in 200 - 500 µl H₂O. For complete solubility, the tube was incubated at 42°C for 20 min using a shaking device. The concentration was determined using a Nanodrop ND-1000.

DNA quantification (tumors and cell lines)

For DNA quantification, the Qubit Fluorometer was used according to the manufacturer's protocol. The fluorometer detects highly specific dyes of dsDNA broad range and high sensitivity assay kit fluorescence when bound to dsDNA. First, the working solution was prepared and mixed in the ratio 1:20 with two provided standards and 1:200 with each sample to a final volume of 200 µl. After incubation for 2 min, calibration was performed by measuring the two standards.

Fragmentation

The Covaris S series was used for sample preparation and shearing of the genomic DNA to a size of 160 - 200 bp. The Covaris S series uses the AFA-technology (Adaptive Focused Acoustics) for fragmentation. Therefore, 5 µg of genomic sample DNA were transferred into a Covaris micro tube and filled up to 120 µl with H₂O. The micro tube was load in the Covaris tube holder and DNA was sheared 3 times with 200 cycles per burst at 4°C for 120 sec.

Purification

The sheared DNA was purified using the Agencourt AMPure XP and a magnetic device. The DNA was eluted after purification in 30 µl H₂O and transferred into a fresh tube.

DNA library preparation and WGS

For using the "Next Generation Sequencing" platform and especially the Illumina paired-end sequencing assay, the sample genomic DNA had to be prepared. All subsequent reactions were performed according to the NEBNext Ultra DNA Library Prep Kit for Illumina (NEB) manufacturer's protocol.

3. Results

3.1 Global enhancer hijacking landscape in NB

The principle of alternative oncogene activation by locating enhancers in the proximity of oncogenes was described for different cancer entities and is referred to as “enhancer hijacking” (Taub et al. 1982; Bakhshi et al. 1987; Groschel et al. 2014; Northcott et al. 2014). Shedding light on the global landscape of enhancer and hijacking events for the first time in NB, was a central task of this work. As depicted in Figure 9 enhancer hijacking describes a rearrangement of a gene or oncogene joined with other chromosome segments harboring strong regulatory elements like super-enhancer (SE).

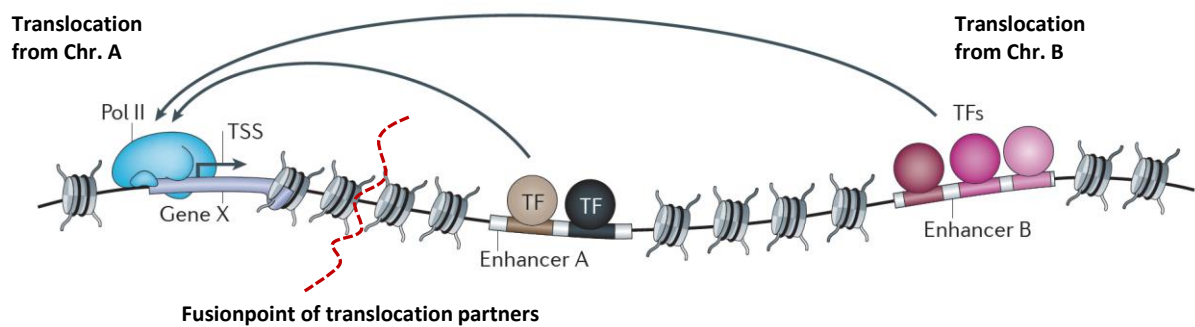


Figure 9: The mechanism of enhancer hijacking.

Structural rearrangements lead to juxtaposition of gene X locus to strong enhancer elements (A and B) that up regulates the transcription of gene X. Adapted from (Shlyueva et al. 2014) – licence obtained.

3.1.1 Telomerase activation by genomic rearrangements in high-risk NB

In a study performed together with colleagues from the university children’s hospital cologne, whole genome sequencing (WGS) of 56 NB primary tumors and matched normal controls (17 low-risk and 39 high-risk patients) was performed (Peifer et al. 2015). All bioinformatics work of this study was performed by Martin Pfeifer. The WGS data confirmed a low overall mutation rate (13.3 mutations/genome) and four recurrent genomic alterations in total (Wang et al. 2011; Molenaar et al. 2012). Three of these alterations are established alterations in NB including amplified *MYCN*, *ATRX* deletion and gain of chromosome 17 (Figure 10) (Schwab et al. 1983; Savelyeva et al. 1994). A novel recurrent genomic aberration located at chromosome 5p15.33 was found in 12 of 56 NB primary tumors (21%). All the 12 cases were high-risk tumors with

rearrangements that clustered upstream of the *TERT* gene without affecting the promoter. No *TERT* gene or promoter mutations were detected and structural aberrations were intra- (n = 7) as well as inter- (n = 5) chromosomal and included balanced translocations with single-copy gains or amplifications. In 56 primary tumors, *ATRX* mutations (n = 7), amplified *MYCN* (n=10) or *TERT* rearrangements (n = 12) were observed in a mutually exclusive fashion.

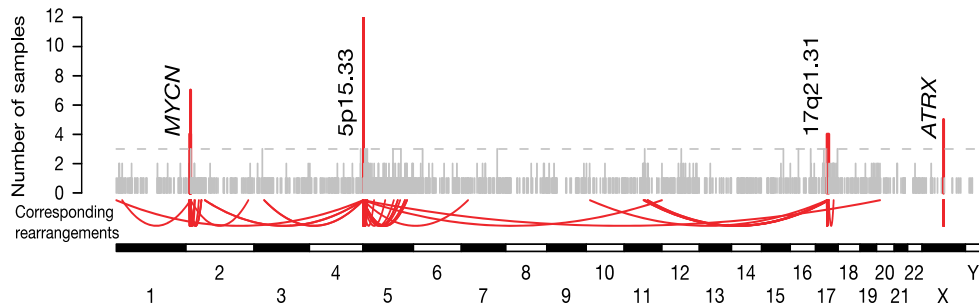


Figure 10: WGS revealed recurrent genomic rearrangements in NB.

WGS of 56 NB primary tumors revealed recurrent genomic rearrangements like amplified MYCN, ATRX deletion, gain of chromosome 17 and TERT rearrangement in high risk patients (recurrence in more than three tumors is marked red). Adapted from (Peifer et al. 2015).

Screening for *TERT* genomic aberrations by fluorescent *in situ* hybridization (FISH) and locus-specific targeted sequencing in an extended cohort of 217 primary NB tumors revealed a total of 28 *TERT* rearrangements (13%; Figure 11A). Almost all *TERT*-rearranged cases were classified as high-risk with the exception of one intermediate-risk sample.

TERT rearrangement was associated with poor survival of NB patients

TERT rearrangements were associated with poor prognosis and poor clinical outcome, which was comparable with patients harboring amplified *MYCN* or remaining high-risk cases (Figure 11B and 11C). The Kaplan-Meier survival probability diagram indicated overall survival (OS) probability of P = 0.056 and event-free survival (EFS) probability of P = 0.038.

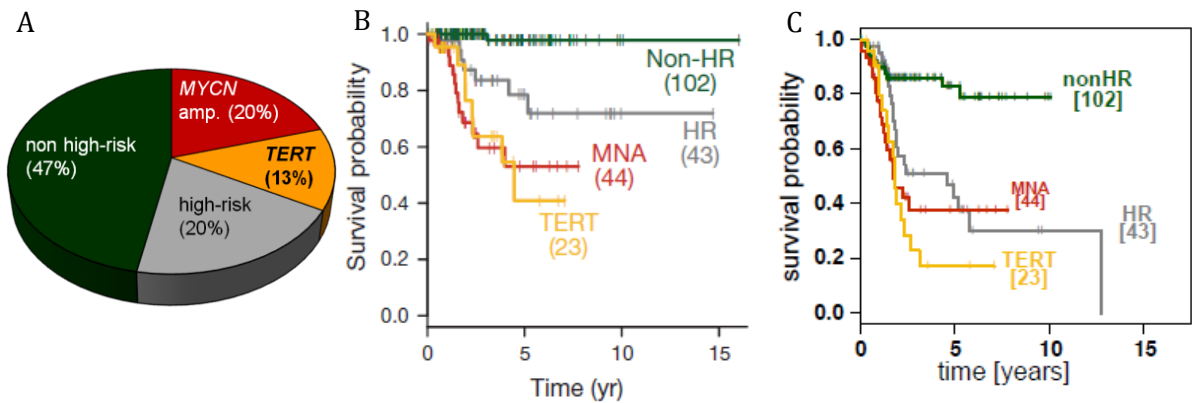


Figure 11: *TERT* rearrangement is associated with poor survival in NB.

(A) Cohort description of 217 primary NB tumors. *TERT* rearrangements were discovered by WGS or FISH and targeted sequencing. (B) Kaplan-Meier event-free survival diagram (EFS). (C) Kaplan-Meier overall survival probability diagram (OS). All figures are adapted from (Peifer et al. 2015).

mRNA expression of TERT in NB tumors and cell lines

TERT expression level of NB tumors harboring *TERT* rearrangements (*TERT*) were compared with *MYCN*-amplified (*MYCN*) as well as remaining high- (HR) and low-risk (LR) NB primary tumors (Figure 12A). The highest *TERT* expression was observed in *TERT*-rearranged cases, with a median expression of 12.3 and significantly higher than that of *MYCN*-amplified tumors ($P = 0.028$). High-risk tumors without amplified *MYCN* or *TERT* rearrangement expressed significantly lower *TERT* levels than *MYCN*-amplified tumors ($P = 0.021$) but higher *TERT* levels as compared to low-risk tumors. As a next step, the *TERT* expression level in the RNA-sequencing (RNA-seq) dataset of 32 NB cell lines, 18 *MYCN*-amplified and 14 *MYCN* non-amplified (MNA), was evaluated (Figure 12B). The highest *TERT* expression was detected in *MYCN*-amplified NGP cells (FPKM of 10.7). This was followed by two MNA cell lines CLB-GA (FPKM of 3.9), GI-ME-N (FPKM of 3.2) and finally by the *MYCN*-amplified cell line KELLY (FPKM of 2.6). The lowest *TERT* expression level in the NB cell line cohort was detected for MNA cell line SK-N-FI with almost no detectable *TERT* mRNA (FPKM of 0.01).

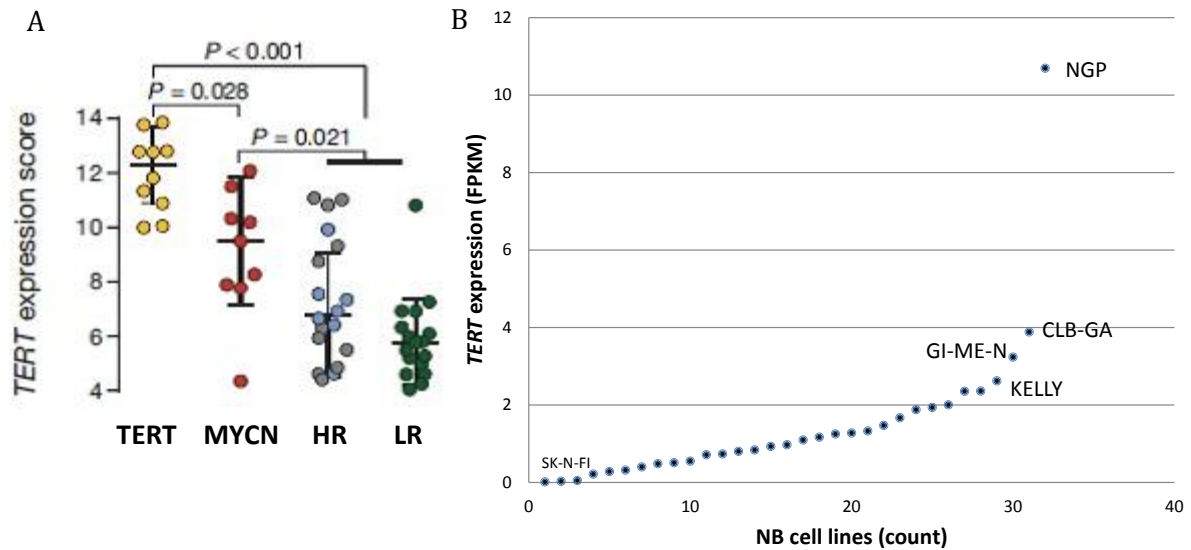


Figure 12: *TERT* mRNA expression in NB.

(A) *TERT* mRNA expression in tumors with *TERT* rearrangement ($n=10$, yellow), amplified *MYCN* ($n = 9$, red) in high-risk tumors without *TERT* rearrangement or amplified *MYCN* ($n = 18$, grey); tumors with additional *ATRX* mutations are shown in blue ($n = 7$) and in low-risk tumors ($n = 17$, green). Adapted from (Peifer et al. 2015). (B) *TERT* mRNA expression in NB cell lines ($n = 32$).

FISH identified structural aberrations involving *TERT*

A technique to detect DNA sequences of genomic locations on chromosomes (2.2.9), fluorescence *in situ* hybridization (FISH), was performed with *TERT* locus-specific probes to identify structural aberrations in NB cell lines (Figure 13). Chromosomal rearrangement partners joining chromosome 5 including the *TERT* locus (green) were evaluated.

In MNA cell line CLB-GA two chromosome 5 derivatives were detected carrying the *TERT* gene (der(5) and der(20)) with translocation events (t(5;11), t(5;20)) (Figure 13A). Derivatives comprise structurally rearranged chromosomes indicating the chromosome with an intact centromere. In the case of t(5;20), a rearrangement of chromosome 5 and 20 occurred, with the breakpoint on chromosome 5 located close to the *TERT* gene. MNA cell line GI-ME-N had six copies of the *TERT* gene (Figure 13B). Two copies were located on a derivate of chromosome 6, der(6), with translocation event t(5;6;19) and two copies on der(16) with the rearrangements including t(5;16;19). The *TERT* gene locus was juxtaposed to genomic regions on chromosome 19 in der(6) as well as der(16). In *MYCN*-amplified KELLY cells, three copies of *TERT* were detected (Figure 13C). Two translocation events were present carrying the *TERT* gene joined to

the genomic regions on chromosome 2 (der(2) and der(5)). A large duplication event on chromosome 5 was identified in *MYCN*-amplified cell line NGP, but was not further characterized within this study (data not shown). Chromosome painting visualizing numerical and structural chromosomal aberrations also revealed evidence for a *TERT* rearrangement in LAN2 cells (data not shown).

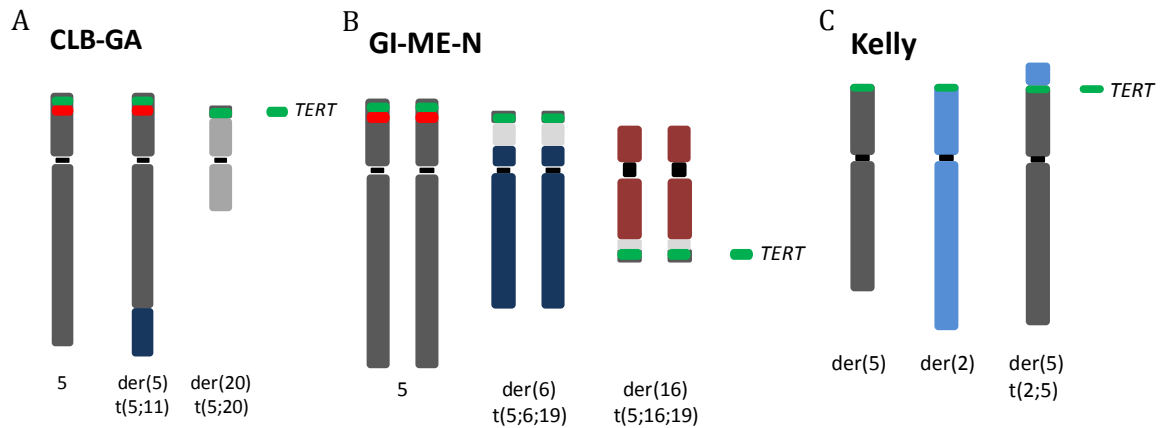


Figure 13: Structural aberrations involving TERT.

Fluorescence in situ hybridization (FISH) of NB cell lines CLB-GA (A), GI-ME-N (B) and KELLY (C). TERT locus-specific probes were labelled in green. Analyses were performed by Larissa Savelyeva.

4C-seq confirmed physical TERT promoter-enhancer interactions in rearranged cell lines

Circular chromatin conformation capturing with subsequent sequencing (4C-seq) was used for detection of physical enhancer-promoter interactions of a specific region, which is called the viewpoint, with all other locations of the genome (2.2.14). Such a viewpoint matching the *TERT* promoter was designed and tested in NB cell lines CLB-GA, GI-ME-N, KELLY and LAN2 (Figure 14 and Figure 15). In cell lines CLB-GA and GI-ME-N, interactions were confirmed between the *TERT* promoter and juxtaposed enhancers at chromosome 20 and 19, respectively (Figure 14).

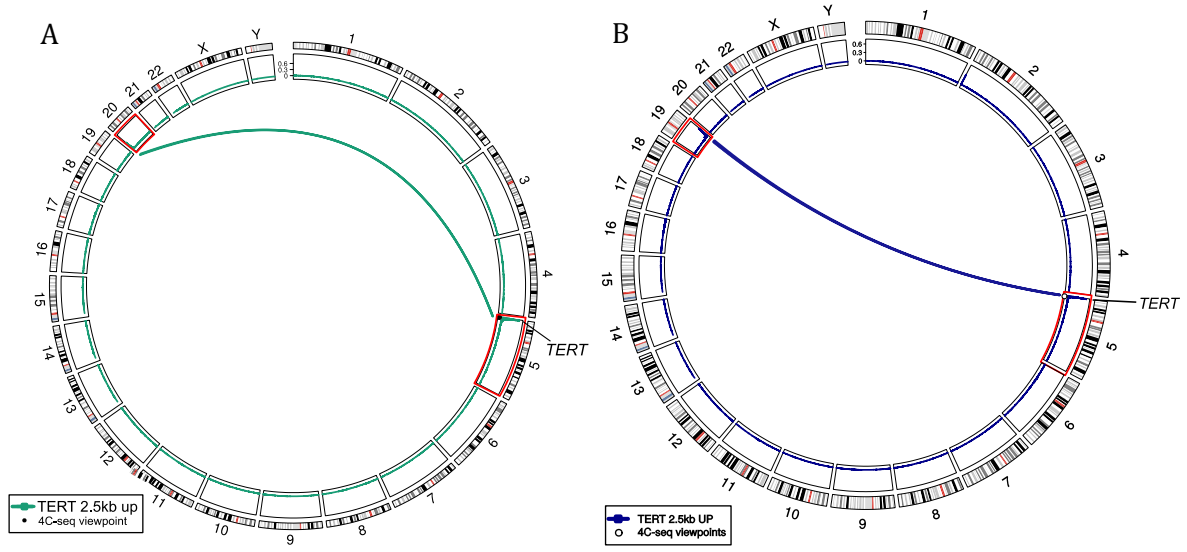


Figure 14: Genome-wide interactions of *TERT* promoter.

Genome-wide circos plot interaction profile of the *TERT* promoter with regulatory elements on chromosome 20 in NB cell line CLB-GA (A) and elements on chromosome 19 in GI-ME-N (B) as determined via 4C-seq. Different viewpoints were applied (green and blue = *TERT* TSS)

In KELLY, 4C-seq identified two SE regions on chromosome 2 close to the *ALK* gene as interaction partners of the *TERT* promoter (Figure 15A).

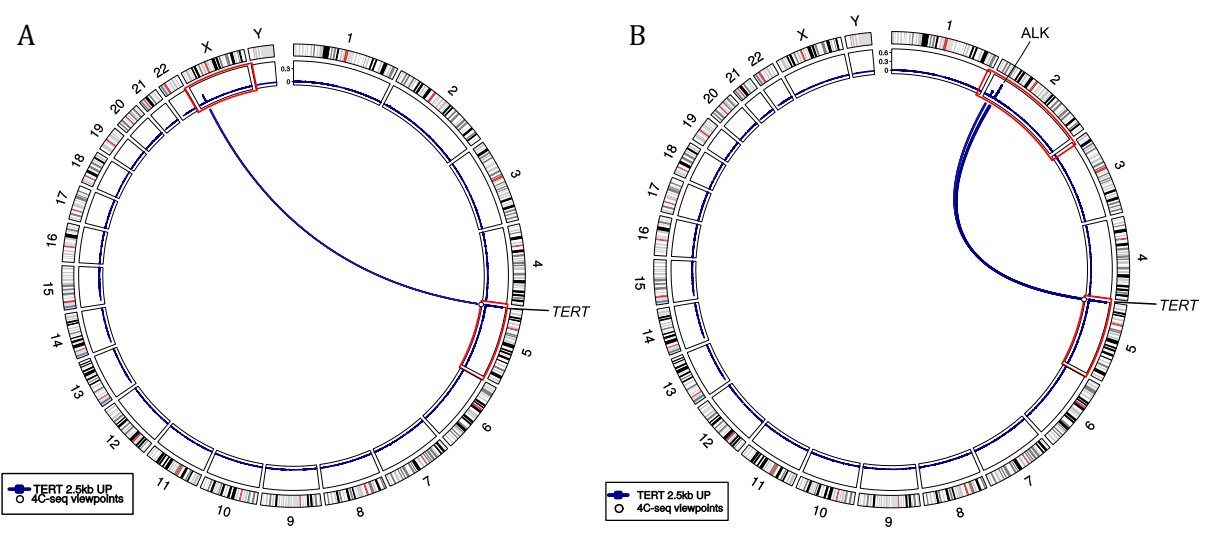


Figure 15: Genome-wide interactions of *TERT* promoter.

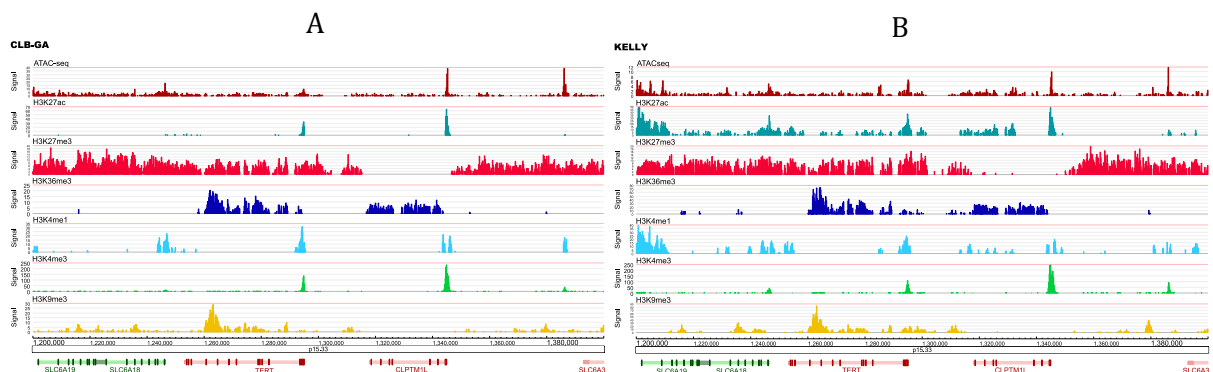
Genome-wide circos plot interaction profile of the *TERT* promoter with regulatory elements on chromosome X in NB cell line LAN2 (A) and elements on chromosome 2 in NB cell line KELLY (B) as determined via 4C-seq. Different viewpoints were applied (blue = *TERT* TSS)

Finally, in LAN2 cells, the rearranged chromosome 5 region carrying *TERT* was located next to chromosome X and enhancer regions that are physically interacting with the *TERT* promoter (Figure 15B). All *TERT* promoter assays provided various *cis*-interactions in the surrounding of the *TERT* viewpoint on chromosome 5.

*ChIP-seq of histone marks identified the epigenetic status
of TERT locus in rearranged NB cell lines*

CLB-GA, GI-ME-N and KELLY cells showed high *TERT* expression level due to a *TERT* rearrangement and interaction of the *TERT* promoter with juxtaposed enhancer regions close to the breakpoint of new interacting chromosomal regions. As a next step, the epigenetic status and chromatin state of *TERT* gene acceptor region was explored by ChIP-seq of histone marks (H3K4me3, H3K4me1, H3K27ac, H3K36me3, H3K27me3 and H3K9me3) or ATAC-seq (Figure 16). The cell lines SK-N-FI and LAN6 without elevated *TERT* genes expression or *TERT* rearrangement served as controls (Figure 17).

TERT-rearranged CLB-GA cells demonstrated the strongest *TERT* expression in the cohort, followed by *MYCN*-amplified NGP cells (Figure 12B). The ATAC-seq profile, a characteristic of open chromatin, was enriched for peaks at the *TERT* locus and surroundings (Figure 16A). This was accompanied by enrichment of H3K27ac, H3K4me1 and H3K4me3 at the *TERT* TSS, which are all associated with actively transcribed protein-coding promoters. The *TERT* gene body was marked by H3K36me3, which is enriched at the gene body of active genes, as well as by H3K27me3 and some distinct peaks of H3K9me3, which are both associated with gene silencing and repressive function. The epigenetic status of KELLY was comparable to that of CLB-GA, except for additional strong enrichment of histone mark H3K27ac at the TSS of *TERT*, surrounding genes as well as at intergenic and intronic regions (Figure 16B).



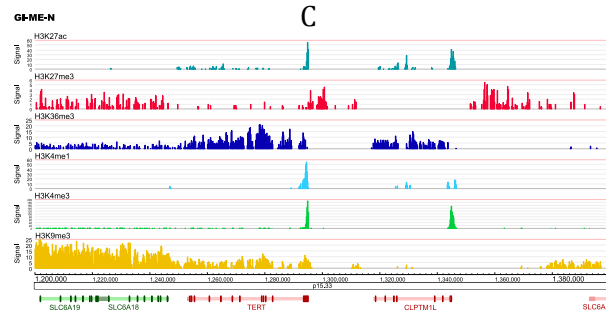


Figure 16: Epigenetic profiling of *TERT* locus.

Input normalized read counts of histone marks H3K4me3, H3K4me1, H3K27ac, H3K36me3, H3K27me3 and H3K9me3 and ATAC-seq peaks (only CLB-GA and KELLY) at the TERT locus. Peaks are shown of cell lines with rearrangements close to the TERT locus (CLB-GA (A), KELLY (B), GI-ME-N (C)).

GI-ME-N cells, which express comparable *TERT* levels to CLB-GA, showed similar epigenetic profile of enrichment of histone modifications H3K4me3, H3K4me1, H3K27ac and H3K36me3 as did CLB-GA at gene body and TSS (Figure 16C). However, the patterns of H3K27me3 and H3K9me3 were different. While histone H3K27me3 was nearly absent at the *TERT* locus, H3K9me3 was heavily enriched upstream of the *TERT* gene.

The two *TERT* non-rearranged and *TERT* non-expressing control cell lines LAN6 and SK-N-FI, showed a comparable epigenetic pattern (Figure 17). H3K4me3, H3K4me1, H3K27ac and H3K36me3 were nearly absent at *TERT* TSS and gene body. However, strong enrichment for histone modification H3K27me3 and moderate peaks for H3K9me3 were observed, which are associated with gene silencing and repressive function.

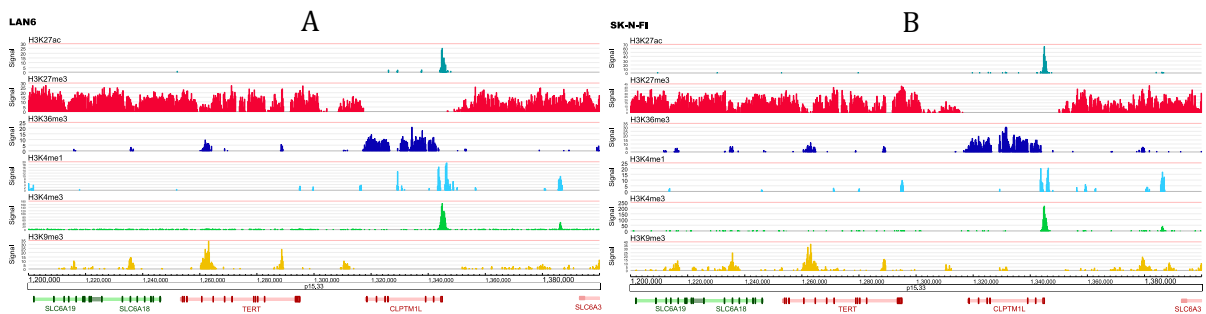


Figure 17: Epigenetic profiling of *TERT* locus.

Input normalized read counts of histone marks H3K4me3, H3K4me1, H3K27ac, H3K36me3, H3K27me3 and H3K9me3 at the TERT locus. Peaks are shown of cell lines lacking TERT alterations (LAN6 (A) and SK-N-FI (B)).

*ChIP-seq of histone marks identified active enhancers
with TERT promoter in rearranged NB tumors*

The epigenetic status and chromatin state of *TERT* gene acceptor region and donor region of the corresponding translocation partner was examined by ChIP-seq for histone marks H3K4me3 and H3K27ac in three *TERT*-rearranged tumors (Figure 18). Two tumors had inter-chromosomal chromosome 5 rearrangements (NB-2 and NB-3; Figure 18B and 18C) and one tumor harbored a translocation event of chromosome 7 and 5, close to the *TERT* gene (NB-1; Figure 18A). In all three cases, there was strong enrichment of histone mark H3K27ac in the translocated region adjacent to the breakpoints. For an additional tumor, a *TERT* translocation close to the *HAND2* (heart and neural crest derivatives expressed 2) downstream enhancer region was identified (NB-4; ChIP-seq data not shown).

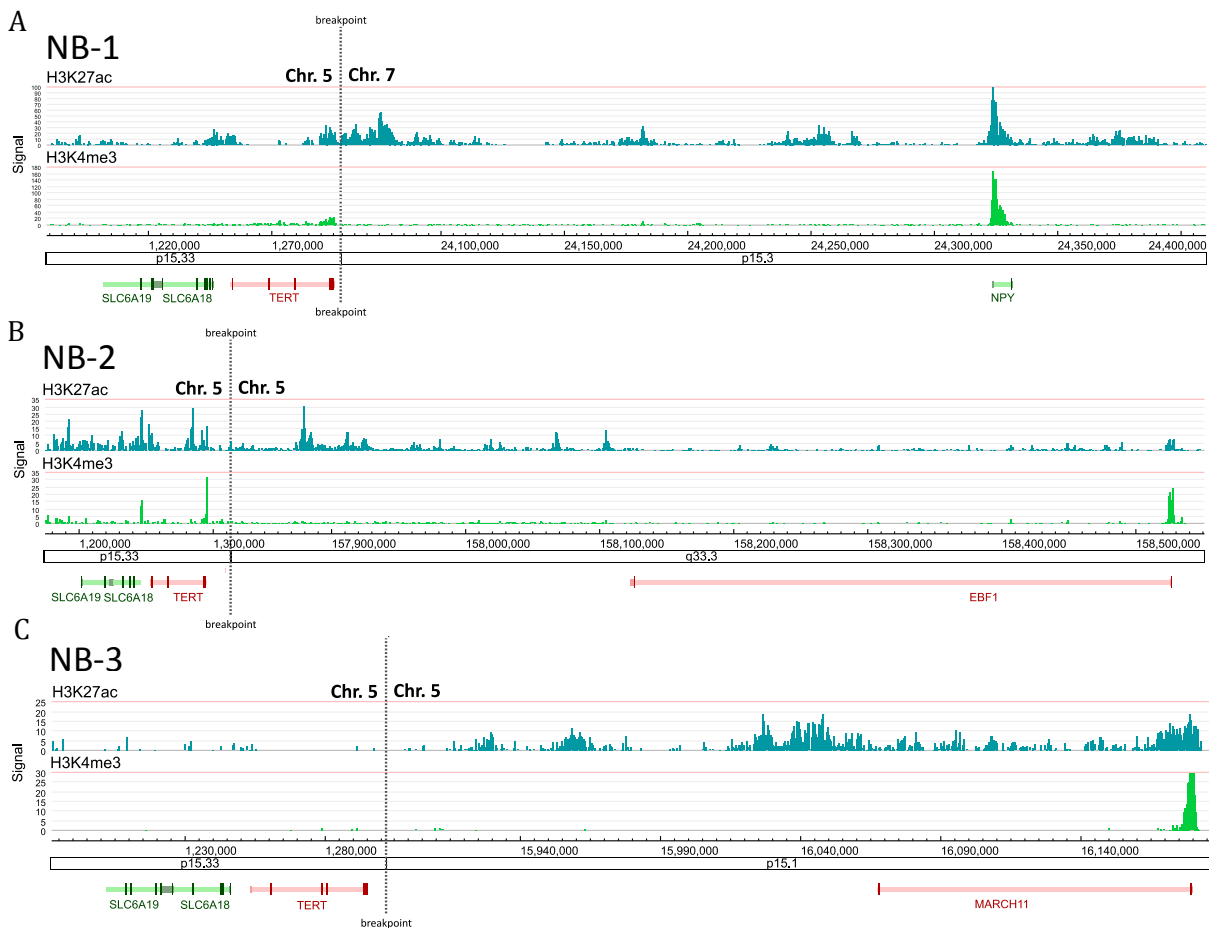


Figure 18: Epigenetic profiling of rearranged regions involving TERT.

Input normalized read counts of histone marks H3K4me3 and H3K27ac within the rearranged genomic regions of NB primary tumors NB-1 (A), NB-2 (B) and NB-3 (C).

Individual ranking of histone mark H3K27ac signal according to SE definition (1.2.3) revealed that strong SE regions juxtaposed the *TERT* gene in all three tumors investigated (Figure 19A, B and C).

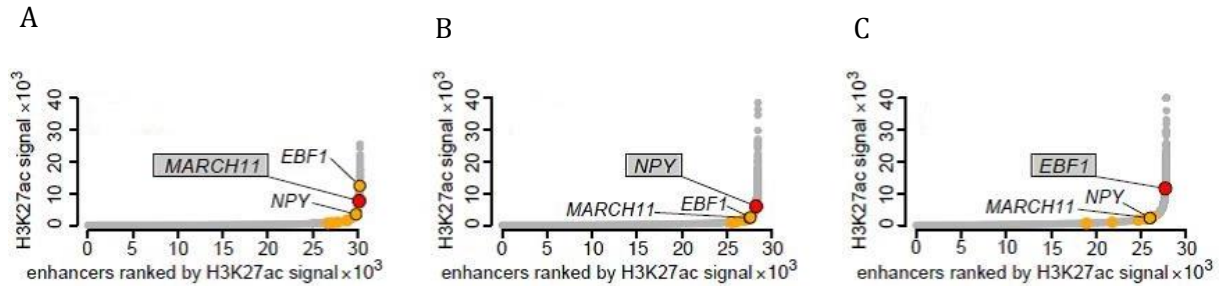


Figure 19: Ranking of histone mark H3K27ac signal.

Ranking of histone mark H3K27ac signal (enhancer elements) in tumors NB-3 (A), NB-1 (B) and NB-2 (C). Enhancers close to the breakpoint of *TERT* rearrangements are marked red and encircled. SE definition was applied according to (1.2.3; Figure 7). H3K27ac ChIP-seq peaks within 12.5 kb distance were stitched and defined as one single enhancer entity. All enhancers and combined enhancer entities were ranked according to their H3K27ac signal within the genomic region. Enhancers with H3K27ac signal above the point where the curve slope exceeds one were considered as SEs. Adapted from (Peifer et al. 2015).

450K analysis identified DNA methylation status

of CpG islands at *TERT* locus in primary NB tumors

DNA methylation analysis of CpG islands at the *TERT* locus of 39 NB primary tumors were compared in *TERT*-rearranged samples (*TERT*), *MYCN*-amplified samples (*MYCN*) and tumors without *TERT* or *MYCN* events (Figure 20). *MYCN* tumors harbored highest CpG islands methylation across the *TERT* gene locus, followed by *TERT*-rearranged cases. Strongly enriched methylation was observed at a CpG site close to the *TERT* promoter of *MYCN* and *TERT* samples as compared to the others.

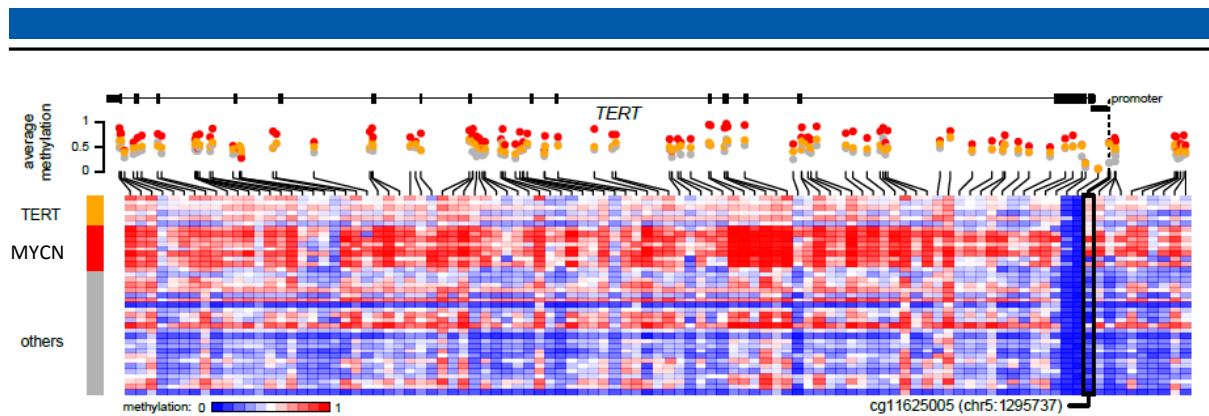


Figure 20: DNA methylation of CpG islands at *TERT* locus in NB.

DNA methylation of CpG islands at the *TERT* locus in 39 primary NB tumors (HumanMethylation450K arrays). Samples were classified in *TERT*-rearranged (*TERT*, $n = 6$), *MYCN*-amplified (*MYCN*, $n = 9$) and cases without *TERT* or *MYCN* events (*others*, $n = 24$). Adapted from (Peifer et al. 2015).

Taken together, a recurrent rearrangement affecting the *TERT* gene was identified in up to 24% of high-risk NB cases using integrated data from WGS and FISH analyses of primary tumors. *TERT* rearrangements upstream of the TSS caused high *TERT* expression and were associated with poor clinical outcome.

In both, tumors and cell lines, ChIP-seq data identified highly active SE regions juxtaposed to the *TERT* gene, which led to activated chromatin state and likely drove high *TERT* expression observed in these cases. In NB cell lines, physical interactions of juxtaposed enhancer elements with the *TERT* promoter were confirmed by 4C-seq studies.

3.1.2 Further rearrangements affecting oncogenes

The principle of oncogene activation by chromosomal rearrangements bringing together active enhancers and oncogenes has been described for several cancer entities and is referred to as the phenomenon of “enhancer hijacking”. With the discovery of recurrent rearrangements of SE elements activating the *TERT* gene, we provided the first evidence for “enhancer hijacking” in NB. Due to the absence of coding mutations or amplifications, extraordinary high expression levels for several oncogenes including *MYCN*, *MYC* (summarized as *MYC(N)*) in NB remained unexplained for a long period and will be elucidated in this study using primary tumor and cell line data sets including FISH, WGS, RNA-seq, ChIP-seq, ATAC-seq and interaction data like 4C and HiChIP.

mRNA expression of MYC(N) in NB tumors and cell lines

As a first step, the mRNA expression level of NB tumors and cell lines was evaluated using RNA-seq data (Figure 21). Therefore, 498 cases with RNA seq data were included consisting of stage 1 (n = 121, 24.3%), stage 2 (n = 78, 15.7%), stage 3 (n = 63, 12.7%), stage 4 (n=183, 36.7%), stage 4S (n = 53, 10.6%) and *MYCN*-amplified (92, 18.5%) samples (Zhang et al. 2015)) (Figure 21A). In tumors classified as *MYCN* non-amplified (MNA), no elevated *MYCN* expression was detected (Figure 21A). Within the RNA-seq dataset of 32 NB cell lines, 18 harbored amplified *MYCN* while 14 were defined as MNA (Figure 21B). All 18 cases of amplified *MYCN* were accompanied by high *MYCN* expression (FPKM of 258.1 for SIMA - 1534.1 for SMS-KCNR). In contrast, for all MNA cell lines, with the exception of NBL-S and SK-N-FI (FPKM of 118.6 and 33.6), a relatively low *MYCN* expression was observed (FPKM of 0.17 for GI-ME-N).

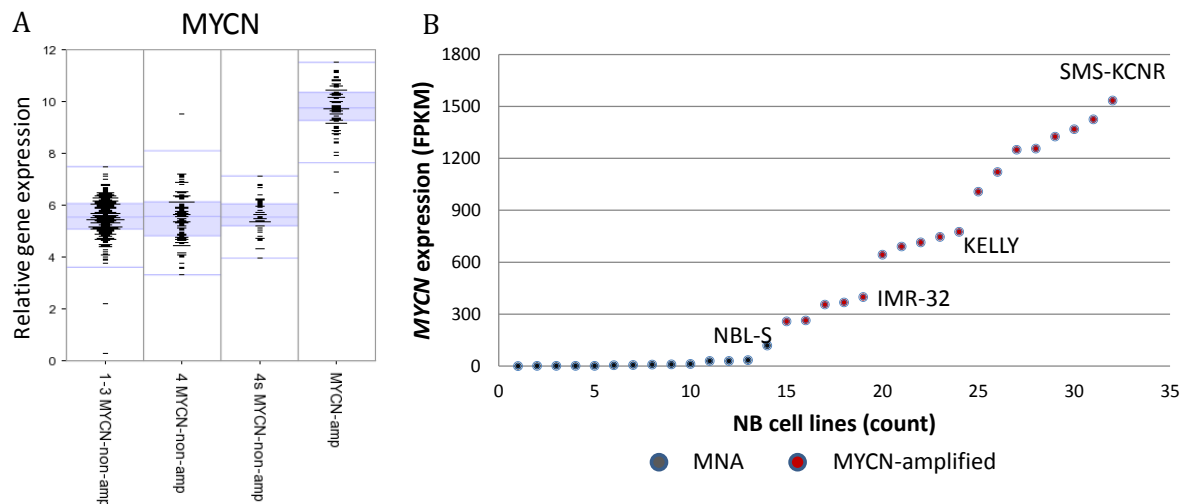


Figure 21: MYCN mRNA expression in NB.

(A) MYCN mRNA expression according to stage and MYCN status in NB tumors by RNA-seq (n = 498; log2 scaling). (B) MYCN mRNA expression in NB cell lines by RNA-seq (n = 32; Sample MNA (blue) or MYCN-amplified (red)).

MYC gene expression was highest in stage 4 patients followed by stage 1-3 and 4S within the RNA-seq cohort of 498 NB primary tumors (Figure 22A). Patients harboring amplified *MYCN* revealed the lowest *MYC* expression, which was in line in NB cell lines (Figure 22B). While *MYCN*-amplified cell lines like CHP126 with the high *MYCN* expression harbored lowest *MYC* expression levels, MNA cell lines like GI-ME-N were among the top *MYC* expressing cell lines.

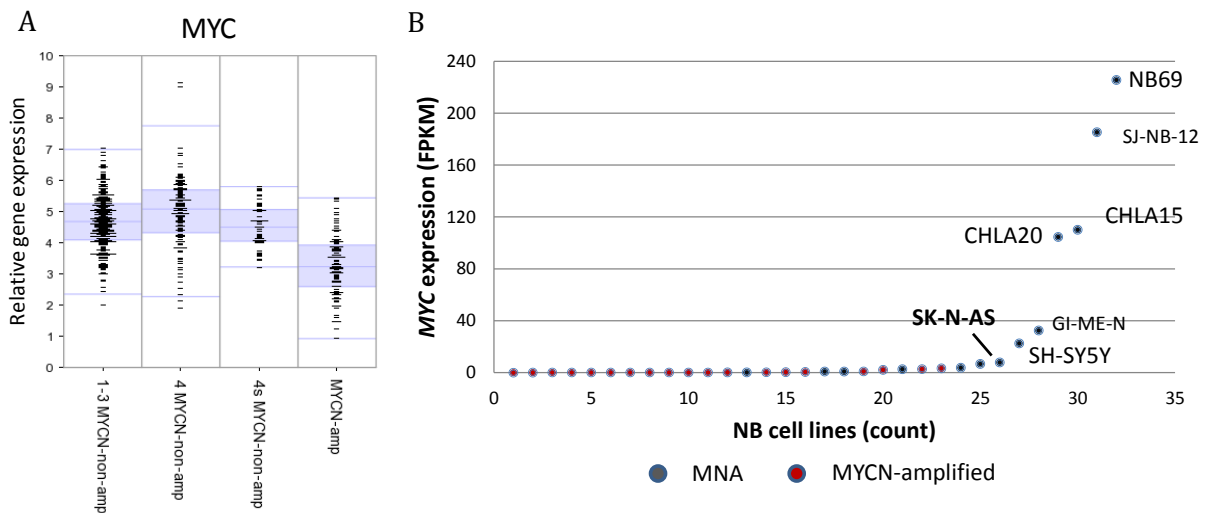


Figure 22: MYC mRNA expression in NB.

(A) MYC mRNA expression according to stage and MYCN status in NB tumors by RNA-seq ($n = 498$; log2 scaling). (B) MYC mRNA expression in NB cell lines by RNA-seq ($n = 32$; Sample MNA (blue) or MYCN-amplified (red)).

Protein quantification of MYC(N) in NB cell lines

The MYCN mRNA expression pattern of MNA cell lines ($n = 7$) was translated to the protein level as determined by western blotting. While no MYCN protein was detectable in most MNA cell lines (SK-N-AS, SH-SY5Y, CHLA20, CHLA15 and NB69) SK-N-FI and especially NBL-S cells displayed high MYCN protein signals (Figure 23)

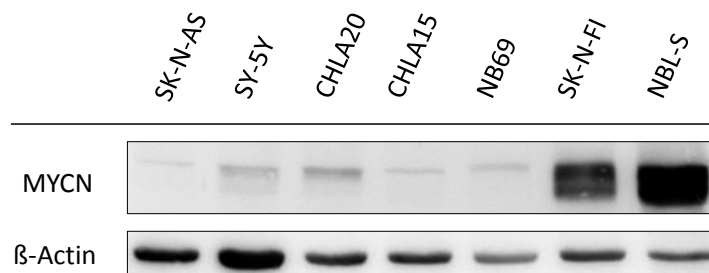


Figure 23: MYCN protein expression in NB cell lines.

MYCN protein expression was quantified by western blotting using β -actin as a loading control in a set of MYCN-non amplified (MNA) NB cell lines ($n = 7$).

Western blot analysis of MYC expression in MNA NB cell lines ($n = 7$) revealed highest MYC protein levels in cell lines NB69 and CHLA20, followed by SH-SY5Y and SK-N-AS (Figure 24).

MYC protein expression was undetectable in the top *MYCN* expressing MNA cell lines NBL-S and SK-N-FI.

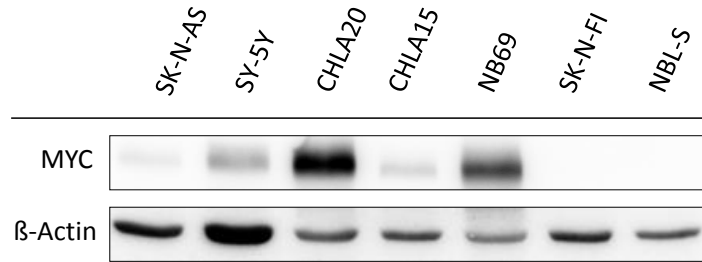


Figure 24: MYC protein expression in NB cell lines.

MYC protein expression was quantified by western blotting using β -actin as a loading control in a set of *MYCN*-non amplified (MNA) NB cell lines ($n = 7$).

High MYC(N) expression was associated with poor survival of NB patients

Increased *MYCN* expression levels significantly correlated with poor event free (EFS) as well as overall survival (OS) in a cohort of 498 primary NBs (Figure 25). EFS probability (Figure 25A) in *MYCN* high cases accounted roughly 0.3 in contrast to less than 0.7 in patients with low *MYCN* expression while OS probability (Figure 25B) resulted in 0.4 and 0.85, respectively.

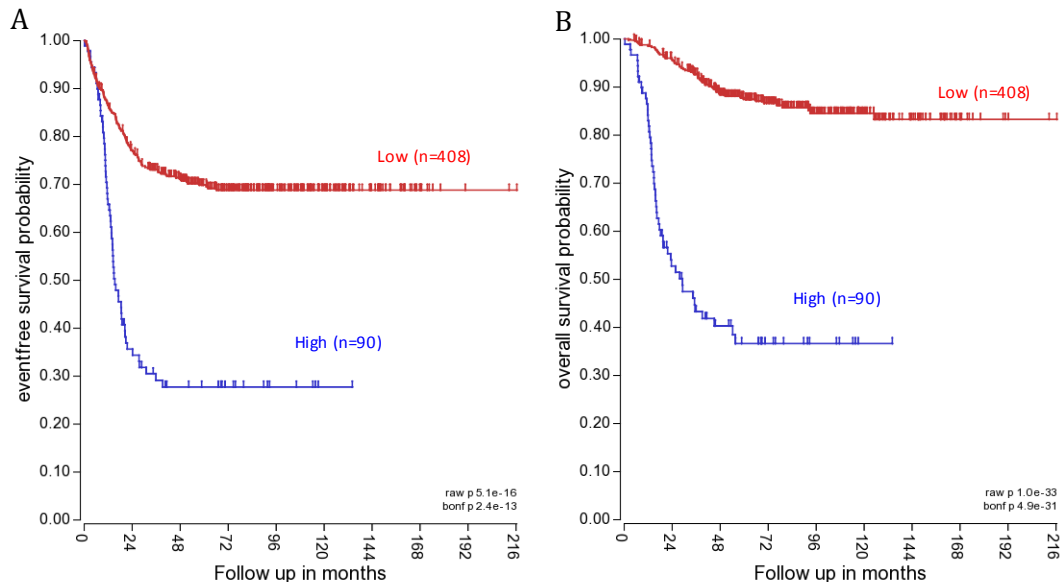


Figure 25: High *MYCN* is associated with poor survival in NB.

Kaplan-Meier analyses for event-free survival (EFS) (A) and overall survival (OS) (B) in respect to *MYCN* expression in a set of 498 NB primary tumors. Uncorrected (raw p) and Bonferroni-

corrected (*bonf p*) *p*-values are shown. Cut-off values for dichotomization of *MYCN* expression were estimated by maximally selected log-rank statistics.

FISH identified structural aberrations involving MYC(N)

To trace the cause for high expression levels of *MYCN* and *MYC* in several NB cell lines, chromosome painting, which allows to visualize numerical and structural chromosomal aberrations, was performed (Ried et al. 1998) (data not shown). For identification of a more specific focus on the rearranged location, FISH analysis, which helps to spot structurally rearranged chromosomes using locus specific BAC probes (100 – 200 kb) was performed in NBL-S cells (Figure 26). Labeling the *MYCN* region (green) and a genomic region on chromosome 4 (red), close to the *HAND2* gene (hereinafter referred to as *HAND2*), revealed two derivatives (der) including the *MYCN* gene (Figure 26). The two translocation events t(2;4) corresponded to the rearrangements of chromosome 2 and 4 (top-down) while the breakpoint was in close proximity to the *MYCN* (chromosome 2) and *HAND2* (chromosome 4) gene (Figure 26).

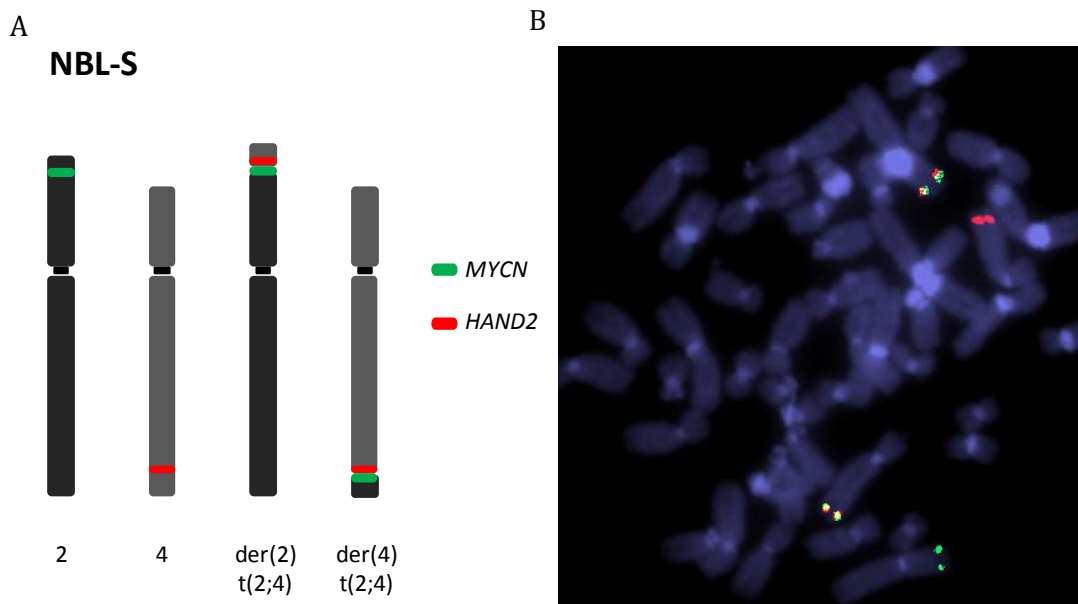
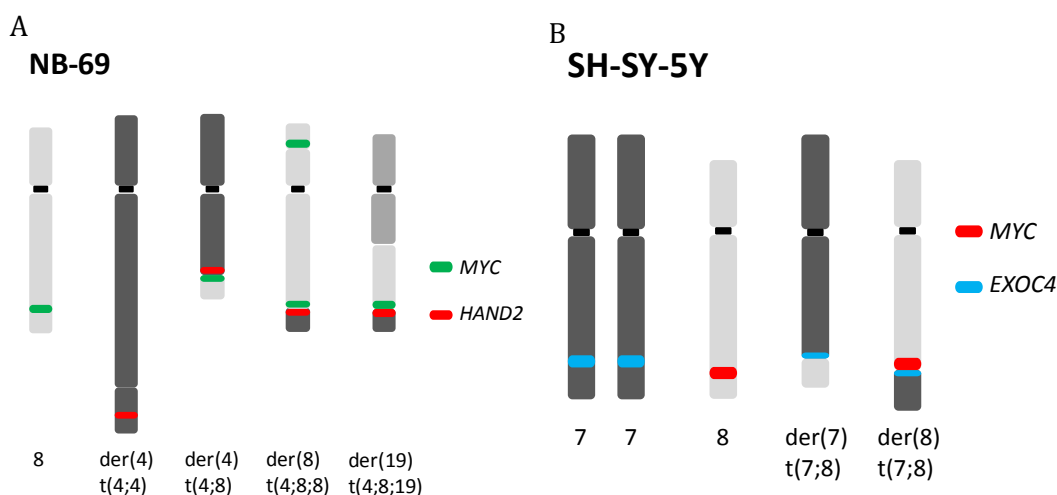


Figure 26: Structural aberrations involving MYCN.

Fluorescence in situ hybridization (FISH) (A) and karyogram (B) of NB cell line NBL-S. Specific probes for MYCN and a genomic region on chromosome 4 (hereinafter referred to as HAND2) close to the HAND2 gene were labelled in green and red, respectively. Analyses were performed by Olga Sepman and Larissa Savelyeva.

Similar to *MYCN*, multicolor FISH using *MYC* locus-specific probes was performed to identify structural aberration events in cell lines with extraordinary high *MYC* expression levels. We focused on the composition of derivatives (der), which describe structurally rearranged chromosomes indicating the chromosome with an intact centromere. Fusion chromosomes on chromosome 8 with the *MYC* locus (green), chromosome 4 with *HAND2* (red) and further chromosomal translocation partners were examined. In cell line NB69, we identified that all three derivatives ((der(4), der(8) and der(19)) containing *MYC* in chromosome 8 segments were flanked by chromosome 4 sections containing the *HAND2* locus (Figure 27A). These translocation events (t(4;4), t(4;8;8)) and t(4;8;19)) included complex rearrangements and duplications. Cell line SH-SY-5Y harbored one translocation event on der(8) including the *MYC* gene (Figure 27B). We identified that der(8) was joined to chromosome segments close to the *EXOC4* gene on chromosome 7 (t(7;8)) in SH-SY5Y cells.

Two derivatives (der(8) and der(18)) containing the *MYC* gene that was joined to chromosome segments close to the *HAND2* locus on chromosome 4 were identified in the isogenic cell lines CHLA15 and CHLA20, which derived from the same patient (CHLA15 was isolated prior to treatment; CHLA20 was isolated after treatment) (Figure 27C and D). Der(8) comprised the translocation event of chromosome 4 and 8 (t(4;8)), while in der(18) large chromosomal fragments of chromosome 18 (t(4;8;18)) were involved. The duplications of these fragments were found in cell line CHLA20, but not in CHLA15. Finally, one derivative (der(8)) was discovered containing translocated segments of chromosome 4 with *HAND2* locus flanking the *MYC* locus (t(4;8)) in SK-N-AS cells (Figure 27E). Derivate (der(9)) explained rearrangement of *MYC* locus with chromosome 9.



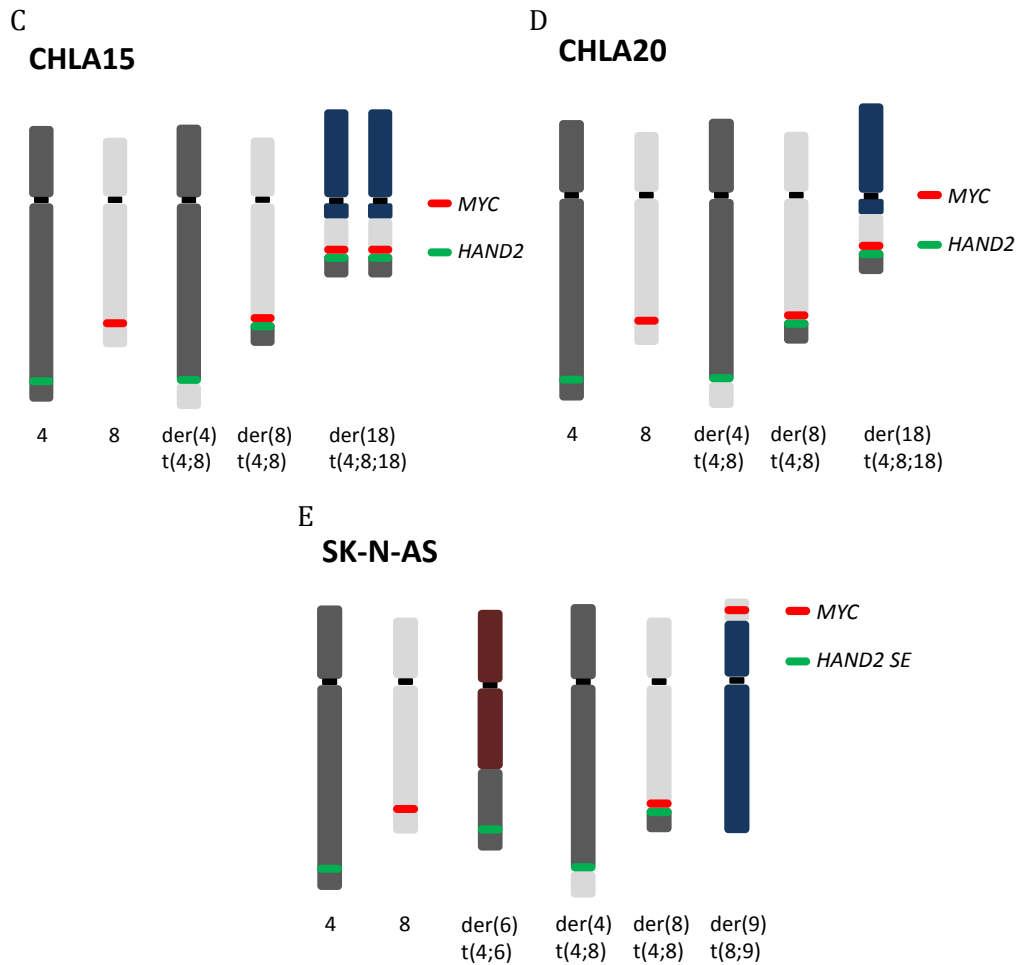


Figure 27: Structural aberrations involving MYC.

Fluorescence in situ hybridization (FISH) image of NB cell line NB69 (A), SH-SY-5Y (B), CHLA15 (C), CHLA20 (D) and SK-N-AS (E). MYC and HAND2 locus-specific probes were labelled in red and green, respectively. In SH-SY5Y, EXOC4 locus-specific probe was labelled in blue. Analyses were performed by Olga Sepman and Larissa Savelyeva.

Combined 4C-seq and ChIP-seq of histone marks identified interactions of active enhancers with MYC(N) promoter in rearranged cell lines

4C-seq was used to validate the FISH defined *MYC(N)* rearrangements by detecting functional and genome wide physical interactions of a specific region, named viewpoint (Figure 28 - Figure 30). Such a viewpoint, matching the *MYC* and *MYCN* promoter was designed and used in *MYC*- and *MYCN*-rearranged cell lines, respectively. For a reciprocal assay, three different viewpoints, using P300 ChIP-seq peaks as enhancer surrogates, were designed, which were close to the breakpoint on chromosome 4.

In NBL-S cells the *trans*-interaction of *MYCN* promoter on chromosome 2 and SEs on chromosome 4 were the only observed interactions (Figure 28). The reciprocal assays starting from the SE peaks confirmed this *trans*-interaction.

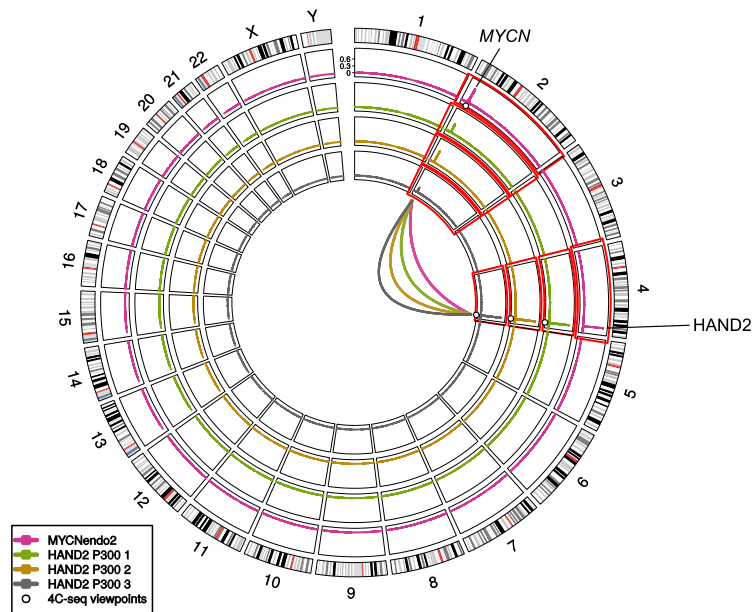


Figure 28: Genome-wide interactions involving *MYCN* promoter.

Genome-wide interaction profile of regulatory elements on chromosome 4 with the *MYCN* promoter in NB cell line NBL-S as determined via 4C-seq. Different viewpoints were applied (pink = *MYCN* TSS; green = *HAND2* P300 position 1; yellow = *HAND2* P300 position 2; grey = *HAND2* P300 position 3)

Trans-interactions of *MYC* promoter with the enhancer regions on chromosome 4 (NB69, SK-N-AS and CHLA20; Figure 29 and Figure 30B) or chromosome 7 (SH-SY5Y; Figure 30A) were identified in all *MYC*-rearranged cells. A reciprocal assay including three different viewpoints was designed as previously described, applied to cell lines NB69 and SK-N-AS and confirmed these *trans*-interactions (Figure 29A and B).

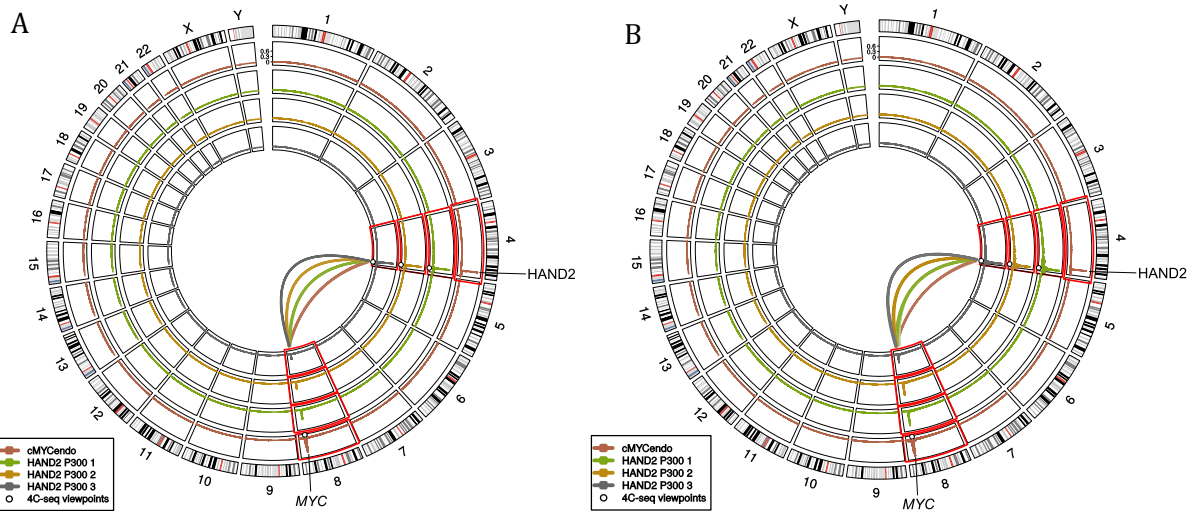


Figure 29: Genome-wide interactions involving MYC promoter.

Genome-wide interaction profile of regulatory elements on chromosome 4 with the MYC promoter in NB69 (A) and SK-N-AS (B) cells as determined via 4C-seq. Different viewpoints were applied in NB69 and SK-N-AS cells, respectively (orange = MYC TSS; green = HAND2 P300 position 1; yellow = HAND2 P300 position 2; grey = HAND2 P300 position 3)

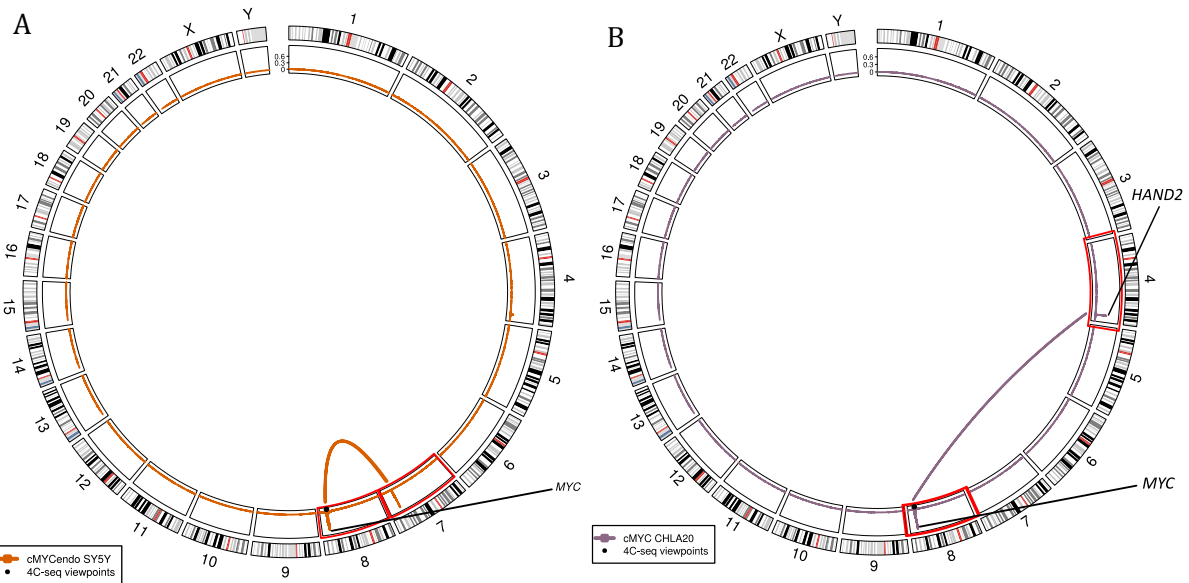


Figure 30: Genome-wide interactions of MYCN promoter.

Genome-wide interaction profile of regulatory elements on chromosome 7 and chromosome 4 in SH-SY5Y (A) cells and regulatory elements on chromosome 4 in CHLA20 (B) cells with the MYC promoter as determined via 4C-seq. MYC promoter viewpoint was applied (orange and purple = MYC TSS in SH-SY5Y and CHLA20, respectively).

For a more detailed view on the donor- and acceptor regions of *MYC(N)*-rearranged cells, all 4C-seq interactions were examined further at the loci and complemented with CHIP-seq profiles (Figure 31 - Figure 35).

In NBL-S cells, two histone modifications, H3K4me3, associated with active transcription at the transcription start sites (TSS) and H3K36me3, associated with transcriptional elongation at the gene body, were enriched at *MYCN* on chromosome 2 as well as *CEP44* (centrosomal protein 44) and *FBXO8* (F-box protein 8) on chromosome 4 indicating active transcription (Figure 31). Repressive marks including K27me3 and K9me3 showed only minor enrichment on chromosome 4 fragment. Patterns for H3K27ac and H3K4me1, in the absence of H3K4me3, generally used as surrogates for active regulatory enhancer elements, were significantly enriched downstream of the *FBXO8* gene on chromosome 4 fragment. This region of multiple enhancer clusters was located directly adjacent to the breakpoint and therefore to the *MYCN* gene.

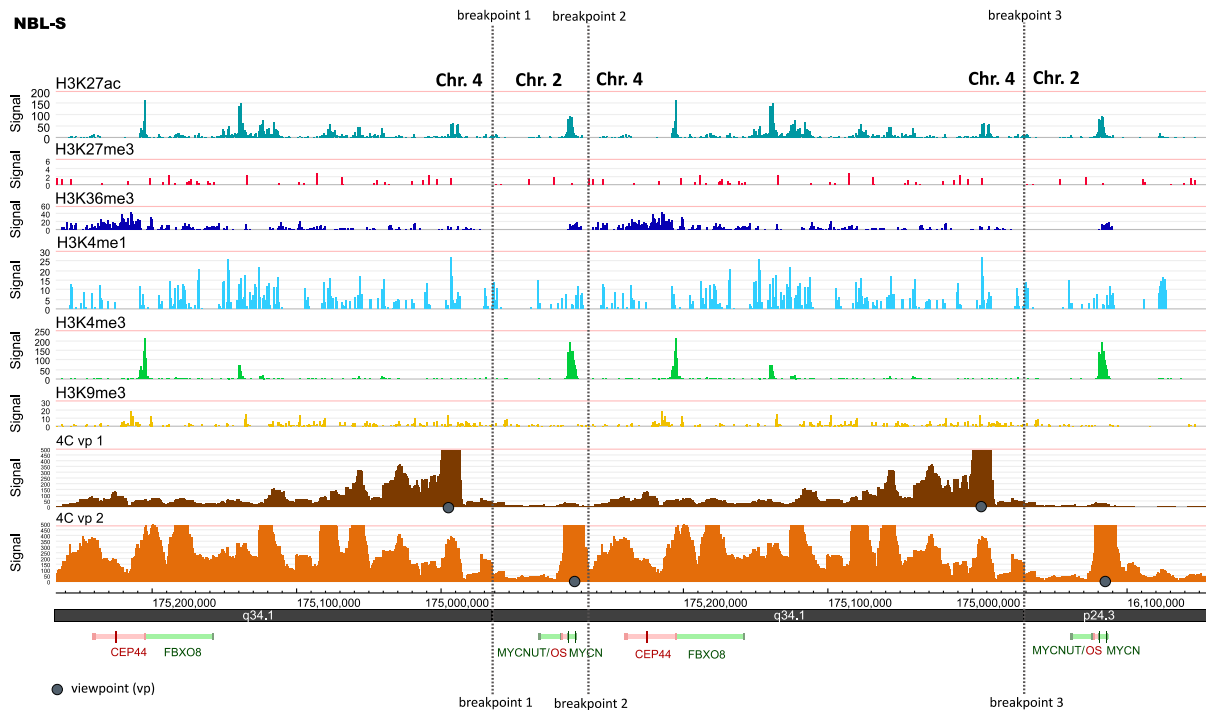


Figure 31: Epigenetic profiling of rearranged regions involving *MYCN*.

Input normalized read counts of histone marks H3K4me3, H3K4me1, H3K27ac, H3K36me3, H3K27me3 and H3K9me3 within the rearranged genomic regions in NBL-S cells. Interaction profiles of potential enhancer elements (VP1 on chr. 4) with the MYCN promoter (VP2 on chr. 2) were determined via circular chromatin conformation capturing with subsequent sequencing (4C-seq).

A large cluster of H3K27ac and H3K4me1 peaks was detected upstream of *FBXO8* on chromosome 4 in NB69 cells (Figure 32). In general, the absence of concurrent H3K4me3 promoter mark is considered as evidence that this cluster was a strong SE. The strong peak of H3K4me3 on chromosome 8 marked the active promoter of the *MYC* gene. In addition, enrichment of the transcriptional elongation mark H3K36me3 in the absence of repressive marks, H3K27me3 or H3K9me3, revealed active *MYC* transcription. 4C-seq analyses of the enhancer viewpoints on chromosome 4 (vp1-vp3) revealed *cis*-interactions close to the chosen viewpoint, which were decreasing with distance to the promoter from vp1 to vp3. This decrease of *cis*-interactions was accompanied by increased *trans*-interactions with the *MYC* promoter. The reciprocal assay with a viewpoint at the *MYC* promoter confirmed interactions with several enhancers of the chromosome 4 segment.

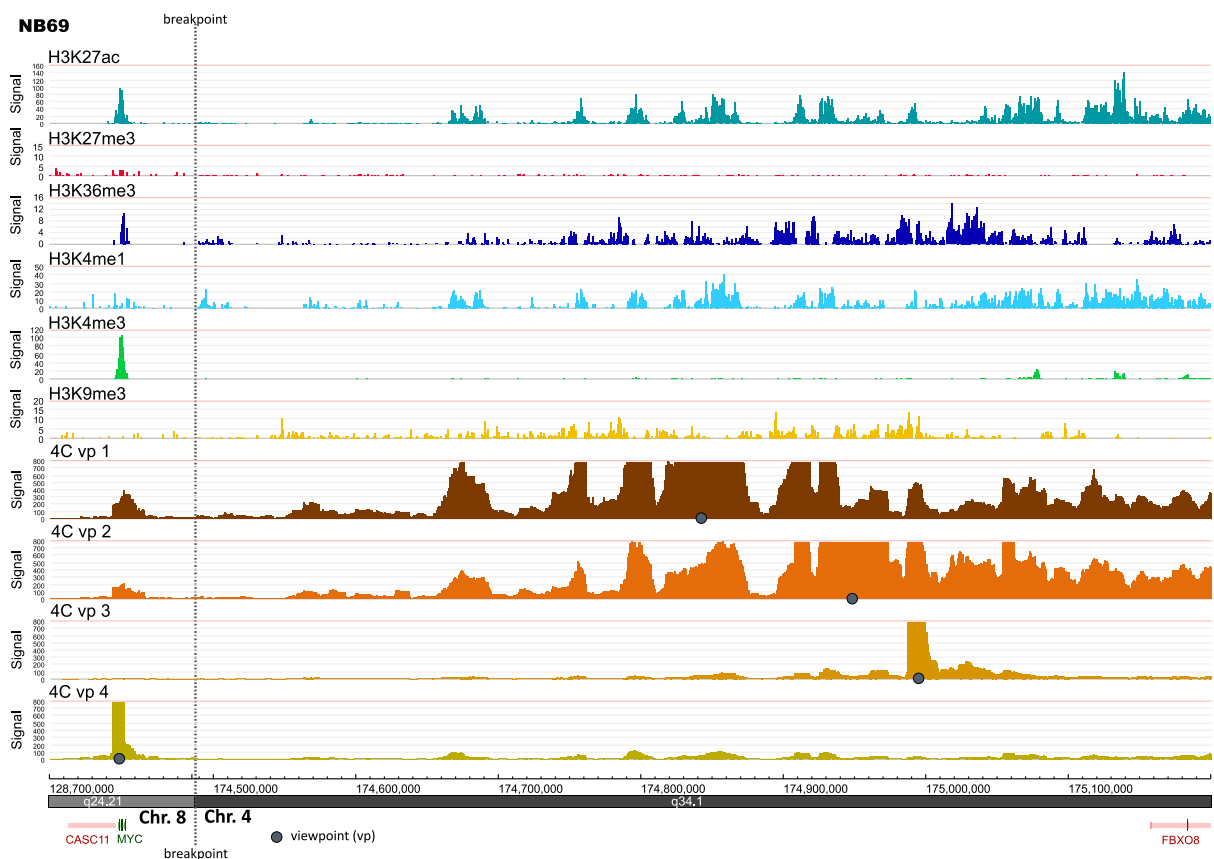


Figure 32: Epigenetic profiling of rearranged regions involving *MYC*.

Input normalized read counts of histone marks H3K4me3, H3K4me1, H3K27ac, H3K36me3, H3K27me3 and H3K9me3 at the junction between chromosome 4 and chromosome 8 in NB69 cells. Interaction profile peaks of potential enhancer elements (VP1-3 on chr. 4) with the *MYC* promoter (VP4 on chr. 8) were determined via circular chromatin conformation capturing with subsequent sequencing (4C-seq).

In SK-N-AS cells, the distance between *MYC* and the downstream breakpoint on chromosome 8 was more than 1 Mb compared to NB69 cells (Figure 33; compare Figure 77 in appendix and Figure 51). Besides the H3K27ac- and H3K4me1-marked SE region of the translocation partner on chromosome 4, several enhancer regions were identified within the *PVT1* gene close to *MYC*. This was confirmed by ATAC-seq, which revealed an open chromatin region matching the potential SE cluster area identified by CHIP-seq. The 4C-seq viewpoint at the *MYC* promoter (vp4) confirmed strong *cis*-interactions of SE region located close to the *PVT* gene on chromosome 8 and the *MYC* promoter. Additional *trans*-interactions were observed with the SEs on the chromosome 4 segment, which decreased with inverse correlation to the distance (vp1-3).

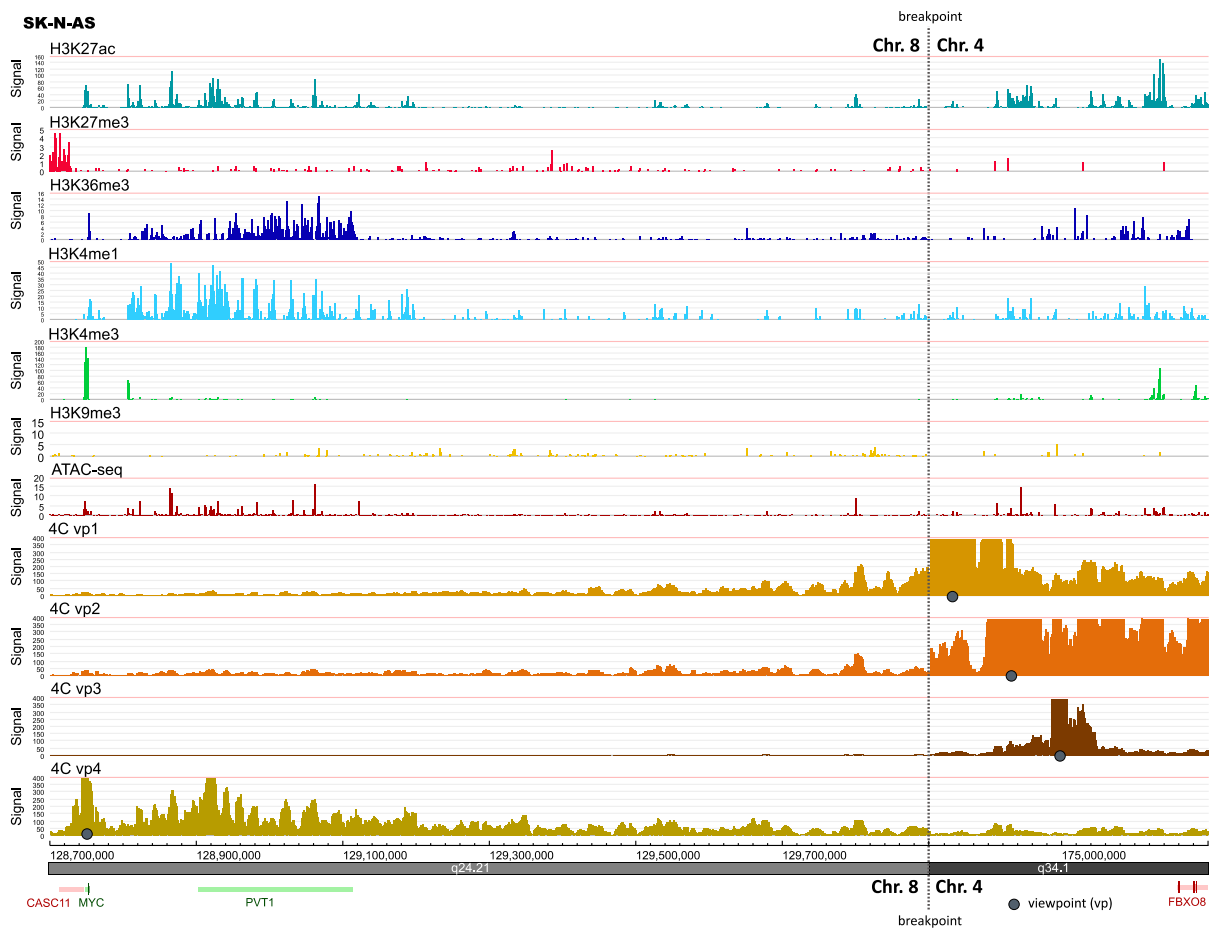


Figure 33: Epigenetic profiling of rearranged regions involving *MYC*.

Input normalized read counts of histone marks *H3K4me3*, *H3K4me1*, *H3K27ac*, *H3K36me3*, *H3K27me3* and *H3K9me3* and ATACseq peaks at the junction between chromosome 4 and chromosome 8 in SK-N-AS cells. Interaction profile peaks of potential enhancer elements (VP1-3 on chr. 4) with the *MYC* promoter (VP4 on chr. 8) were determined via circular chromatin conformation capturing with subsequent sequencing (4C-seq).

The rearrangement in cell line SH-SY-5Y revealed that *MYC* gene was joined with chromosome segments close to the *EXOC4* gene on chromosome 7 (Figure 27). These chromosome segments harbored strong enrichment of SE associated histone marks (H3K27ac, H3K4me1 without H3K4me3) and additional minor enrichments of histone marks associated with repressive functions (H3K27me3 and H3K9me3) (Figure 34). The *MYC* locus was enriched for H3K4me3 and RNA polymerase II (RPB1), indicating transcriptional activation. On the other hand, the repressive H3K27me3 mark was enriched at the *MYC* locus. 4C-seq using a viewpoint at the *MYC* promoter identified weak *cis*-interactions and strong *trans*-interactions with SE elements on chromosome 7.

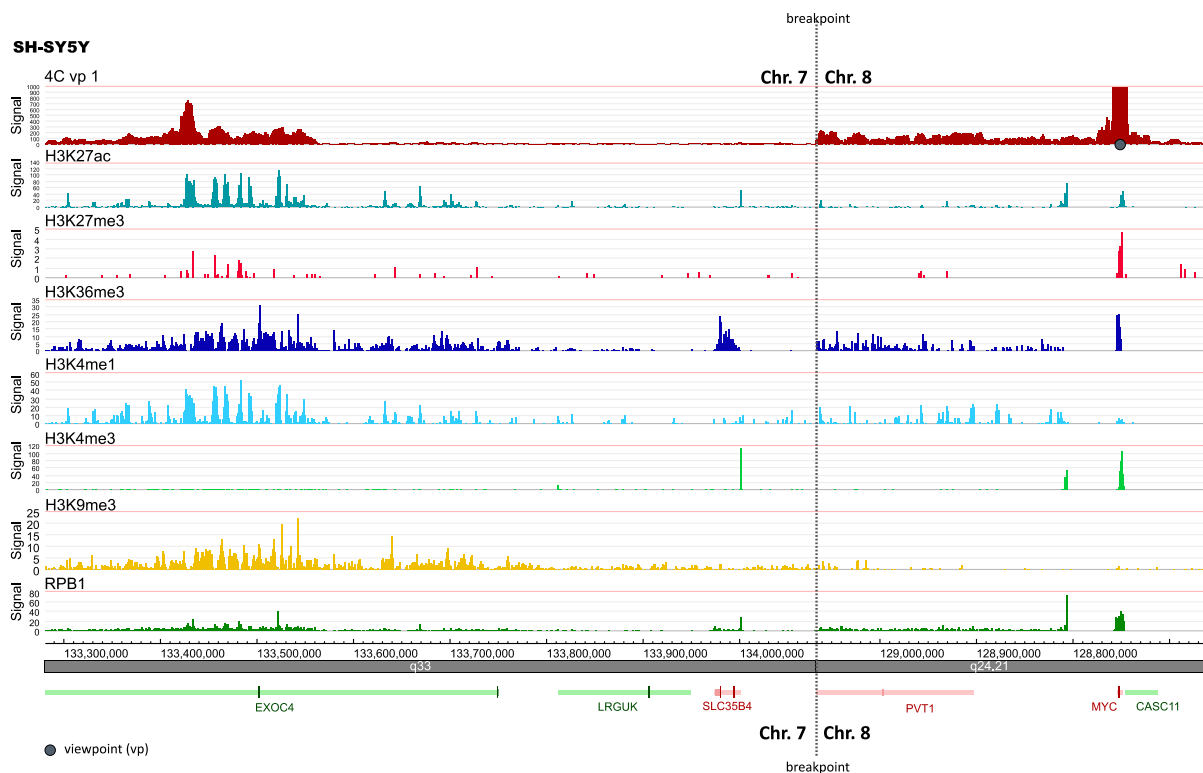


Figure 34: Epigenetic profiling of rearranged regions involving MYC.

Input normalized read counts of histone marks H3K4me3, H3K4me1, H3K27ac, H3K36me3, H3K27me3 and H3K9me3 and RNA PolII peaks at the junction between chromosome 7 and chromosome 8 in SH-SY5Y cells. Interaction profile peaks of the MYC promoter (VP1 on chr. 8) with potential enhancer elements on chr. 7 were determined via circular chromatin conformation capturing with subsequent sequencing (4C-seq).

A large cluster of SE associated histone marks (H3K27ac and H3K4me1 in the absence of H3K4me3) was detected upstream of the *FBXO8* gene on chromosome 4 in CHLA20 cells (Figure 35). This chromosomal segment was joined with chromosome 8 including the *MYC* gene. ChIP-seq peaks of the architectural protein CTCF (CCCTC-Binding Factor) could indicate TAD borders

that prevent interactions between neighboring domains. Even though there were several CTCF peaks at chromosome 4, potentially disrupting the interaction of *MYC* promoter and SE elements, 4C-seq using *MYC* promoter viewpoints revealed significant *trans*-interactions with the SE elements on chromosome 4.

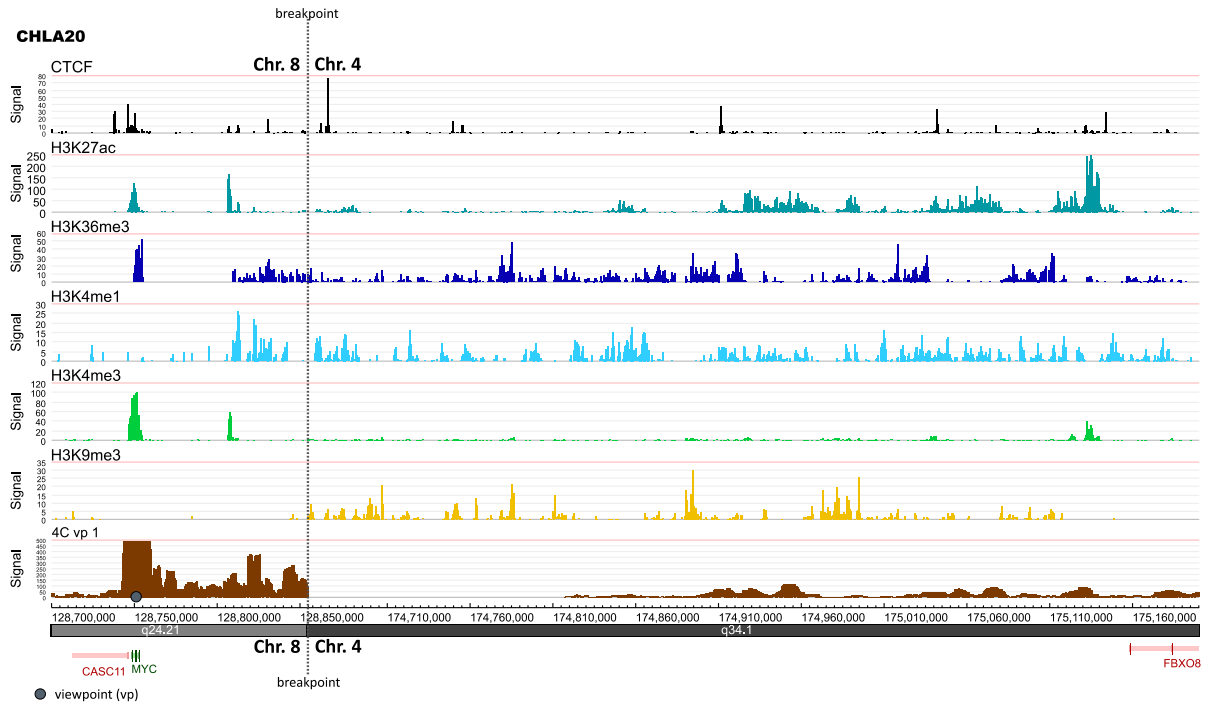


Figure 35: Epigenetic profiling of rearranged regions involving MYC.

Input normalized read counts of histone marks H3K4me3, H3K4me1, H3K27ac, H3K36me3, H3K27me3 and H3K9me3 and CTCF peaks at the junction between chromosome 4 and chromosome 8 in CHLA20 cells. Interaction profile peaks of the MYC promoter (VP1 on chr. 8) with potential enhancer elements on chr. 4 were determined via circular chromatin conformation capturing with subsequent sequencing (4C-seq).

The H3K27ac enhancer profiles of the *MYC(N)*-rearranged cell lines were analyzed towards SEs ranking according to the strategy proposed by Hnisz and colleagues (Hnisz et al. 2013) (Figure 36 and Figure 37).

The analysis and ranking revealed that the enhancer cluster from Chr. 4 juxtaposed to *MYCN* in NBL-S cells was a SE (Figure 36). *HAND2* associated SE region was defined as SE, which was outperformed by the SE with the highest signal of H3K27ac assigned to *CAMTA1*.

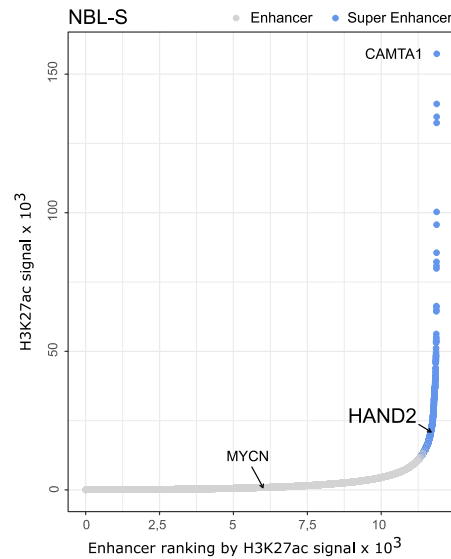


Figure 36: Ranking of histone mark H3K27ac signal.

Ranking of histone mark H3K27ac signal (enhancer elements) of NB cell line NBL-S according to Hnisz and colleagues (Hnisz et al. 2013). Therefore, enhancer above the cut-off considered as SEs are marked as blue circles. HAND2 enhancer close to the breakpoint of MYCN rearrangements is highlighted (enlarged letters). SE assignment to HAND2 was supported by HAND2 4C-seq interaction data.

The analysis and ranking revealed strong SE clusters which were juxtaposed to *MYC* in all *MYC*-rearranged cell lines (Figure 37).

The enhancer region downstream of *HAND2* in NB69 cells, was ranked third after first ranked SE assigned to *MAML3* (Figure 37A). The *HAND2* SE region juxtaposed to *MYC* in SK-N-AS cells was defined as a SE although the H3K27ac signal was moderate as compared to other SE regions including *MYC* itself in these cells (Figure 37B). *ZMIZ1* was the highest ranked SE. Also the *HAND2* associated enhancer region in CHLA20 cells was defined as SE. The SE with the highest signal of H3K27ac was assigned to *GLIS1* (Figure 37C). The highest ranked SE in SH-SY-5Y genome-wide was the *EXOC4* enhancer which was juxtaposed to the *MYC* gene (Figure 37D).

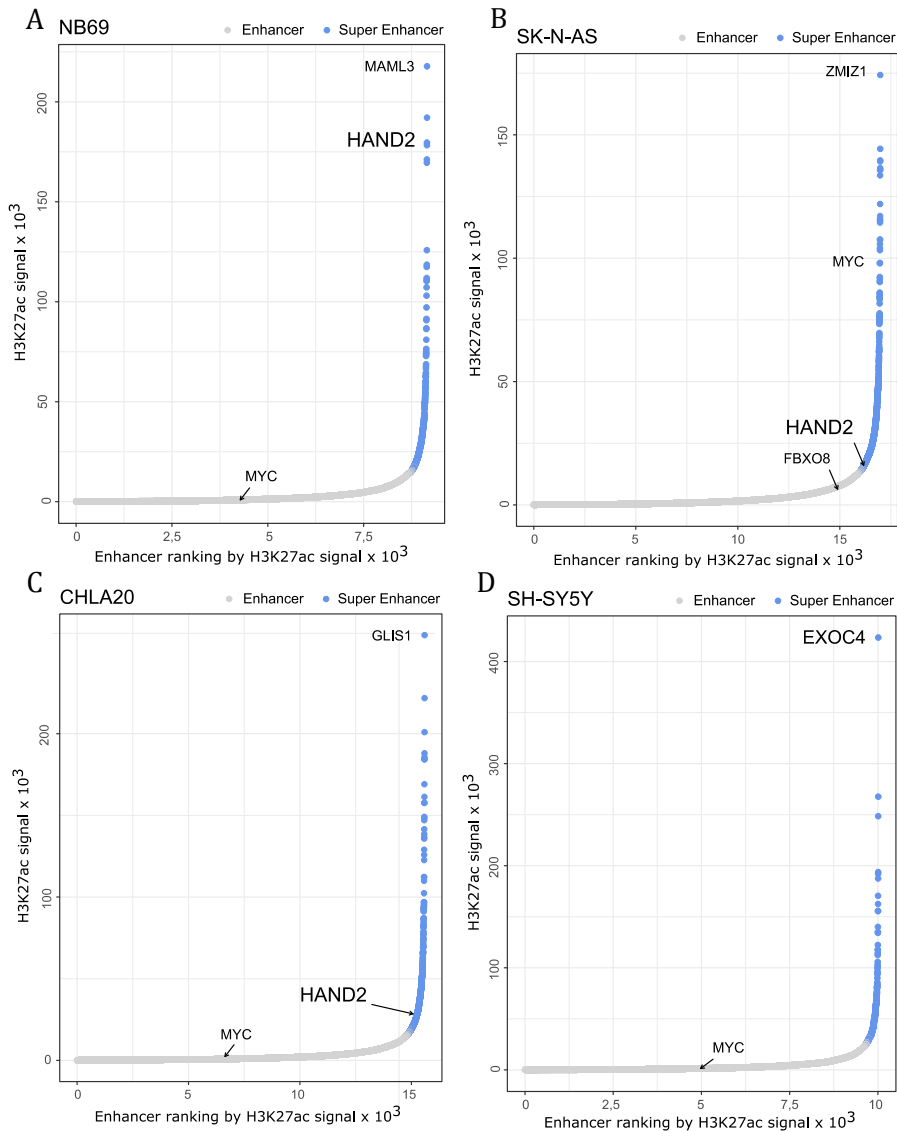


Figure 37: Ranking of histone mark H3K27ac signal.

Ranking of histone mark H3K27ac signal (enhancer elements) of NB cell line NB69 (A), SK-N-AS (B), CHLA20 (C) and SH-SY5Y (D) according to Hnisz and colleagues (Hnisz et al. 2013). Therefore, enhancer above the cut-off considered as SEs are marked as blue circles. HAND2 enhancer close to the breakpoint of MYC rearrangements is highlighted (enlarged letters). SE assignment to HAND2 was supported by HAND2 4C-seq interaction data.

RNAi-mediated knockdown of MYC and its impact on cell viability

Two different siRNAs were used for RNAi-mediated knockdown in four NB cell lines (SK-N-AS, SH-EP and GI-ME-N = MNA, NMB = *MYCN*-amplified). The knockdown experiments and subsequent analysis using two different assays were performed in two replicates (Figure 38).

The Celltiter Blue (CTB) viability assay measures the metabolic activity, while the colony formation assay after GIEMSA staining was used to assess colony formation capacity (2.2.5 and 2.2.6). SK-N-AS cells were most sensitive to RNAi-mediated knockdown of *MYC* using siRNA#2 in both assays with remaining colonies or viability of 57% and 82%, respectively (Figure 38) (74% remaining colonies and 87% remaining viability using siRNA#1). All other tested cell lines (SH-EP, GI-ME-N and NMB) persisted almost unaffected with remaining colonies or viability of more than 95%.

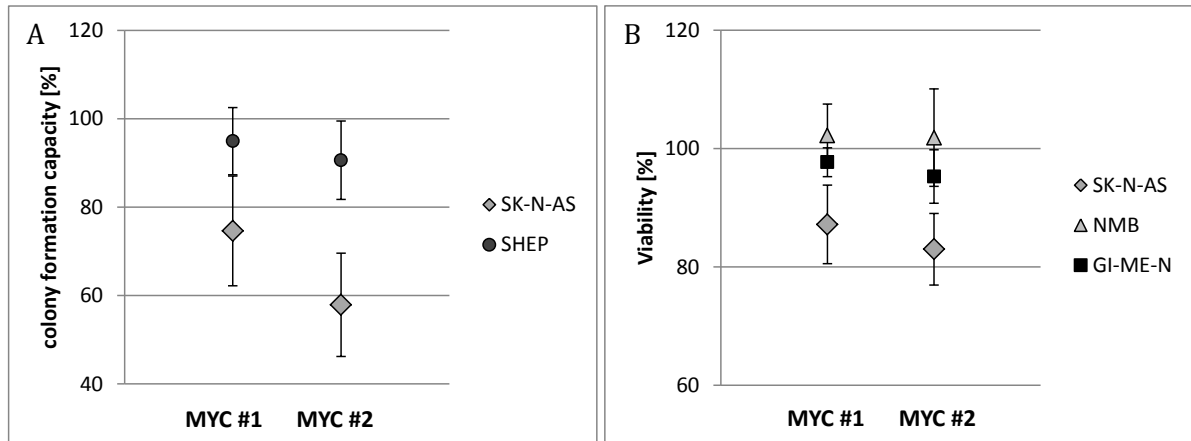


Figure 38: Impact of RNAi-mediated knockdown targeting MYC.

Impact of RNAi-mediated knockdown using two different siRNA targeting MYC on colony formation capacity (A) and cell viability (B) analyzed using colony formation assay after GIEMSA staining or CTB assay, respectively. RNAi-mediated knockdown was performed in four NB cell lines (SH-EP, GI-ME-N and SK-N-FI = MNA, NMB = MYCN-amplified).

Taken together, FISH data, of NB cell line NBL-S without *MYCN* copy number changes and high *MYCN* expression at mRNA and protein level, revealed a rearrangement affecting the *MYCN* gene. Likewise, FISH data of highly *MYC* expressing (*MYC*-non amplified) NB cell lines NB69, SK-N-AS, CHLA20/15 and SH-SY5Y revealed rearrangements affecting chromosome 8 in the vicinity of *MYC* in all cases. In tumors, high *MYCN* expression was associated with poor clinical outcome. ChIP-seq data revealed that highly active SE regions juxtaposed to *MYC(N)*, likely led to activated chromatin state and increased *MYC(N)* expression in these cells. Physical interaction of rearranged enhancer elements with the *MYC(N)* promoter was confirmed by 4C-seq analyses. RNAi-induced silencing of *MYC* revealed increased vulnerability in *MYC*-rearranged SK-N-AS cells as compared to *MYC* high expressing GI-ME-N and *MYCN*-amplified NMB, both without *MYC* rearrangement.

3.1.3 WGS identified rearrangements affecting oncogenes

Further on in this study, due to recurring events of rearrangements, a combined comprehensive set of WGS (n = 111) and RNA-seq data was screened with the support of EPISTEME analysis for further enhancer hijacking events including *IGF2BP1* (insulin-like growth factor 2 mRNA-binding protein 1) and *ATOH1* (atonal bHLH transcription factor 1). EPISTEME is a structural variation (SV) algorithm similar to the published DELLY, which identifies SVs by integrating paired-end and split-reads (Rausch et al. 2012). Further on, *IGF2BP1* and *ATOH1* rearrangements, identified in NB tumors via WGS data, were functionally validated in NB cell lines or tumors, respectively.

mRNA expression of IGF2BP1 in NB tumors and cell lines

The expression of *IGF2BP1* was compared between stage 1-3, stage 4, stage 4s (all MNA) and *MYCN*-amplified NB subgroups (Figure 39A). Stage 4s patients revealed a moderate higher expression of *IGF2BP1* compared to the other groups. With the exception of several outlier cases, *IGF2BP1* expression was low in all clinical subgroups. In NB cell lines, there were only few cell lines including CHLA90, SK-N-AS or SH-N-SH with almost undetectable *IGF2BP1* expression (Figure 39B). Most cell lines showed an elevated expression starting from an FPKM of 4.5 for SK-N-BE2(C), FPKM of 29 for IMR32 up to an FPKM of 35 and 45 for LS and NMB, respectively. The *IGF2BP1* top expressing cell line CLB-GA (FPKM of 86.8) displayed outlier expression of almost twice the *IGF2BP1* expression levels observed for second ranked NMB cells. In contrast to the moderate correlation of higher *IGF2BP1* expression with stage 4s MNA tumors, the 12 top expressing cell lines had amplified *MYCN* with the exception of CLB-GA.

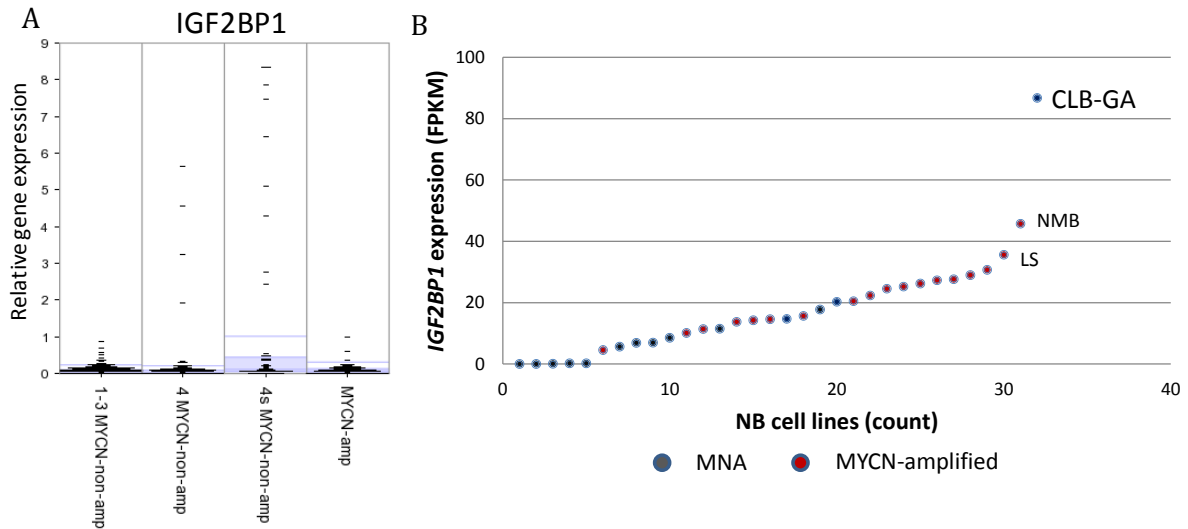


Figure 39: IGF2BP1 mRNA expression in NB.

(A) IGF2BP1 mRNA expression according to stage and MYCN status in NB tumors by RNA-seq ($n=498$; log₂ scaling). (B) IGF2BP1 mRNA expression in NB cell lines by RNA-seq ($n = 32$; Sample MNA (blue) or MYCN-amplified (red)).

Protein quantification of IGF2BP1 in NB cell lines

Western blot analysis was used to validate IGF2BP1 protein expression in a set of three selected NB cell lines representing the complete spectrum of *IGF2BP1* gene expression. There was no IGF2BP1 protein detectable in MNA cell line SK-N-FI while MYCN-amplified cell line IMR32 revealed elevated IGF2BP1 protein. The highest gene expression level of MNA cell line CLB-GA was validated on the protein level via western blot (Figure 40).

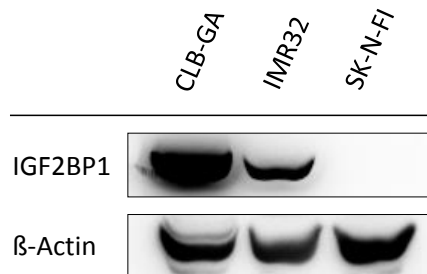


Figure 40: IGF2BP1 protein expression in NB cell lines.

IGF2BP1 protein expression was quantified by western blotting using β -actin as a loading control in three NB cell lines (CLB-GA and SK-N-FI = MNA, IMR32 = MYCN-amplified)

High IGF2BP1 expression was associated with poor survival of NB patients

Increased *IGF2BP1* levels significantly correlated with poor EFS as well as OS in a cohort of 498 primary NBs (Figure 41). EFS probability in *IGF2BP1* high expressing cases accounted roughly 0.6 in contrast to less than 0.85 in patients with low *IGF2BP1* expression while OS probability resulted in 0.7 and 0.9, respectively.

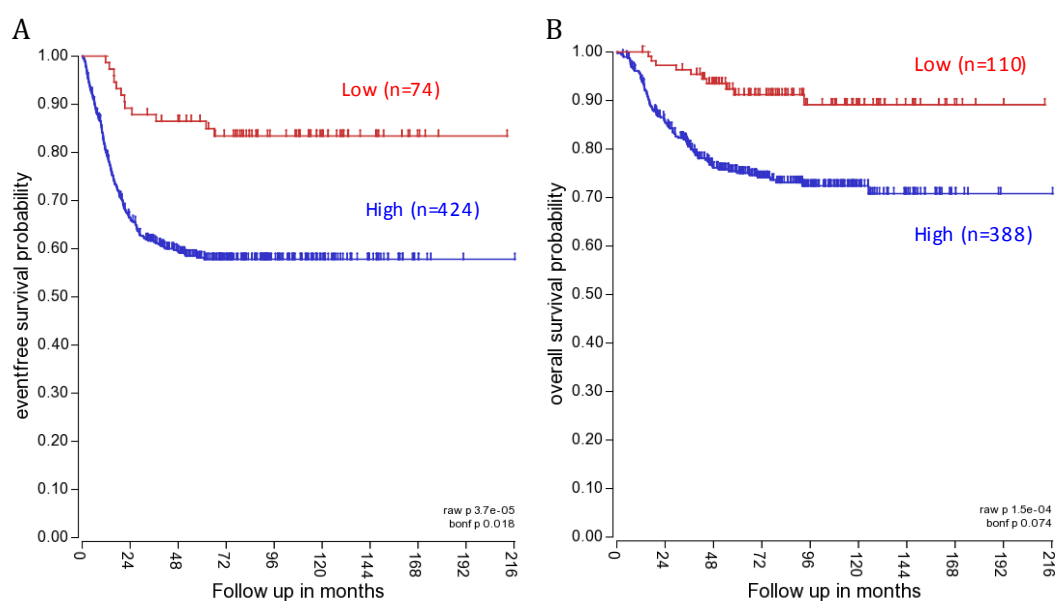


Figure 41: High IGF2BP1 is associated with poor survival.

Kaplan-Meier survival probability diagram indicates event-free survival (EFS) (A) and overall survival (OS) (B) in respect to IGF2BP1 expression in a set of 498 NB primary tumors. An uncorrected (raw p) and corrected (bonf p) p-value for multiple testing according to the Bonferroni method is shown. Cut-off values for dichotomization of IGF2BP1 expression were estimated by maximally selected log-rank statistics.

FISH identified structural aberrations involving IGF2BP1

The top *IGF2BP1* expressing cell line CLB-GA was examined for chromosomal rearrangements by FISH using *IGF2BP1* locus-specific probes (Figure 42). The composition of derivative (der) of chromosome 17, close to the *IGF2BP1* locus (pink), was examined for joined segments including the genomic region on chromosome 4 close to *HAND2* enhancers (green). Two derivatives ((der(4) and der(3)) containing joined elements of chromosome 17 segments including

IGF2BP1 and chromosome 4 segments including *HAND2* were identified. They consisted of one translocation event involving only two chromosome partners (t(4;17) and in the case of der(3) a complex rearrangement containing parts of chromosome 3, 4, 16 and 17 (t(3;4;16;18)).

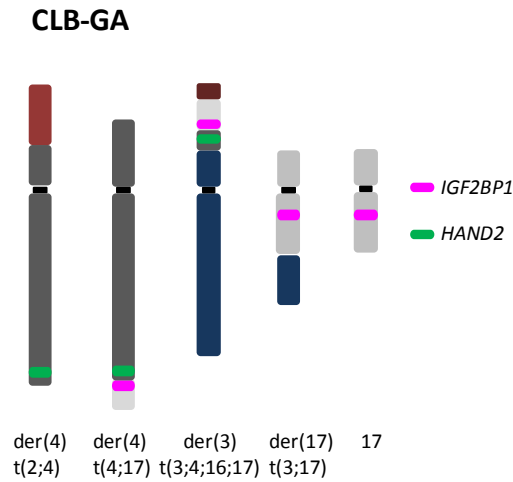


Figure 42: Structural aberrations involving IGF2BP1.

Fluorescence in situ hybridization (FISH) image of NB cell line CLBGA. IGF2BP1 or HAND2 specific probes were labelled in pink or green, respectively. Analyses were performed by Larissa Savelyeva.

Combined ChIP-seq of histone marks, 4C-seq and HiChIP identified interactions of active enhancers with IGF2BP1 promoter in rearranged cell line

4C-seq was used to validate the FISH defined *IGF2BP1* rearrangements by identifying functional and genome wide physical interaction of enhancer regions on chromosome 4, downstream of *HAND2*. Strong *trans*-interaction signals of enhancer regions at chromosome 4 and the *IGF2BP1* promoter were detected in cell line CLB-GA (Figure 43).

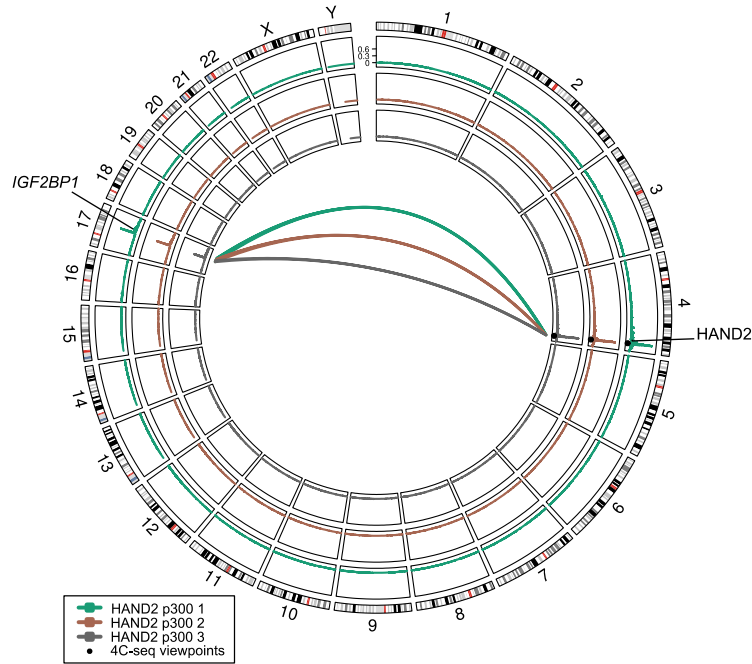


Figure 43: Genome-wide interactions involving *IGF2BP1*.

Genome-wide interaction profile of regulatory elements on chromosome 4 with the *IGF2BP1* promoter in NB cell line CLB-GA as determined via 4C-seq. Different viewpoints were applied (green = *HAND2* P300 position 1; orange = *HAND2* P300 position 2; grey = *HAND2* P300 position 3)

In addition to the 4C-seq-based validation of *trans*-interactions, which depends on a viewpoint and therefore has a limited capacity, we performed HiChIP allowing all possible interactions in CLB-GA cells (Figure 44). Antibodies targeting H3K27ac and SMC1A were used for enrichment. Three *trans*-interactions between chromosome 4 and 17 were detected in CLB-GA, while there was no interaction observed in SK-N-AS (Figure 44). The strongest *trans*-interaction (read count of 11 versus 6 and 7) confirmed the by 4C-seq identified interaction of the *IGF2BP1* promoter and the SE region downstream of *HAND2* with a defined breakpoint on chromosome 4 position 174.455.247-174.460.067 bps (hg19) and on chromosome 17 position 47.072.951-47.075.129 bps (hg19).

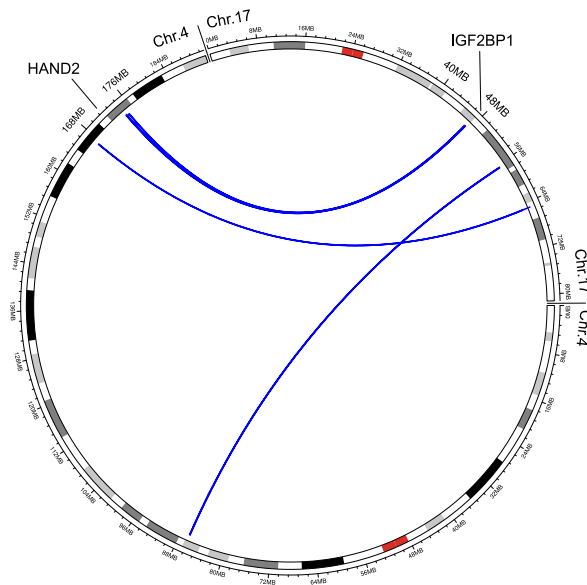


Figure 44: Genome-wide interactions involving *IGF2BP1*.

Genome-wide circos plot interaction profile of regulatory elements on chromosome 4 with chromosome 17 and the *IGF2BP1* promoter in NB cell line CLB-GA as determined via HiChIP. (H3K27ac and SMC1A antibodies were used for enrichment).

For a more detailed view on the donor- and acceptor regions of *IGF2BP1*-rearranged cells, all 4C-seq interactions were examined further at the loci and complemented with ChIP- and ATAC-seq profiles (Figure 45). The acceptor region of *IGF2BP1* on chromosome 17 consisted of open chromatin and was marked by active histone modifications (H3K4me, H3K4m1, H3K27ac and H3K36me). In addition, there was H3K27me3 enrichment at the *IGF2BP1* locus and the surrounding region, which is associated with repressive functions. A large cluster of H3K27ac and H3K4me1 histone marks peaks was detected downstream of the *HAND2* locus on chromosome 4. Since a H3K4me3 mark was absent, this region could be considered as an enhancer. Enhancer viewpoints on chromosome 4 (vp1-vp3) showed *cis*-interactions close to the chosen viewpoint of the *HAND2* promoter. The strongest *trans*-interactions with the *IGF2BP1* promoter occurred with vp2 and vp1 and the least interaction happened with vp3, which was closest to the breakpoint. Using the *HAND2* promoter as a viewpoint (vp5), *cis*-interactions were identified with the enhancer elements downstream as well as *trans*-interactions with the *IGF2BP1* promoter on chromosome 17. The 4C-seq tracks of the reciprocal assay starting from the *IGF2BP1* promoter (vp4) confirmed *trans*-interactions with the region of interest on chromosome 4.

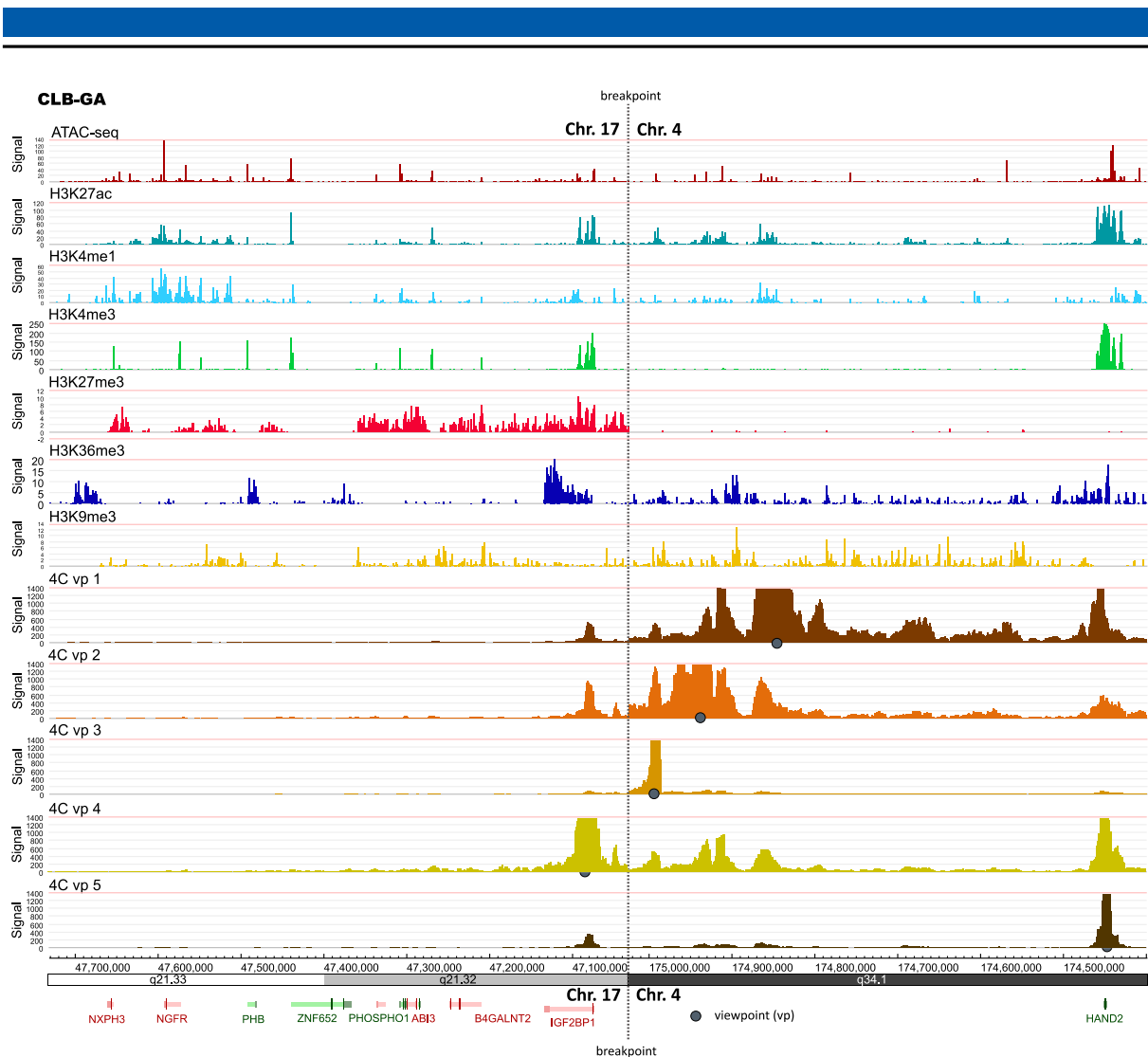


Figure 45: Epigenetic profiling of rearranged regions involving *IGF2BP1* locus.

Input normalized read counts of histone marks (*H3K4me3*, *H3K4me1*, *H3K27ac*, *H3K36me3*, *H3K27me3* and *H3K9me3*) and ATAC-seq peaks at the junction between chromosome 4 and chromosome 17 in SK-N-AS cells. Interaction profile peaks of potential enhancer elements (VP1-3 on chr. 4) as well as the *HAND2* promoter (VP 5 on chr. 4) with the *IGF2BP1* promoter (VP4 on chr. 17) were determined via circular chromatin conformation capturing with subsequent sequencing (4C-seq).

The H3K27ac enhancer profile of the *IGF2BP1*-rearranged cell line CLB-GA was analyzed towards SEs ranking according to the strategy proposed by Hnisz and colleagues (Hnisz et al. 2013). The analysis and ranking revealed that the enhancer cluster assigned to *HAND2* from Chr.4 juxtaposed to *IGF2BP1* indeed was a SE in CLB-GA cells (Figure 46). The SE with the highest signal of H3K27ac was assigned to *MVK* (mevalonate kinase) gene.

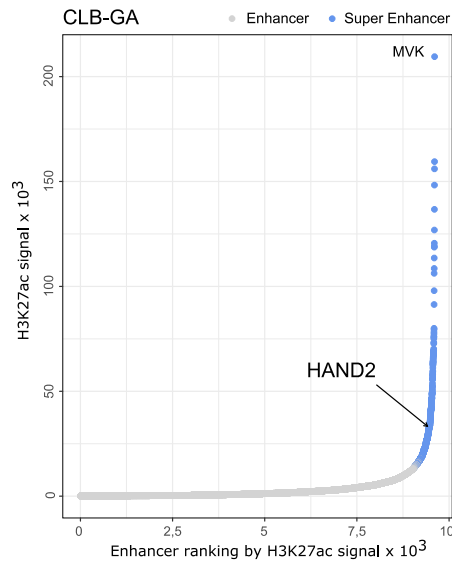


Figure 46: Ranking of histone mark H3K27ac signal.

Ranking of histone mark H3K27ac signal (enhancer elements) of NB cell line CLB-GA according to Hnisz and colleagues (Hnisz et al. 2013). Therefore, enhancer above the cut-off considered as SEs are marked as blue circles. HAND2 enhancer close to the breakpoint of IGF2BP1 rearrangements is highlighted (enlarged letters). SE assignment to HAND2 was supported by HAND2 4C-seq interaction data.

Taken together, using a combined approach of WGS (n = 111) and RNA-seq data including a downstream SV algorithm called EPISTEME, an *IGF2BP1* rearrangement in one tumor and one cell lines was identified. Functionally, high *IGF2BP1* expression was associated with poor clinical outcome in NB tumors. In addition, FISH data of NB cell line CLB-GA with high *IGF2BP1* expression at mRNA and protein level, revealed a rearrangement affecting the *IGF2BP1* gene. ChIP-seq data in CLB-GA cell line, revealed highly active SE regions juxtaposed to the *IGF2BP1* gene, likely leading to activated chromatin state and increased *IGF2BP1* expression. Physical interactions of rearranged enhancer elements with the *IGF2BP1* gene promoter were confirmed by 4C-seq and genome wide HiChIP studies.

mRNA expression of ATOH1 in NB tumors and cell lines

The gene expression of *ATOH1* was compared between stage 1-3, stage 4, stage 4s (all MNA) and *MYCN*-amplified NB subgroups (Figure 47A). With the exception of some outlier expressers, present in all but the 4S subgroup, no subtype-specific increased gene expression for *ATOH1* was detectable. In NB cell lines, only SK-N-FI (FPKM = 3.9) showed increased *ATOH1* expression (Figure 47B). Most NB cell lines had an expression level below FPKM of 1 or no *ATOH1* expression at all.

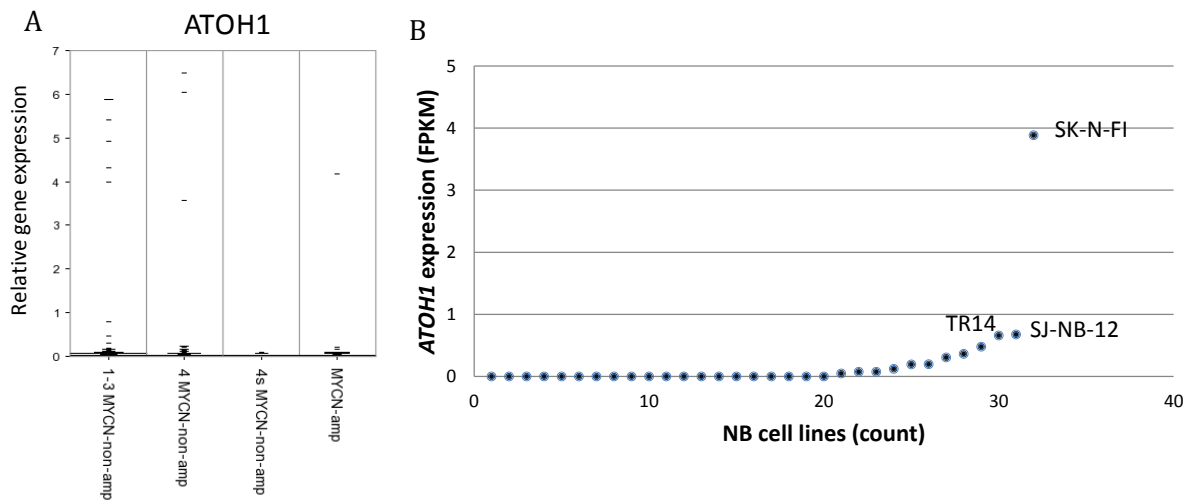


Figure 47: ATOH1 mRNA expression in NB.

ATOH1 mRNA expression according to stage and *MYCN* status in NB tumors by RNA-seq ($n = 498$; log₂ scaling). (B) *ATOH1* mRNA expression in NB cell lines by RNA-seq ($n = 32$).

High ATOH1 expression was associated with poor survival of NB patients

Increased *ATOH1* levels significantly correlated with poor EFS as well as OS in a cohort of 498 primary NBs (Figure 48). EFS probability in *ATOH1* high cases accounted roughly 0.55 in contrast to less than 0.80 in patients with low *ATOH1* expression while OS probability resulted in 0.65 and 0.9, respectively.

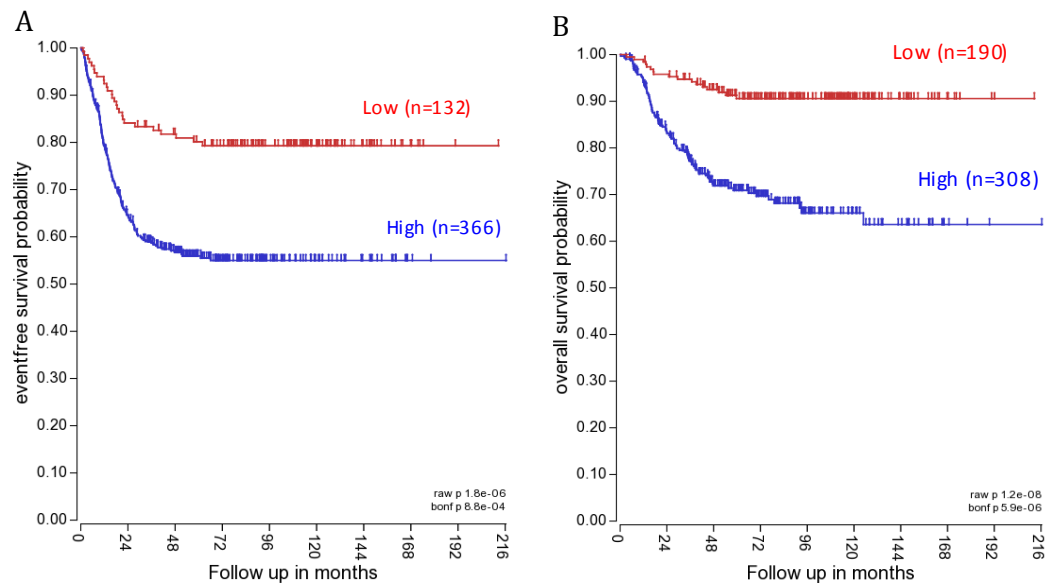


Figure 48: High ATOH1 is associated with poor survival.

Kaplan-Meier survival probability diagram indicates event-free survival (EFS) (A) and overall survival (OS) (B) in respect to ATOH1 expression in a set of 498 NB primary tumors. An uncorrected (raw p) and corrected (bonf p) p-value for multiple testing according to the Bonferroni method is shown. Cut-off values for dichotomization of ATOH1 expression were estimated by maximally selected log-rank statistics.

*ChIP-seq of histone marks identified active enhancers
close to the junctions in rearranged tumor*

An intra-chromosomal (chromosome 4) rearrangement of *HAND2* to *ATOH1* was identified in two NB tumors via WGS data. For a more detailed view on the donor- and acceptor region, epigenetic profiling was examined performing H3K4me3 and H3K27ac ChIP-seq analysis in one of the two NB tumors (Figure 49). The acceptor-side breakpoint on chromosome 4 was located approximately 50 kB downstream of the *ATOH1* gene locus, which was fused to the donor site at the *CEP44* and *FBXO8* locus on chromosome 4. Upstream of *FBXO8* there was a cluster of H3K27ac histone modification marks without any active TSS, which would be considered as enhancer and stretches towards the *HAND2* gene (Figure 49).

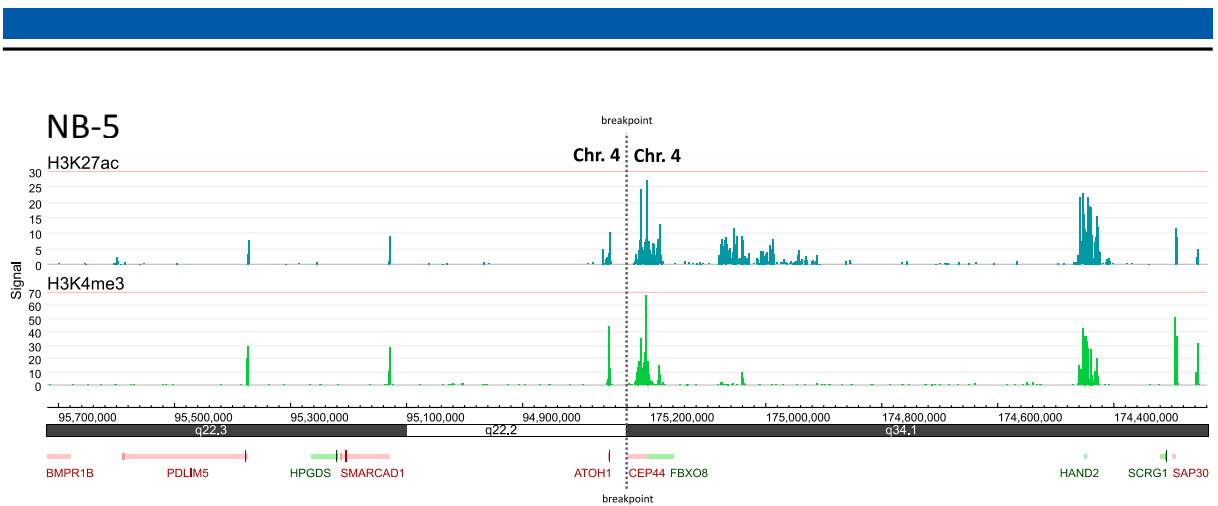


Figure 49: Epigenetic profiling of rearranged regions involving *ATOH1* locus.

Input normalized read counts of histone marks *H3K4me3* and *H3K27ac* within the rearranged genomic regions of NB primary tumor NB-5.

The *H3K27ac* enhancer profile of the *ATOH1*-rearranged tumor NB-5 was analyzed towards SE ranking according to the strategy proposed by Hnisz and colleagues (Hnisz et al. 2013). The ranking revealed strong enhancer regions that were joined to the *ATOH1* gene segment (Figure 37). The donor region of *HAND2* associated enhancer was ranked higher than the *ATOH1* assigned enhancer. The SE with the highest signal of *H3K27ac* was assigned to *CELF4* (CUGBP elav-like family member 4).

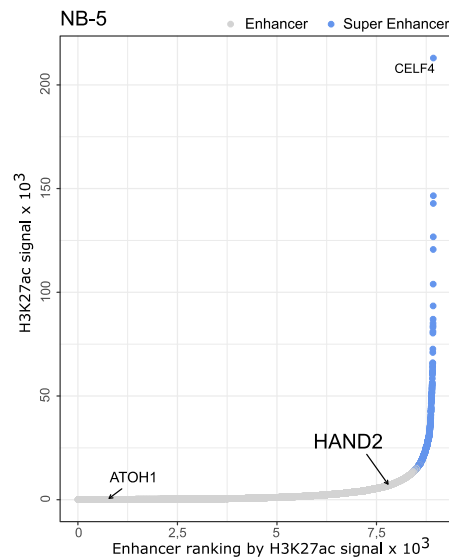


Figure 50: Ranking of histone mark *H3K27ac* signal.

Ranking of histone mark *H3K27ac* signal (enhancer elements) of NB primary tumor NB-5 according to Hnisz and colleagues (Hnisz et al. 2013). Therefore, enhancer above the cut-off considered as SEs are marked as blue circles. *HAND2* enhancer close to the breakpoint of *ATOH1*

rearrangements is highlighted (enlarged letters). SE assignment to HAND2 was supported by HAND2 4C-seq interaction data.

Taken together, using a combined approach of WGS (n = 111) and RNA-seq data including a downstream SV algorithm called EPISTEME, an *ATOH1* rearrangement in two tumors was identified. Functionally, high *ATOH1* expression was associated with poor clinical outcome in NB tumors. In one of the two identified primary tumors, ChIP-seq data revealed highly ranked enhancer regions juxtaposing the *ATOH1* gene, which likely leads to activated chromatin state and increased *ATOH1* expression.

3.1.4 HAND2 SE cluster is recurrent donor-region in rearrangement events

The SE cluster downstream of *HAND2* and upstream of the *FBXO8* gene locus was described in this study as a recurrent donor-region juxtaposing to oncogenes in NB cell lines and tumors, likely leading to increased expression of enhancer targets (Figure 51). *HAND2* SE rearrangements were discovered as enhancer hijacking events joining to the *MYCN* locus (NB cell line NBL-S), *MYC* locus (NB cell lines NB69, SK-N-AS and CHLA20), *IGF2BP1* locus (NB cell line CLB-GA), *ATOH1* locus (NB primary tumor NB-5) and *TERT* locus (NB primary tumor NB-4). In all cases, ranking of histone mark H3K27ac signal for SE definition (according to Figure 7) determined the region between *HAND2* and *FBXO8* as a strong enhancer region juxtaposed to the described oncogenes. Intriguingly, the *HAND2* enhancer stretch was ranked as the third strongest SE region genome-wide in NB69 cells.

*ChIP-seq of histone marks and RNA-seq identified active enhancers
resulting in increased gene expression in rearranged cell lines*

Figure 51 shows the fusion junction of the *MYC* and *HAND2* SE rearrangement in NB cell lines CHLA20, NB69 and SK-N-AS. In CHLA20 and NB69 the breakpoint is located 100 and 50 kbps apart the *MYC* gene locus, respectively, while in SK-N-AS it is localized approximately one Mb downstream. The mRNA expression of *MYC* and nearby genes was evaluated in the context of a NB cell line set (n = 32) highlighting five cell lines with a rearrangement event (NB69, CHLA29 and SK-N-AS = *MYC* rearrangement; CLB-GA = *IGF2BP1* rearrangement, NBL-S = *MYCN* rearrangement) (Figure 51 – lower panel). The genes upstream of *MYC* displayed overall low

expression in the cell line cohort. Exceptions were observed for *PCAT2* (prostate cancer associated transcript 2), *CCAT1* (colon cancer associated transcript 1) and *POU5F1B* (POU class 5 homeobox 1B) (FPKM = 2.7; 0.4; 0.7) or *CASC8* and *CASC11* (cancer susceptibility 8 and 11) (FPKM = 0.4; 0.5) displaying outlier expression in NGP cells or MHH-NB-11 cells, respectively (Figure 51 - lower panel). CHLA20 and NB69 cells, harboring breakpoints close to *MYC*, expressed high levels of *MYC* in contrast to lower *MYC* expression in SK-N-AS cells. Expression of genes was decreasing, downstream of the *MYC* locus on chromosome 8, from *PVT1* to *TMEM75* and further from *CCDC26* to *GSDMC* (Gasdermin C), which were both excluded on the translocated allele by the three *MYC*-rearranged cell lines. Outlier expression was observed for *PVT1* (FPKM = 7.6) in MHH-NB-11 cells, for *TMEM75* (FPKM = 3.3) in SMS-KCNR cells and for *CCDC26* and *GSDMC* (FPKM = 0.7; 0.6) in TR14 cells. Comparing *PVT1* expression in the *MYC*-rearranged cell lines, identified highest gene expression in CHLA20, which is truncated, followed by SK-N-AS cells (FPKM = 4.4; 2.5). In cell line NB69 *PVT1* was not included in the translocated region and *PVT1* displayed the lowest expression (FPKM = 2.1) as compared to the other *MYC*-rearranged cell lines (Figure 51). A similar trend was observed for *TMEM75*, which is located further downstream on chromosome 8. *TMEM75* was solely included in the rearrangement of SK-N-AS cells (breakpoint on chromosome 8 position 129.902.921 bps; hg19) and displayed a slightly increased expression in SK-N-AS (FPKM = 0.6) as compared to CHLA20 and NB69 cells (FPKM = both 0.1) (Figure 51).

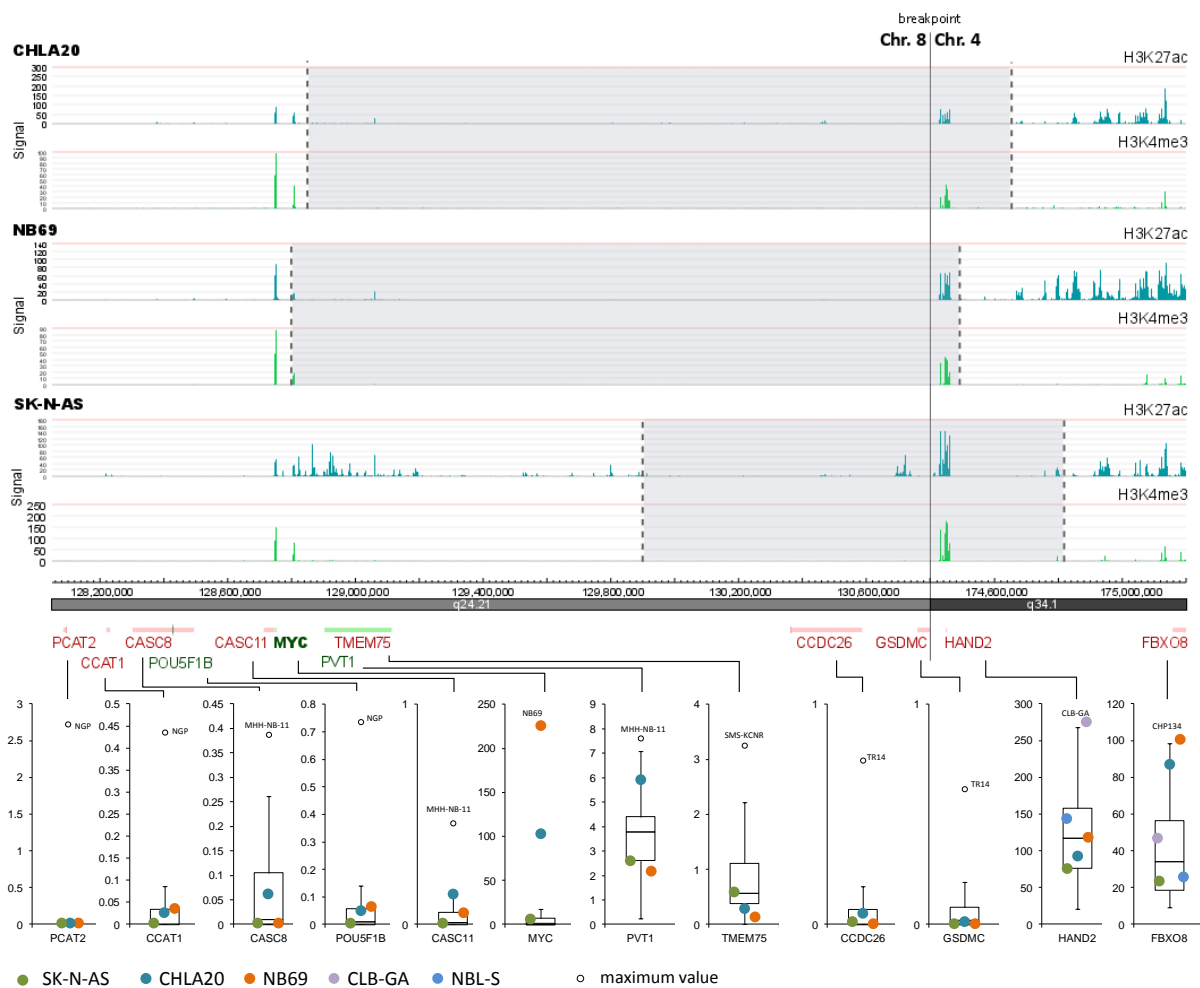


Figure 51: Epigenetic profiling and mRNA expression of genes within rearranged regions.

Input normalized read counts of histone marks H3K4me3 and H3K27ac at the junction between chromosome 4 and chromosome 8 in NB cell lines CHLA20, NB69 and SK-N-AS and mRNA expression values (FPKM) of set of NB cell lines ($n = 32$; highlighted with colors). The area shown greyed out is excluded by the newly formed cell line-specific junction between chromosome 4 and chromosome 8. In addition mRNA expression of HAND2 and FBXO8 of NB cell lines CLB-GA ($t(4;17)$) and NBL-S ($t(2;4)$) was colored.

The genes *HAND2* and *FBXO8*, flanking the SE cluster on chromosome 4, were highly expressed in the whole set of NB cell lines (Figure 51 – upper panel). Extraordinary high *HAND2* expression was observed in *IGF2BP1*-rearranged cell line CLB-GA (Figure 51 – lower part). According to the CLB-GA 4C-seq interaction data (Figure 45), the *HAND2* gene retained in contact with the downstream enhancer cluster and joined upstream with chromosome 17 segment containing the *IGF2BP1* gene. In *MYCN*-rearranged NBL-S cells, *HAND2* interacted with the strong *MYCN* enhancer downstream of *MYCN* (Figure 31). In *MYC*-rearranged cell lines

CHLA20, NB69 and SK-N-AS, *HAND2* expression was just average or below with an FPKM between 72 up to 87 within the panel of NB cells (Figure 51 – lower panel).

Protein quantification of HAND2 in NB cell lines

HAND2 protein expression was analyzed via western blotting in *HAND2*-rearranged cell lines NB69 and SK-N-AS (*MYC*-rearranged), NBL-S (*MYCN*-rearranged) and CLB-GA (*IGF2BP1*-rearranged) (Figure 52). Non-rearranged SK-N-FI cells served as a control. NBL-S expressed highest levels of *HAND2* protein, followed by SK-N-FI. In cell lines CLB-GA, SK-N-AS and NB69 almost no *HAND2* protein was detected.

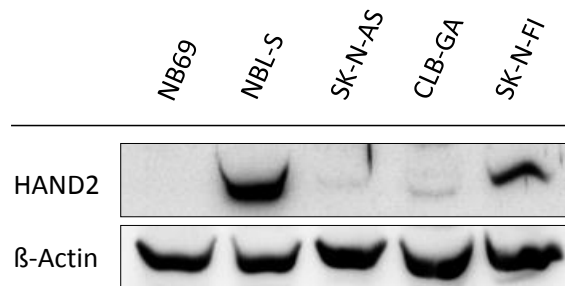


Figure 52: HAND2 protein expression of NB cells.

HAND2 protein expression was quantified by western blotting using β -actin as a loading control in a set of *MYCN*-non amplified (MNA) NB cell lines.

RNAi-mediated knockdown of HAND2 and its impact on cell viability

RNAi-mediated knockdown of *HAND2* was performed in two replicates using two different siRNAs in *HAND2*-rearranged NB cell lines SK-N-AS (MNA) and NBL-S (*MYCN*-amplified). The impact on cell growth was analyzed via colony formation assay of GIEMSA stained cells. Both siRNAs decreased cell growth in both cell lines (Figure 53). However, *HAND2* siRNA#1 had stronger impact on reduction of colony formation capacity with less than 70% in NBL-S and almost 80% in SK-N-AS cells. In contrast, siRNA#2 decreased colony formation capacity to 90% in the case of SK-N-AS and down to 85% in NBL-S cells.

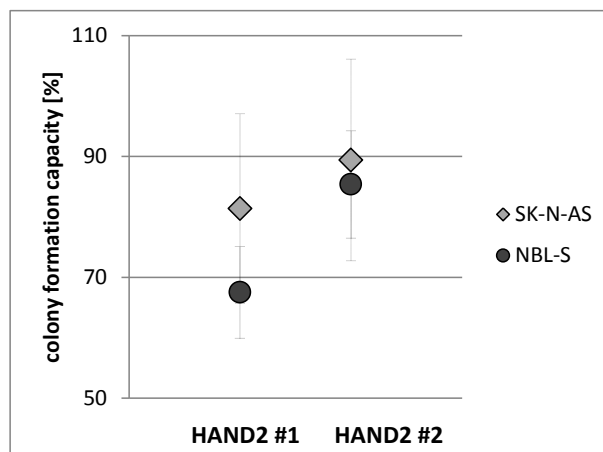


Figure 53: Impact of RNAi-mediated knockdown targeting *HAND2*.

Impact of RNAi-mediated knockdown using two different siRNA targeting *HAND2* by subsequent colony formation assay analyzed after GIEMSA staining in SK-N-AS and NBL-S cells (both MNA).

Taken together, these data indicated that SE regions between *HAND2* and *FBXO8* genes were recurrently translocated into the proximity of oncogenes like *TERT*, *MYCN*, *MYC*, *IGF2BP1* and *ATOH1* in NB cell lines and primary tumors. Rearrangements of *HAND2* SE elements caused massive chromatin remodeling and upregulation of adjacent genes. The data indicated that the characteristic expression gains of genes in the acquired genomic context and expression losses of the genes in the old genomic context were breakpoint dependent (Figure 51).

3.2 Global super enhancer landscape analysis in NB

To get deeper insights into NB epigenetics and to define the NB SE landscape *in vivo*, a protocol for ChIP-seq of primary tissues was established in the course of the present study. Continuous optimization and streamlining of this protocol allowed the analysis of 60 tumor ChIP-seq profiles of histone mark H3K27ac. All bioinformatic work of this study was performed in collaboration with the department of cancer regulatory genomics at the DKFZ headed by Carl Herrmann.

SEs were defined using the ROSE tool, based on H3K27ac peaks called by MACS2 and only peaks lacking H3K4me3 signal or those that are at least 2.5 kbs away from any H3K4me3 peak were considered. A tumor-specific SEs consensus list was generated containing all SEs identified in at least two samples (n = 1959).

3.2.1 Epigenetic profiling defines NB SE landscape

The ChIP-seq-analyzed cohort consisted of 60 samples of which 49 were primary NBs (including 3 matched relapsed cases), eight were relapsed cases and three were metastases (all from one relapsed case) (Figure 54). The NB primary cohort consisted of 20 *MYCN*-amplified and 40 MNA tumors. According to INSS staging 25 cases were considered as 1-3 and 4s stage, which were referred to hereinafter as low- to intermediate-risk due to missing risk information within this study. Likewise, 35 stage 4 cases were also referred to as high-risk patients. 52 patients were older and 8 patients were younger than 18 months at diagnosis. The NB primary tumor ChIP-seq cohort was complemented with ChIP-seq profiles from 26 NB cell lines (*MYCN* amplified = 10; MNA = 14) including two neural crest-derived cell lines provided by Hauser and colleagues (Hauser et al. 2012).

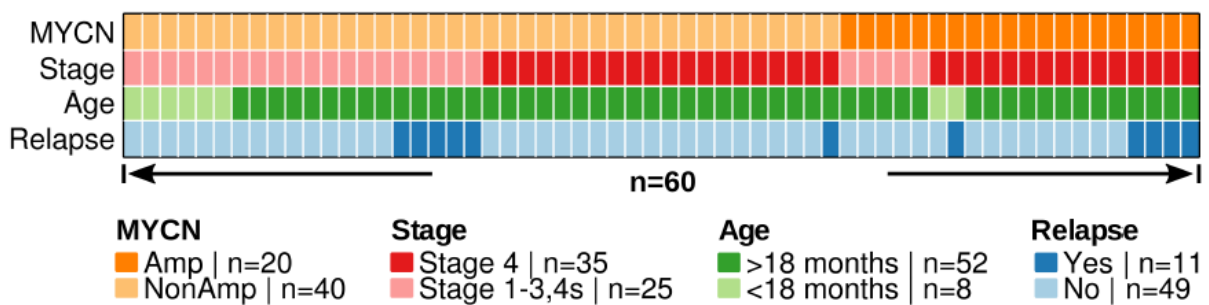


Figure 54: NB tumor cohort composition of SE landscape.

Composition of the NB tumor ChIP-seq cohort ($n = 60$) in respect *MYCN* status (*MYCN*-amplified and MNA), stage (INSS), age (age at diagnosis) and relapsed case.

To estimate the expected total amount of SE regions in NB tumors and their coverage in the 60 tumor cohort, saturation analysis revealed that 130 Mbs of predicted 200 Mbs SE regions (65%) were covered (Figure 55A). The model estimated a sample size of more than 900 primary tumor samples to cover all expected SE regions. To evaluate the specificity of our NB SE cohort, comparison analyses with public available profiles from 24 human primary tissues and 15 cell lines were performed (Hnisz et al. 2013). Therefore, the Jaccard index was calculated, which is a statistic tool to demonstrate the overlap of sample sets in terms of similarities. Cross-tissue comparison of NB-specific SE regions revealed a maximum overlap of 11% with SEs (Figure 55B). The tissues overlapping most with NB-specific SE regions were lung, osteoblasts and brain tissues. Comparing median expression of the predicted NB-specific SE target genes with public available expression profiles from 53 normal and 34 tumor tissues (GTEx (<https://gtexportal.org/home/>), TCGA (<http://cancergenome.nih.gov/>) and TARGET

(<https://ocg.cancer.gov/programs/target>) identified highest overlap with an external NB data set followed by brain and nerve tissue (Figure 55C).

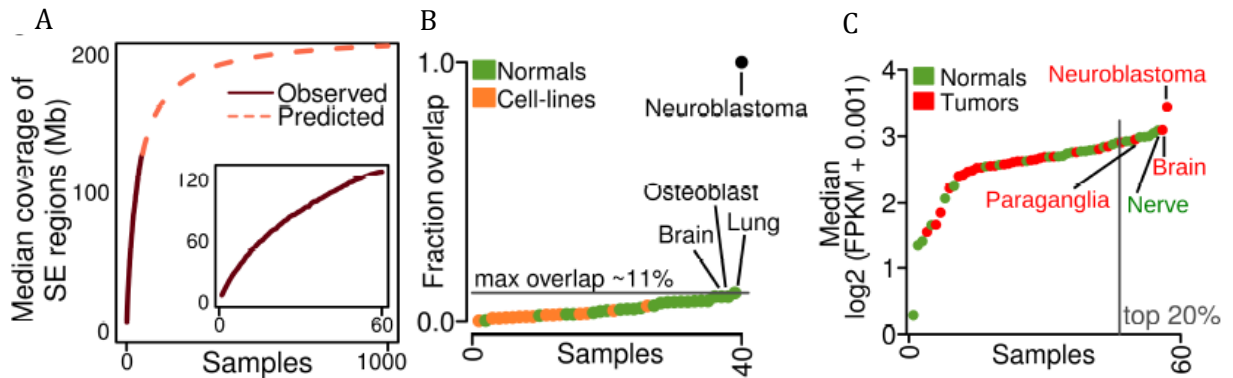


Figure 55: Tissue specificity of NB SE cohort.

(A) SE regions in Mbs covered by the NB tumor ChIP-seq cohort ($n = 60$) and predicted saturation of region coverage computed by Michaelis-Menten model fit. (B) Cross-tissue comparison of the NB SE regions with SE regions of other human tissues and cell lines. (C) Median expression of the predicted SE target gene cohort compared to publicly available profiles from 53 normal (GTEx - <https://gtexportal.org/home/>) and 34 tumor tissues including NB (TCGA - <http://cancergenome.nih.gov/> and TARGET- <https://ocg.cancer.gov/programs/target>).

The median cohort-wide signal intensity of the enhancer mark H3K27ac was calculated for all primary NB SEs and was used for a genome-wide ranking of NB SEs and their assigned target genes ($n = 1424$ SE target genes) (Figure 57). The identification of SE target genes was performed hierarchically, starting by prioritizing physical chromatin interactions that were confirmed by experimental HiChIP data in SK-N-AS and KELLY NB cells (hichip; green). Assignment of SE target genes was followed by public available HiC profiles (hic; dark purple) (Rao et al. 2014), correlation of the H3K27ac signal intensity with gene expression within the tumor samples (correlation; orange) and finally, proximity of SE to target gene (Figure 57).

The SE to target gene assignment strategy was exemplified for *CCND1* and *MAML3*, two top ranked candidates, in SK-N-AS and KELLY NB cells and NB primary tumor consensus H3K27ac and consensus SEs tracks (Figure 56). In both cell lines, H3K27ac-defined SE regions harbored open chromatin as indicated by enrichment of ATAC-seq peaks in these regions. HiChIP chromatin interaction data, using H3K27ac and SMC1A for enrichment, confirmed physical interactions between the SEs and the *CCND1* (cyclin D1) or *MAML3* TSS, as indicated by the arches (Figure 56). It is of note, that similar enrichment peaks were observed in consensus H3K27ac and SE data of primary NB tumors at these locations, further confirming the results obtained here.

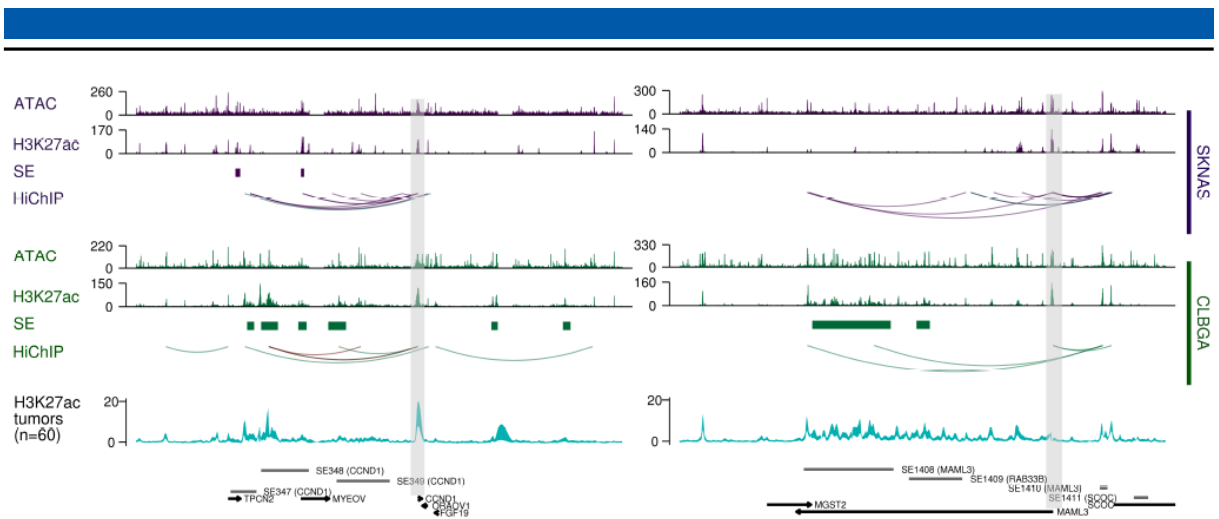


Figure 56: Validation of SE to target gene assignment using chromatin conformation data.

Epigenetic landscape using ATAC-seq and H3K27ac ChIP-seq (H3K27ac) profiles, MACS2-called SEs (horizontal bars) and physical interactions (HiChIP chromatin interactions (HiChIP; arches)) of two top ranked SE regions (CCND1 and MAML3) in NB cell lines SK-N-AS (purple) and CLB-GA (green). A consensus H3K27ac track (turquoise) and consensus SEs (grey horizontal bars) including predicted target genes are depicted at the bottom. Promoter regions of CCND1 and MAML3 are shaded in grey and gene orientation is given by black arrows.

Among the top ranked SE assigned target genes several previously published and well described NB-specific genes like *MYCN*, *ALK*, *CAMTA1* and *CCND1* were identified (Figure 57) (Schwab et al. 1983; Molenaar et al. 2003; Caren et al. 2008; Chen et al. 2008; George et al. 2008; Janoueix-Lerosey et al. 2008; Mosse et al. 2008; Henrich et al. 2011). Further genes previously associated with NB SEs, including *MAML3*, *GATA3*, *LMO1*, *HAND2* and *PHOX2B* were highly ranked on the extended SE list, which further confirms the robustness and reproducibility of the underlying epigenetic data (Figure 57 - upper panel) (Oldridge et al. 2015; Boeva et al. 2017; van Groningen et al. 2017).

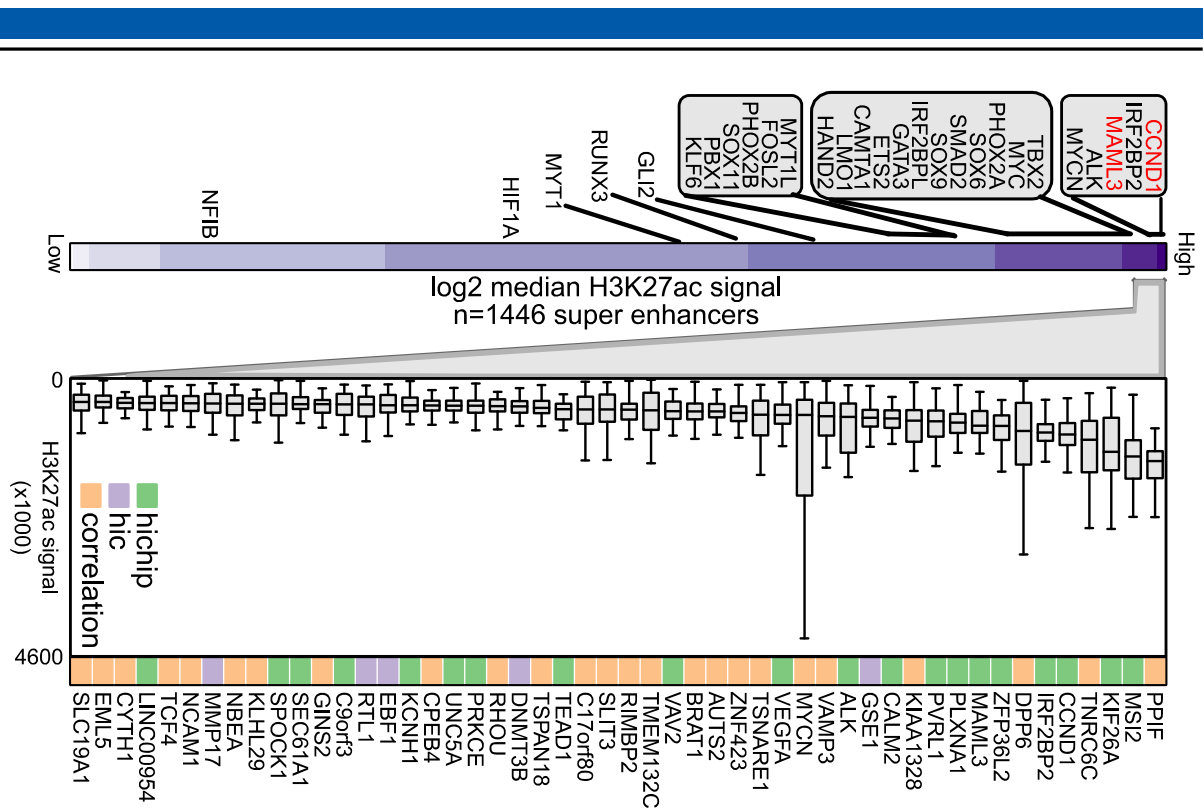


Figure 57: Ranking of target gene assigned SEs in NB tumor cohort.

Ranked boxplots of top 50 SEs in NB primary tumors derived from H3K27ac ChIP-seq profiles ($n = 60$; bottom panel). Whiskers denote the interval within 1.5 times the interquartile range (box edges) of the median (center line). Target genes were predicted hierarchically by (i) HiChIP interactions (hichip; green), (ii) public Hi-C profiles (hic; purple) (Rao et al. 2014) (iii) H3K27ac signal versus expression correlation (correlation; orange) or (iv) SE target gene proximity (closest). An activity map of the whole set of 1424 SEs is given in the top panel, highlighting genes previously assigned to NB SEs.

3.2.2 SE defined NB epigenetic subtypes

H3K4me3-subtracted H3K27ac ChIP-seq profiles of primary tumors were further used to define the SE landscape of NB by applying non-negative matrix factorization (NMF) analysis (Figure 58). NMF was described by Huebschmann and colleagues in 2017 and can be used to subdivide higher-dimensional datasets into several lower-dimensional signatures (Huebschmann et al. 2017). Each individual sample (tumor or cell line H3K27ac ChIP-seq profiles) that was included in the data set, received an exposure value of each signature. Samples with similar exposure patterns composed a subset of samples. For the tumor NMF, four signatures produced the most stable factorization and subdivision of the tumor cohort (Figure 58). According to the clinical annotation (Figure 54; MYCN status, INSS stage, age and relapse) MYCN signature defined a subset of MYCN-amplified samples (MYCN). MNA-LR and MNA-HR were both composed of MNA samples, which were associated with low-risk disease (MNA-LR)

or high-risk disease (MNA-HR), respectively. Many samples showed exposure to more than one signature, which impeded a clear signature assignment for some cases. The remaining signature revealed no clear enrichment for one of the clinical annotations. Due to missing clinico-biological parameters describing the subgroup that was formed by the remaining signature, gene set enrichment analysis (GSEA) for gene sets defined by all four signatures SEs was performed (Figure 58). The GSEA revealed significant enrichment of epithelial mesenchymal transition (EMT) terms and cell migration for this mesenchymal (Mes) signature, which was not the case for all other signatures. MNA-HR signature was enriched for gene sets associated with transcriptional regulation and signaling while MNA-LR and MYCN signatures showed no significant enrichment.

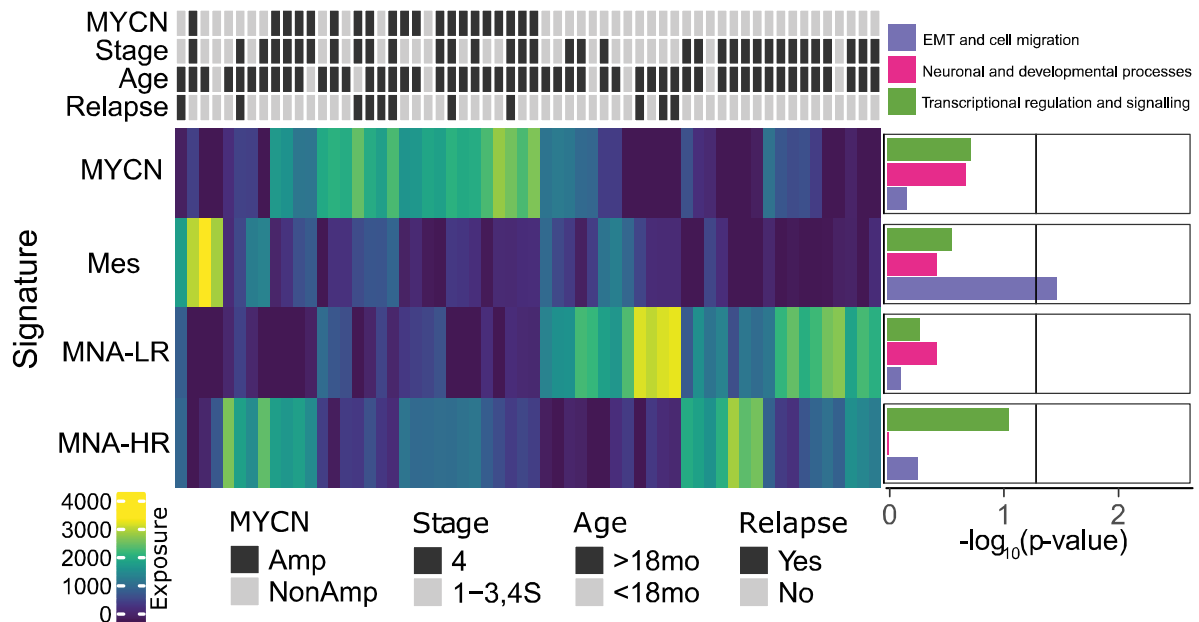


Figure 58: NMF analysis of NB tumors.

Non-negative matrix factorization (NMF) analysis of NB tumors ($n = 60$) based on H3K27ac histone mark ChIP-seq signal at NB SEs leading to four signatures (MYCN, Mes, MNA-LR and MNA-HR). Degree of exposure from high to low is depicted by a color gradient from yellow to blue. Information on clinico-biological parameters of the tumors is given as previously described (Figure 54) regarding MYCN status (MYCN amplified = black; MNA = grey), stage (INSS stage 1-3 and 4s (grey) or 4 (black)), age (age at diagnosis or 18 months (black) or younger 18 months (grey)) and relapsed case (yes (black) or no (grey)). Gene set enrichment analysis (GSEA) of the predicted SE target genes defining the NMF signatures are given on the right. GSEA was performed using the MSigDB (<https://software.broadinstitute.org/gsea/msigdb/>).

For the cell lines, three NMF signatures produced the most stable factorization and subdivision of the cohort (Figure 59). With the exception of MYCN-amplified SMS-KCNR, which was assigned

to MNA signature, all *MYCN*-amplified cell lines were assigned to MYCN signature, defining this signature as *MYCN*-amplified (MYCN). The Mes signature revealed high exposure values for all contained samples and consisted exclusively of MNA samples. With the exception of SMS-KCNR, MNA signature displayed highest exposure values for MNA samples. NB cell lines are exclusively derived from high-risk tumors so that, in analogy to tumor MNA-HR, signature was termed cell line MNA signature. To identify specific subtype characteristics of the three cell line NMF signatures, GSEA was performed (Figure 59). Similar to GSEA of tumor NMF, the non-clinico-biologically defined Mes cell line signature was significantly enriched for terms associated with EMT and cell migration and minor enrichment for the two other gene sets. Both signatures, MYCN and MNA were enriched for terms linked to transcriptional regulation and signalling while MNA showed additionally enrichment for gene sets associated with neuronal and developmental processes.

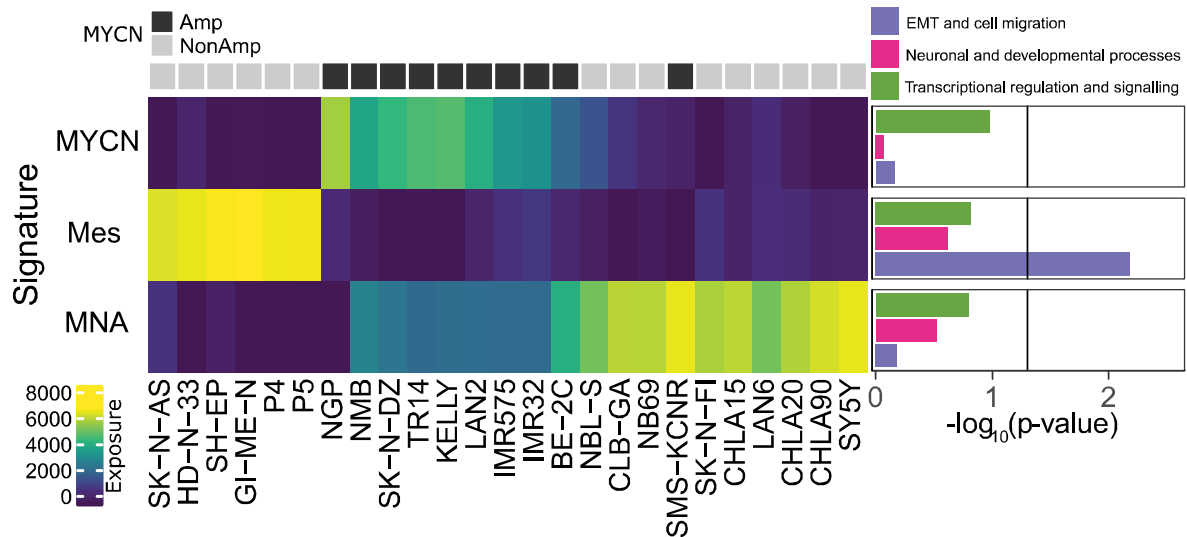


Figure 59: NMF analysis of NB cell lines.

Non-negative matrix factorization (NMF) analysis of the NB cell lines ($n = 25$) based on H3K27ac histone mark ChIP-seq signal at NB SEs leading to three signatures (MYCN, Mes and MNA). Information is given on the MYCN status (MYCN amplified (black) and MNA (grey)). Gene set enrichment analysis (GSEA) of the predicted SE target genes defining the NMF signatures are given on the right. GSEA was performed using the MSigDB (<https://software.broadinstitute.org/gsea/msigdb/>).

Tumor and cell line H3K27ac histone mark ChIP-seq data were combined and analyzed by t-distributed stochastic neighbor embedding (t-SNE) to validate NMF-defined subgrouping (Figure 60). Another aspect was to assay for stable subgroups, which would be reflected by defined clusters made up of tumors and cell lines. Intriguingly, tumors and cell lines previously

assigned to a Mes signature by NMF and GSEA (Mes in Figure 58 and Figure 59) were arranged together in a cluster and distinct from all other samples. The mesenchymal tumor and cell line samples mixed cluster was the only intermixed cluster in the t-SNE analysis. Cell line samples of MYCN and MNA NMF signature (Figure 58) grouped close together and did not mix with tumor samples. Similarly, tumor samples of MYCN, MNA-HR and MNA-LR NMF signature were arranged without obvious pattern and without mixing with cell line samples.

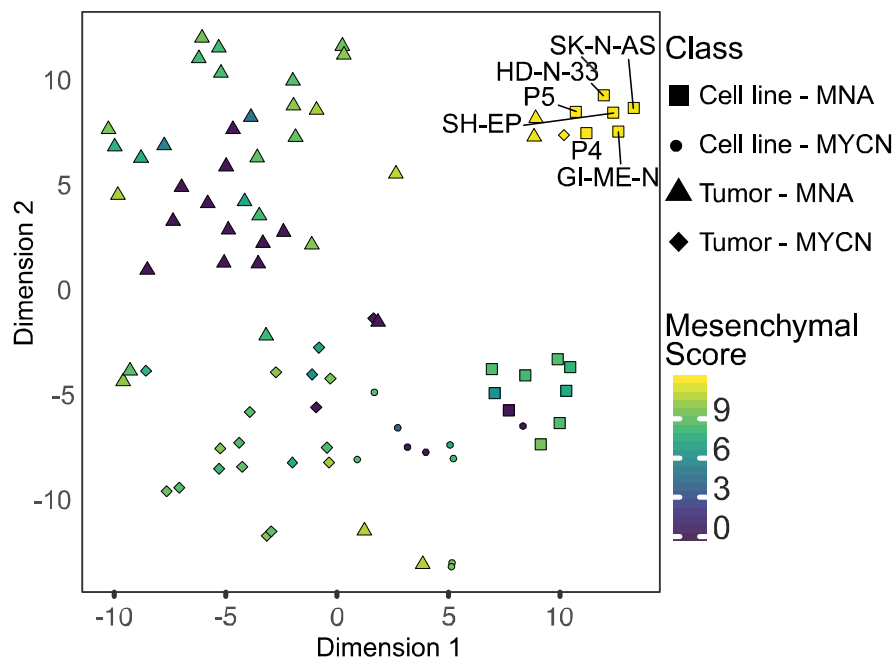


Figure 60: t-SNE analysis of NB tumors and cell lines.

T-distributed stochastic neighbor embedding (t-SNE) analysis of NB primary tumors ($n = 60$; triangles) and NB cell lines ($n = 26$; squares) based on H3K27ac histone mark ChIP-seq signal. NB tumor and cell line samples were separated in MYCN-amplified (MYCN) and MNA cases and colored to NMF signature two exposures (Mesenchymal Score).

60 NB tumors of the ChIP-seq cohort allowed the identification of a novel epigenetically-defined four NB subtypes including a new one with mesenchymal characteristics (Figure 58). To further extent the cohort, the set of assigned NB SE target genes (as described for Figure 56 and Figure 58) was used to perform NMF analysis based on expression in an available RNA-seq cohort of 598 NB tumors (Figure 61). For both tumor NMFs based on ChIP-seq and RNA-seq data, four signatures produced the most stable factorization and subdivision of the tumor cohort. According to the clinical annotation (Figure 54; MYCN status, INSS stage, age and relapse) the MYCN RNA-seq NMF signature defined a subset of MYCN-amplified samples. The Mes signature

revealed enrichment for relapsed cases, while MNA-LR signature defined almost exclusively MNA cases with low-risk features. In contrast to this, MNA-HR signature was enriched for high-risk samples and contained only 2 (of 107) *MYCN* amplified-samples. As described for the results of tumor ChIP-seq NMF (Figure 58), many samples in the tumor RNA-seq NMF were exposed to more than one signature. Similar to GSEA of tumor and cell line ChIP-seq NMF, the non-clinico-biologically defined Mes RNA-seq signature was significantly enriched for terms associated with EMT and cell migration and for transcriptional regulation and signaling in the RNA-seq cohort (Figure 61). MNA-LR signature was significantly enriched for gene sets associated with transcriptional regulation and signaling as well as neuronal and developmental processes while MNA-HR and *MYCN* signatures showed no significant enrichment.

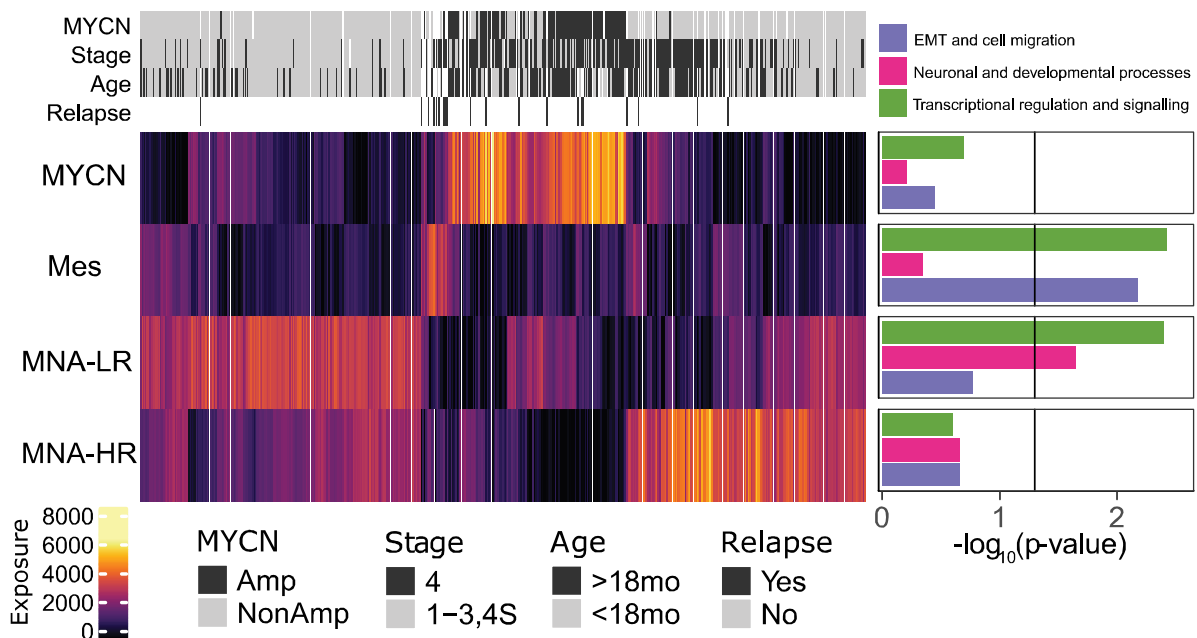


Figure 61: Extended NMF analysis of NB tumors based on RNA-seq data.

Non-negative matrix factorization (NMF) analysis of NB tumors ($n = 589$) based on predicted NB primary tumor SE target gene expression defined by RNA-seq leading to four signatures (*MYCN*, *Mes*, *MNA-LR* and *MNA-HR*). Information on clinico-biological parameters of the tumors is given as previously described (Figure 54) regarding *MYCN* status (*MYCN* amplified (black) and *MNA* (grey)), stage (INSS stage 1-3 and 4s (grey) or 4 (black)), age (age at diagnosis or 18 months (black) or younger 18 months (grey)) and relapsed case (yes (black) or no (grey)). Gene set enrichment analysis (GSEA) of the predicted SE target genes defining the NMF signatures are given on the right. GSEA was performed using the MSigDB (<https://software.broadinstitute.org/gsea/msigdb/>).

To compare ChIP-seq- and RNA-seq-defined NMF signatures, signature exposure values of tumors represented in both cohorts were plotted in scatter plots (Figure 62). Samples with high

exposure to MYCN signature and Mes in the ChIP-seq NMF also displayed high exposure to the respective signature in the RNA-seq NMF, thus confirming the robustness of these signatures. In contrast to this, LR-MNA signature and HR-MNA showed discrepancies between the two datasets when samples with high exposure in the ChIP-seq based NMF had low exposure in the RNA-seq based NMF and vice versa.

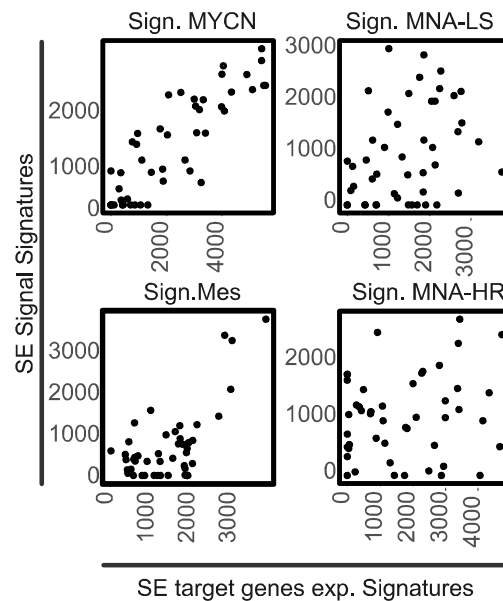


Figure 62: Scatterplots of NMF-based signatures for NB tumors.

Scatterplots of NMF-based signature exposure values for NB primary tumors present in both, the ChIP-seq (SE signal signatures, from Figure 58) and the RNA-seq cohort (SE target genes expression signatures, from Figure 61).

All four NB subtypes defined by NMF of NB tumors SEs were analyzed for association with the clinical characteristics high-risk and relapsed disease (Figure 63). Therefore, Recovery analyses were performed, revealing strong association of relapse disease with tumors highly exposed to the Mes as well as the MYCN signature and strong association of the MYCN signature with high-risk disease.

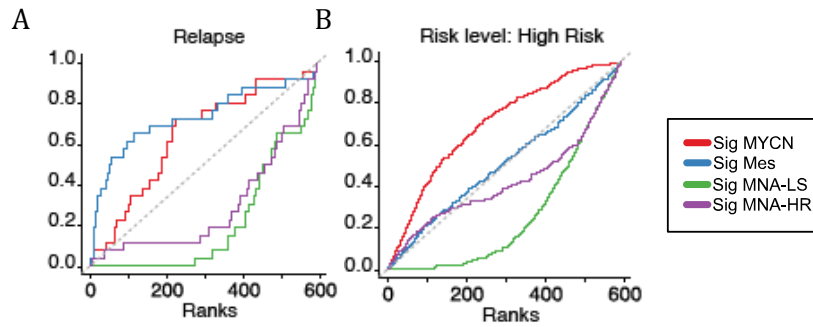


Figure 63: Recovery analysis of clinical variables of NMF-based signatures for NB tumors.

Recovery analysis of clinical variables of relapse (A) and high-risk disease (B) in the SE-defined subgroups. The x-axis depicts the samples of the extended NB RNA-seq NMF cohort ($n = 589$) sorted by descending exposure to the respective signature. On the y-axis the percent recovery of the considered clinical variable is given within the respective fraction of samples. Curve progression above or below the diagonal represent positive or negative association of the particular signature with the clinical variable, respectively (Sig = signature).

3.2.3 Core regulatory circuitries of NB subtypes

NMF analysis of the NB tumor SE landscape revealed distinct epigenetically defined NB subtypes, which were also manifested through the expression of the SE assigned target genes. We hypothesized that specific sets of master regulator or a core regulatory circuitry (CRC) is driving and regulating each individual subtype and making it distinct from one another. NB subtype-specific CRCs were explored by a bioinformatic approach.

For the reconstruction of NB-specific gene regulatory network of transcription factors (TFs) and their target genes, the ARACNE (Algorithm for the Reconstruction of Accurate Cellular Networks) algorithm was used. The ARACNE or improved ARACNE-AP (Adaptive Partitioning strategy) algorithm requires gene expression data as an input and omits interactions due to co-expression (Margolin et al. 2006; Lachmann et al. 2016). The method estimated an NB regulome consisting of 239,499 significant TF-gene interactions using expression profiles of the extended NB RNA-seq cohort ($n = 589$) and a list of human specific TFs ($n = 1471$) from the FANTOM5 (Functional ANnotation Of the Mammalian genome) project (Forrest et al. 2014) (<http://fantom.gsc.riken.jp/>).

As regulatory elements, like SEs that recruit and build up transcription factor networks and are thereby involved in aberrant gene regulation in human cancers we tried to identify these relevant regulators, using the concept of CRCs (Saint-Andre et al. 2016). CRCs are defined as regulating their own and the expression of other CRC TFs and consequently forming an interconnected auto-regulatory loop. Therefore, NB subtype-specific CRCs were determined by

integrating the NB regulome data and the subtype-specific transcription factor activities defined by VIPER as well as the previously published CRCmapper (Saint-Andre et al. 2016). VIPER infers transcription factor activity by analysing RNA-seq gene expression data of the transcription factors target genes (Alvarez et al. 2016).

The CRC TFs in the network were established and displayed colour coded and clustered according to their observed frequency of CRCs in tumors (n = 60) and cell lines (n = 25) assigned to each per sample and per signature as well as TF activity analyzed by VIPER algorithm, which was assigned to the respective CRC (Figure 64). A set of 75 NB CRC TFs was identified, based on the criteria of being present in at least 5% of tumor samples as well as in the ARACNE defined NB regulome. All 24 cluster one CRC TFs were observed in the Mes cell line subtype but only 14 of them in the Mes tumor subtype. Some of the CRC TFs including *RARB* (retinoic acid receptor beta), *KLF4* (kruppel like factor 4) and *RUNX2* (runt related transcription factor 2) were exclusively observed in the Mes subtype of cell lines and tumors. All 24 cluster one CRC TFs were significantly enriched for mesenchymal (Mes) TF activity.

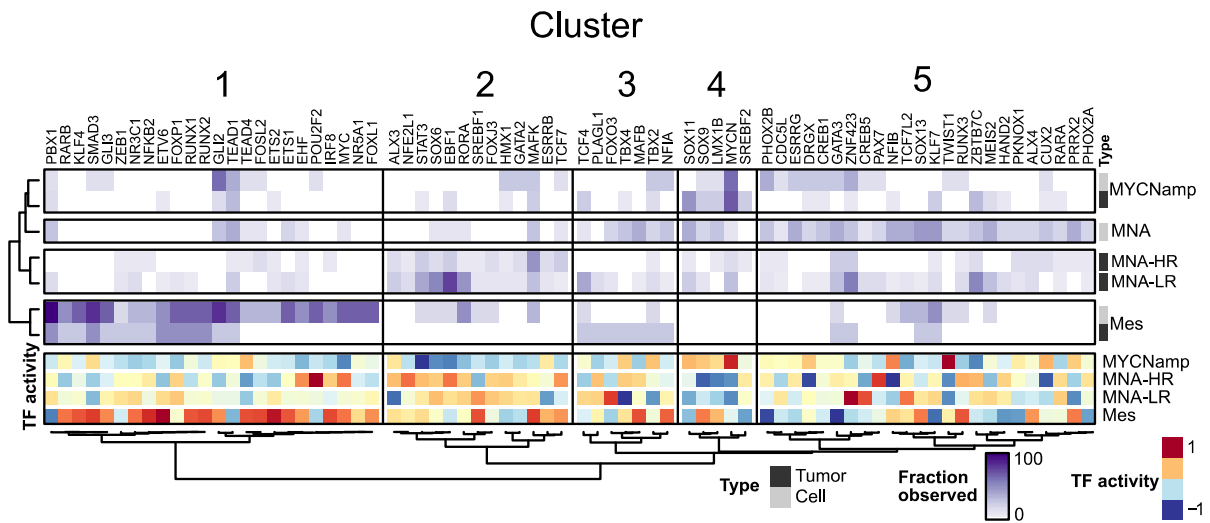


Figure 64: Definition of NB-specific CRCs.

Definition of NB-specific core regulatory circuitry (CRC) clusters by integration of ARACNE regulome analysis and identification of subtype-specific transcription factor activity via VIPER's regulon analysis. CRC TF abundance in the networks of the respective samples is colour coded ascending from white (not present) to purple (observed in up to 100%) for NB cell lines (n = 24) and NB tumors (n = 60). NB cell line and tumor cohorts were subdivided in three or four subgroups, respectively based on the signatures derived from NMF (Huebschmann et al. 2017). MNA, mesenchymal (Mes) and MYCN-amplified high-risk (HR) and low-risk (LR) (MNA in NB cell lines) as previously defined by NMF.

Cluster two CRC TFs were mainly observed in both MNA subtypes of tumors and Mes cell line signature, while MYCN signature for both and Mes subtype exclusively in tumor revealed low and no presents at all, respectively (Figure 64). TF activities of the 13 CRC TFs within cluster two were enriched for Mes and both MNA (HR and LR) tumor subtypes, while TF activity for MYCN subtypes was low. In cluster three and five neither any increased abundance of CRC TFs of any subtype nor obvious enrichment for TF activity were observed. Cluster four CRC TF *MYCN* was increased and almost exclusively observed within MYCN subtype of cell lines and tumors. CRC TFs were enriched for MYCN TF activity in tumors.

Validation of the CRC networks of SE-driven TFs was exemplified in SK-N-AS cells (mes subtype) by exploring the epigenetic status of three CRC candidates loci *FOSL2* (FOS like 2), *MYC* and *SMAD3* (Figure 65). The chromatin status at these loci was analyzed by ATAC-seq, SE identification by H3K27ac ChIP-seq and predicted CRC TF binding by PIQ algorithm, which uses DNase I hypersensitivity profiles for TF binding site prediction (Sherwood et al. 2014). SE regions assigned to *FOSL2*, *MYC* and *SMAD3* harbored open chromatin structure and revealed binding motifs for their own and the respective two other CRC TFs.

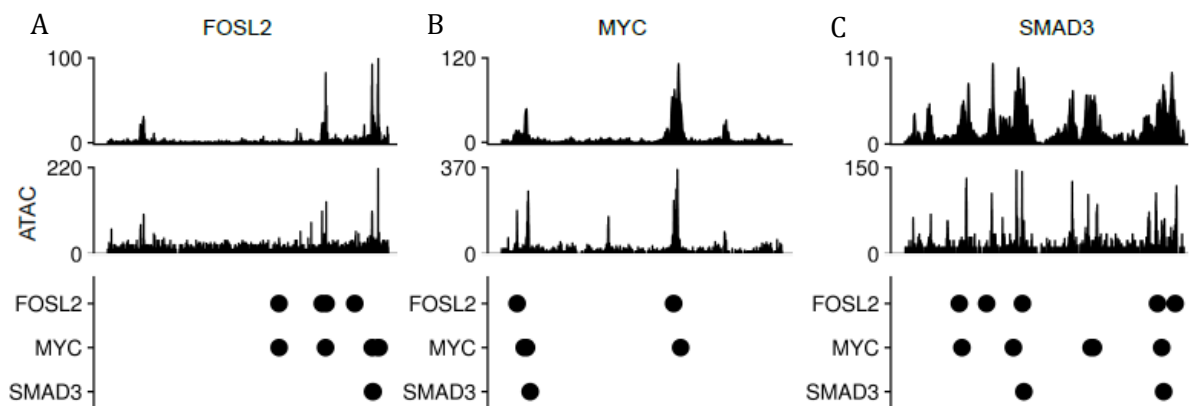


Figure 65: Validation of exemplar CRC TFs using chromatin conformation data.

*Chromatin status and conformation at SE elements (*FOSL2* - SE1028, *MYC* - SE1838 and *SMAD3* - SE642) assigned to the three active CRC transcription factors *FOSL2* (A), *MYC* (B) and *SMAD3* (C) in SK-N-AS cells. H3K27ac ChIP-seq (top lane), ATAC-seq (second lane) and motif prediction analysis by protein interaction quantitation (PIQ) were performed for validation of innate and reciprocal transcription factor binding.*

RNAi-induced knockdown of CRC TFs and its impact on viability and gene expression

For functional validation of the NB CRCs, RNAi-induced knockdown of a set of CRC TFs (n = 28) was performed in GI-ME-N (Mes subtype) and NMB (MYCN subtype) cells (Figure 66A).

Knockdown (KD) sensitivity was evaluated by a colony formation assay using GIEMSA staining and transcription factor activity of the CRC TFs in the Mes subtypes was displayed. RNAi-induced knockdown of CRC TFs *NFKB2* (nuclear factor kappa B subunit 2), *RUNX1* or *RARB* from cluster one, which was enriched for the Mes subtype and Mes TF activity (Figure 64), had strong effect on KD sensitivity in mesenchymal GI-ME-N cells. In contrast, RNAi-induced knockdown of CRC TFs from other clusters, including *GATA2* (cluster two), *PHOX2B* (cluster five) or *SOX11* (cluster four) revealed a higher impact on KD sensitivity in NMB cells. To identify the impact of RNAi-induced knockdown of a set of CRC TFs, the expression profiles after Mes-specific *RARB*, *ETS1* or *SMAD3* RNAi were resolved by RNA-seq in Mes SH-EP cells (Figure 66B). RNAi-induced knockdown of *RARB* led to downregulation of EMT, KRAS signalling as well as TNF signalling via *NFKB2*. In contrast, MYC target genes were upregulated. *ETS1* knockdown caused downregulation of gene sets involved in cell cycle regulation (i.e. mitotic spindle regulators, E2F targets as well as G2M checkpoint genes). Finally, RNAi-induced knockdown of *SMAD3* decreased the expression of oxidative phosphorylation and fatty acid metabolism gene sets and furthermore, TNF signalling via *NFKB2* was significantly upregulated.

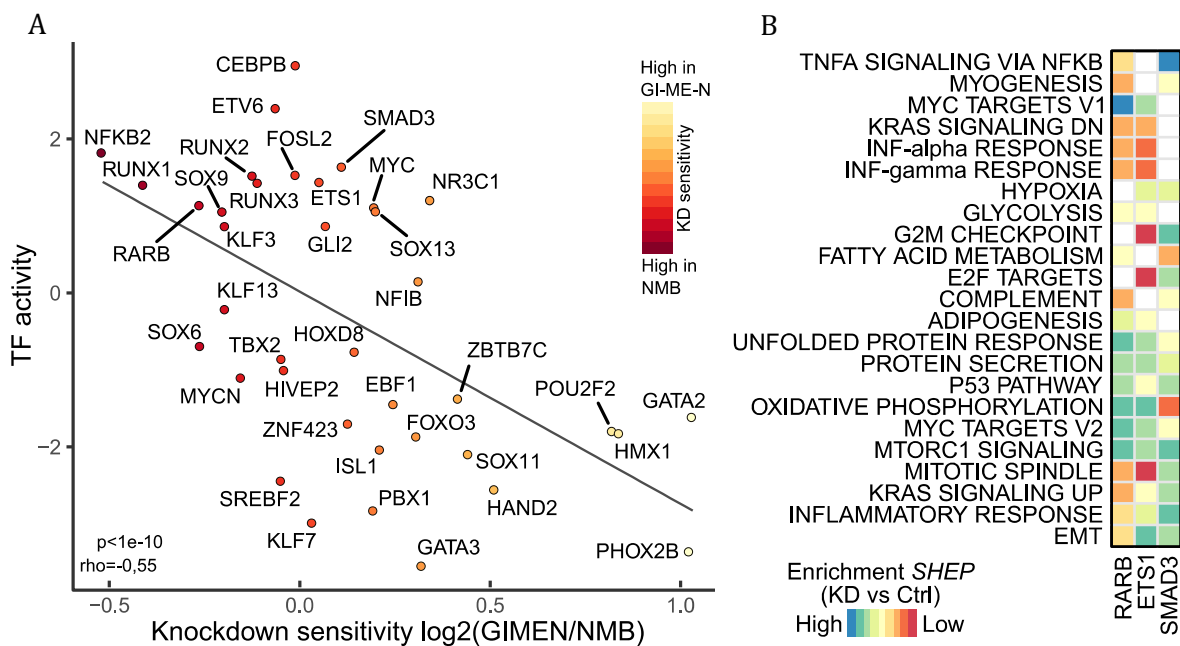


Figure 66: Functional validation via RNAi-induced knockdown of exemplar CRC TFs.

(A) *Log*₂ ratio of RNAi-induced knockdown (KD) sensitivity (x-axis) in GI-ME-N versus NMB for a subset of CRC TFs (n = 28) in dependence of Mes transcription factor activity (y-axis). KD sensitivity was defined by colony formation assay using GIEMSA staining and subsequent colony count via ImageJ version 1.47 using the ColonyArea plugin. In addition, KD sensitivity was depicted by colour code (light yellow = high sensitivity in NMB; dark red = high sensitivity in GI-ME-N). (B) Expression changes (red = decrease; blue = increase) of GSEA after RNAi-induced knockdown of *RARB*, *ETS1* or *SMAD3* in SH-EP (Mes subtype) cells defined by RNA-seq. GSEA was performed using the MSigDB (<https://software.broadinstitute.org/gsea/msigdb/>).

For validation of RNAi-induced knockdown efficiency prior to RNA-seq, protein levels of the respective genes were quantified using western blotting (Figure 67). RNAi-induced knockdown of *ETS1* caused protein reduction down to 9.6% and 5.7% remaining protein for siRNA one and two, respectively. After *SMAD3* knockdown 6.7% (siRNA#1) and 2.6% (siRNA#2) protein was left and RNAi-induced knockdown of *RARB* reduced the protein level to 32.5% (siRNA#1) and 93.8% (siRNA#2). For each of the targets, the siRNA causing the most efficient gene knockdown and protein reduction was used for subsequent functional experiments.

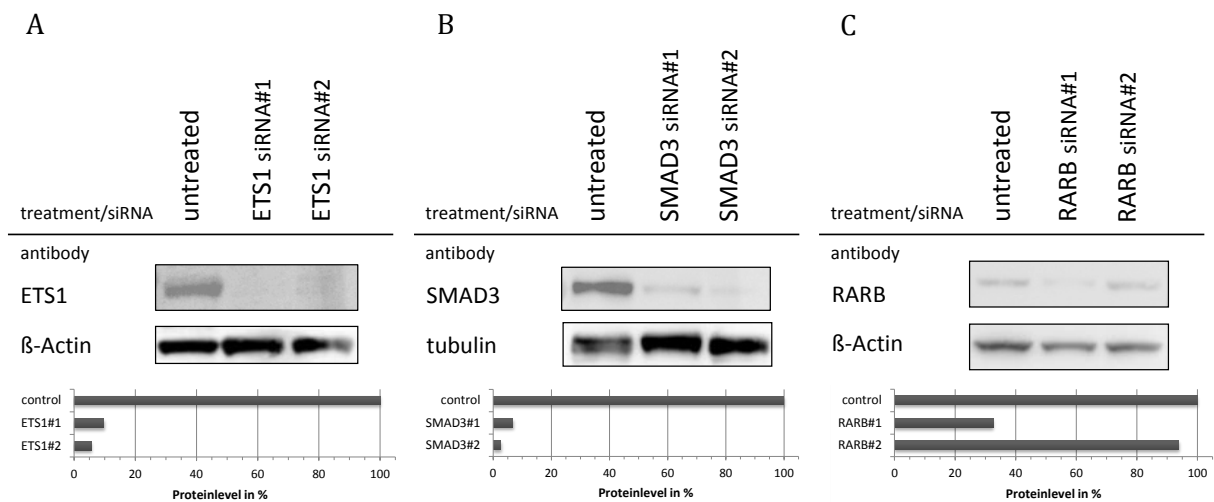


Figure 67: Validation of RNAi-induced knockdown of exemplar CRC TFs.

Validation of RNAi-induced knockdown of (A) *ETS1* (#1 = 9.6% and #2 = 5.7% protein left), (B) *SMAD3* (#1 = 6.7% and #2 = 2.6% protein left) and (C) *RARB* (#1 = 32.5% and #2 = 93.8% protein left) in SH-EP (Mes subtype) cells by protein quantification (Western blotting). Protein quantification after RNAi-induced knockdown was performed via ImageJ by normalization using the loading control and the untreated control.

The four NMF-defined NB subtypes exposed clear differences in SEs and their predicted target gene activities, which allowed the identification of a network of master transcription factors that likely drive expression programs associated with distinct clinical associations.

To further define the epigenetic regulation, the genome-wide physical interactions of CLB-GA (MNA subtype) and SK-N-AS (Mes subtype) cells were analyzed by HiChIP chromatin capturing assay (Figure 68A). In SK-N-AS cells, the fraction of interactions with SEs assigned to the Mes signature was three times higher as compared to CLB-GA cells (SK-N-AS = 64%; CLB-GA = 20.3%). In contrast, CLB-GA cells harbored more than twice the amount of interactions with SEs associated with the non-mesenchymal (nonMes) signature as compared to SK-N-AS (CLB-GA = 79.7%; SK-N-AS = 36%). Comparing the chromatin status and accessibility in KELLY (MYCN

Retinoic acid (RA) receptor *RARB*, identified as a mesenchymal CRC TF in this work, was reported to reduce RA signaling and suppresses EMT-transition in basal-like breast cancer in mice (Liu and Giguere 2014). Since RA receptors, including *RARB*, are the downstream mediators of RA, the effect of all-trans retinoic acid (ATRA) on Mes signature was analyzed. ATRA is known as an inducer of differentiation of malignant cells, used in therapy for patients with low- and intermediate-risk NB (Matthay et al. 1999). ChIP-seq of the enhancer associated histone mark H3K27ac was performed at two time points of ATRA treatment in BE(2)-C and KELLY cells (both MYCN subtype). Exposure values to each NMF signature obtained from cell line ChIP-seq were computed for these experiments (Figure 69). These analyses, called radar plots, visualize exposure of different samples to the NMF-defined subtypes representing highest exposure (100% of indicated signature) on the outer and lowest (0% of indicated signature) on the inner circle (Figure 69).

In BE(2)-C cells, a clear shift towards increasing exposure values of Mes signature was observed upon ATRA treatment as compared to controls (Figure 69A). Mes exposure values, starting from 44 in the control, increased upon treatment in a time-dependent manner to 1081 after 24 h up to almost 2231 after 144 h of ATRA treatment. BE(2)-C exposure values for MNA were slightly increased (4847 (EtOH control) to 5006) or for MYCN signature highly decreased (3506 (EtOH control) to 113) after 144 h of ATRA treatment. In KELLY cells no shift of exposure values was observed for the Mes or MYCN signature (Figure 69B). At the 24 h time point of ATRA treatment MNA signature was slightly increased (1243 (EtOH control) to 1935) but decreased again after 144 h compared to the EtOH control (1243 (EtOH control) to 818).

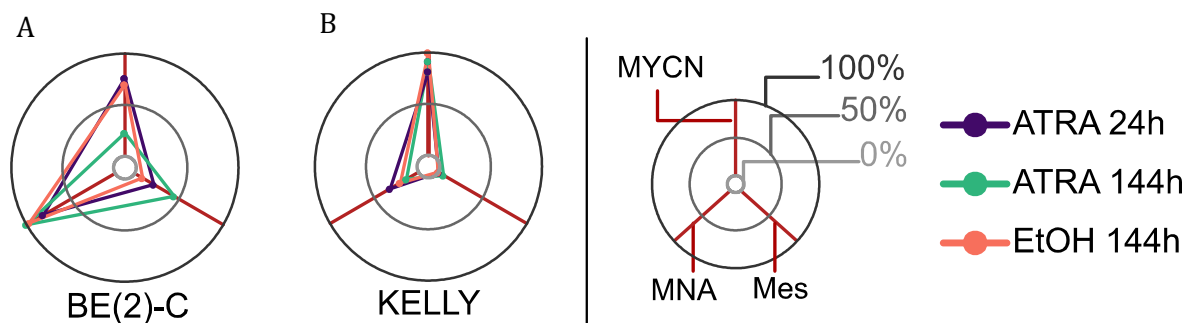


Figure 69: ATRA-induced shifts of NB subtype exposure values of ChIP-seq data.

Radar plots visualizing exposure changes to the NMF-defined subtypes MYCN, Mes, MNA (red lines) obtained from cell line RNA-seq upon ATRA treatment in BE(2)-C (A) and KELLY (B) (both MYCN subtype) cells based on ChIP-seq H3K27ac data. ATRA- or EtOH- (pink) treated cells were harvested at the indicated time points as replicates for ChIP-seq 24 h (purple) and 144 h (green) after ATRA treatment.

In analogy to the ChIP-seq analysis, RNA-seq time course data of ATRA-treated BE(2)-C and KELLY cells were used to compute exposure values to each NMF signature obtained from cell line RNA-seq data (Figure 70). ATRA treatment resulted in decreased MYCN signature exposure and increased Mes signature exposure in BE(2)-C cells, while exposure to the MNA signature remained unchanged compared to the EtOH control (Figure 70A). Both changes in signature exposure occurred in a time-dependent manner up to 144 h upon ATRA treatment. In KELLY cells no apparent changes in any of the three signature exposures were detected (Figure 70B). Since NB cell lines are exclusively derived from high-risk tumors, ChIP-seq NMF of cell lines is incapable of resolving high-risk and low-risk MNA tumor signatures. To circumvent this limitation, the RNA-seq time course data of ATRA-treated BE(2)-C and KELLY cells was used to compute exposure values for the tumor derived LR- and HR-MNA NMF signature (Figure 70C). BE(2)-C cells showed an increase of LR-MNA tumor signature exposure in a time-dependent manner as compared to the EtOH control while no changes were observed in the exposure to the HR-MNA tumor signature. The replicates for KELLY showed no consistent or directed exposure shift of any type.

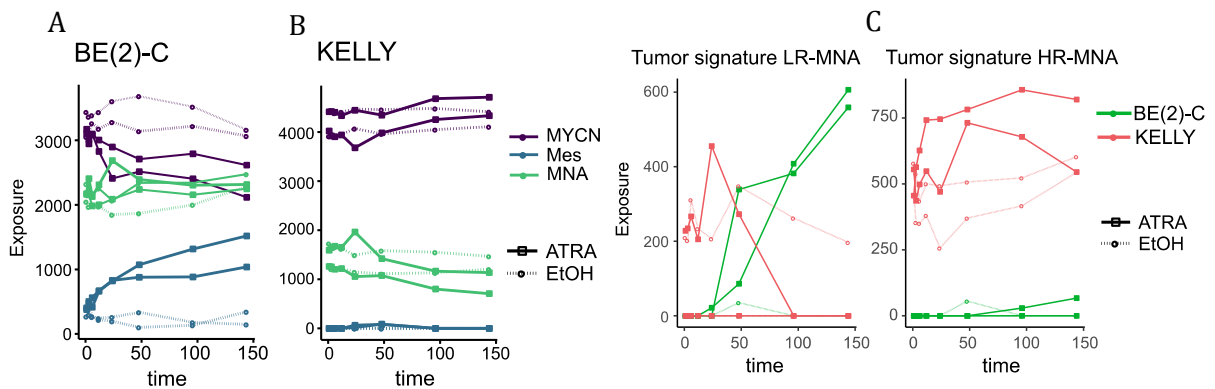


Figure 70: ATRA-induced shifts of NB subtype exposure values of RNA-seq data.

RNA-seq data of ATRA-treated BE(2)-C (A) and KELLY (B (both MYCN subtype) cells was used to compute exposure values to each NMF signature (MYCN, Mes and MNA) obtained from cell line RNA-seq. (C) RNA-seq data of ATRA-treated BE(2)-C and KELLY (both MYCN subtype) cells was used to compute exposure values to tumor MNA-LR and MNA-HR NMF signatures obtained from tumor RNA-seq. ATRA (continuous line) or EtOH- control (dotted line) treated cells were harvested at the indicated time points (0 h, 1 h, 3 h, 6 h, 12 h, 24 h, 48 h, 96 h and 144 h after ATRA treatment) as replicates for RNA-seq analysis.

As strong clinical association of relapsed disease with tumors exposed to the Mes signature was revealed already (Figure 63), RNA-seq data of three primary tumors and matching relapsed samples was used to compute exposure values to each NMF signature obtained from tumor

RNA-seq. All three patient samples revealed a shift towards a stronger Mes signature exposure in the relapsed as compared to the primary tumor sample (Figure 71). Furthermore, slight decrease of exposure to the HR-MNA signature and minor increase of exposure to the MYCN signature was observed after relapse in all three cases. Exposure to the LR-MNA signature was slightly decreased upon relapse in the first patient while an increase of exposure to this signature was observed upon relapse in patients two and three. The sample from a metastasis during second relapse (pink) of patient one revealed the same but less pronounced trend in shifting signature exposure values.

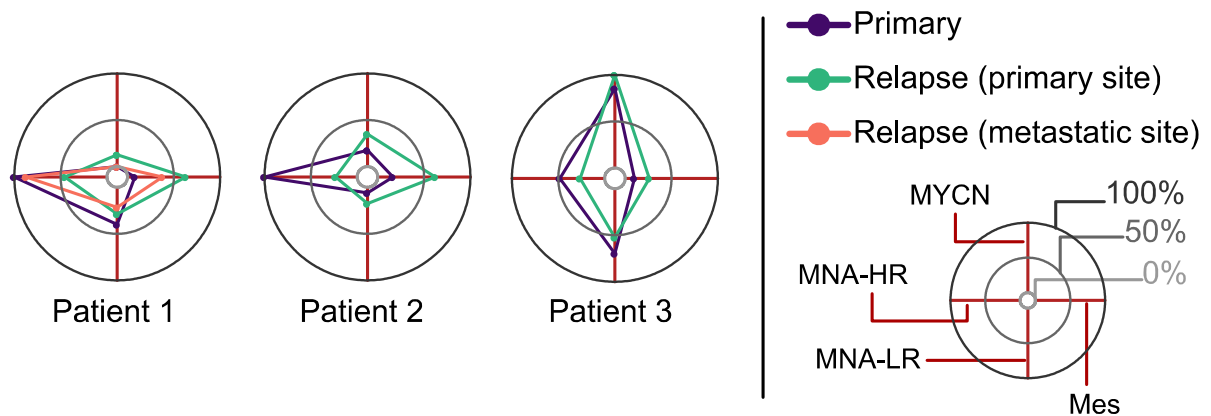


Figure 71: NB subtype exposure values of relapsed patients.

Radar plots visualizing exposure changes to the NMF-defined subtypes MYCN, Mes, MNA-LR and MNA-HR obtained from tumor RNA-seq of primary tumors (purple) to matched relapsed samples (primary site = green; metastatic site = pink) based on RNA-seq data.

Taken together, these data indicate that samples from relapsed tumors showed higher exposure to the tumor ChIP-seq NMF-derived Mes signature as compared to matched primary samples, regardless of whether the primary or metastatic site at relapse was analyzed. In addition, ATRA treatment caused a time-dependent shift towards the Mes signature. Given this dynamic shifts of the Mes signature, we wanted to search for an involved pathway or underlying mechanism of this Mes signature. First evidence of *JUN* and *FOSL2* being associated with highly accessible chromatin in mesenchymal SK-N-AS cells (Figure 68B) suggested involvement of JUN/FOS associated genes with the Mes signature. An enrichment of activating *RAS*-MAPK pathway gene mutations in relapsed NBs was already described (Eleveld et al. 2015). Our results pointed towards a possible involvement of RAS associated genes with the Mes signature. Therefore, the Mes signature was analyzed for enrichment of JUN/FOS or RAS pathway signature or target genes. A strong positive correlation was identified for the RAS signature ($\rho=0.83$) and JUN/FOS target genes ($\rho=0.72$) (Figure 72).

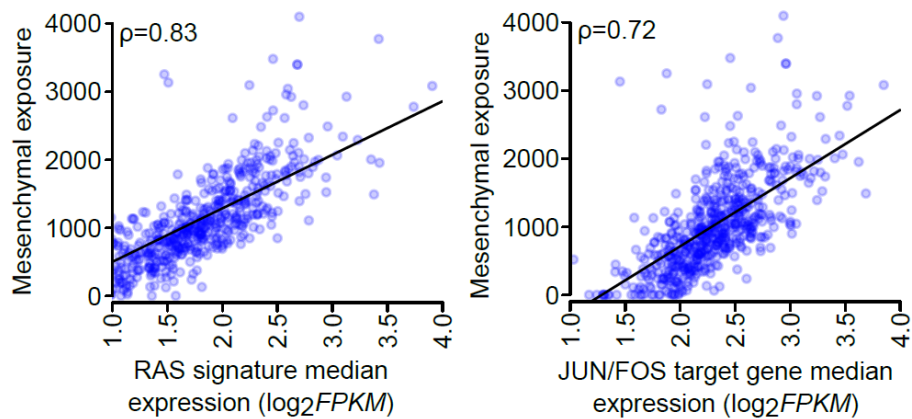


Figure 72: Pathway gene correlation of Mes signature.

Correlation analysis of (A) RAS signature (public available gene expression signature of RAS pathway (Loboda et al. 2010)) or (B) JUN/FOS (based on previously defined ARACNE regulom including AP-1 transcription factor subunits: FOS, FOSB, FOSL1, FOSL2, JUN, JUNB, JUND). Median expression ($\log_2\text{FPKM}$) of a set of genes (signature) representing RAS or JUN/FOS activation (x-axis) versus patients' mesenchymal exposure derived from ChIP-seq NMF.

Intriguingly, gene expression of RAS signature genes was strongly increased in relapsed samples as RAS signature genes were enriched in the top 25% of expressed genes in relapsed samples (Figure 73A). In primary samples, only a few RAS signature genes showed increased expression. Similarly, JUN/FOS target genes with high expression were enriched in relapsed samples, particularly in the top 25% of expressed genes (Figure 73B). In contrast, in the top 25% expressed genes in primary tumors the JUN/FOS target genes were represented to a much lesser extent.

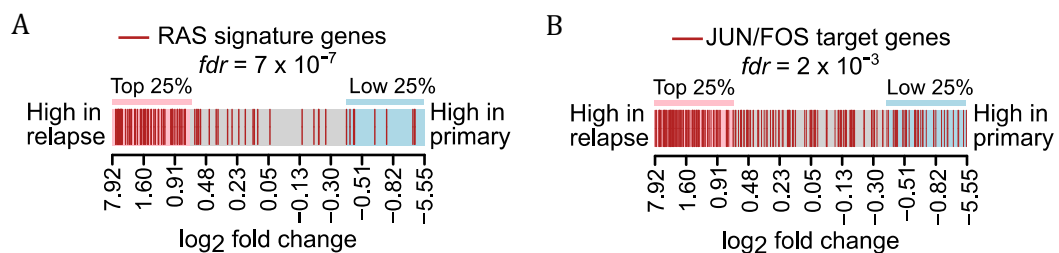


Figure 73: Pathway gene enrichment in primary and relapsed cases.

Enrichment analysis of (A) RAS signature target genes (public available gene expression signature of RAS pathway (Loboda et al. 2010)) or (B) JUN/FOS target genes (based on previously defined ARACNE regulom including FOS, FOSB, FOSL1, FOSL2, JUN, JUNB, JUND) in differentially expressed genes between primary and relapsed tumor samples.

NB relapsed samples showed increase in Mes signature exposure as well as increased expression of RAS signature genes and JUN/FOS target genes in contrast to matched primary samples. To deepen the insight into regulatory networks governing gene expression of primary and relapsed tumors, the enrichment of NB-specific CRC TF target genes defined in the present study (3.2.3) in primary versus relapsed NB samples was analyzed (Figure 74). In line with previously described results of the present study, target genes of CRC TFs that harbored a high Mes TF activity were accumulated and highly expressed in relapsed samples. Among those CRC TFs *IRF8* (interferon regulatory factor 8), *RUNX1*, *FOXL1* (forkhead box L1) and *NFKB2* displayed highest expression and normalized enrichment score in relapsed cases in contrast to primary samples. On the other hand, target genes of CRC TFs that occupied a high nonMes TF activity were accumulated and highly expressed in primary samples. Here, *PBX1* (PBX homeobox 1) and *SREBF2* (sterol regulatory element binding transcription factor 2) revealed highest expression and normalized enrichment score in primary in contrast to relapsed samples. It is of note, that most target genes of NB CRC TFs showed a clear assignment to either primary or relapsed samples according to enrichment score and expression level. Only a few genes including *MYC* or *TCF4* (transcription factor 4) were expressed comparably low and showed low enrichment values.

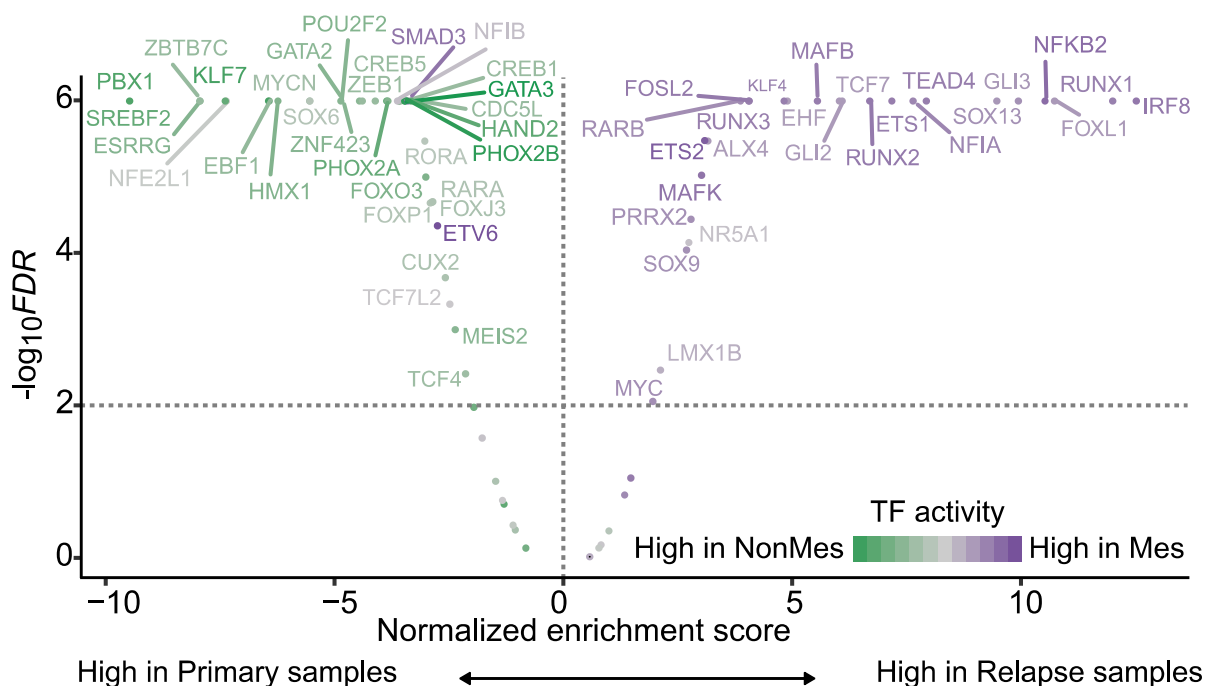


Figure 74: CRC TF enrichment in primary and relapsed cases.

Normalized enrichment score of NB-specific core regulatory circuitry (CRC) transcription factor (TF) target genes in primary or relapsed NB samples arranged by their gene expression ($-\log_{10}FDR$). Each CRC TF is coloured according to VIPER defined mesenchymal TF activity (green - high in Mes; purple - high in nonMes).

4. Discussion

4.1 Global enhancer hijacking landscape in NB

Shedding light on the global landscape of oncogene activating enhancer hijacking events in NB was a central task of this work. Regulatory elements, like SEs that recruit and build up transcription factor complexes and thereby regulate gene expression play an essential role in aberrant function of many human cancers. Several mechanisms of enhancer malfunction that lead to cancer development due to altered oncogene expression are known. These include mutations, insertions or deletions within enhancer elements that change transcription factor binding sites as well as their *de novo* formation (Demichelis et al. 2012; Huang et al. 2014; Mansour et al. 2014; Oldridge et al. 2015). The principle of alternative oncogene activation through translocation of enhancers in the proximity of oncogenes was described in several cancer types and is referred to as enhancer-hijacking (Taub et al. 1982; Bakhshi et al. 1987; Groschel et al. 2014; Northcott et al. 2014). The present study reports enhancer-hijacking for several NB-specific oncogenes including *TERT*, *MYCN*, *MYC*, *IGF2BP1* and *ATOH1* that play an essential role in NB tumorigenesis. Intriguingly, in NB cell lines and primary tumors, a strong, lineage-specific SE region downstream of *HAND2* and upstream the *FBXO8* gene locus was recurrently rearranged into the proximity of these oncogenes, thereby leading to increased expression. Given the predominant role of epigenetic deregulation in NB, high-frequency of enhancer-hijacking events, reported in the present study, emphasizes a strong epigenetic involvement in NB tumorigenesis (Henrich et al. 2016). A better understanding of the epigenetic landscape could pave the way towards more specific epigenetic drugs and novel therapies including epigenetic analyses as basic diagnostic methods for NB tumors.

4.1.1 Telomerase activation by genomic rearrangements in high-risk NB

WGS (n = 59) and FISH (n = 217) analysis of primary NB tumors revealed recurrent rearrangements affecting the *TERT* gene and leading to alternative telomere activation in up to 24% of high-risk NB cases. Overcoming the Hayflick limit by escaping replicative senescence and gaining indefinite proliferation capacity is a well-known hallmark of cancer, which can be implemented by reactivation of telomerase activity (Hayflick 1965; Kim et al. 1994; Shay and Bacchetti 1997). Telomerase is the most important component of telomere maintenance in humans. It consists of the catalytic subunit TERT (telomerase reverse transcriptase) and TERC (telomerase RNA component), which is essential for template repeat elongation at gDNA

telomeres (Greider and Blackburn 1989; Lendvay et al. 1996; Lingner and Cech 1996). The protective function of telomere maintenance is usually inactive in somatic cells, while it is reactivated in germ cells, stem cells and 80 – 90% of malignant tumors where it is commonly associated with poor prognosis (Liu et al. 2004; Pestana et al. 2017). Increased telomere activity due to *TERT* promoter mutations is associated with metastasis and reduced survival in melanoma, thyroid carcinomas and gliomas (Melo et al. 2014; Populo et al. 2014; Heidenreich et al. 2015). In line with these observations, *TERT* rearrangements in the present study were associated with poor prognosis and poor clinical outcome in NB patients, comparable to that observed for patients harboring amplified *MYCN*. It has been previously shown that short telomeres were associated with favorable prognosis whereas maintained telomeres were accompanied with unfavorable outcome in a cohort of 51 NB primary tumors (Ohali et al. 2006). A recent study revealed that tumors with intact telomere maintenance mechanism in combination with RAS/p53 pathway mutations were associated with fatal outcome in a cohort of 416 untreated NB tumors. In contrast, occurrence of spontaneous regression was restricted to tumors lacking RAS/p53 pathway mutations and simultaneous telomere maintenance (Ackermann et al., 2018, submitted). Genomic rearrangements, especially those upstream of the *TERT* gene, were already described as an alternative process of transcriptional activation of *TERT* and thereby telomerase activation (Zhao et al. 2009). This study from 2009 was conducted in genetically modified fibroblast cells to describe cellular immortalization and a novel mechanism to alter the epigenetic condensed chromatin landscape upstream the *TERT* locus.

Besides the discovery of *TERT* rearrangements, WGS in this study confirmed established genomic aberrations including amplified *MYCN*, *ATRX* deletion and gain of chromosome 17 in NB tumors, which is in line with recently published studies (Maris et al. 2007; Molenaar et al. 2012; Pugh et al. 2013). Inactivating *ATRX* mutations are common in several cancer entities like pancreatic neuroendocrine tumors (PanNETs) and are associated with alternative telomere maintenance and alternative lengthening of telomeres (ALT) (Heaphy et al. 2011). *ATRX* protein is involved in chromatin remodeling but ALT mechanism is not only restricted to *ATRX*-mutated tumors (Cheung et al. 2012). In the present study, *ATRX* mutations (n=7), amplified *MYCN* (n = 10) or *TERT* rearrangement (n = 12) were observed in a mutually exclusive fashion in a cohort of 56 primary NBs. Intriguingly, all of these three high-risk associated aberrations induce one of the two telomerase maintenance mechanisms. Either by increasing *TERT* expression through activating *TERT* rearrangements, transcriptional activation by amplified *MYCN* or by activating the homologous recombination-based ALT pathway through *ATRX* inactivation (Duan and Zhao 2018).

In the present study, no mutations of the *TERT* gene or promoter region were detected in 59 analyzed primary NBs, whereas these aberrations are commonly activating *TERT* and telomere activity in various cancer entities. Recurrent somatic mutations within the *TERT* promoter were found in 44% (n = 225) of thyroid cancer types and 33% (n = 77) of primary melanomas (Landa et al. 2013). In melanomas it was shown that somatic mutations within the promoter region of *TERT* can establish ETS transcription factor binding motifs causing up to two fold upregulation of *TERT* (Horn et al. 2013; Huang et al. 2013). Recurrent *TERT* promoter mutations were detected in 6.4% of renal cell carcinomas (n = 188) and in more than 65% of bladder cancers (n = 327) (Hosen et al. 2015; Hosen et al. 2015). In addition, *TERT* promoter mutations were identified in 66% of gliomas (n = 303) with 80% in primary glioblastomas, 70% in oligodendrogliomas and 39% in astrocytomas (Heidenreich et al. 2015). On the DNA level, the present study determined a low overall mutation frequency of only 13.3 mutations per genome, which confirms previous NB sequencing studies (Pugh et al. 2013). In an analysis of 12 major cancer types lowest median mutation frequency of 0.28 mutations per megabase (Mb) was found in acute myeloid leukemia (AML) whereas highest mutation frequency was observed in lung squamous cell carcinoma with 8.15 mutations per Mb (Kandoth et al. 2013). A recent pan-cancer study revealed that mutation frequencies across 24 non-adult cancer types (n = 961) were up to 14 times lower (0.02 – 0.49 mutations per Mb) compared to adult cancer entities. In this study, NB samples (n = 59), including three relapsed samples with increased mutation rates, harbored a median mutation frequency of 0.22 mutations per Mb (Grobner et al. 2018).

In NB cells (n = 32), three of the six top *TERT* expressing lines (CLB-GA, GI-ME-N and KELLY) harbored a *TERT* rearrangement which was confirmed by FISH. Despite the fact that *TERT* expression was significantly higher in *TERT*-rearranged versus *MYCN*-amplified cases in NB tumors, *MYCN*-amplified and non-*TERT*-rearranged NGP cells exhibited the highest *TERT* expression of all NB cell lines. In NGP cells, as well as in two further MNA cell lines, among the six top *TERT* expressing cell lines, additional activating aberrations like *TERT* promoter mutations might be present, which should be analyzed by e.g. WGS and subsequent analyses. Particularly, in *MYCN*-amplified NGP cells a duplication event of *TERT* locus was identified but not further characterized in this study. If high expression of *TERT* in NGP cells is due to duplication or correlation with amplified *MYCN* has to be clarified. For all the three *TERT*-rearranged tumors analyzed, ChIP-seq profiles of TSS associated H3K4me3 and enhancer surrogate H3K27ac histone marks revealed repositioning of enhancer elements into the proximity of the *TERT* gene. Genome wide enhancer ranking by H3K27ac signal identified all three translocated enhancers as SEs. The three *TERT*-rearranged cell lines with high *TERT*

expression harbored a heavily silenced region upstream of *TERT* with condensed chromatin represented by H3K27me3 and H3K9me3. However, *TERT* was enriched for activating histone modifications like H3K4me3, H3K4me1 and H3K27ac at the promoter and H3K36me3 at the gene body in all *TERT*-rearranged cell lines and were absent in the non-rearranged control cell lines. Such co-occurrence of activating and repressive marks at the same locus is termed as a bivalent state and is described in colon cancer and further tissues and cancers. Dysregulation of such bivalent genomic regions (promoters and gene bodies) through loss of the repressive marks can cause oncogene activation (Baylin and Jones 2011; Hahn et al. 2014). Changes in the epigenetic landscape, including transformation from repressive polycomb-mediated trimethylation of H3K27 to long-term silencing by DNA methylation (epigenetic switching), are reported in many cancer types and reduces epigenetic plasticity (Gal-Yam et al. 2008). In this study, DNA methylation analysis of CpG islands at the *TERT* locus of 39 NB primary tumors revealed highest methylation of CpG islands across the *TERT* gene in *MYCN*-amplified and *TERT*-rearranged tumors. In contrast to this silenced region the *CLPTM1L* (cisplatin resistance-related protein 9) gene further upstream of *TERT* showed lack of repressive marks in all analyzed cell lines (*TERT*-rearranged and control). *CLPTM1L* was even enriched for ATAC-seq peaks, which marks open chromatin, as well as for histone marks associated with transcriptional elongation (H3K36me3) and active transcription (H3K4me1, H3K4me3 and H3K27ac). *TERT* rearrangements in NB cell lines CLB-GA, GI-ME-N and KELLY were validated using FISH, as described before. The principle of alternative oncogenes activation by enhancer rearrangements into the proximity of oncogenes and upregulating their expression was described for many cancer types (Taub et al. 1982; Bakhshi et al. 1987; Groschel et al. 2014; Northcott et al. 2014). As a proof of principle, 4C-seq using a viewpoint matching the *TERT* promoter was performed in NB cell line CLB-GA, GI-ME-N, KELLY. Using this validation of physical interaction with the *TERT* promoter, the location of the hijacked enhancer was identified. Likewise, enhancer elements assigned to *GATA2* on chromosome 3 were replaced into the proximity of *EVII* as detected by 4C-seq analysis in AML. This caused downregulation and upregulation of both genes, *GATA2* and *EVII*, respectively (Groschel et al. 2014).

Finally, there are treatment opportunities by targeting tumor cells with uncontrolled telomerase maintenance through e.g. the activation of *TERT* as demonstrated in NB cells. Treatment approaches with telomestatin that inhibits telomere activity and results in telomere shortening, growth arrest and apoptosis *in vitro* are particularly promising (Binz et al. 2005).

4.1.2 Further rearrangements affecting oncogenes

The principle of oncogene activation by chromosomal rearrangements bringing together active enhancers and oncogenes has been described for several cancer entities and is referred to as “enhancer hijacking” (Taub et al. 1982; Bakhshi et al. 1987; Groschel et al. 2014; Northcott et al. 2014). With the discovery of recurrent rearrangements of SE elements activating the *TERT* gene, we provided the first evidence for “enhancer hijacking” in NB. Due to the absence of coding mutations or amplifications, extraordinary high expression levels known for several oncogenes in NB remained unexplained for a long period. The present study followed the hypothesis that “enhancer hijacking” might be the driving force of activation for oncogenes including *MYCN*, *MYC*, *IGF2BP1* and *ATOH1*, which will be discussed in the following section.

MYCN and MYC

Examining mRNA levels of NB cell lines (n = 32) using RNA-sequencing data, revealed extraordinary high *MYCN* expression levels in NBL-S despite the fact that they bear no changes in *MYCN* copy number. Similarly, outlier expression of *MYC* was observed in *MYC* single-copy cell lines NB69, SK-N-AS, CHLA20 and SH-SY5Y. High mRNA expression of either *MYCN* or *MYC* in the respective cell lines were mirrored by protein expression as could be confirmed by western blotting. *MYC* and *MYCN* expression is mutually exclusive, which is in accordance with previous studies that identified a lack of *MYC* expression in *MYCN*-amplified NB tumors, which is explained by regulatory interactions of both (Breit and Schwab 1989). In another study, high expression of *MYCN* and *MYC* target genes was identified as marker for poor survival and was driven by *MYC* in stage 4 tumors lacking amplified *MYCN* (Westermann et al. 2008). In addition, immunohistochemistry (IHC) staining for *MYCN* and *MYC* protein appeared almost mutually exclusive in a cohort of 157 NB primary tumors. The tumors defined as *MYC*-positive (11%) in a subset of high-risk cases were associated with worse prognosis than *MYCN*-positive tumors or tumors negative for both (Wang et al. 2013). This fosters prognostic significance of *MYC* in addition to *MYCN* as described in a group of patients with undifferentiated NB (Wang et al. 2015). In general, *MYCN* and *MYC* share several homolog regions and hold similar cellular functions especially during development since *MYCN* was discovered as *MYC* homolog that is subject to amplification in NB tumors (Gustafson and Weiss 2010). Both, ectopic *MYCN* and *MYC* expression can drive neuroblastoma tumorigenesis *in vivo* in mice or zebrafish (Althoff et al. 2015; Zimmerman et al. 2018). To evaluate *MYC* dependency, RNAi-mediated *MYC* knockdown was performed in NB cell lines. Among the MNA cell lines, the strongest decrease of viability was observed in SK-N-AS, which harbored intermediate *MYC* expression as compared to GI-ME-N (higher *MYC* expression) and SHEP (lower *MYC* expression). *MYCN*-amplified NMB cells

displayed only marginal levels of *MYC* expression and viability remained unaffected by RNAi-mediated *MYC* knockdown. This emphasizes a unique *MYC* dependency of *MYC*-rearranged cell line SK-N-AS, which is lower in GI-ME-N cells with a higher *MYC* expression.

In contrast to *MYCN*, which is amplified in advanced stage disease in approximately half of the cases and in 20% of all NB, amplification of *MYC* is a very rare event (Brodeur et al. 1984). An exception was found by a WGS study in NB primary tumors (n = 87), identifying chromothripsis as causa for amplification and strong upregulation of *MYC* in one patient of the study (Molenaar et al. 2012). However, *MYC* amplification is not always associated with high *MYC* expression or increased protein level due to posttranscriptional modifications or due to a short half-life of *MYC* protein, as described in breast cancer (Mariani-Costantini et al. 1988). *MYC* itself is deregulated in many ways in many cancer entities and is described as the most frequently deregulated oncogene in cancer (Kalkat et al. 2017). Amplification of the *MYC* locus as well as co-amplification of adjacent genes within the *MYC* surrounding “gene desert” is a well described phenomenon in many cancer entities, like ovarian and small cell lung cancer or prostate carcinoma (Sato et al. 1999; Kim et al. 2006; Haverty et al. 2009). Co-amplified genes downstream of *MYC* are the long non-coding RNA genes *PVT1* and *CCDC26* as well as the *GSDMC* gene (Gasdermin C), which regulates apoptosis of the gastric epithelium (Saeki et al. 2009). *PVT1-MYC* co-amplification was found in medulloblastoma group 3 as the first recurrent translocation involving *PVT1* and *MYC*, due to chromosome 8 chromothripsis events (Northcott et al. 2012). Interestingly, high *MYC* expression was particularly depending on increased levels of *PVT1*, a long non-coding RNA gene downstream of *MYC*, through a positive feedback loop. Both genes are co-amplified and co-expressed in 98% of all *MYC*-amplified tumors (Tseng et al. 2014). However, no correlation between *MYC* and *PVT1* expression was observed in NB cell lines. On the contrary, NB69 cells that highly express *MYC* revealed low *PVT1* expression, which was even lower expressed than the first quartile of 32 NB cells. Furthermore, highest *PVT1* expression co-occurred with low *MYC* expression in MHH-NB11 cells. According to this, *MYC* amplification is most probably not the reason for high *MYC* expression in NB cases and there will be another cause for *MYC* activation. Since there are hardly any genes within the *MYC* surrounding “gene desert”, most of the adjacent enhancer elements are assigned to regulate or deregulate *MYC* expression. Alterations including focal amplifications of *MYC*-interacting enhancer elements in these non-coding regions were reported for lung adenocarcinoma as well as for NB (Zhang et al. 2016; Zimmerman et al. 2018). Among four *MYC*-rearranged NB cell lines with highest *MYC* expression, only SK-N-AS and SH-SY5Y cells contained the *PVT1* gene on the rearranged strand. In addition, all four cell lines lack *PVT1*, *CCDC26* as well as *GSDMC*, downstream of *MYC* on the translocated allele. For *CCDC26* and *GSDMC* only average expression

level was detected in *MYC*-rearranged cell lines. All *MYC*-rearranged NB cell lines exhibited only one chromosome 8 wild-type allele carrying *MYC*, *PVT1*, *CCDC26* as well as *GSDMC* genes. Only a region-gain including *MYC* and three downstream genes was able to promote cancer in mice, which was impossible for amplified *MYC* gene alone (Tseng et al. 2014).

In search for the reason for high *MYCN* expression at mRNA and protein level in NB NBL-S cells and extraordinary high *MYC* expression and protein level in NB69, SK-N-AS, CHLA20 and SH-SY5Y cells these lines were studied via FISH in the present study. *MYC* and *MYCN* rearrangements were identified in all tested cell lines, while almost all translocated SE elements juxtaposed to *MYC* or *MYCN* originated from the same genomic location at chromosome 4 (Chr.4 q34). The phenomenon of enhancer hijacking was first described in 1982 in Burkitt's lymphoma, where structural rearrangements juxtapose immunoglobulin H (IgH) enhancers to *MYC* thereby driving increased *MYC* expression (Taub et al. 1982). As described for *TERT* rearrangements, 4C-seq confirmed interactions of the *MYCN* or *MYC* promoter with translocated enhancer elements in NB cell lines NBL-S or, NB69, SK-N-AS, CHLA20 and SH-SY5Y, respectively. These experiments identified further the precise positions of the interacting enhancers. Genome wide enhancer ranking by H3K27ac signal identified all four *MYC*- as well as the *MYCN*-rearranged enhancers as SEs, which was directly associated with increased oncogene expression. In addition to this epigenetic profiling, *MYC* rearrangement with chromosome 7 segments in SH-SY5Y revealed enriched repressive H3K27me3 marks at the *MYC* locus. This bivalent state, with activating and repressive marks at the same locus is described in colon cancer and further entities. Dysregulation of such bivalent genomic regions by loss of the repressive marks can cause oncogene activation (Baylin and Jones 2011; Hahn et al. 2014).

As the principle of alternative oncogene activation by enhancer rearrangements plays an important role in NB biology by regulating *TERT*, *MYCN* and *MYC*, we screened for further potential "enhancer hijacking" events in NB tumors and cells. Therefore, combination of WGS and supplemented RNA-seq data of primary tumors without amplified *MYCN* (n = 111) and a small set of NB cell lines were used as input for our EPISTEME analysis platform developed by Umut Toprak (Neuroblastoma Genomic, DKFZ). EPISTEME is a structural variation (SV) algorithm similar to the published DELLY, which identifies SVs by integrating paired-end and split-reads (Rausch et al. 2012). Within this study, *IGF2BP1* and *ATOH1* two candidates for alternative activation by rearrangements were examined further.

IGF2BP1

The present study revealed cases of enhancer-hijacking involving *IGF2BP1*, in NB cell lines and tumors, providing evidence for recurrent targeting of this gene. *IGF2BP1*, which is located on

17q21.32, was first described in 2015 by Bell and colleagues to play a role in NB biology (Bell et al. 2015). *IGF2BP1* family members including RNA-binding protein Vg1 RBP are involved in neural crest cell migration as well as neurite development (Yaniv et al. 2003; Bell et al. 2015). *IGF2BP1* involvement in LIN28/Let-7 pathway, which is described to induce NB in mice, confirms prognostic significance for NB tumors independently of *MYCN* status (Molenaar et al. 2012). In further cancer entities, like cutaneous squamous cell carcinoma (cSCC) increased *IGF2BP1* is associated with higher staging, decreased cell differentiation and increased proliferation (Kim et al. 2017). In melanoma, *IGF2BP1* expression was increased in metastatic disease and associated with chemotherapeutic resistance (Kim et al. 2018). *IGF2BP1* was highly expressed throughout our NB cell line cohort (n = 32) revealing a strong positive correlation with amplified *MYCN*, which was less pronounced in NB tumors. However, in an external NB tumor cohort *IGF2BP1* is associated with amplified *MYCN* and high *MYCN* expression (Bell et al. 2015). Interestingly, the candidate cell line for *IGF2BP1* rearrangement, CLB-GA, exhibited by far the highest *IGF2BP1* gene expression, which was almost two fold increased as compared to the next in line. This finding of elevated IGF2BP1 in CLB-GA was confirmed on the protein level in a small set of NB cell lines. The RNA-binding protein IGF2BP1 was shown to be involved in supporting high *MYC* expression level by protecting its mRNA, which might explain correlation with *MYCN* or *MYC* (Lemm and Ross 2002). In a previous study of two NB tumor cohorts, *IGF2BP1* was found to be expressed and increased expression was associated with poor patient survival, which was both confirmed in the NB tumor cohort of the present study (Bell et al. 2015). It was described previously that NB tumors display elevated *IGF2BP1* expression due to frequent gains of chromosome 17q21 in NB (Bell et al. 2015).

In one tumor an *IGF2BP1* rearrangement with chromosome 4 was predicted by WGS data and the EPISTEME SV algorithm that integrates paired-end and split-reads and finally RNA-seq analysis. Chromatin interaction analyses via 4C-seq confirmed physical interactions between the *IGF2BP1* promoter and the *HAND2* enhancer cluster on chromosome 4 in CLB-GA cells. This was validated independently using genome wide interactions identified by HiChIP in CLB-GA. *IGF2BP1* resides on chromosome 17q, which is the most frequently gained region in NB. Furthermore, *IGF2BP1* was identified as a *MYCN* transcriptional target. Despite this complex high-risk associated network of *IGF2BP1* upregulation, we could resolve *IGF2BP1* rearrangement as an additional and novel mechanism of *IGF2BP1* upregulation, in the present study. Analyzing the rearranged regions at the *IGF2BP1* locus by ChIP-seq confirmed that strong enhancers reside on the chromosome 4 translocation partner region in CLB-GA cells. In addition, the *IGF2BP1* locus was enriched for repressive H3K27me3 marks and further marks associated with active transcription. Similar to *TERT* rearrangements or *MYC* rearrangement in

SH-SY5Y cells, this could be defined as a bivalent promoter as well as the repressed epigenetic status of wild-type allele. This should be clarified in further experiments choosing a monoallelic RNA-seq or allele-specific ChIP- or ATAC-seq approach using QuASAR (Quantitative Allele Specific Analysis of Reads), which recognizes allelic imbalance at heterozygous sites (Harvey et al. 2015). A tumor suppressive function of indirect reduction of *IGF2BP1* via knockdown of regulator miR-506 was reported in glioblastoma (Luo et al. 2015). Taken together, *IGF2BP1* has been identified as a promising candidate for a therapeutic approach in other entities, like glioblastoma. In terms of the epigenetic deregulation and novel mechanism of *IGF2BP1* upregulation by rearrangement as described in the present study, targeting *IGF2BP1* would be also a promising approach for NB tumors.

ATOH1

The present study revealed cases of enhancer-hijacking involving *ATOH1* in three NB tumors, providing evidence for recurrent targeting of this gene. This demonstrates that recurrence of enhancer hijacking events *in vivo* is not restricted to the *TERT* gene. The role of NOTCH pathway transcription factor *ATOH1* is contradictory in different cancer entities. Dependent on the tumor type, *ATOH1* is reported to exert oncogenic or tumor suppressive functions. *ATOH1* is described to have a tumor suppressive role preventing transcriptional repression of *ARID2* (AT-rich interaction domain 2) in hepatocellular carcinoma (Gao et al. 2017). In most colorectal cancers *ATOH1* is silenced and high *ATOH1* activity is associated with cell differentiation (Kazanjan and Shroyer 2011). In the NB cohort of the present study, increased *ATOH1* expression (EFS n = 366; OS n = 308) was associated with decreased EFS and OS probability, which is pointing towards an oncogenic function. This is in line with findings in another neuronal pediatric tumor, aggressive medulloblastomas, displaying high *ATOH1* expression in recurrent and metastatic medulloblastoma (Grausam et al. 2017). Further adding to this, *ATOH1* enhances oncogenic function via *GLI2* (GLI family zinc finger 2) target genes and inhibits neuronal differentiation in medulloblastoma-initiating cells (Ayrault et al. 2010). In the present study, *ATOH1* displayed outlier expression for one MNA cell line SK-N-FI as well as for several tumors of different stages. Integrated analysis of structural rearrangements and expression data did not detect any *ATOH1* rearrangements in NB cell lines, which have not been confirmed by FISH or 4C-seq analysis yet. The epigenetic status was determined exemplary for one tumor with predicted *ATOH1* rearrangement and revealed strong enhancer elements within the recurrently translocated region coming into the proximity of *ATOH1* gene locus and most likely driving the expression. In mouse NB and neural progenitor cells, β -catenin increases *ATOH1* expression by *ATOH1* enhancer binding and vice versa RNAi-mediated knockdown of β -catenin decreased *ATOH1* expression (Shi et al. 2010). In medulloblastoma, Jak2 (janus kinase 2) inhibition reduced tumor

growth *in vivo* through reduction of tyrosine 78 phosphorylation of ATOH1. This effect on tumor growth caused protein destabilization and reduced ATOH1 activity presenting a promising way of targeting *ATOH1* (Klisch et al. 2011; Klisch et al. 2017). Taken together, targeting *ATOH1* has been a promising candidate for a therapeutic approach in other entities, like medulloblastoma. In terms of the epigenetic deregulation and novel mechanism of *ATOH1* upregulation by rearrangement described in the present study, targeting *ATOH1* would be a promising approach for NB tumors.

4.1.3 HAND2 SE cluster is recurrent donor-region in rearrangement events

The present study identified structural rearrangements, which recurrently juxtaposed a particular enhancer region in the proximity of different NB oncogenes including *TERT*, *MYCN*, *MYC*, *IGF2BP1* and *ATOH1*. This enhancer region downstream of the *HAND2* (referred to as *HAND2SE* region in the following) and upstream of the *FBXO8* gene was characterized by strong H3K27ac signal in NB cell lines and tumors. An increased H3K27ac signal, which is an established enhancer surrogate, was observed in the presence or absence of rearrangement events at this locus, which points towards an important regulatory role and also lineage specificity in wild-type NB.

FBXO8 gene, a member of the F-box gene family mediates protein-protein interactions and is involved in developmental processes, even though its exact function is still unknown (Calcia et al. 2013). In contrast, the functions of DNA binding protein *HAND2* are diverse and regulate development and cell specification in different tissues and cell types like heart, cardiac cushion, bone and noradrenergic sympathetic ganglion neurons. *Hand2* inactivation is lethal *in vivo* in mice (Hendershot et al. 2008) and the present study showed that RNAi-mediated knockdown of *HAND2* caused reduced viability in two *HAND2* SE-rearranged NB cell lines, independent of amplified *MYCN*. Both genes, *HAND2* and *FBXO8*, were highly expressed across NB cell lines, while expression of both genes was slightly increased in rearranged cases and revealed *HAND2* outlier expression in CLB-GA cells as well as *FBXO8* outlier expression in NB69 and CHLA20 cells. In addition, 4C-seq analysis of the *HAND2* enhancer regions demonstrated physical interaction with the *HAND2* as well as the *FBXO8* transcription start site (TSS), which are likely driving the increased expression observed for both genes. Interestingly, CLB-GA with the highest *HAND2* expression of the NB cell line cohort was the only rearranged cell line harboring both, the *HAND2* gene and *HAND2* enhancer region, on the translocated allele which indicates strong breakpoint dependency of expression. Surprisingly, high *HAND2* mRNA expression did not result in increased *HAND2* protein level. *HAND2* protein levels were relatively low in CLB-GA

and undetectable in NB69 cells. In endometrial cancer, *HAND2* is associated with potential tumor suppressive functions through *HAND2*-mediated proteasomal degradation of estrogen receptor α (ER α) protein by ubiquitination (Fukuda et al. 2015). Potential proteasomal degradation functions or self-degradation might be the cause of the discrepancy between *HAND2* mRNA and *HAND2* protein expression observed in NB and will be an interesting topic for future investigations. A reason for recurrent rearrangements of *HAND2* enhancer region could be the presence of a “hot spot” like a fragile site with predisposition to breakage as described for subtypes of lymphomas and leukemia (Barski et al. 2007). Such common fragile sites (CFS) are defined as highly unstable genomic regions that are prone to non-random gaps, breaks or even rearrangements under replication stress (Fungtammasan et al. 2012). Many genomic and epigenetic markers for CFS prediction have been described, although several of those including gene density measures, TSS location and enrichment of certain histone modifications are under discussion. While Jiang and colleagues identified association of CFSs with histone marks for condensed and repressive elements (Jiang et al. 2009), opposing findings revealed an open chromatin structure and DNase hypersensitive sites at the regions of recurrent breaks (Zhang and Rowley 2006). In line with the hypothesis that active chromatin sites, as the NB *HAND2* enhancer region, might be prone to breakage, TSS or enhancer marks like H3K4me3, H3K4me1 and H3K27ac were associated with recurrent breakpoints cell type-specific in T-cell cancer (Barski et al. 2007).

Taken together, these data indicate that recurrent rearrangements of the lineage-specific SE region downstream of *HAND2* and upstream the *FBXO8* gene locus has a predisposition to breakage leading to aberrant expression of oncogenes as described in this study for *TERT*, *MYCN*, *MYC*, *IGF2BP1* and *ATOH1*. In case of targeting aberrant SE activity there are several treatment strategies existing as SE regulation and transcription is dependent on BRD4 and CDK-containing (cyclin dependent kinase) complexes.

4.2 Global super enhancer landscape analysis in NB

Active enhancer elements are defined as DNA regulatory units bound by transcription factors that control cell type-specific gene expression and thereby cell identity in mammalian cells (Bulger and Groudine 2011; Thurman et al. 2012). In a cancer context, there is an urgent need to define entity-specific enhancer and SE profiles. These regulatory elements are often enriched at driving oncogenes essential for cancer cell survival, offering vulnerability for targeted therapy (Wong et al. 2017). Especially highly active SEs are described to regulate entity specific master

transcription factors composing a CRC. CRC TFs regulating their own expression and expression of other CRC TFs forming hierarchically an interconnected auto-regulatory loop are crucial elements of many epigenetic driven cancer types (Saint-Andre et al. 2016).

4.2.1 Epigenetic profiling defines NB SE landscape

For the identification of enhancer and super-enhancer (SE) profiles, histone mark H3K27ac profiles were generated by ChIP-seq for a representative cohort of 60 primary NB tumors including *MYCN*-amplified high-risk, low-risk as well as relapsed patient samples. The obtained data were used to generate the first comprehensive global NB tumor-specific enhancer and SE landscape map, which was additionally supplemented with the data of 23 NB cell lines and two neural crest-derived human cells. Similar approaches identifying enhancer or SE profiles in primary tumor samples have been undertaken in cancer entities including ependymoma or colorectal cancer (Cohen et al. 2017; Mack et al. 2018). In primary gastric adenocarcinoma (GC) epigenetic SE profiles (n = 110) using GC and normal tissues as well as cell lines were used to generate an enhancer and SE landscape. In tumor tissues a large scale reprogramming of the epigenetic landscape was reported, which caused dysregulation and cancer gene expression (Ooi et al. 2016). Enhancer profiling in adult T-cell leukemia/lymphoma (ATL), revealed SE elements at cancer driving genes including *CCR4* (C-C motif chemokine receptor 4) and *TP73* (tumor protein P73), which were absent in normal T-cells (Wong et al. 2017). Identification of new subtypes was the result of an enhancer profiling study in 66 AML patients. The study defined six novel subtypes with distinct leukemic cell states and *RARA* (retinoic acid receptor alpha) as a new transcriptional driver gene that was functionally validated in further approaches (McKeown et al. 2017). In the present study, all tumor-derived SE regions as well as their predicted target genes were validated for tissue specificity in a cross-tissue comparison. High tissue specificity of the NB SE set was confirmed, with a maximum of 11% overlap with SE regions defined in other tissues and strongest overlap with an external NB data set of predicted SE target genes. The strategy to derive SEs and their targets in primary NB tumors from H3K27ac ChIP-seq profiles was based on the method described by Hnisz and colleagues and a hierarchical assignment approach, respectively (Hnisz et al. 2013). To generate a stringent list of NB consensus SEs, all H3K27ac peaks closer than 2.5 kb to H3K4me3 promoter peaks were omitted prior to calling. Stringency was further increased by considering only those SEs which were called in two or more samples. Target genes were predicted hierarchically based on i) physical HiChIP and Hi-C interactions, followed by ii) H3K27ac signal versus expression correlation and iii) SE target gene proximity. The strategy of inferring causal enhancer-gene

interaction has previously been proven to be valid in a pan-cancer enhancer analysis using 8928 tumor samples of 33 cancer entities. Here, HiC data and co-expression of mRNA was used to predict physical enhancer-gene interaction, which was validated experimentally exemplified for *PD-L1* (programmed death-ligand 1) enhancer interaction (Chen et al. 2018). The robustness and reproducibility of the underlying epigenetic data and subsequent gene assignment strategy was rendered by the huge overlap of the highly ranked genes and previously identified NB-specific and SE associated genes. Similar to the study by Chen et al., the validity of the applied SE to target gene assignment strategy was demonstrated in the present study for *CCND1* and *MAML3*, two top ranked candidates, in SK-N-AS and KELLY NB cell lines by ChIP-seq, ATAC-seq and HiChIP data.

4.2.2 SE defined NB epigenetic subtypes

The SE profiles of NB tumors were used as an input for NMF analysis to search for novel epigenetically defined NB subtypes. NMF computed four SE signatures as most suitable to represent the whole NB tumor cohort based on SE data of the ChIP-seq cohort. Three out of four signatures could be assigned to specific subgroups due to clinical parameters (*MYCN*-amplified, MNA low-risk and high-risk). Importantly, an additional, previously undefined NB tumor subtype was identified by NMF of SE data which could be defined as enriched for mesenchymal terms including “EMT” or “migratory potential” by gene set enrichment analysis (GSEA). NMF analysis of NB cell line SE profiles computed three stable signatures, namely *MYCN*-amplified, MNA and, similar to the tumors, a third group displaying strong enrichment for mesenchymal terms (hereinafter referred to as Mes subgroup). In parallel to the proceeding of the present study, a related study was published based solely on SE data from nine NB cell lines. This study identified two distinguishable cell line populations, described as undifferentiated mesenchymal and adrenergic cells (van Groningen et al. 2017). This dichotomy was further validated in a joint study in an extended cohort of 25 NB cell lines, which was subdivided in a sympathetic noradrenergic, a neural crest cell like and a mixed identity subgroup (Boeva et al. 2017).

To further access the depth of information in the primary tumor SE cohort and the large cohort of cell lines, t-SNE analysis on joint tumor and cell line SE profiles was performed. These analyses revealed that most cell line and tumor samples grouped apart from each other, representing inherent and disclosed differences that are distinct for tumors and cell lines. This indicates the relevance of the NB tumor SE landscape to judge the actual *in vivo* situation in NB. Interestingly, only samples with the highest exposure to the Mes signature grouped intermixed between tumors and cell lines. This emphasizes the prominence of the mesenchymal character

and confirmed the stability of the Mes signature. Interestingly, NMF signature exposure values of cell lines compared to tumors reflects the selective nature of numerous passages of cell lines under cell culture conditions. For tumors, NMF signature exposures are more continuous with several intermediate samples, which reflects the situation in nature and the importance of a tumor based epigenetic approach.

Despite the fact that the cohort with available ChIP-seq data has grown to a considerable size of 60 tumors during the study, a cohort increase promised to gain even deeper insights in the NB regulatory networks. Therefore, the cohort size was extended by using predicted SE-target genes to perform NMF on RNA-seq data from 589 primary NBs. The four NMF signatures derived directly from SE profiles could be confirmed using gene expression data and robustness was validated in scatterplots and GSEA. Particularly, the *MYCN*-amplified- and the Mes signature displayed high congruence between the two underlying data sets. The extended RNA-seq based NMF analysis, which was based on the epigenetic profiling, was able to recapitulate the ChIP-seq NMF analysis. *De novo* RNA-seq based NMF analysis alone could not reflect the distinct and robust Mes signature. Intriguingly, the robust Mes and *MYCN*-amplified signatures displayed a strong association with relapsed cases for tumors. The mesenchymal subtype of cells and EMT is associated with loss of cell adhesion, increased tumor invasion and metastatic initiation in different cancer entities including breast cancer or NB (Taube et al. 2010; Nozato et al. 2013). This goes along with poor patient outcome and drug resistance mechanisms as defined by the clinical association in the present study since metastasis in NB patients is still one of the main causes of death of the disease (Naiditch et al. 2015; Shao et al. 2017).

Despite the identification of this distinct and robust Mes signature in NB tumors it remains still uncertain if the mesenchymal cells are an independent subgroup of the NB entity or rather a transferable population by changing the expression pattern as described by van Groningen and colleagues. Here, the mesenchymal SE associated TF *PRRX1* (paired related homeobox 1) was overexpressed in an adrenergic NB cell line resulting in a more mesenchymal state (van Groningen et al. 2017).

4.2.3 Core regulatory circuitries of NB subtypes

With the SE NMF-based definition of four distinct and clinically relevant NB subtypes, the basis was proven for defining the transcriptional network driving and regulating these discrete subtypes. This SE based approach was used in combination with significant TF interactions using expression profiles to generate a set of the 75 most essential core regulatory circuitry TFs

within four distinct NB subtypes. The analysis identified regulatory networks which were exclusively present in the Mes signature (driven by CRC TFs including *RARB* and *KLF4*) of tumors and cell lines. Consistently, the comprised CRC TFs harbored high activity exclusively in samples with high exposure to the Mes signature. However, some exceptions were found among CRC TFs including *POU2F2* in MNA-HR, which were present in particular signatures but did not show any TF activity in those. Activators of regulatory networks have been identified for further entities. The pioneer factor FOXF1 (forkhead box F1), regulates the two master transcription factors *KIT* (KIT proto-oncogene receptor tyrosine kinase) and *ETV1* providing evidence that FOXF1 is essential for *in vivo* tumor growth and maintenance in gastrointestinal stromal tumors (Ran et al. 2018). Another study presented the overlap of regulatory circuitries of glioblastoma and neural stem cells, which proved to be extensive. The study focused mainly on the transcriptional network of *KLF4* that have both populations in common (Riddick et al. 2017). *KLF4* is part of the 75 NB CRC TFs identified in this study and was observed in the Mes cell line and tumor subtype. An interesting finding of the present study was the discovery of a group of TFs that were observed as CRC in the Mes subtype exclusively in cell lines but displayed a high Mes TF activity which was derived from tumor RNA-seq (e.g. *TEAD4* (TEA domain transcription factor 4), *FOSL2* and *ETS1/2* among others). This shows the strength of combining both analyses, TF activity and observed CRC TFs, since all of those TFs lacking CRC classification in tumors might have still essential functions in Mes tumors. In this case the function might be irrespective of an auto regulatory feedback-loop, which is the requirement for CRC classification. The combination of TF activity and CRC analysis confirmed consistency of the Mes signature. This is in line of *MYC* TF, which was observed only in the Mes cell line subtype but was heavily enriched for Mes TF activity in tumors. Missing the requirements for CRC classification in tumors does not change the *MYC* assignment as a Mes TF. Involvement of *MYC* in EMT and a relevance in the Mes subtype was observed and confirmed in breast cancer where high *MYC* expression induces EMT (Cho et al. 2010).

Despite the fact that the definition of an entity-specific regulatory network solely by CRCs might ignore important TFs that do not fulfil CRC criteria, the auto-regulatory aspect of defined CRC networks could be confirmed via ATAC-seq as exemplified for the network of *FOSL2*, *MYC* and *SMAD3*. The present study revealed that RNAi-induced knockdown of Mes or nonMes TFs had a greater impact on viability in a mesenchymal or non-mesenchymal cell line, respectively. This confirms that targeting a core component of a subtype-specific regulatory network has impact on the cells of the corresponding subtype and their function is essential for NB subtype maintenance. RNAi-induced knockdown or overexpression of one or more TFs central for a specific subtype might have the power to collapse the whole regulatory network, which might

pave the way for high-risk subtype-specific targeted therapy. A subtype-specific network collapse was demonstrated by RNAi-induced knockdown of three Mes TFs in Mes SH-EP cells. While RNAi-induced knockdown of *RARB* is in line with reduction of EMT processes targeting, *ETS1* and *SMAD3* revealed the opposite. It is of note that defining a subtype-specific list of a regulatory network is only an approximation as *ETS1* and *SMAD3* were defined as Mes CRC TF but have different function in Mes SH-EP cells. This emphasizes sample-specific CRC TF definition for experiments and potential therapies.

A similar functional validation of central TF of regulatory networks was performed in ependymoma and decreased survival upon RNAi-induced knockdown of central factors including *SOX2/9* and *RFX2* (regulatory factor X2) in contrast to control shRNA constructs (Mack et al. 2018). In glioblastoma stem cells, knockdown of regulatory core component *KLF4* by shRNA, caused downregulation of *HRAS* and increased abundance of differentiated cells. On the other hand, overexpression of *KLF4* blocked differentiation and was negatively correlated with patient's survival, indicating a cellular context dependent role in tumor progression for this master TF (Rowland and Peeper 2006; Riddick et al. 2017). This emphasizes the entity- and also cell type-specific role of an identified core component and confirms results from the present study. As described previously, the identified Mes CRC components *ETS1* and *SMAD3* revealed an opposing effect after RNAi-induced knockdown in Mes SH-EP cells.

4.2.4 Functional and clinical relevance of NB epigenetic subtypes

In the final part of the present study, epigenetic subtype signatures were analyzed for novel clinical implications or vulnerabilities in view of potential specific treatment options. Finding a therapeutic window for a Mes subgroup is crucial as Mes cells of several entities revealed increased chemo-resistance (Arumugam et al. 2009). For the Mes CRC TF and RA receptor *RARB*, which was tested after RNAi-induced knockdown in Mes SH-EP cells in this study, it is reported that reduced RA signaling through *RARB* suppresses EMT-transition in basal-like breast cancer in mice (Liu and Giguere 2014). As RA receptors, including *RARB*, are the downstream mediators of RA signalling, the effect of all-trans retinoic acid (ATRA) was analyzed. ChIP- and RNA-seq profiles of ATRA-treated sensitive or resistant NB cells were used to compute exposure to each of the four NB tumor NMF signatures. Intriguingly, ATRA treatment caused a reduction of exposure to the *MYCN*-amplified signature and an increased exposure to the Mes signature in ATRA sensitive BE(2)-C cell line in both, RNA-seq and ChIP-seq based analyses. In contrast, no such effect was observed in the ATRA-resistant KELLY cell line. The reduction of *MYCN* expression in NB cell lines upon ATRA-treatment is a well described

phenomenon (Reynolds et al. 1991). RA, an inducer of differentiation of malignant cells, is used as therapy for patients with low- and intermediate-risk, while it is ineffective for many patients with high-risk neuroblastoma (Matthay et al. 1999; Reynolds et al. 2003). The reason for an unsuccessful therapy of many high-risk patients was previously explained by MYCN-induced resistance as high *MYCN* prevents neuronal differentiation (Duffy et al. 2017). The present data provides the basis for an alternative explanation of RA resistance for many high-risk patients that might initially respond to this therapy approach but finally establish a population of resistant, mesenchymal tumor cells. The fact, that NB tumors are a heterogeneous cell population with mesenchymal cells was already described previously. Within this recent study a mesenchymal SE associated TF *PRRX1* was overexpressed in an adrenergic NB cell line, resulting in a time dependent increasing mesenchymal state (van Groningen et al. 2017).

Further dissecting the MNA cell line signature, which remained unaffected by ATRA treatment, into the LR- and HR-MNA tumor signature revealed increased exposure to the LR-MNA signature in BE(2)-C effect of RA on differentiation, which is phenotypically detectable by neurite-like outgrowth, cell cycle arrest and expression of neuronal differentiation marker like *TrkA* (tropomyosin receptor kinase A) and *CDH5* (Sidell et al. 1986; Higashi et al. 2015). Further on, clinical association analysis of the Mes NB subtype revealed strong association with relapsed disease, which is in line with the radar plot results and the shift of exposure towards a Mes cell type of primary tumors samples compared to matching relapsed samples. This might be due to resistance mechanisms of a cellular subpopulation of the tumor with mesenchymal character, which was described previously. Chemotherapeutic treatment using drugs including doxorubicin or cisplatin in Mes cells revealed higher resistance compared to nonMes cells (Boeva et al. 2017; van Groningen et al. 2017). This is supported by the finding that Mes subtype-specific CRC TFs in the present study were enriched and highly expressed in relapsed samples compared to primary tumors that rather showed enrichment for the non-mes regulatory networks. First evidence for *JUN* and *FOSL2* association with highly accessible chromatin in Mes SK-N-AS cells suggested involvement of JUN/FOS associated genes with the Mes signature. A WGS study of NB relapsed patients (n = 32) identified an enrichment of activating RAS-MAPK pathway gene mutation in relapsed NBs, which points towards a possible involvement of RAS associated genes with the Mes signature (Eleveld et al. 2015). Our study follows this hypothesis further and provides evidence for a strong correlation of exposure to the Mes signature with activation of the RAS pathway and JUN/FOS target genes. This suggests involvement of RAS and JUN/FOS pathway genes in the Mes component and EMT in NB tumor pathways which showed enrichment in relapsed samples. Aberrant activation of EMT has been

already described for oncogenic RAS signaling and RAS effectors like AP-1 (activator protein-1) family members FOS (Reichmann et al. 1992; Shao et al. 2014).

In concert, this data emphasizes the robustness of the defined Mes subgroup including their core regulatory component, which is in line with characterized cancer pathways and clinical correlations in NB. Involvement of RAS and JUN/FOS pathway genes in the Mes component might open a therapeutic window targeting this distinct subgroup of NB tumors.

4.3 Conclusion and perspective

A central finding of the first part of the present study is the discovery of recurrent chromosomal rearrangements juxtaposing SE elements in the proximity of the oncogene *TERT*. These rearrangements are associated with telomerase activation and occur in up to 24% of high-risk NB cases providing the first evidence for “enhancer hijacking” in NB tumors. Further omics analyses, integrating genome-wide expression, enhancer signal and chromatin interaction data, reveal that enhancer hijacking is not restricted to *TERT* but also affects other oncogenes including *MYCN*, *MYC*, *IGF2BP1* and *ATOH1* in NB cell lines and tumors sporadically and in a recurrent manner. Intriguingly, a strong lineage-specific SE region, assigned to the *HAND2* gene in the wild-type situation, is recurrently involved in enhancer hijacking events with all the above mentioned oncogenes, implicating the relevance of strong lineage-specific enhancers in tumorigenesis.

As a proof of principle, the present study provides evidence that NB cells are “addicted” to enhancer hijacking activated *MYC* via RNAi experiments in NB cell lines. However, the relevance of other enhancer hijacking candidate genes, identified in this study, remains to be determined. A strong focus should be placed on the identification of further candidates using the established EPISTEM structural variant algorithm approach coupled with RNA-seq data. At the moment, functional validation of physical SE-promoter interactions is still restricted to cell culture material. Enhancer hijacking validation approaches for primary material have to be optimized and can be based on chromatin interaction assays (e.g. 4C-seq), monoallelic RNA expression or allele-specific ChIP-seq and should be object for future investigations. A bidirectional approach should be undertaken to further elucidate the contribution of SE hijacking events as NB drivers. First, CRISPR/Cas9-based deletion of hijacked SE elements in NB model cell lines should be conducted. A particular focus should be placed on the lineage-specific *HAND2*-associated SE involved in various NB hijacking events. Such experiments would directly verify the causal link of SE regulation and targeted gene expression. A reciprocal approach to determine the

tumorigenic impact of a SE proto-oncogene interaction would be the introduction of a highly active SE element into the proximity of a candidate oncogene in non-tumor neural crest-derived cell lines. Neural crest-derived cells are missing a tumorigenic background, thereby reflecting the full impact of genome editing approach by CRISPR/Cas9. To elaborate on this aspect further, the described genome editing approach should be conducted in genetic mouse models. Reasonable treatment options for enhancer hijacking-activated genes include targeting (i) the gene directly, (ii) its downstream networks indirectly or (iii) driving SE. The enhancer hijacking candidate *IGF2BP1* is a potentially druggable target and can be selectively inhibited by the recently identified small molecule BTYNB (Kim et al. 2018). Also, several therapeutic targeting strategies are available for TERT, which should be examined for efficiency in the available *TERT* rearrangement model systems. The most promising approaches of telomerase inhibition are G-quadruplex stabilizer including telomestatin or guanine-rich oligonucleotides (GROs). In case of targeting aberrant SE activity, several treatment options exist, as SE regulation and transcription is dependent on BRD4 and CDK-containing complexes. The most commonly used small-molecule inhibitor targeting SE complexes is a BET bromodomain inhibitor. Several bromodomain inhibitors targeting BRD2, BRD3 and BRD4 (iBET726) combined or BRD4 (OTX015) alone are currently tested in clinical studies including NB in a *MYCN*-dependent context. Functional studies should include CDK7 (THZ1) and CDK 4/6 (Lee011) inhibitors in order to identify to potential synergy. Promising results towards this direction were recently published for a covalent CDK7 inhibitor, which reduced SE-associated *MYCN* expression in *MYCN*-amplified NB while CDK4/6 inhibitors reduced cyclin D1-associated SE and their target genes (Chipumuro et al. 2014).

The second part of the present study defines the first NB- and NB subgroup-specific SE landscape of primary tumors and cell lines with assigned target genes and their inherent downstream core transcription factor networks. In depth analysis of tumor ChIP-seq data resolves three SE signatures underlying distinct clinico-biologically-defined NB subtypes of *MYCN*-amplified, MNA high-risk and MNA low-risk cases. Intriguingly, a fourth signature is discovered harboring mesenchymal (Mes) features, which is stably validated also in NB cells, indicating a profound role of the underlying signature in the biology of affected NBs. The Mes signature shows an ATRA-inducible dynamic, association with clinical features of relapsed cases as well as correlation with RAS and JUN/FOS signature genes.

In view of the indicated clinical implications and pathway associations of the newly defined Mes subgroup, the cohort size has to be extended. Therefore, an applicable screening method for detection, probably H3K27ac ChIP- or RNA-seq based, as well as bioinformatic processing are needed. The impact of entity- as well as subgroup-specific SE regulated genes should be clarified

in further functional studies. From the NB entity perspective, the potential of assigned genes including *CCND1* or *MAML3*, of the cohort-wide top ranked SE in terms of H3K27ac activity, should be assessed. The dependency on subgroup-specific key player genes should be elucidated by further RNAi-induced knockdown experiments with subsequent viability measurement. This has been successfully applied for three Mes-specific transcription factors (TF) ETS1, RARB and SMAD3 in in the present study. Here, the choice of the NB cell line is crucial as the expression of subgroup specific genes is assumed to be indispensable for cell survival. A subgroup-specific core TF is not necessarily active in every cell line assigned to this subgroup. As already stated in the enhancer hijacking part, selective inhibition of dysregulated key genes within the networks would be a promising venue towards identifying therapeutical approaches. Targeting enhancer-mediated transcription, e.g. by epigenetic drugs including bromodomain or CDK7 inhibitors, might be another promising strategy. The implication of RAS and JUN/FOS signaling in the Mes subgroup of NB tumors demands a better understanding of the pathways in the subgroup. Since gain-of-function mutations of *RAS* are relatively common in human cancers and frequently detected in NB relapsed tumors, it should be clarified whether there is any connection of RAS mutations and the Mes subgroup in NB. Targeting RAS, either directly or indirectly, with recently developed pan-RAS inhibitors (e.g. compound 3144) or downstream pathway inhibitors might be a promising approach for the treatment of Mes subgroup NBs.

In conclusion, the present study identifies a major involvement of epigenetic deregulation on the chromatin and enhancer level in the pathogenesis of NB. A better understanding of aberrant enhancer functions leading to patient-specific targeting could pave the way towards an individualized and more efficient therapy for this deadly disease.

5. Appendix

5.1 CHIP-seq step-by-step protocol

Cells in a 15 cm dish should have a confluency of approximately 70-80% before fixation.

(~1x10⁶ cells for histone marks and at least 10x10⁶ cells for transcription factors)

Formaldehyde fixation and harvesting of cells

1. Crosslink by adding 1.7 ml of a fresh 16% formaldehyde (FA) ampulla to ~25 ml media (1% FA final conc.).
 2. Shake for 10 min (Polymax 2040 shaker, Heidolph).
 3. Add 2.6 ml of 1.25 M fresh glycine solution.
 4. Shake for 5 min (Polymax 2040 shaker, Heidolph).
 5. Scrape cells and collect medium into 50 ml tubes (working on ice!).
 6. Centrifuge at 1250 rpm for 7 min and remove supernatant.
 7. Resuspend pellet with 1x PBS with proteinase inhibitor and transfer into 1.5 ml tubes.
 8. Centrifuge at 2000 rpm at 4°C for 7min and remove supernatant.
 9. Repeat the washing step 4 times.
- Pellets can be snap-frozen in liquid nitrogen and stored at -80°C.

Cell lysis and sonication

1. Resuspend pellet with 900 µl RIPA I lysis buffer and incubate on ice for 30 min.
2. Aliquot 300 µl into Bioruptor Pico 1.5 ml microtubes with caps.
3. For sonication with a Bioruptor Pico cool down the system to 4°C. Use 30 – 60 cycles of each 30 sec ON and 30 sec OFF intervals.
4. After sonication spin for 15 min at 13300 rpm and 4°C and pool the samples arising from one experiment into a new tube.
5. Take a 15 µl aliquot of the sample as the input control and store at 4°C until next step 6 of the “Immunoprecipitation (IP) and reverse cross-linking” chapter.

Antibody coupling with magnetic beads (prepare during sonication)

1. Wash 75 µl magnetic protein G beads per IP twice with 300 µl binding/blocking buffer using a magnetic device.

-
2. Resuspend the magnetic beads in 100 μ l binding/blocking buffer per IP and add the desired antibody (10 μ g for TF and 3 μ g for histone modifications).
 3. Add 300 μ l of binding/blocking buffer und mix by flicking.
 4. Collect beads using a magnetic device and discard supernatant.
 5. Wash twice with 300 μ l of binding/blocking buffer and proceed immediately with the next step.

Immunoprecipitation (IP) and reverse cross-linking

1. Combine sonicated material for one IP with specific antibodies coupled to beads and tumble the tubes over night at 4°C.
2. Collect beads on a magnetic device and discard supernatant.
3. Transfer magnetic beads in 180 μ l ice cold RIPA buffer to a 96-well plate.
4. Wash beads five times with 200 μ l ice cold RIPA, twice with 200 μ l RIPA-500, twice with 200 μ l LiCl and finally with 200 μ l TE-buffer (no aspirator for TE-buffer).
5. Discard the supernatant and let the beads as dry as possible.
6. Include 8 μ l of input sample from step 5 of the cell lysis and sonication part.
7. Add 50 μ l direct elution buffer to each sample and 42 μ l to each input control.
8. Add per sample a mix of 3 μ l direct elution buffer and 1 μ l RNase A (10 mg/mL, DNase and protease-free) and incubate mix for 30 min at 37°C.
9. Add per sample a mix of 2.5 μ l Proteinase K (10 mg/ml), 1 μ l glycogen (10901393001, Roche) and 1.5 μ l direct elution buffer and incubate 1 h at 37°C.

DNA purification of ChIP DNA

1. Add 135 μ l of SPRI beads to the sample and elute in 44 μ l 10 mM Tris-HCL (pH 8.0).

End repair of ChIP DNA (NEBNext)

1. Add 5 μ l of end repair reaction buffer and 2.5 μ l end repair enzyme mix.
2. Incubate reaction plate for 30 min at 20°C.
3. Add 90 μ l of SPRI beads to the sample and elute in 44 μ l 10 mM Tris-HCL (pH 8.0)

A-tailing of end repaired DNA

1. Add 5 μ l of A-tailing reaction buffer and 3 μ l Klenow Fragment.
2. Incubate reaction plate for 30 min at 37°C.
3. Add 90 μ l of SPRI beads to the sample and elute in 21 μ l 10 mM Tris-HCL (pH 8.0).

Adaptor ligation of A-Tailed DNA

1. Add 6 μ l of Quick ligation reaction buffer, 1 μ l of diluted Adaptor (1.5 μ M) and 5 μ l of Quick T4 DNA Ligase.

2. Incubate reaction plate for 15 min at 20°C.
3. Add 54 µl of SPRI beads to the sample and elute in 25 µl 10 mM Tris-HCL (pH 8.0).

PCR enrichment of adaptor ligated DNA and small size selection

1. Add 25 µl of High-Fidelity PCR Master Mix, 1 µl Universal PCR Primer (25 µM) and 2.5 µl individual Index primer (25 µM) to each sample.
2. Incubate reaction plate:
 - 2.1. 98°C– 0:30 min,
 - 2.2. 98°C– 0:10 min
 - 2.3. 65°C – 0:30 min
 - 2.4. 72°C – 0:30 min (repeat step 2.2. – 2.4. for 10 cycles),
 - 2.5. 72°C – 5:00 min
 - 2.6. 4°C forever
3. Add 37 µl of SPRI beads to the sample and elute in 25 µl 10mM Tris-HCL (pH 8.0)

QC of fragment size distribution and concentration using a Bioanalyzer and Qubit assay

1. Determine the mean peak size and fragment size distribution (e.g. primer dimer). Pool size cutoff as needed.

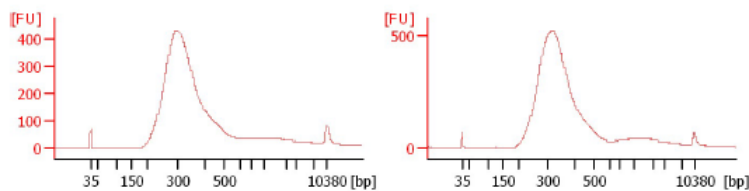


Figure 75: Fragment distribution of ChIP-seq library.

Fragment distribution of ChIP-seq library using a chip of the Bioanalyser Agilent High Sensitivity DNA Kit.

2. Measure the PCR-enriched DNA concentration using the Qubit dsDNA HS kit.
3. Pool equimolar amounts of each sample and sequence multiplexed libraries (50 bases single-end) on the Illumina sequencing platform (German Cancer Research Center Core facility).

5.2 Tumor ChIP-seq step-by-step protocol

Hereinafter, only the different parts to the previous ChIP-seq protocol like cutting, fixation and sonication of the tumor material are described. All downstream procedure has to be performed according to the “ChIP-seq step-by-step protocol (5.1)”.

Preparation of tumor material and formaldehyde fixation

1. Add 500 μ l of 1% formaldehyde in PBS solution with proteinase inhibitor. Vortex 5 sec and incubate 10 min at RT.
2. Add 57 μ l of 1.25 M fresh glycine solution and incubate 5 minutes.
3. Centrifuge 10 min at 2000 rpm and 4°C and remove supernatant.
4. Add 500 μ l ice-cold PBS with proteinase inhibitor and mix.
5. Centrifuge 10 min at 2000 rpm and 4°C and remove supernatant except for 10 μ l. Store at -80°C.

Cell lysis and sonication

1. Resuspend pellet with 120 μ l lysis buffer and use a homogenizer until solution is cloudy. Subsequently incubate on ice for 5 min.
2. For sonication with a Bioruptor Pico cool down the system to 4°C. Use 5 cycles of each 30 sec ON and 30 sec OFF intervals.
3. Centrifuge 10 min at 11200 rpm and 4°C and transfer supernatant into Bioruptor Pico 1.5 ml microtubes with caps.
4. Add 30 μ l lysis buffer to the pellet and mix. Subsequently, centrifuge 10 min at 11200 rpm and 4°C and transfer supernatant into the same Bioruptor Pico 1.5 ml microtubes with caps from step 3.
5. Add 150 μ l RIPA (without SDS) and use Bioruptor Pico for 40 cycles of each 30 sec ON and 30 sec OFF intervals.
6. Add 220 μ l RIPA I (without SDS), centrifuge 10 min at 11200 rpm and 4°C and transfer 500 μ l of supernatant into a new tube.
7. Add 220 μ l RIPA I (without SDS) to the pellet, mix and centrifuge 10 min at 11200 rpm and 4°C.
8. Transfer 400 μ l of the supernatant with the supernatant from step 6.
9. Store 50 μ l of the supernatant for the input at -20°C.

5.3 CHIPmentation step-by-step protocol

Hereinafter, only the different parts to the previous ChIP-seq protocol like reduced sonication time and the whole library preparation of cells or tumor material are described. All downstream procedure has to be performed according to the “ChIP-seq step-by-step protocol” (5.1).

Sonication

1. Resuspend pellet with 900 μ l RIPA I lysis buffer and incubate on ice for 30 min.
2. Aliquot 300 μ l into Bioruptor Pico 1.5 ml microtubes with caps.
3. For sonication with a Bioruptor Pico cool down the system to 4°C. Use 20 cycles of each 30 sec ON and 30 sec OFF intervals.
4. After sonication, spin for 15 min at 13300rpm and 4°C and pool the samples arising from one experiment into a new tube.
5. Take a 15 μ l aliquot of the samples as the input control and store it at 4°C until step 6 of the “Immunoprecipitation (IP) and reverse cross-linking” chapter in (5.1).

Immunoprecipitation (IP) and tagmentation reaction

1. Combine sonicated material for one IP with specific antibodies coupled to beads and tumble the tubes over night at 4°C.
2. Collect beads on a magnetic device and discard supernatant.
3. Transfer magnetic beads in 180 μ l ice cold RIPA buffer to a 96-well plate.
4. Wash beads five times with 200 μ l ice cold RIPA, twice with 200 μ l RIPA-500, twice with 200 μ l LiCl buffer.
5. Wash beads twice with 10 nM Tris-Cl pH 8.0 and transfer the beads-Tris-HCl solution during the second wash into a new tube.
6. Collect beads on a magnetic device.
7. Resuspend beads in 25 μ l of 1x Tagment DNA buffer (Illumina, Nextera DNA Library Prep Kit) and add 1 μ l Tagment DNA Enzyme. Mix and incubate for 1 min at 37°C.
8. Collect beads on an ice-cold magnetic device and discard supernatant.
9. Wash beads twice with 200 μ l ice cold RIPA- and twice with 200 μ l TE-buffer and transfer the beads-TE-solution during the second wash into a new tube.
10. Discard the supernatant and let the beads as dry as possible.
11. Include 8 μ l of input sample from step 5 of the cell lysis and sonication part.
12. Add 50 μ l direct elution buffer to each sample and 42 μ l to each input control.
13. Add per sample a mix of 3 μ l direct elution buffer and 1 μ l RNase A (10 mg/mL, DNase and protease-free) and incubate mix for 30 min at 37°C.

-
14. Add per sample a mix of 2.5 μ l Proteinase K (10mg/ml), 1 μ l glycogen (10901393001, Roche) and 1.5 μ l direct elution buffer and incubate 1 h at 37°C.

DNA purification of CHIP and input DNA

1. Add 135 μ l of SPRI beads to the CHIP and input DNA sample and elute in 25 μ l 10 mM Tris-HCL (pH 8.0)

Input sample preparation

1. Concentration of purified input DNA was measured and diluted in 10 mM Tris-HCl to 2.5 ng/ μ l.
2. Add 0.5 μ l of 1:10-diluted Tagment DNA enzyme and 2.5 μ l 2x Tagment DNA buffer.
3. Mix and incubate for 5 min at 55°C.
4. Clean up the reaction mix by using the Qiagen MinElute kit according to manufacturers' protocol and elute in 25 μ l Tris-HCl.

PCR Enrichment of CHIP and input DNA and small size selection

1. The 25 μ l CHIP- and input samples were PCR amplified using 25 μ l Illumina or KAPA Biosystems PCR Master Mix, 5 μ l of Illumina or KAPA Biosystems PCR Primer Cocktail and each 5 μ l of compatible Illumina index primer i7 and i5.
2. Incubate reaction plate:
 1. 72°C– 3:00 min,
 2. 98°C– 0:30 min
 3. 98°C– 0:10 min
 4. 63°C – 0:30 min
 5. 72°C – 0:30 min (repeat step 2. – 5. for 12 cycles),
 6. 72°C – 3:00 min
 7. 4°C forever
4. Add 91 μ l of SPRI beads to the sample and elute in 25 μ l 10 mM Tris-HCL (pH 8.0).

5.4 4C-seq step-by-step protocol

Protocol for cell culture material and approximately 10^7 loose cells.

Harvesting cells

1. Remove media completely and wash cells briefly with 5 ml versene.
2. Add 3 ml trypsin (0.25 mg/ml; Lonza) per plate and incubate 5 min at 37°C.
3. Detach cells gently and inactivate trypsin by adding 9 ml media with 10% FCS.
4. Collect cell solution in 50 ml falcon.
5. Count cells (10 μ l trypan blue (TB) + 10 μ l cells) Luna - automated cell counter) and prepare aliquots of 10^7 cells in 50 ml reaction tubes.
6. Centrifuge 5 min at 1100 rpm and RT in swing out centrifuge.
7. Discard supernatant by pouring and resuspend pellet in 5 ml PBS with 10% FCS.

Formaldehyde fixation

1. Add 5 ml 4% formaldehyde to the cell suspension in PBS with 10% FCS.
2. Incubate 10 min at RT while tumbling.
3. Add 1.425 ml 1M glycine, mix and put tubes immediately on ice.
4. Continue immediately and centrifuge 8 min at 1300 rpm and RT and remove supernatant.

Cell lysis

1. Resuspend pellet in 1 ml freshly prepared 4C lysis buffer and incubate 5 min at RT, then 5 min in 65°C waterbath and transfer on ice.
2. Perform verification of successful cell lysis by mixing 2 μ l TB with 3 μ l cells and microscopic evaluation.
 - In the case of insufficient cell lysis repeat step lysis at 65°C or try to homogenize cells mechanically.
3. Centrifuge 8 min at 1800 rpm and RT and remove supernatant.
4. Resuspend pellets in 1 ml PBS and transfer to 1.5 ml tube.
5. Centrifuge 2 min at 2400 rpm and 4°C and remove supernatant.
 - Pellets could be snap frozen in liquid nitrogen and stored at -80°C.

First digestion (Restriction enzyme (RE) *DpnII*; NEB)

1. Resuspend cell pellet in 440 μ l and 60 μ l 10x RE-buffer.

-
2. Add 15 µl 10% SDS and incubate at 37°C for 1 h while shaking at 900 rpm.
 3. Add 75 µl 20% Triton X-100 and incubate at 37°C for 1 h while shaking at 900 rpm.
 4. Take a 5 µl aliquot of the sample as the “undigested control”.
 5. Add 200 U RE *DpnII*, incubate 4 h at 37°C while shaking at 900 rpm.
 6. Add 200 U RE *DpnII*, incubate o/n at 37°C while shaking at 900 rpm.
 7. Add 200 U RE *DpnII*, incubate 4 h at 37°C while shaking at 900 rpm.
 8. Take 5 µl aliquot of the sample as the “digested control”.
 9. Verification of digestion efficiency:
Add 2.5 µl Prot K (20 mg/ml) and incubate for 1 h at 65°C. Compare 20 µl of digested and undigested control sample on a 0.6% agarose gel.

- In case of insufficient digestion efficiency repeat step 5-7.

First ligation

1. Inactivate enzyme (*DpnII*) by incubating 20 min at 65°C.
2. For diluted ligation, transfer each sample to a 50 ml reaction tube.
3. Add 700 µl 10X 4C ligation buffer and H₂O up to 7 ml.
4. Add 10 µl T4 Ligase (Roche 5U/µl) and incubate o/n at 16°C.
5. Take a 100 µl aliquot of the sample as the “ligated control”.
6. Verification of ligation efficiency:
Add 2.5µl Prot K (20 mg/ml) and incubate for 1 h at 65°C. Compare 20 µl of digested and undigested control sample on a 0.6% agarose gel.

- In case of insufficient ligation efficiency repeat step 5-7 and add fresh ATP to ligation buffer.

Reverse crosslinking and precipitation

1. In case of sufficient ligation efficiency add Prot K (20 mg/ml) to the samples and de-crosslink o/n at 65°C (waterbath).
2. Add 30 µl RNase A (10 mg/ml) and incubate 45 min at 37°C.
3. Add 7 ml phenol-chloroform, mix vigorously.
4. Centrifuge at 3750 rpm for 15 min at RT and transfer water phase carefully to a new 50 ml reaction tube.
5. Add 7 ml H₂O, 7 µl Glycogen, 1.5 ml 2M NaAC (pH 5.6) and 35 ml 100% ethanol.
6. Mix and place at -80°C until the sample is completely frozen (o/n).
7. Centrifuge at 4500 rpm for 45 min at 4°C and remove the supernatant.

-
8. Add 10 ml ice cold 70% ethanol and centrifuge 15 min at 4500 rpm and 4°C.
 9. Remove the supernatant and briefly dry the pellet at RT.
 10. Resuspend and dissolve the pellet in 150 µl pre-warmed Tris (10 mM, pH 7.5, 37°C).
 11. Samples can be stored at this point at -20 °C.

Second digestion (RE *Csp6I* (NEB) /*Bfal* (Thermo Fisher Scientific))

1. To 150 µl 4C sample add 50 µl 10X RE buffer, 50 U RE *Csp6I* or *Bfal*, fill up with water to 500 µl and incubate o/n at 37°C.
2. Take a 5 µl aliquot of the sample as the “second digested control”.
3. Verification of digestion efficiency:
Add 95 µl 10 mM Tris pH 7.5 to the 5 µl sample second digested control. Compare 20 µl of “undigested” and “second digested” control sample on a 0.6% agarose gel.

In case of insufficient digestion efficiency repeat step 1-3.

Second ligation

1. Inactivate enzyme (*DpnII*) by incubating 20 min at 65°C.
2. For diluted ligation, transfer each sample to a 50 ml reaction tube.
3. Add 1.4 ml 10X 4C ligation buffer and H₂O up to 14 ml.
4. Add 20 µl T4 Ligase (Roche 5 U/µl) and incubate o/n at 16°C.

Precipitation

1. Add 1.4 ml 2M NaAC (pH 5.6), 14 µl glycogen and 35 ml 100% ethanol.
2. Mix and place at -80°C until the sample is completely frozen (o/n).
3. Centrifuge at 3750 rpm for 45 min at 4°C and remove the supernatant.
4. Remove supernatant and add 15 ml cold 70% ethanol.
5. Centrifuge at 3750 rpm for 15 min at 20°C, remove the supernatant and briefly dry the pellet at RT.
6. Resuspend and dissolve the pellet in 150 µl pre-warmed Tris (10 mM, pH 7.5, 37°C).

Purification of 4C samples

1. Use 3 columns of the QIAquick PCR purification kit per 4C sample according to the manufacturer’s protocol.
2. Elute columns in total 50 µl of 10 mM Tris (pH 7.5) and measure the concentration.
3. Samples can be stored at this point at -20°C.

Primer design and preliminary amplification

1. Forward and reverse primer for each viewpoint were designed according to the published protocol (van de Werken et al. 2012).
2. A preliminary PCR was performed for each sample to assess the quality of primers and the best amount of 4C material for the final preparative amplification step.

Preparative amplification

1. For preparative PCR the Expand Long Template PCR System (Roche) was used.
2. A master mix sufficient for 16 PCR reactions with a volume of 50 µl each was prepared. for each viewpoint and sample.

Prepare and mix (single reaction):

5 µl 10X PCR buffer 1.1 µl dNTPs (10 mM), 1.5 µl forward primer (1 µg/µl), 1 µl reverse primer (1 µg/µl), 0.7 µl Polymerase ELT and 50 – 200 ng 4C-PCR template.

3. Run the following PCR program:
 1. 94°C– 2:00 min,
 2. 94°C– 00:15 min
 3. 55°C– 1:00 min
 4. 68°C – 3:00 min (repeat step 2. – 4. for 35 cycles),
 5. 68°C – 7:00 min
 6. 4°C forever

Purification of PCR products

1. Pooling of all samples per 4C-PCR and purification to get rid of primer dimer by using 2 columns of the high pure PCR template preparation kit (Roche) according to the manufacturer's protocol.
2. Elute each column in 50 µl of 10 mM Tris (pH 7.5) - of each 4C-PCR.
3. As a last purification step, use 2 columns of the QIAquick PCR purification kit (Qiagen) per 4C sample according to the manufacturer's protocol.
4. Elute each column in 50 µl of 10 mM Tris (pH 7.5) and measure the concentration using a Nanodrop ND-1000.
5. Check fragment size of each 4C-PCR sample on a 1% agarose gel.

Sample preparation of sequencing

1. Prepare a 1:3 (sample 4-6) and 1:6 (sample 7-9) dilution of the pooled 4C libraries and measure fragment distribution by loading triplicates on a chip of the Bioanalyser Agilent DNA 12000 Kit according to the manufacturer's protocol.
2. Determine the mean peak size and the overall molarity of the pooled 4C libraries and adjust to a final concentration of 10 nM for submission.

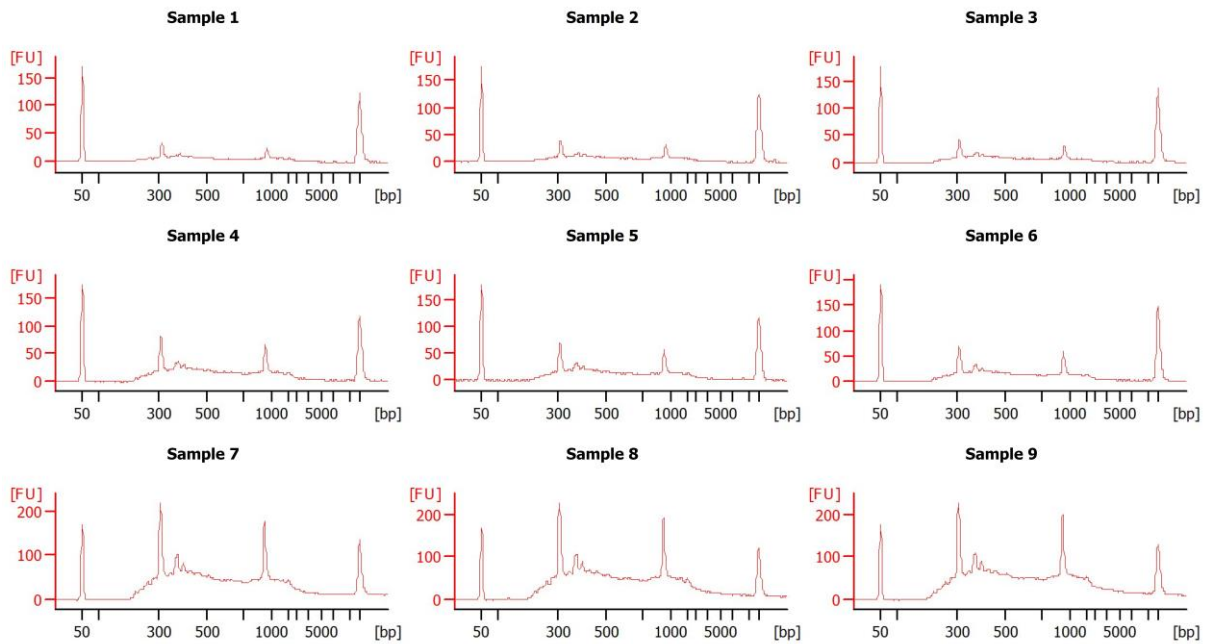


Figure 76: Fragment distribution of 4C-seq library.

Fragment distribution using a chip of the Bioanalyser Agilent DNA 12000 Kit of undiluted (sample 1-3), 1:3 (sample 4-6) and 1:6 (sample 7-9) diluted pooled 4C libraries.

3. Libraries were sequenced (50 bases single-end) on the Illumina sequencing platform (German Cancer Research Center Core facility).

5.5 Further figures and tables

Enjancer hijacking events in NB cell lines					
cell line	Acceptor region	Genomic position	Donor region	Genomic position	associated gene
GI-ME-N	<i>TERT</i>	/	Chr. 19	/	/
LAN2	<i>TERT</i>	/	Chr. X	/	/
KELLY	<i>TERT</i>	/	Chr. 2	/	<i>ALK</i>
CLB-GA	<i>TERT</i>	/	Chr. 20	/	/
NBL-S	<i>MYCN</i>	chr2:16,023,867	Chr. 4	chr4:174,964,065	<i>HAND2</i>
NB69	<i>MYC</i>	chr8:128,803,002	Chr. 4	chr4:174,487,645	<i>HAND2</i>
SK-N-AS	<i>MYC</i>	chr8:129,902,921	Chr. 4	chr4:174,820,996	<i>HAND2</i>
SH-SY-5Y	<i>MYC</i>	chr8:129,065,737	Chr. 7	chr7:134,080,765	<i>EXOC4</i>
CHLA15/20	<i>MYC</i>	chr8:128,855,087	Chr. 4	chr4:174,661,821	<i>HAND2</i>
CLB-GA	<i>IGF2BP1</i>	chr17:47,031,746	Chr. 4	chr4:175,024,980	<i>HAND2</i>

Figure 77: Summary of rearrangements in NB cell lines (hg19) including genomic position and assigned gene of acceptor and donor region.

References

- Abel, F., K. Ejeskar, et al. (1999). "Gain of chromosome arm 17q is associated with unfavourable prognosis in neuroblastoma, but does not involve mutations in the somatostatin receptor 2(SSTR2) gene at 17q24." *Br J Cancer* **81**(8): 1402-1409.
- Ali, T., R. Renkawitz, et al. (2016). "Insulators and domains of gene expression." *Curr Opin Genet Dev* **37**: 17-26.
- Allfrey, V. G., R. Faulkner, et al. (1964). "Acetylation and Methylation of Histones and Their Possible Role in the Regulation of Rna Synthesis." *Proc Natl Acad Sci U S A* **51**: 786-794.
- Allfrey, V. G. and A. E. Mirsky (1964). "Structural Modifications of Histones and their Possible Role in the Regulation of RNA Synthesis." *Science* **144**(3618): 559.
- Althoff, K., A. Beckers, et al. (2015). "A Cre-conditional MYCN-driven neuroblastoma mouse model as an improved tool for preclinical studies." *Oncogene* **34**(26): 3357-3368.
- Alvarez, M. J., Y. Shen, et al. (2016). "Functional characterization of somatic mutations in cancer using network-based inference of protein activity." *Nat Genet* **48**(8): 838-847.
- Amiel, J., B. Laudier, et al. (2003). "Polyalanine expansion and frameshift mutations of the paired-like homeobox gene PHOX2B in congenital central hypoventilation syndrome." *Nat Genet* **33**(4): 459-461.
- Arumugam, T., V. Ramachandran, et al. (2009). "Epithelial to mesenchymal transition contributes to drug resistance in pancreatic cancer." *Cancer Res* **69**(14): 5820-5828.
- Astuti, D., A. Agathangelou, et al. (2001). "RASSF1A promoter region CpG island hypermethylation in phaeochromocytomas and neuroblastoma tumours." *Oncogene* **20**(51): 7573-7577.
- Aviel-Ronen, S., F. H. Blackhall, et al. (2006). "K-ras mutations in non-small-cell lung carcinoma: a review." *Clin Lung Cancer* **8**(1): 30-38.
- Ayrault, O., H. Zhao, et al. (2010). "Atoh1 inhibits neuronal differentiation and collaborates with Gli1 to generate medulloblastoma-initiating cells." *Cancer Res* **70**(13): 5618-5627.
- Bakhshi, A., J. J. Wright, et al. (1987). "Mechanism of the t(14;18) chromosomal translocation: structural analysis of both derivative 14 and 18 reciprocal partners." *Proc Natl Acad Sci U S A* **84**(8): 2396-2400.
- Bannister, A. J. and T. Kouzarides (2011). "Regulation of chromatin by histone modifications." *Cell Res* **21**(3): 381-395.
- Barski, A., S. Cuddapah, et al. (2007). "High-resolution profiling of histone methylations in the human genome." *Cell* **129**(4): 823-837.
- Baylin, S. B. and P. A. Jones (2011). "A decade of exploring the cancer epigenome - biological and translational implications." *Nat Rev Cancer* **11**(10): 726-734.
- Bell, A. C. and G. Felsenfeld (2000). "Methylation of a CTCF-dependent boundary controls imprinted expression of the Igf2 gene." *Nature* **405**(6785): 482-485.
- Bell, J. L., R. Turlapati, et al. (2015). "IGF2BP1 harbors prognostic significance by gene gain and diverse expression in neuroblastoma." *J Clin Oncol* **33**(11): 1285-1293.
- Berger, S. L., T. Kouzarides, et al. (2009). "An operational definition of epigenetics." *Genes Dev* **23**(7): 781-783.
- Bernstein, B. E., T. S. Mikkelsen, et al. (2006). "A bivalent chromatin structure marks key developmental genes in embryonic stem cells." *Cell* **125**(2): 315-326.
- Binz, N., T. Shalaby, et al. (2005). "Telomerase inhibition, telomere shortening, cell growth suppression and induction of apoptosis by telomestatin in childhood neuroblastoma cells." *Eur J Cancer* **41**(18): 2873-2881.
- Blecher-Gonen, R., Z. Barnett-Itzhaki, et al. (2013). "High-throughput chromatin immunoprecipitation for genome-wide mapping of in vivo protein-DNA interactions and epigenomic states." *Nat Protoc* **8**(3): 539-554.

-
- Boeva, V., C. Louis-Brennetot, et al. (2017). "Heterogeneity of neuroblastoma cell identity defined by transcriptional circuitries." *Nat Genet* **49**(9): 1408-1413.
- Boros, J., N. Arnoult, et al. (2014). "Polycomb repressive complex 2 and H3K27me3 cooperate with H3K9 methylation to maintain heterochromatin protein 1alpha at chromatin." *Mol Cell Biol* **34**(19): 3662-3674.
- Bown, N. (2001). "Neuroblastoma tumour genetics: clinical and biological aspects." *J Clin Pathol* **54**(12): 897-910.
- Bown, N., S. Cotterill, et al. (1999). "Gain of chromosome arm 17q and adverse outcome in patients with neuroblastoma." *N Engl J Med* **340**(25): 1954-1961.
- Bradford, M. M. (1976). "A rapid and sensitive method for the quantitation of microgram quantities of protein utilizing the principle of protein-dye binding." *Anal Biochem* **72**: 248-254.
- Breit, S. and M. Schwab (1989). "Suppression of MYC by high expression of NMYC in human neuroblastoma cells." *J Neurosci Res* **24**(1): 21-28.
- Brodeur, G. M. (2003). "Neuroblastoma: biological insights into a clinical enigma." *Nat Rev Cancer* **3**(3): 203-216.
- Brodeur, G. M., J. Pritchard, et al. (1993). "Revisions of the international criteria for neuroblastoma diagnosis, staging, and response to treatment." *J Clin Oncol* **11**(8): 1466-1477.
- Brodeur, G. M., R. C. Seeger, et al. (1984). "Amplification of N-myc in untreated human neuroblastomas correlates with advanced disease stage." *Science* **224**(4653): 1121-1124.
- Brodeur, G. M., G. Sekhon, et al. (1977). "Chromosomal aberrations in human neuroblastomas." *Cancer* **40**(5): 2256-2263.
- Brueckner, L. M., E. M. Hess, et al. (2013). "Instability at the FRA81 common fragile site disrupts the genomic integrity of the KIAA0146, CEBPD and PRKDC genes in colorectal cancer." *Cancer Lett* **336**(1): 85-95.
- Buenrostro, J. D., P. G. Giresi, et al. (2013). "Transposition of native chromatin for fast and sensitive epigenomic profiling of open chromatin, DNA-binding proteins and nucleosome position." *Nat Methods* **10**(12): 1213-1218.
- Buenrostro, J. D., B. Wu, et al. (2015). "ATAC-seq: A Method for Assaying Chromatin Accessibility Genome-Wide." *Curr Protoc Mol Biol* **109**: 21 29 21-29.
- Bulger, M. and M. Groudine (2011). "Functional and mechanistic diversity of distal transcription enhancers." *Cell* **144**(3): 327-339.
- Calcia, A., G. Gai, et al. (2013). "Bilaterally cleft lip and bilateral thumb polydactyly with triphalangeal component in a patient with two de novo deletions of HSA 4q32 and 4q34 involving PDGFC, GRIA2, and FBXO8 genes." *Am J Med Genet A* **161A**(10): 2656-2662.
- Caren, H., F. Abel, et al. (2008). "High incidence of DNA mutations and gene amplifications of the ALK gene in advanced sporadic neuroblastoma tumours." *Biochem J* **416**(2): 153-159.
- Castleberry, R. P. (1997). "Biology and treatment of neuroblastoma." *Pediatr Clin North Am* **44**(4): 919-937.
- Castleberry, R. P. (1997). "Neuroblastoma." *Eur J Cancer* **33**(9): 1430-1437; discussion 1437-1438.
- Chen, H., C. Li, et al. (2018). "A Pan-Cancer Analysis of Enhancer Expression in Nearly 9000 Patient Samples." *Cell* **173**(2): 386-399 e312.
- Chen, Y., J. Takita, et al. (2008). "Oncogenic mutations of ALK kinase in neuroblastoma." *Nature* **455**(7215): 971-974.
- Cheung, N. K., J. Zhang, et al. (2012). "Association of age at diagnosis and genetic mutations in patients with neuroblastoma." *JAMA* **307**(10): 1062-1071.
- Chipumuro, E., E. Marco, et al. (2014). "CDK7 inhibition suppresses super-enhancer-linked oncogenic transcription in MYCN-driven cancer." *Cell* **159**(5): 1126-1139.
- Cho, K. B., M. K. Cho, et al. (2010). "Overexpression of c-myc induces epithelial mesenchymal transition in mammary epithelial cells." *Cancer Lett* **293**(2): 230-239.

-
- Cohen, A. J., A. Saiakhova, et al. (2017). "Hotspots of aberrant enhancer activity punctuate the colorectal cancer epigenome." *Nat Commun* **8**: 14400.
- Cox, D., C. Yuncken, et al. (1965). "Minute Chromatin Bodies in Malignant Tumours of Childhood." *Lancet* **1**(7402): 55-58.
- Creyghton, M. P., A. W. Cheng, et al. (2010). "Histone H3K27ac separates active from poised enhancers and predicts developmental state." *Proc Natl Acad Sci U S A* **107**(50): 21931-21936.
- Dahl, J. A. and P. Collas (2008). "A rapid micro chromatin immunoprecipitation assay (microChIP)." *Nat Protoc* **3**(6): 1032-1045.
- Decock, A., M. Ongenaert, et al. (2011). "Neuroblastoma epigenetics: from candidate gene approaches to genome-wide screenings." *Epigenetics* **6**(8): 962-970.
- Demichelis, F., S. R. Setlur, et al. (2012). "Identification of functionally active, low frequency copy number variants at 15q21.3 and 12q21.31 associated with prostate cancer risk." *Proc Natl Acad Sci U S A* **109**(17): 6686-6691.
- Derks, S., L. J. Bosch, et al. (2009). "Promoter CpG island hypermethylation- and H3K9me3 and H3K27me3-mediated epigenetic silencing targets the deleted in colon cancer (DCC) gene in colorectal carcinogenesis without affecting neighboring genes on chromosomal region 18q21." *Carcinogenesis* **30**(6): 1041-1048.
- Dreidax, D., S. Bannert, et al. (2014). "p19-INK4d inhibits neuroblastoma cell growth, induces differentiation and is hypermethylated and downregulated in MYCN-amplified neuroblastomas." *Hum Mol Genet* **23**(25): 6826-6837.
- Duan, X. F. and Q. Zhao (2018). "TERT-mediated and ATRX-mediated Telomere Maintenance and Neuroblastoma." *J Pediatr Hematol Oncol* **40**(1): 1-6.
- Duffy, D. J., A. Krstic, et al. (2017). "Retinoic acid and TGF-beta signalling cooperate to overcome MYCN-induced retinoid resistance." *Genome Med* **9**(1): 15.
- Edelmann, J., K. Holzmann, et al. (2012). "High-resolution genomic profiling of chronic lymphocytic leukemia reveals new recurrent genomic alterations." *Blood* **120**(24): 4783-4794.
- Egger, G., G. Liang, et al. (2004). "Epigenetics in human disease and prospects for epigenetic therapy." *Nature* **429**(6990): 457-463.
- Eleveld, T. F., D. A. Oldridge, et al. (2015). "Relapsed neuroblastomas show frequent RAS-MAPK pathway mutations." *Nat Genet* **47**(8): 864-871.
- Emanuel, B. S., G. Balaban, et al. (1985). "N-myc amplification in multiple homogeneously staining regions in two human neuroblastomas." *Proc Natl Acad Sci U S A* **82**(11): 3736-3740.
- Feinberg, A. P. and B. Vogelstein (1983). "Hypomethylation distinguishes genes of some human cancers from their normal counterparts." *Nature* **301**(5895): 89-92.
- Feinberg, A. P. and B. Vogelstein (1983). "Hypomethylation of ras oncogenes in primary human cancers." *Biochem Biophys Res Commun* **111**(1): 47-54.
- Filippakopoulos, P., J. Qi, et al. (2010). "Selective inhibition of BET bromodomains." *Nature* **468**(7327): 1067-1073.
- Flavahan, W. A., Y. Drier, et al. (2016). "Insulator dysfunction and oncogene activation in IDH mutant gliomas." *Nature* **529**(7584): 110-114.
- Fong, C. T., N. C. Dracopoli, et al. (1989). "Loss of heterozygosity for the short arm of chromosome 1 in human neuroblastomas: correlation with N-myc amplification." *Proc Natl Acad Sci U S A* **86**(10): 3753-3757.
- Foret, M. R., R. S. Sandstrom, et al. (2014). "Molecular targets of chromatin repressive mark H3K9me3 in primate progenitor cells within adult neurogenic niches." *Front Genet* **5**: 252.
- Forrest, A. R., H. Kawaji, et al. (2014). "A promoter-level mammalian expression atlas." *Nature* **507**(7493): 462-470.
- Forrester, K., C. Almoguera, et al. (1987). "Detection of high incidence of K-ras oncogenes during human colon tumorigenesis." *Nature* **327**(6120): 298-303.

-
- Fukuda, T., A. Shirane, et al. (2015). "HAND2-mediated proteolysis negatively regulates the function of estrogen receptor alpha." *Mol Med Rep* **12**(4): 5538-5544.
- Fungtammasan, A., E. Walsh, et al. (2012). "A genome-wide analysis of common fragile sites: what features determine chromosomal instability in the human genome?" *Genome Res* **22**(6): 993-1005.
- Gal-Yam, E. N., G. Egger, et al. (2008). "Frequent switching of Polycomb repressive marks and DNA hypermethylation in the PC3 prostate cancer cell line." *Proc Natl Acad Sci U S A* **105**(35): 12979-12984.
- Gallego, S., J. Reventos, et al. (1998). "Differential polymerase chain reaction with serial dilutions for quantification of MYCN gene amplification in neuroblastoma." *Anticancer Res* **18**(2A): 1211-1215.
- Gao, Q., K. Wang, et al. (2017). "HBx protein-mediated ATOH1 downregulation suppresses ARID2 expression and promotes hepatocellular carcinoma." *Cancer Sci* **108**(7): 1328-1337.
- George, R. E., T. Sanda, et al. (2008). "Activating mutations in ALK provide a therapeutic target in neuroblastoma." *Nature* **455**(7215): 975-978.
- Goldberg, A. D., C. D. Allis, et al. (2007). "Epigenetics: a landscape takes shape." *Cell* **128**(4): 635-638.
- Goll, M. G. and T. H. Bestor (2005). "Eukaryotic cytosine methyltransferases." *Annu Rev Biochem* **74**: 481-514.
- Grau, E., F. Martinez, et al. (2011). "Hypermethylation of apoptotic genes as independent prognostic factor in neuroblastoma disease." *Mol Carcinog* **50**(3): 153-162.
- Grausam, K. B., S. D. R. Dooyema, et al. (2017). "ATOH1 Promotes Leptomeningeal Dissemination and Metastasis of Sonic Hedgehog Subgroup Medulloblastomas." *Cancer Res* **77**(14): 3766-3777.
- Greider, C. W. and E. H. Blackburn (1989). "A telomeric sequence in the RNA of Tetrahymena telomerase required for telomere repeat synthesis." *Nature* **337**(6205): 331-337.
- Grobner, S. N., B. C. Worst, et al. (2018). "The landscape of genomic alterations across childhood cancers." *Nature* **555**(7696): 321-327.
- Groschel, S., M. A. Sanders, et al. (2014). "A single oncogenic enhancer rearrangement causes concomitant EVI1 and GATA2 deregulation in leukemia." *Cell* **157**(2): 369-381.
- Gu, Z., L. Gu, et al. (2014). "circlize Implements and enhances circular visualization in R." *Bioinformatics* **30**(19): 2811-2812.
- Guenther, M. G., S. S. Levine, et al. (2007). "A chromatin landmark and transcription initiation at most promoters in human cells." *Cell* **130**(1): 77-88.
- Gustafson, W. C. and W. A. Weiss (2010). "Myc proteins as therapeutic targets." *Oncogene* **29**(9): 1249-1259.
- Hahn, M. A., A. X. Li, et al. (2014). "Loss of the polycomb mark from bivalent promoters leads to activation of cancer-promoting genes in colorectal tumors." *Cancer Res* **74**(13): 3617-3629.
- Harvey, C. T., G. A. Moyerbrailean, et al. (2015). "QuASAR: quantitative allele-specific analysis of reads." *Bioinformatics* **31**(8): 1235-1242.
- Hata, Y., H. Naito, et al. (1990). "Fifteen years' experience of neuroblastoma: a prognostic evaluation according to the Evans and UICC staging systems." *J Pediatr Surg* **25**(3): 326-329.
- Hatzis, P. and I. Talianidis (2002). "Dynamics of enhancer-promoter communication during differentiation-induced gene activation." *Mol Cell* **10**(6): 1467-1477.
- Hauser, S., D. Widera, et al. (2012). "Isolation of novel multipotent neural crest-derived stem cells from adult human inferior turbinate." *Stem Cells Dev* **21**(5): 742-756.
- Haverty, P. M., L. S. Hon, et al. (2009). "High-resolution analysis of copy number alterations and associated expression changes in ovarian tumors." *BMC Med Genomics* **2**: 21.
- Hayashi, Y., N. Kanda, et al. (1989). "Cytogenetic findings and prognosis in neuroblastoma with emphasis on marker chromosome 1." *Cancer* **63**(1): 126-132.

-
- Hayes, F. A., A. Green, et al. (1983). "Surgicopathologic staging of neuroblastoma: prognostic significance of regional lymph node metastases." *J Pediatr* **102**(1): 59-62.
- Hayflick, L. (1965). "The Limited in Vitro Lifetime of Human Diploid Cell Strains." *Exp Cell Res* **37**: 614-636.
- He, Y. F., B. Z. Li, et al. (2011). "Tet-mediated formation of 5-carboxylcytosine and its excision by TDG in mammalian DNA." *Science* **333**(6047): 1303-1307.
- Heaphy, C. M., R. F. de Wilde, et al. (2011). "Altered telomeres in tumors with ATRX and DAXX mutations." *Science* **333**(6041): 425.
- Heidenreich, B., P. S. Rachakonda, et al. (2015). "TERT promoter mutations and telomere length in adult malignant gliomas and recurrences." *Oncotarget* **6**(12): 10617-10633.
- Heintzman, N. D. and B. Ren (2009). "Finding distal regulatory elements in the human genome." *Curr Opin Genet Dev* **19**(6): 541-549.
- Heintzman, N. D., R. K. Stuart, et al. (2007). "Distinct and predictive chromatin signatures of transcriptional promoters and enhancers in the human genome." *Nat Genet* **39**(3): 311-318.
- Hendershot, T. J., H. Liu, et al. (2008). "Conditional deletion of Hand2 reveals critical functions in neurogenesis and cell type-specific gene expression for development of neural crest-derived noradrenergic sympathetic ganglion neurons." *Dev Biol* **319**(2): 179-191.
- Henrich, K. O., T. Bauer, et al. (2011). "CAMTA1, a 1p36 tumor suppressor candidate, inhibits growth and activates differentiation programs in neuroblastoma cells." *Cancer Res* **71**(8): 3142-3151.
- Henrich, K. O., S. Bender, et al. (2016). "Integrative Genome-Scale Analysis Identifies Epigenetic Mechanisms of Transcriptional Deregulation in Unfavorable Neuroblastomas." *Cancer Res* **76**(18): 5523-5537.
- Henrich, K. O., M. Fischer, et al. (2006). "Reduced expression of CAMTA1 correlates with adverse outcome in neuroblastoma patients." *Clin Cancer Res* **12**(1): 131-138.
- Hermann, A., R. Goyal, et al. (2004). "The Dnmt1 DNA-(cytosine-C5)-methyltransferase methylates DNA processively with high preference for hemimethylated target sites." *J Biol Chem* **279**(46): 48350-48359.
- Herranz, D., A. Ambesi-Impiombato, et al. (2014). "A NOTCH1-driven MYC enhancer promotes T cell development, transformation and acute lymphoblastic leukemia." *Nat Med* **20**(10): 1130-1137.
- Herz, H. M. (2016). "Enhancer deregulation in cancer and other diseases." *Bioessays* **38**(10): 1003-1015.
- Higashi, M., V. Kolla, et al. (2015). "Retinoic acid-induced CHD5 upregulation and neuronal differentiation of neuroblastoma." *Mol Cancer* **14**: 150.
- Hnisz, D., B. J. Abraham, et al. (2013). "Super-enhancers in the control of cell identity and disease." *Cell* **155**(4): 934-947.
- Hoebbeck, J., E. Michels, et al. (2009). "Aberrant methylation of candidate tumor suppressor genes in neuroblastoma." *Cancer Lett* **273**(2): 336-346.
- Holliday, R. and J. E. Pugh (1975). "DNA modification mechanisms and gene activity during development." *Science* **187**(4173): 226-232.
- Hon, G. C., R. D. Hawkins, et al. (2009). "Predictive chromatin signatures in the mammalian genome." *Hum Mol Genet* **18**(R2): R195-201.
- Horn, S., A. Figl, et al. (2013). "TERT promoter mutations in familial and sporadic melanoma." *Science* **339**(6122): 959-961.
- Hosen, I., P. S. Rachakonda, et al. (2015). "Mutations in TERT promoter and FGFR3 and telomere length in bladder cancer." *Int J Cancer* **137**(7): 1621-1629.
- Hosen, I., P. S. Rachakonda, et al. (2015). "TERT promoter mutations in clear cell renal cell carcinoma." *Int J Cancer* **136**(10): 2448-2452.
- Huang, F. W., E. Hodis, et al. (2013). "Highly recurrent TERT promoter mutations in human melanoma." *Science* **339**(6122): 957-959.

-
- Huang, Q., T. Whittington, et al. (2014). "A prostate cancer susceptibility allele at 6q22 increases RFX6 expression by modulating HOXB13 chromatin binding." *Nat Genet* **46**(2): 126-135.
- Huang, Y. and A. Rao (2012). "New functions for DNA modifications by TET-JBP." *Nat Struct Mol Biol* **19**(11): 1061-1064.
- Huether, R., L. Dong, et al. (2014). "The landscape of somatic mutations in epigenetic regulators across 1,000 paediatric cancer genomes." *Nat Commun* **5**: 3630.
- Iacobuzio-Donahue, C. A. (2009). "Epigenetic changes in cancer." *Annu Rev Pathol* **4**: 229-249.
- Imamura, J., C. R. Bartram, et al. (1993). "Mutation of the p53 gene in neuroblastoma and its relationship with N-myc amplification." *Cancer Res* **53**(17): 4053-4058.
- Iolascon, A., M. Badiali, et al. (1993). "Rare frequency of point mutations for codon 12, 13 and 61 of ras gene in italian neuroblastoma." *Int J Oncol* **3**(3): 529-533.
- Irizarry, R. A., C. Ladd-Acosta, et al. (2009). "The human colon cancer methylome shows similar hypo- and hypermethylation at conserved tissue-specific CpG island shores." *Nat Genet* **41**(2): 178-186.
- Ito, S., L. Shen, et al. (2011). "Tet proteins can convert 5-methylcytosine to 5-formylcytosine and 5-carboxylcytosine." *Science* **333**(6047): 1300-1303.
- Janoueix-Lerosey, I., D. Lequin, et al. (2008). "Somatic and germline activating mutations of the ALK kinase receptor in neuroblastoma." *Nature* **455**(7215): 967-970.
- Jiang, M., J. Stanke, et al. (2011). "The connections between neural crest development and neuroblastoma." *Curr Top Dev Biol* **94**: 77-127.
- Jiang, Y., I. Lucas, et al. (2009). "Common fragile sites are characterized by histone hypoacetylation." *Hum Mol Genet* **18**(23): 4501-4512.
- Johnsen, J. I., P. Kogner, et al. (2009). "Embryonal neural tumours and cell death." *Apoptosis* **14**(4): 424-438.
- Jones, P. A. (2012). "Functions of DNA methylation: islands, start sites, gene bodies and beyond." *Nat Rev Genet* **13**(7): 484-492.
- Kalkat, M., J. De Melo, et al. (2017). "MYC Deregulation in Primary Human Cancers." *Genes (Basel)* **8**(6).
- Kandoth, C., M. D. McLellan, et al. (2013). "Mutational landscape and significance across 12 major cancer types." *Nature* **502**(7471): 333-339.
- Kaneko, Y., N. Kanda, et al. (1987). "Different karyotypic patterns in early and advanced stage neuroblastomas." *Cancer Res* **47**(1): 311-318.
- Kazanjian, A. and N. F. Shroyer (2011). "NOTCH Signaling and ATOH1 in Colorectal Cancers." *Curr Colorectal Cancer Rep* **7**(2): 121-127.
- Kim, N. W., M. A. Piatyszek, et al. (1994). "Specific association of human telomerase activity with immortal cells and cancer." *Science* **266**(5193): 2011-2015.
- Kim, T., T. Havighurst, et al. (2018). "Targeting insulin-like growth factor 2 mRNA-binding protein 1 (IGF2BP1) in metastatic melanoma to increase efficacy of BRAF(V600E) inhibitors." *Mol Carcinog* **57**(5): 678-683.
- Kim, T., T. Havighurst, et al. (2017). "RNA-Binding Protein IGF2BP1 in Cutaneous Squamous Cell Carcinoma." *J Invest Dermatol* **137**(3): 772-775.
- Kim, T. H., L. O. Barrera, et al. (2005). "A high-resolution map of active promoters in the human genome." *Nature* **436**(7052): 876-880.
- Kim, Y. H., L. Girard, et al. (2006). "Combined microarray analysis of small cell lung cancer reveals altered apoptotic balance and distinct expression signatures of MYC family gene amplification." *Oncogene* **25**(1): 130-138.
- Kirby, K. S. (1956). "A new method for the isolation of ribonucleic acids from mammalian tissues." *Biochem J* **64**(3): 405-408.
- Klein, F. A., T. Pakozdi, et al. (2015). "FourCSeq: analysis of 4C sequencing data." *Bioinformatics* **31**(19): 3085-3091.
- Klisch, T. J., A. Vainshtein, et al. (2017). "Jak2-mediated phosphorylation of Atoh1 is critical for medulloblastoma growth." *Elife* **6**.

-
- Klisch, T. J., Y. Xi, et al. (2011). "In vivo Atoh1 targetome reveals how a proneural transcription factor regulates cerebellar development." *Proc Natl Acad Sci U S A* **108**(8): 3288-3293.
- Kohl, N. E., N. Kanda, et al. (1983). "Transposition and amplification of oncogene-related sequences in human neuroblastomas." *Cell* **35**(2 Pt 1): 359-367.
- Kolasinska-Zwierz, P., T. Down, et al. (2009). "Differential chromatin marking of introns and expressed exons by H3K36me3." *Nat Genet* **41**(3): 376-381.
- Kornberg, R. D. (1974). "Chromatin structure: a repeating unit of histones and DNA." *Science* **184**(4139): 868-871.
- Kornberg, R. D. and J. O. Thomas (1974). "Chromatin structure; oligomers of the histones." *Science* **184**(4139): 865-868.
- Lachmann, A., F. M. Giorgi, et al. (2016). "ARACNe-AP: gene network reverse engineering through adaptive partitioning inference of mutual information." *Bioinformatics* **32**(14): 2233-2235.
- Landa, I., I. Ganly, et al. (2013). "Frequent somatic TERT promoter mutations in thyroid cancer: higher prevalence in advanced forms of the disease." *J Clin Endocrinol Metab* **98**(9): E1562-1566.
- Lemm, I. and J. Ross (2002). "Regulation of c-myc mRNA decay by translational pausing in a coding region instability determinant." *Mol Cell Biol* **22**(12): 3959-3969.
- Lendvay, T. S., D. K. Morris, et al. (1996). "Senescence mutants of *Saccharomyces cerevisiae* with a defect in telomere replication identify three additional EST genes." *Genetics* **144**(4): 1399-1412.
- Lingner, J. and T. R. Cech (1996). "Purification of telomerase from *Euplotes aediculatus*: requirement of a primer 3' overhang." *Proc Natl Acad Sci U S A* **93**(20): 10712-10717.
- Liu, L., S. Lai, et al. (2004). "Genetic and epigenetic modulation of telomerase activity in development and disease." *Gene* **340**(1): 1-10.
- Liu, X. and V. Giguere (2014). "Inactivation of RARbeta inhibits Wnt1-induced mammary tumorigenesis by suppressing epithelial-mesenchymal transitions." *Nucl Recept Signal* **12**: e004.
- Loboda, A., M. Nebozhyn, et al. (2010). "A gene expression signature of RAS pathway dependence predicts response to PI3K and RAS pathway inhibitors and expands the population of RAS pathway activated tumors." *BMC Med Genomics* **3**: 26.
- Look, A. T., F. A. Hayes, et al. (1984). "Cellular DNA content as a predictor of response to chemotherapy in infants with unresectable neuroblastoma." *N Engl J Med* **311**(4): 231-235.
- Loven, J., H. A. Hoke, et al. (2013). "Selective inhibition of tumor oncogenes by disruption of super-enhancers." *Cell* **153**(2): 320-334.
- Luo, Y., R. Sun, et al. (2015). "miR-506 inhibits the proliferation and invasion by targeting IGF2BP1 in glioblastoma." *Am J Transl Res* **7**(10): 2007-2014.
- Mack, S. C., K. W. Pajtler, et al. (2018). "Therapeutic targeting of ependymoma as informed by oncogenic enhancer profiling." *Nature* **553**(7686): 101-105.
- Mansour, M. R., B. J. Abraham, et al. (2014). "Oncogene regulation. An oncogenic super-enhancer formed through somatic mutation of a noncoding intergenic element." *Science* **346**(6215): 1373-1377.
- Margolin, A. A., I. Nemenman, et al. (2006). "ARACNE: an algorithm for the reconstruction of gene regulatory networks in a mammalian cellular context." *BMC Bioinformatics* **7 Suppl 1**: S7.
- Margueron, R. and D. Reinberg (2011). "The Polycomb complex PRC2 and its mark in life." *Nature* **469**(7330): 343-349.
- Mariani-Costantini, R., C. Escot, et al. (1988). "In situ c-myc expression and genomic status of the c-myc locus in infiltrating ductal carcinomas of the breast." *Cancer Res* **48**(1): 199-205.
- Maris, J. M., M. D. Hogarty, et al. (2007). "Neuroblastoma." *Lancet* **369**(9579): 2106-2120.
- Matthay, K. K., H. N. Sather, et al. (1989). "Excellent outcome of stage II neuroblastoma is independent of residual disease and radiation therapy." *J Clin Oncol* **7**(2): 236-244.

-
- Matthay, K. K., J. G. Villablanca, et al. (1999). "Treatment of high-risk neuroblastoma with intensive chemotherapy, radiotherapy, autologous bone marrow transplantation, and 13-cis-retinoic acid. Children's Cancer Group." *N Engl J Med* **341**(16): 1165-1173.
- McKeown, M. R., M. R. Corces, et al. (2017). "Superenhancer Analysis Defines Novel Epigenomic Subtypes of Non-APL AML, Including an RARalpha Dependency Targetable by SY-1425, a Potent and Selective RARalpha Agonist." *Cancer Discov* **7**(10): 1136-1153.
- Meddeb, M., G. Danglot, et al. (1996). "Additional copies of a 25 Mb chromosomal region originating from 17q23.1-17qter are present in 90% of high-grade neuroblastomas." *Genes Chromosomes Cancer* **17**(3): 156-165.
- Melo, M., A. G. da Rocha, et al. (2014). "TERT promoter mutations are a major indicator of poor outcome in differentiated thyroid carcinomas." *J Clin Endocrinol Metab* **99**(5): E754-765.
- Molenaar, J. J., R. Domingo-Fernandez, et al. (2012). "LIN28B induces neuroblastoma and enhances MYCN levels via let-7 suppression." *Nat Genet* **44**(11): 1199-1206.
- Molenaar, J. J., J. Koster, et al. (2012). "Sequencing of neuroblastoma identifies chromothripsis and defects in neuritogenesis genes." *Nature* **483**(7391): 589-593.
- Molenaar, J. J., P. van Sluis, et al. (2003). "Rearrangements and increased expression of cyclin D1 (CCND1) in neuroblastoma." *Genes Chromosomes Cancer* **36**(3): 242-249.
- Moley, J. F., M. B. Brother, et al. (1991). "Low frequency of ras gene mutations in neuroblastomas, pheochromocytomas, and medullary thyroid cancers." *Cancer Res* **51**(6): 1596-1599.
- Monclair, T., G. M. Brodeur, et al. (2009). "The International Neuroblastoma Risk Group (INRG) staging system: an INRG Task Force report." *J Clin Oncol* **27**(2): 298-303.
- Mosse, Y. P., M. Laudenslager, et al. (2004). "Germline PHOX2B mutation in hereditary neuroblastoma." *Am J Hum Genet* **75**(4): 727-730.
- Mosse, Y. P., M. Laudenslager, et al. (2008). "Identification of ALK as a major familial neuroblastoma predisposition gene." *Nature* **455**(7215): 930-935.
- Muller, P. A. and K. H. Vousden (2014). "Mutant p53 in cancer: new functions and therapeutic opportunities." *Cancer Cell* **25**(3): 304-317.
- Mumbach, M. R., A. J. Rubin, et al. (2016). "HiChIP: efficient and sensitive analysis of protein-directed genome architecture." *Nat Methods* **13**(11): 919-922.
- Naiditch, J. A., C. Jie, et al. (2015). "Mesenchymal change and drug resistance in neuroblastoma." *J Surg Res* **193**(1): 279-288.
- Northcott, P. A., C. Lee, et al. (2014). "Enhancer hijacking activates GF11 family oncogenes in medulloblastoma." *Nature* **511**(7510): 428-434.
- Northcott, P. A., D. J. Shih, et al. (2012). "Subgroup-specific structural variation across 1,000 medulloblastoma genomes." *Nature* **488**(7409): 49-56.
- Nozato, M., S. Kaneko, et al. (2013). "Epithelial-mesenchymal transition-related gene expression as a new prognostic marker for neuroblastoma." *Int J Oncol* **42**(1): 134-140.
- Ohali, A., S. Avigad, et al. (2006). "Telomere length is a prognostic factor in neuroblastoma." *Cancer* **107**(6): 1391-1399.
- Okano, M., D. W. Bell, et al. (1999). "DNA methyltransferases Dnmt3a and Dnmt3b are essential for de novo methylation and mammalian development." *Cell* **99**(3): 247-257.
- Oldridge, D. A., A. C. Wood, et al. (2015). "Genetic predisposition to neuroblastoma mediated by a LMO1 super-enhancer polymorphism." *Nature* **528**(7582): 418-421.
- Ong, C. T. and V. G. Corces (2014). "CTCF: an architectural protein bridging genome topology and function." *Nat Rev Genet* **15**(4): 234-246.
- Ooi, W. F., M. Xing, et al. (2016). "Epigenomic profiling of primary gastric adenocarcinoma reveals super-enhancer heterogeneity." *Nat Commun* **7**: 12983.
- Paul, F. and I. Amit (2014). "Plasticity in the transcriptional and epigenetic circuits regulating dendritic cell lineage specification and function." *Curr Opin Immunol* **30**: 1-8.
- Peifer, M., F. Hertwig, et al. (2015). "Telomerase activation by genomic rearrangements in high-risk neuroblastoma." *Nature* **526**(7575): 700-704.

-
- Pestana, A., J. Vinagre, et al. (2017). "TERT biology and function in cancer: beyond immortalisation." *J Mol Endocrinol* **58**(2): R129-R146.
- Peters, A. H., J. E. Mermoud, et al. (2002). "Histone H3 lysine 9 methylation is an epigenetic imprint of facultative heterochromatin." *Nat Genet* **30**(1): 77-80.
- Peters, J. M., A. Tedeschi, et al. (2008). "The cohesin complex and its roles in chromosome biology." *Genes Dev* **22**(22): 3089-3114.
- Phanstiel, D. H., A. P. Boyle, et al. (2015). "Mango: a bias-correcting ChIA-PET analysis pipeline." *Bioinformatics* **31**(19): 3092-3098.
- Populo, H., P. Boaventura, et al. (2014). "TERT promoter mutations in skin cancer: the effects of sun exposure and X-irradiation." *J Invest Dermatol* **134**(8): 2251-2257.
- Pott, S. and J. D. Lieb (2015). "What are super-enhancers?" *Nat Genet* **47**(1): 8-12.
- Pritchard, J. and J. A. Hickman (1994). "Why does stage 4s neuroblastoma regress spontaneously?" *Lancet* **344**(8926): 869-870.
- Pugh, T. J., O. Morozova, et al. (2013). "The genetic landscape of high-risk neuroblastoma." *Nat Genet* **45**(3): 279-284.
- Raabe, E. H., M. Laudenslager, et al. (2008). "Prevalence and functional consequence of PHOX2B mutations in neuroblastoma." *Oncogene* **27**(4): 469-476.
- Ramirez, F., F. Dundar, et al. (2014). "deepTools: a flexible platform for exploring deep-sequencing data." *Nucleic Acids Res* **42**(Web Server issue): W187-191.
- Ran, L., Y. Chen, et al. (2018). "FOXF1 Defines the Core-Regulatory Circuitry in Gastrointestinal Stromal Tumor." *Cancer Discov* **8**(2): 234-251.
- Rao, S. S., M. H. Huntley, et al. (2014). "A 3D map of the human genome at kilobase resolution reveals principles of chromatin looping." *Cell* **159**(7): 1665-1680.
- Rausch, T., T. Zichner, et al. (2012). "DELLY: structural variant discovery by integrated paired-end and split-read analysis." *Bioinformatics* **28**(18): i333-i339.
- Raviram, R., P. P. Rocha, et al. (2016). "4C-ker: A Method to Reproducibly Identify Genome-Wide Interactions Captured by 4C-Seq Experiments." *PLoS Comput Biol* **12**(3): e1004780.
- Reddy, E. P., R. K. Reynolds, et al. (1982). "A point mutation is responsible for the acquisition of transforming properties by the T24 human bladder carcinoma oncogene." *Nature* **300**(5888): 149-152.
- Reichmann, E., H. Schwarz, et al. (1992). "Activation of an inducible c-FosER fusion protein causes loss of epithelial polarity and triggers epithelial-fibroblastoid cell conversion." *Cell* **71**(7): 1103-1116.
- Reynolds, C. P., D. J. Kane, et al. (1991). "Response of neuroblastoma to retinoic acid in vitro and in vivo." *Prog Clin Biol Res* **366**: 203-211.
- Reynolds, C. P., K. K. Matthay, et al. (2003). "Retinoid therapy of high-risk neuroblastoma." *Cancer Lett* **197**(1-2): 185-192.
- Riddick, G., S. Kotliarova, et al. (2017). "A Core Regulatory Circuit in Glioblastoma Stem Cells Links MAPK Activation to a Transcriptional Program of Neural Stem Cell Identity." *Sci Rep* **7**: 43605.
- Ried, T., E. Schrock, et al. (1998). "Chromosome painting: a useful art." *Hum Mol Genet* **7**(10): 1619-1626.
- Riggs, A. D. (1975). "X inactivation, differentiation, and DNA methylation." *Cytogenet Cell Genet* **14**(1): 9-25.
- Rowland, B. D. and D. S. Peeper (2006). "KLF4, p21 and context-dependent opposing forces in cancer." *Nat Rev Cancer* **6**(1): 11-23.
- Rowley, J. D. (1973). "Letter: A new consistent chromosomal abnormality in chronic myelogenous leukaemia identified by quinacrine fluorescence and Giemsa staining." *Nature* **243**(5405): 290-293.
- Saeki, N., T. Usui, et al. (2009). "Distinctive expression and function of four GSDM family genes (GSDMA-D) in normal and malignant upper gastrointestinal epithelium." *Genes Chromosomes Cancer* **48**(3): 261-271.

-
- Saint-Andre, V., A. J. Federation, et al. (2016). "Models of human core transcriptional regulatory circuitries." *Genome Res* **26**(3): 385-396.
- Sato, K., J. Qian, et al. (1999). "Clinical significance of alterations of chromosome 8 in high-grade, advanced, nonmetastatic prostate carcinoma." *J Natl Cancer Inst* **91**(18): 1574-1580.
- Savelyeva, L., R. Corvi, et al. (1994). "Translocation involving 1p and 17q is a recurrent genetic alteration of human neuroblastoma cells." *Am J Hum Genet* **55**(2): 334-340.
- Sawyers, C. (2004). "Targeted cancer therapy." *Nature* **432**(7015): 294-297.
- Schmidl, C., M. Klug, et al. (2009). "Lineage-specific DNA methylation in T cells correlates with histone methylation and enhancer activity." *Genome Res* **19**(7): 1165-1174.
- Schmidl, C., A. F. Rendeiro, et al. (2015). "ChIPmentation: fast, robust, low-input ChIP-seq for histones and transcription factors." *Nat Methods* **12**(10): 963-965.
- Schuettengruber, B. and G. Cavalli (2009). "Recruitment of polycomb group complexes and their role in the dynamic regulation of cell fate choice." *Development* **136**(21): 3531-3542.
- Schwab, M., K. Alitalo, et al. (1983). "Amplified DNA with limited homology to myc cellular oncogene is shared by human neuroblastoma cell lines and a neuroblastoma tumour." *Nature* **305**(5931): 245-248.
- Schwab, M., H. E. Varmus, et al. (1984). "Chromosome localization in normal human cells and neuroblastomas of a gene related to c-myc." *Nature* **308**(5956): 288-291.
- Seeger, R. C., G. M. Brodeur, et al. (1985). "Association of multiple copies of the N-myc oncogene with rapid progression of neuroblastomas." *N Engl J Med* **313**(18): 1111-1116.
- Servant, N., N. Varoquaux, et al. (2015). "HiC-Pro: an optimized and flexible pipeline for Hi-C data processing." *Genome Biol* **16**: 259.
- Shao, D. D., W. Xue, et al. (2014). "KRAS and YAP1 converge to regulate EMT and tumor survival." *Cell* **158**(1): 171-184.
- Shao, J. B., Z. M. Gao, et al. (2017). "The mechanism of epithelial-mesenchymal transition induced by TGF-beta1 in neuroblastoma cells." *Int J Oncol* **50**(5): 1623-1633.
- Shay, J. W. and S. Bacchetti (1997). "A survey of telomerase activity in human cancer." *Eur J Cancer* **33**(5): 787-791.
- Sherwood, R. I., T. Hashimoto, et al. (2014). "Discovery of directional and nondirectional pioneer transcription factors by modeling DNase profile magnitude and shape." *Nat Biotechnol* **32**(2): 171-178.
- Shi, F., Y. F. Cheng, et al. (2010). "Beta-catenin up-regulates Atoh1 expression in neural progenitor cells by interaction with an Atoh1 3' enhancer." *J Biol Chem* **285**(1): 392-400.
- Shi, J., W. A. Whyte, et al. (2013). "Role of SWI/SNF in acute leukemia maintenance and enhancer-mediated Myc regulation." *Genes Dev* **27**(24): 2648-2662.
- Shlyueva, D., G. Stampfel, et al. (2014). "Transcriptional enhancers: from properties to genome-wide predictions." *Nat Rev Genet* **15**(4): 272-286.
- Shukla, S., E. Kavak, et al. (2011). "CTCF-promoted RNA polymerase II pausing links DNA methylation to splicing." *Nature* **479**(7371): 74-79.
- Sidell, N., T. Sarafian, et al. (1986). "Retinoic acid-induced differentiation of human neuroblastoma: a cell variant system showing two distinct responses." *Exp Cell Biol* **54**(5-6): 287-300.
- Simon, J. A. and R. E. Kingston (2009). "Mechanisms of polycomb gene silencing: knowns and unknowns." *Nat Rev Mol Cell Biol* **10**(10): 697-708.
- Splinter, E., E. de Wit, et al. (2012). "Determining long-range chromatin interactions for selected genomic sites using 4C-seq technology: from fixation to computation." *Methods* **58**(3): 221-230.
- Squire, J. A., P. Thorner, et al. (1996). "Identification of MYCN Copy Number Heterogeneity by Direct FISH Analysis of Neuroblastoma Preparations." *Mol Diagn* **1**(4): 281-289.
- Stadler, M. B., R. Murr, et al. (2011). "DNA-binding factors shape the mouse methylome at distal regulatory regions." *Nature* **480**(7378): 490-495.

- Stewart, M. D., J. Li, et al. (2005). "Relationship between histone H3 lysine 9 methylation, transcription repression, and heterochromatin protein 1 recruitment." *Mol Cell Biol* **25**(7): 2525-2538.
- Tahiliani, M., K. P. Koh, et al. (2009). "Conversion of 5-methylcytosine to 5-hydroxymethylcytosine in mammalian DNA by MLL partner TET1." *Science* **324**(5929): 930-935.
- Taub, R., I. Kirsch, et al. (1982). "Translocation of the c-myc gene into the immunoglobulin heavy chain locus in human Burkitt lymphoma and murine plasmacytoma cells." *Proc Natl Acad Sci U S A* **79**(24): 7837-7841.
- Taube, J. H., J. I. Herschkowitz, et al. (2010). "Core epithelial-to-mesenchymal transition interactome gene-expression signature is associated with claudin-low and metaplastic breast cancer subtypes." *Proc Natl Acad Sci U S A* **107**(35): 15449-15454.
- Teitz, T., T. Wei, et al. (2000). "Caspase 8 is deleted or silenced preferentially in childhood neuroblastomas with amplification of MYCN." *Nat Med* **6**(5): 529-535.
- Thurman, R. E., E. Rynes, et al. (2012). "The accessible chromatin landscape of the human genome." *Nature* **489**(7414): 75-82.
- Tie, F., R. Banerjee, et al. (2009). "CBP-mediated acetylation of histone H3 lysine 27 antagonizes *Drosophila* Polycomb silencing." *Development* **136**(18): 3131-3141.
- Trochet, D., F. Bourdeaut, et al. (2004). "Germline mutations of the paired-like homeobox 2B (PHOX2B) gene in neuroblastoma." *Am J Hum Genet* **74**(4): 761-764.
- Tsankova, N., W. Renthal, et al. (2007). "Epigenetic regulation in psychiatric disorders." *Nat Rev Neurosci* **8**(5): 355-367.
- Tseng, Y. Y., B. S. Moriarity, et al. (2014). "PVT1 dependence in cancer with MYC copy-number increase." *Nature* **512**(7512): 82-86.
- Valton, A. L. and J. Dekker (2016). "TAD disruption as oncogenic driver." *Curr Opin Genet Dev* **36**: 34-40.
- van de Werken, H. J., P. J. de Vree, et al. (2012). "4C technology: protocols and data analysis." *Methods Enzymol* **513**: 89-112.
- van Groningen, T., J. Koster, et al. (2017). "Neuroblastoma is composed of two super-enhancer-associated differentiation states." *Nat Genet* **49**(8): 1261-1266.
- Van Roy, N., G. Laureys, et al. (1994). "1;17 translocations and other chromosome 17 rearrangements in human primary neuroblastoma tumors and cell lines." *Genes Chromosomes Cancer* **10**(2): 103-114.
- Vaquerizas, J. M., S. K. Kummerfeld, et al. (2009). "A census of human transcription factors: function, expression and evolution." *Nat Rev Genet* **10**(4): 252-263.
- Venkatesh, S. and J. L. Workman (2015). "Histone exchange, chromatin structure and the regulation of transcription." *Nat Rev Mol Cell Biol* **16**(3): 178-189.
- Vogan, K., M. Bernstein, et al. (1993). "Absence of p53 gene mutations in primary neuroblastomas." *Cancer Res* **53**(21): 5269-5273.
- Walker, E. J., C. Zhang, et al. (2012). "Monoallelic expression determines oncogenic progression and outcome in benign and malignant brain tumors." *Cancer Res* **72**(3): 636-644.
- Wang, K., S. J. Diskin, et al. (2011). "Integrative genomics identifies LMO1 as a neuroblastoma oncogene." *Nature* **469**(7329): 216-220.
- Wang, L. L., R. Sukanuma, et al. (2013). "Neuroblastoma of undifferentiated subtype, prognostic significance of prominent nucleolar formation, and MYC/MYCN protein expression: a report from the Children's Oncology Group." *Cancer* **119**(20): 3718-3726.
- Wang, L. L., R. Teshiba, et al. (2015). "Augmented expression of MYC and/or MYCN protein defines highly aggressive MYC-driven neuroblastoma: a Children's Oncology Group study." *Br J Cancer* **113**(1): 57-63.
- Wang, Y., L. Wang, et al. (2016). "Novel ALK inhibitor AZD3463 inhibits neuroblastoma growth by overcoming crizotinib resistance and inducing apoptosis." *Sci Rep* **6**: 19423.

-
- Westermann, F., D. Muth, et al. (2008). "Distinct transcriptional MYCN/c-MYC activities are associated with spontaneous regression or malignant progression in neuroblastomas." *Genome Biol* **9**(10): R150.
- Westermann, F. and M. Schwab (2002). "Genetic parameters of neuroblastomas." *Cancer Lett* **184**(2): 127-147.
- Whyte, W. A., D. A. Orlando, et al. (2013). "Master transcription factors and mediator establish super-enhancers at key cell identity genes." *Cell* **153**(2): 307-319.
- Wiench, M., S. John, et al. (2011). "DNA methylation status predicts cell type-specific enhancer activity." *EMBO J* **30**(15): 3028-3039.
- Wolf, S. F., D. J. Jolly, et al. (1984). "Methylation of the hypoxanthine phosphoribosyltransferase locus on the human X chromosome: implications for X-chromosome inactivation." *Proc Natl Acad Sci U S A* **81**(9): 2806-2810.
- Wong, R. W. J., P. C. T. Ngoc, et al. (2017). "Enhancer profiling identifies critical cancer genes and characterizes cell identity in adult T-cell leukemia." *Blood* **130**(21): 2326-2338.
- Yaniv, K., A. Fainsod, et al. (2003). "The RNA-binding protein Vg1 RBP is required for cell migration during early neural development." *Development* **130**(23): 5649-5661.
- Zhang, W., Y. Yu, et al. (2015). "Comparison of RNA-seq and microarray-based models for clinical endpoint prediction." *Genome Biol* **16**: 133.
- Zhang, X., P. S. Choi, et al. (2016). "Identification of focally amplified lineage-specific super-enhancers in human epithelial cancers." *Nat Genet* **48**(2): 176-182.
- Zhang, Y. and J. D. Rowley (2006). "Chromatin structural elements and chromosomal translocations in leukemia." *DNA Repair (Amst)* **5**(9-10): 1282-1297.
- Zhao, Y., S. Wang, et al. (2009). "Rearrangement of upstream sequences of the hTERT gene during cellular immortalization." *Genes Chromosomes Cancer* **48**(11): 963-974.
- Zimmerman, M. W., Y. Liu, et al. (2018). "MYC Drives a Subset of High-Risk Pediatric Neuroblastomas and Is Activated through Mechanisms Including Enhancer Hijacking and Focal Enhancer Amplification." *Cancer Discov* **8**(3): 320-335.

Publications

Ongoing work:

Moritz Gartlgruber*, Daniel Dreidax*, Ashwini Sharma*, Paul Saary, Andrés Felipe Quintero Moreno, Young-Gyu Park, Elena A. Afanasyeva, Selina Jansky, Daria Doncevic, Rogier Versteeg, Johan van Nes, Carl Herrmann, Frank Westermann *equal contribution

Integrative genome-wide enhancer landscape analysis in primary neuroblastomas reveals distinct epigenetic subtypes. (manuscript in preparation)

Hamed Alborzina*, Andrés F. Flórez*, Sina Gogolin*, Lena M. Brückner*, **Moritz Gartlgruber**, Dorett Odoni, Chunxuan Shao, Michal Nadler-Holly, Matthias Ziehm, Franziska Paul, Jürgen Burhenne, Sebastian Steinhäuser, Emma Bell, Marjan Shaikhkarami, Sabine Hartlieb, Daniel Dreidax, Elisa M. Hess, Jochen Kreth, Gernot Poschet, Michael Büttner, Naveed Ishaque, Matthias Schlesner, Barbara Nicke, Carlo Stresemann, María Llamazares, Jan H. Reiling, Matthias Fischer, Ido Amit, Matthias Selbach, Carl Herrmann, Stefan Wölfl, Kai-Oliver Henrich, Thomas Höfer† and Frank Westermann† *equal contribution; †co-senior authors

MYCN mediates cysteine addiction and sensitizes to ferroptosis. (in revision for *Nature*)

Bieke Decaestecker, Geertrui Denecker, Wouter Van Looche, **Moritz Gartlgruber**, Fanny De Vloed, Pauline Depuydt, Karen Verboom, Dries Rombaut, Shana Claeys, Siebe Loontjens, Carl Herrmann, Daniel Dreidax, Kaat Durinck, Anton Henssen, Rogier Versteeg, Valentina Boeva, Suzanne Vanhauwaert, Gudrun Schleiermacher, Johannes Schulte, Johan van Nes, Pieter Mestdagh, Frank Westermann, Christophe Van Neste, Katleen De Preter, Frank Speleman

TBX2 is a neuroblastoma core regulatory circuitry component enhancing MYCN/FOXM1 reactivation of DREAM targets. (in revision for *Nat. Commun.*)

Elena A. Afanasyeva, **Moritz Gartlgruber**, Tatyana Ryl, Gregor Mönke, Andres Florez, Alica Torkov, Daniel Dreidax, Carl Herrmann, Konstantin Okonechnikov, Vitaliya Sagulenko, Larissa Savelyeva, Kai-Oliver Henrich, Bieke Decaestecker, Geertrui Denecker, Frank Speleman, Frank Westermann

Kalirin-RAC controls nuclear migration in ADRN subtype neuroblastoma. (manuscript in preparation)

Authorships in peer-reviewed journals:

Peifer M*, Hertwig F*, Roels F*, Dreidax D*, **Gartlgruber M***, Menon R, Krämer A, Roncaioli JL, Sand F, Heuckmann J, Ikram F, Schmidt R, Ackermann S, Engesser A, Kahlert Y, Vogel W, Altmüller J, Nürnberg P, Thierry-Mieg J, Thierry-Mieg D, Mariappan A, Heynck S, Mariotti E, Henrich KO, Glöckner C, Bosco G, Leuschner I, Schweiger MR, Savelyeva L, Watkins SC, Shao C, Bell E, Höfer T, Achter V, Lang U, Theissen J, Volland R, Saadati M, Eggert A, de Wilde B, Berthold F, Peng Z, Zhao C, Shi L, Ortman M, Büttner R, Perner S, Hero B, Schramm A, Schulte JH, Herrmann C, O'Sullivan RJ, Westermann F, Thomas RK, Fischer M. *equal contribution

Telomerase activation by genomic rearrangements in high-risk neuroblastoma. *Nature*. 2015 Oct 29

Schramm A, Köster J, Assenov Y, Althoff K, Peifer M, Mahlow E, Odersky A, Beisser D, Ernst C, Henssen AG, Stephan H, Schröder C, Heukamp L, Engesser A, Kahlert Y, Theissen J, Hero B, Roels F, Altmüller J, Nürnberg P, Astrahantseff K, Glöckner C, De Preter K, Plass C, Lee S, Lode HN, Henrich KO, **Gartlgruber M**, Speleman F, Schmezer P, Westermann F, Rahmann S, Fischer M, Eggert A, Schulte JH.

Mutational dynamics between primary and relapse neuroblastomas. *Nat Genet*. 2015 Jun 29

Beckers A, Van Peer G, Carter DR, **Gartlgruber M**, Herrmann C, Agarwal S, Helmsmoortel HH, Althoff K, Molenaar JJ, Cheung BB, Schulte JH, Benoit Y, Shohet JM, Westermann F, Marshall GM, Vandesompele J, De Preter K, Speleman F.

MYCN-driven regulatory mechanisms controlling LIN28B in neuroblastoma. *Cancer Lett*. 2015 Sep 28

Sonja Textor, Felicitas Bossler, Kai-Oliver Henrich, **Moritz Gartlgruber**, Julia Pollmann, Nathalie Fiegler, Annette Arnold, Frank Westermann, Nina Waldburger, Kai Breuhahn, Sven Golfier, Mathias Witzens-Harig and Adelheid Cerwenka. **The proto-oncogene Myc drives expression of the NK cell-activating NKp30 ligand B7-H6 in tumor cells.** *Onc Immunology*. 2016 Jul 28

Henrich KO, Bender S, Saadati M, Dreidax D, **Gartlgruber M**, Shao C, Herrmann C, Wiesenfarth M, Parzonka M, Wehrmann L, Fischer M, Duffy DJ, Bell E, Torkov A, Schmezer P, Plass C, Höfer T, Benner A, Pfister SM, Westermann F.

Integrative Genome-Scale Analysis Identifies Epigenetic Mechanisms of Transcriptional Deregulation in Unfavorable Neuroblastomas. *Cancer Res*. 2016 Sep 15

Acknowledgements

Accomplishing this doctoral thesis was only feasible based on enormous support from various sides and especially due to all patients donating sample material for this research.

First of all, I would like to thank my advisor Frank Westermann for the opportunity to do my PhD in the Neuroblastoma Genomics department at the DKFZ. To pursue my PhD in a challenging environment but at the same time pleasant working atmosphere – where you always get the possibility to ask questions or discuss important issues – makes me grateful. I'm thankful for your understanding support when I left and paused my PhD for several months to take the opportunity working at the BASF. I really appreciated all the inspiring, international conferences you afforded me to participate and your efforts finding solutions for the bioinformatic bottle neck, which was such an important counterpart for my methodical work.

My special thanks go to Daniel Dreidax - frankly I don't know how I would have accomplished this without the perfect mixture of scientific support and fun during each day. From a working perspective, you were the perfect counterpart pushing our projects where we had the greatest success. Thanks for your stunning help with this thesis, the daily tiresome „fights“ and even more important your friendship. I wish you all the luck for you and your family and your new job perspective.

I'm thankful to Carl Herrmann and his group members. Together with you we had the perfect bioinformatic match making all my method implementations possible - during numerous meetings, calls or slack chats. Particularly, I want to mention Ashwin Sharma, Andres Quintero and Paul Saary as well as former group members Sebastian Steinhauser and Daria Doncevic. I'm sure you cursed us every once in a while for all the annoying requests and optimizations but in the end I think we were quite successful and managed to create a great manuscript.

I would like to thank my first examiner Thomas Höfer for his help during my PhD and many people of his lab supporting me with a lot of bioinformatic work. I want to emphasize Chunxuan Shao and especially Verena Körber supporting me with several projects and new ideas.

I also want to express my gratitude to my other PhD examiners, Sylvia Erhardt and Stefan Wiemann for their participation and review of my work.

I owe my deepest gratitude to Young-Gyu Park not only for making the best glass noodle salad and kimchi I ever had, in addition he adapted and optimized our tumor ChIP-seq protocols to the point of genius. Now the Russian gang - first Alica Torkov, I'm thankful that you joined this, compared to you, inactive lab and making it (together with Kai and Daniel) a crazy and much better place. Thanks Elena Afanasyeva for being a good company late in the lab and for your great proof reading skills. I'm grateful to work with Larissa Savelyeva, who was always supporting me with important scientific input. Thanks to Sina Gogolin for a great time at Bayer in Berlin and proofreading and of course Elisa Hess for being a helping hand everywhere in the lab. My special gratitude goes to Kai Henrich for uncountable scientific support and for giving my hessian soul a place in his garden with our annually self-made 'Äppelwoi'. I want to thank Jochi Kreth for several years of support, fun and putting up with me and my moods during this time. He was perfectly replaced by Felix Schuster, who is supporting us reluctantly since then. Thanks to Mona Friedrich for a memorable trip to the Australian outback. I would like to thank the

whole department of B087 for being my colleagues and offered me such a great working atmosphere.

I want to thank Philipp Mallm for introducing me to my first sequencing techniques and later on for having always helpful advises. In addition, I'm thankful to the sequencing core facility team for always being flexible with our requests beyond the usual methodic needs as well as Naveed Ishaque for taking care of my RNA-seq problems.

I want to express my gratitude to our numerous external collaborators namely Frank Speleman and his group members from Ghent, Johan van Nes from Amsterdam and especially Matthias Fischer and his group in Cologne for great collaboration concerning our joint publication as well as for giving me the opportunity to work in his lab for technical training.

I want to thank Ido Amit from the Weizmann institute for the opportunity to stay at his lab and for technical training within the German-Israeli Joint PhD program. Here, I also want to thank Franziska Paul, my PhD counterpart at the WIS, making the stay and communication later on much easier. Thanks to all the 'members' of this small group of German Israeli PhD students, the stays in Israel and Germany and the time we had together as well as Lindsay Murrells and Evelyn Müller for organizing everything.

I would also like to thank all my friends for their support and for making also my life outside of the PhD enjoyable: Sajo, Chrissi, Alica, Sebastian, Alex, Daniel, Johannes, Felix. With most of you we had a great time at BioContact including successful teamwork and outstanding events. Especially, Sajo and Chrissi for listening to my problems, for sharing theirs, and for the funny times we enjoyed besides all the problems while cooking Indian food.

I'm grateful for many friendships besides the DKFZ and really enjoyed the weekly play evenings with Thomas, Freya, Nico and Peter. I'm thankful for my long-time friends Kaldi, Simon, Verena, Joscha, Mark and Steffi as well as Sabine and Sebastian for always bringing stability and support in my life since school or studies.

I am deeply thankful to Nadine for reminding me what is important besides work and PhD and all the sacrifices you made on my behalf the last months.

Personal thanks go to my big Austrian Gartlgruber family that is spread all over Europe and US. I want to express my gratitude to my closest family members Christian, Kristin, Kristina, Gerd and especially my grandmother who sadly can't witness my graduation anymore.

Finally and foremost I am deeply thankful to my loving family, especially my parents Dagmar and Gerd as well as to my sister Miriam, for your unlimited support and for giving me the feeling that you are proud of whatever I'm doing.